GOCE++ Dynamic Topography at the coast and tide gauge unification
GOCE ++ DYCOT

TITLE. D9 Final Report

Authors: Karina Nielsen, Per Knudsen, Ole B. Andersen, Christopher C. Hughes, Médéric Gravelle, Rory Bingham, and Luciana Fenoglio-Marc

ESTEC Ref: ITT AO/1-8194/15/NL/FF/gp "GOCE++ Dynamic Topography at the coast and tide gauge unification"- Coordinator: Ole B. Andersen (DTU)

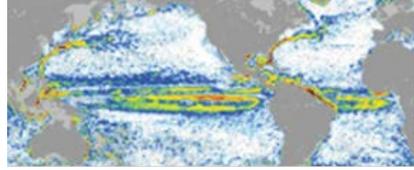| DOCUMENT CHANGE LOG				
Rev.	Date	Sections modified	Comments	Changed by
1	15-06-2017	All	Draft	Karina Nielsen

Contents

1   Introduction

The Final Report is a compilation of the Summary report and the deliverables D1-D8

2 Appendix A, D10: Summary report

GOCE++ Dynamic Topography at the coast and tide gauge unification
GOCE ++ DYCOT

TITLE. D10 Summary Report

Authors: Karina Nielsen, Per Knudsen, Ole B. Andersen, Christopher C. Hughes, Médéric Gravelle, Rory Bingham, and Luciana Fenoglio-Marc

ESTEC Ref: ITT AO/1-8194/15/NL/FF/gp "GOCE++ Dynamic Topography at the coast and tide gauge unification"- Coordinator: Ole B. Andersen (DTU)

DOCUMENT CHANGE LOG				
Rev.	Date	Sections modified	Comments	Changed by
1	15-06-2017	All	Draft	Karina Nielsen
2	17-11-17	All	Input from partners	All

Table of Contents

1   Introduction

The Summary Report will contain a short description of the work carried out within each Work Package of the GOCE++ project.

2   WP1000 Scientific Review and Approach

2.1   WP1100 Scientific Review

A review of current understanding of the issue of the coastal Mean Ocean Dynamic Topography (MODT) was undertaken. This is reported fully in [1]. The main conclusions were as follows.

It has been shown that the coastal MODT is consistent with ocean model predictions at the 5-10 cm level. However, recent improvements and new geoid data available have not yet been fully exploited. There are two approaches: the open ocean approach using satellite altimetry, and the tide gauge approach. For the latter, and to a large extent also for the former approach, the inclusion of small scale gravity information is crucial. Ideally this information is incorporated into a global gravity solution in a consistent way, which is why it has been difficult to demonstrate improvements over the pre-GOCE EGM08 geoid which took this approach. The TUM13 geoid demonstrates that extension of the consistent solution to degree 720 is possible and results in significant improvements over the simple combination with EGM08, but this still requires additional information from EGM08 at higher degrees.

These consistent geoid solutions (TUM13, GGM05C, EIGEN-6C4, and the expected GOCO05C) all use versions of the gravity anomalies associated with the DTU mean sea surface, so should be compatible with that surface when calculating the MODT.

Improved satellite altimeter corrections are pushing to the centimetre level for coastal regions, but there remain important questions about the validity of the sea state bias correction. New techniques involving wave models are addressing part of this issue, but there are additional questions concerning the changing shape of waves in coastal regions which would benefit from further investigation.

Altimeter retracking methods are succeeding in providing more data close to the coast, though in some cases the loss of data is due to a failure of the onboard tracker as the instrument

crosses from land to ocean, and these data losses are irretrievable. More recent onboard trackers do not suffer from this problem.

New SAR altimetry methods are accurate and have higher spatial resolution, allowing closer approach to the coast, but otherwise suffer the same limitations associated with corrections as traditional altimeters, including the important issue of sea state bias.

All methods suffer from important temporal aliasing effects, leading to a requirement for accurate tidal models as well as models for the high frequency response to atmospheric forcing. These issues become much more acute in coastal regions as both sources of variability increase in amplitude, and tides in particular become more complex, requiring more components than are commonly provided in tide models. This issue is mitigated for mean sea level given sufficient data (many years) for exact repeat missions, but remains an issue for the slow or no repeat CryoSat mission. The size of the problem is highly dependent on region, being particularly difficult in wide shelf seas and regions of high tides. SWOT should help in this regard, as its swath capability circumvents the classic trade-off between spatial and temporal sampling for a nadir track altimeter.

2.2   WP1200 Selection of Approach
The initial approach is summarized in Table 1. A more detailed description is found in [4]

Table 1: The initial approach.

MDT	The MDT is derived using a geodetic approach. Hence estimated from altimetry and constrained by tide gauge data.
Geoid	To minimize the residue errors in the final MDT it is recommended to uses the same geoid as applied in the altimetric mean sea surface.
Reference period	The reference period is chosen to be 2003-2007, to achieve the best data collection.
Filter	A spatial filter was selected so the MDT could be derived on a regional scale. The filter is a simple average filter, which is applied iteratively.
MDT gradients	To ensure a more physical correct MDT in the coast area, the altimetric MDT is here constrained by tide gauge data. The tide gauge data is inserted as MDT values over land. After filtering the land values are smoothed into the coastal region and hence aligning the gradients along the coast.

2.3   Test regions and data
The first task of WP1300 was to prepare a database with supporting information, which includes description, format specification, conventions and transformations between data systems, to provide convenient access by ftp to data used in WP2000 and WP3000. The database is located in the server of the University of Bonn. Table 2 below summarizes the data detailed in [2], [3], [5] and updates Table 1 in [2] and [5]. It includes altimeter, in-situ and model data, at different

level of post-processing.

The second task of WP1300 was to select data based on their quality and few test regions based on the data availability. Geodetic tie via GPS@TG was available at 302 tide gauge stations, which include the full SONEL dataset and external German stations. We distinguished between "well-surveyed" and "poorly-surveyed" areas based on the availability of in-situ sea level records and co-located GPS data and selected for each group respectively two (North-Eastern Atlantic and Australia) and three regions (Pacific Islands, the South Eastern African Coast and the North-Eastern coast of South-America)**.** Based on the same criteria we selected the time intervals 2003-2007 and 2008-2012.

Table 2: The database

Data Type	parameter	Name of Products
Altimeter data	Ell. Heights, SLA	AVISO, RADS, CryoSat-2, T/P, Jason, Envisat, SLCCI v2.0
Bathymetry	depth	GEBCO_2014
Geoid	height	TUM2013C, GGM05C, EIGEN6C4, GOCO05C, EGM08, DIR5C
MSS	Ell. height	DTU15MSS, DTU13MSS, CLS
MDT	height	DTU15MDT, DTU13MDT
Ocean Models	height	AVISO, ecco2, eccog, livc,livs,nemo12a,nemo12b,nemoq,tum13
Tide gauge data	height	PSMSL, BSH local organisation
Tide gauge GPS	Ell. Heights	302
Drifter mean velocities	Velocity	UHDTU15MGV
Inverse Barometer	Correction	Dac, IB to be added to ssh (m)

3   WP2000 Implementation and Validation

3.1   WP2100 Software development

The main task of WP2100 was to develop prototype software for estimation of the MDT along the coast. The software is based on the approach outlined in Section 2.2. Its main functionality is the integration of altimetry and tide gauge data in the estimation of the MDT.

3.1.1 Short description

The architecture is illustrated in Figure 1, where green is input data, purple is the functionality and blue is the output, the final MDT. The software is implemented as in the open source programming language "R" (https://www.r-project.org/). It is implemented as an R-package coastMDT, which makes it easy to use. coastMDT can be used with the available demo data, which enables the used to derive a MDT based on altimetry and gauge data for a selected region. CoastMDT can also be used with data provided by the user. Demands related to format are found in [9].
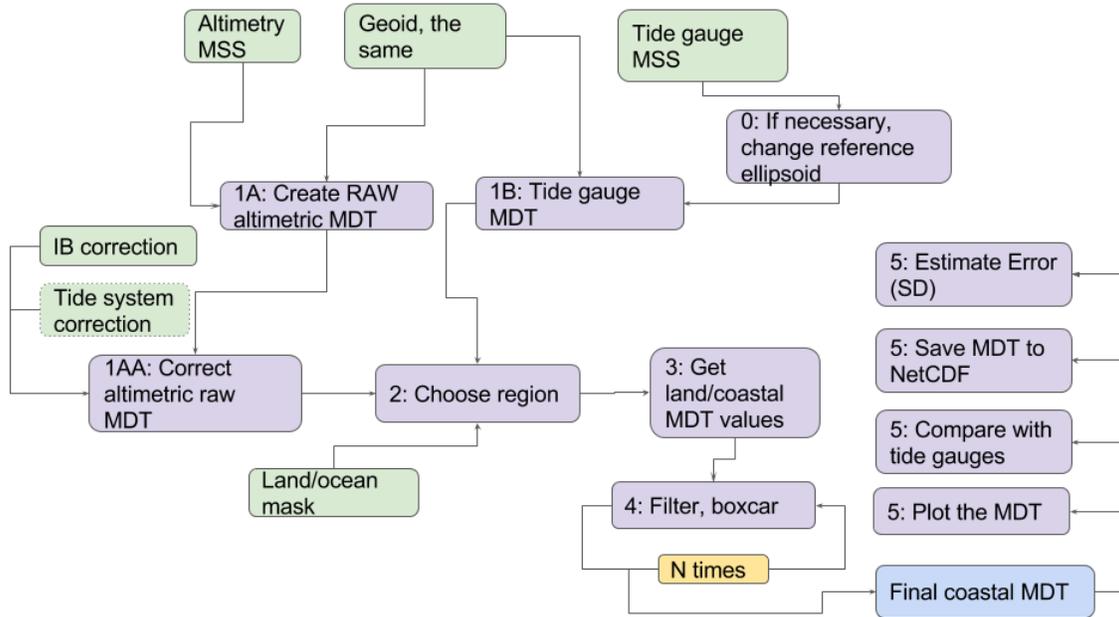
Figure 1: Flowchart of prototype software for estimation of the coastal MDT

3.1.2 Data and functionality

Table 3 and Table 4 list the functionality and available demo data for the coastMDT package.

Table 3: Functionality of the software coastMDT

Function	Description
compareWithTG	Function to compare altimetric and tide gauge based MDT values at tide gauge stations.
ellipsoidTF2MT	Get correction to go from a tide free to a mean tide ellipsoid.
getData	Function that downloads the data used for constructing the coastal MDT.
getError	Function to estimate the Error of the MDT via the bootstrap approach
getLandVal	Function to estimate MDT values over land/coast.

getSubGrid	Function to extract a regional grid from a global grid.
getSubTG	Function to extract a subset of the tide gauge MDT values.
Grid2file	Function to save the MDT grid to a NetCDF file.
iterativeAveSmoother	Iterative average filter.
plotMDT	Function for plotting the MDT.
readncdf1var	Function to read NetCDF file with one variable.
readRegGridBin	Function to read a regular gridded binary file
tideConvert	Function to convert between different permanent tidal systems.
Wgs2topCorr	Function that estimates the height difference between WGS84 and TOPEX ellipsoids.

Table 4: Demo data available for the coastMDT

Data	Description
landmask8	Land/ocean mask on 1/8 degree (0-360 degree) grid.
dDTU15MSS_ref2003_2007	Grid to transform the DTU15 MSS (DTU15MSS) to the MSS of the reference period 2003-2007. The grid is defined on 1/8 degree (0-360 degree) grid.
eigen6c4r	Geoid model based on EIGEN-6C4 on 1/8 degree (0-360 degree) grid.
dacCor5Y_2003_2007	Dynamic atmosphere correction for the 5-year reference period 2003-2007 on 1/8 degree (0-360 degree) grid.
ibCor5Y_2003_2007	Inverse barometer corrections for the 5-year reference period 2003-2007 on 1/8 degree (0-360 degree) grid.
TG	Tide gauge based MSL relative to WGS 84 (tide free) ellipsoid heights. The file also contains geoid height based on eigen6c4r.
mean2TF_addThis	Conversion from mean tide to tide-free system on 1/8 degree (0-360 degree) grid.
TF2mean_AddThis	Conversion from tide-free to mean tide system on 1/8 degree (0-360 degree) grid.
difmss15eig6c4r	Raw MDT based on the mean sea surface

DTU15MSS and the geoid model eigen6c4r.

3.1.3   Documentation

The available functions in coastMDT and how to use these are described in the user manual [9]. The tutorial [10] gives the user an introduction to the package with a thorough example. The demo data available for the package is described in [11]. Further information is given in [4].

3.2   WP2200 Software functionality and validation

Task of WP2200 was to test the software developed in WP2100 described in [4] (D4). We have distinguished two parts: a test of the software functionality and a validation of the software and method in the two well-surveyed areas.

We have first checked that the software is capable of computing coastal and offshore MDT and to evaluate statistically the consistency between the TG MDT and oceanic or altimetric MDT. A number of issues were recognized to be important and have been implemented. The MDTs are evaluated by the geodetic approach separately from altimetry and tide gauge data; a third MDT with error is computed by using the TG MDT as a constraint. A spatial filter can smooth the raw MDT. Similarly, combined TG and oceanic MDT is estimated using ocean model instead of altimetric MDT. The validation metrics include bias and root mean square differences (RMS) computed as following: firstly, for each station the average of the differences between altimetry and TG is computed in a box around the station, their average over all the stations is called "bias" and each TG station is corrected for it. The RMS is the difference at each TG between the corrected TG value and the mean in the box.

We have validated the approach in the two well-surveyed areas North Eastern Atlantic and Australia, by comparing all the MDTs available. Station number is large, 84 in NEA and 35 in Australia (Table 3), RMS after smoothing is 5 cm, bias is 1-2 cm. Filtering causes a large reduction of the STDD in Australia, where unfiltered RMS is 14 cm.
We considered also the poor-surveyed areas and the Gulf of Mexico, being here the number of stations smaller, the statistics are to be interpreted with caution. The Pacific Islands region is characterised by the largest bias (8 cm) and RMS (15 cm) and the South-Eastern African region, with only five stations, has small bias and RMS (3 cm and 5 cm). Method and software give expected results.

Figure 2 shows an example of the graphics output of the toolbox for the German Bight region.
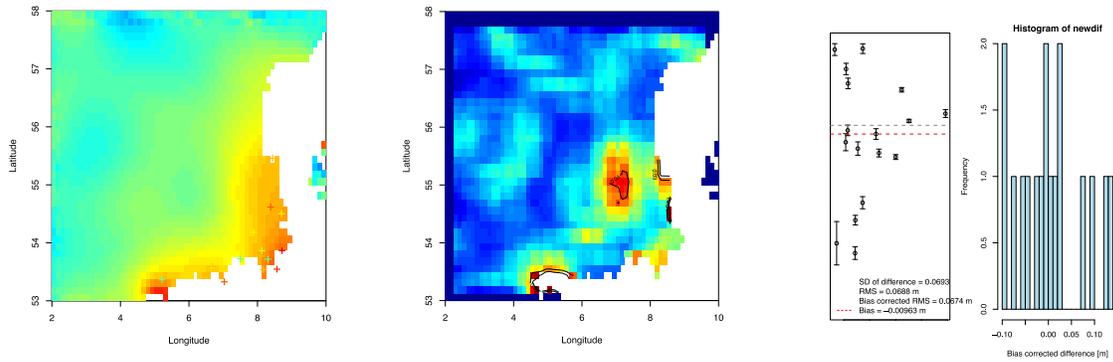
Figure 2: Mean Dynamic Topography from altimetry and tide gauge (left), its estimated error (middle) and histogram of the MDT differences (right). Smoothing is applied. The graphics are output of the coastMDT package developed within this project.

4 WP3000 DT at coast and tide gauge connection

4.1 WP3100 DT along the coast

As described in [6], A coastal dynamic topography from tide gauges was calculated and compared with model and and global altimetry-derived MDTs as shown in Figure 3. Time-dependent measurements from tide gauges were also compared to test their coherence, and along-coast variations in MDT were examined in the ocean models.

In all cases a very heterogeneous picture emerged. Well-surveyed regions (northwest Europe and Australia were taken as test cases) were found to show good agreement with some exceptions (discussed in more detail in the case of Australia). Two poorly-surveyed regions (South America and Africa) produced comparable results, but only a very small number of sites. A third poorly-surveyed region (Pacific Islands) showed large discrepancies, including systematically positive offsets in the MDT. It was conjectured that this results from the similar small-scale geoid variations associated with small islands, in combination with a lack of in situ gravity data to resolve those variations.
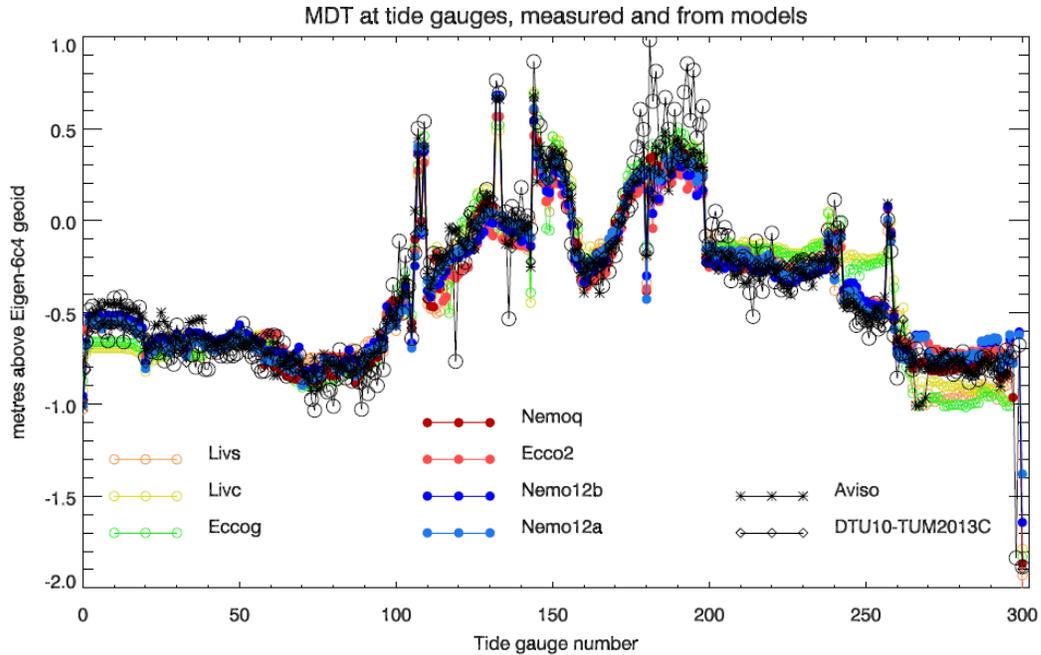
Figure 3: The Mean Dynamic Topography (MDT) of the ocean determined at 302 tide gauges (black circles), compared with values extrapolated to tide gauge positions from three coarse resolution ocean models (open coloured circles), four fine resolution models (solid circles), the Aviso combined observational product (black crosses) and the DTU10 mean sea surface minus the TUM2013C geoid (black diamonds). All curves are set to have the same median values. Gauges up to approximately numer 104 are in Europe and North Africa, 112-146 are in Japan, 149-181 in Australia, 18-200 are Pacific Islands, 201-240 are Pacific North America, and 243-301 are Atlantic and Arctic North America.

Overall, it was found [8] that the statistics could be approximated by a near-Gaussian core with standard deviation 10-14 cm, plus a long tail skewed to positive values, again interpreted as reflecting small scale geoid error at some sites. The core distributions distinguished clearly between ocean models, showing worse agreement with the poorer resolution models.

Coherence between tide gauges was found to be very variable, in some cases reflecting idiosyncrasies of location (some are up rivers, or in semi-enclosed estuaries, some Japanese instances are on islands with intermittent strong currents flowing between the island and the coast). Similarly it was found that, although along-coast gradients of MDT are generally gentler than the cross-coast gradients, there is great spatial variability in the size of those along-coast gradients.

Fortunately, there was found to be quite good consistency between different model estimates of along-coast gradients, as long as the finer resolution models (0.25 degree or better) were considered. These are also the models which clearly perform better in comparison with observations (Figure 3). This suggests that such models can be used to inform the statistical interpretation of coastal MDTs, and to help develop an optimal combination of MDT from tide gauges and from altimetry.

4.2   WP3200 MDT and COCE

This work package assessed our ability to compute a coastal MDT (CMDT) using the latest GOCE gravity models. It began with an assessment of the signal content of the CMDT as represented by a high-resolution ocean model. From this, a model of CMDT omission error was derived. This CMDT omission error was compared with the formal geoid errors from a representative range of gravity models, thereby establishing a likely upper limit (assuming the formal errors to be accurate) on the resolution that can be obtained by the geodetic approach. Based on analysis of the cross-over point between the CMDT omission error, which falls with increasing d/o, and the geoid commission error, that grows with increasing d/o, a clear improvement in the resolution of the geodetic CMDT that can be obtained by including GOCE data is found, with the EIGEN6c4 cross-over points and the other GOCE-based models, exceed those for EGM2008 in all cases (see Figure Figure 4). The impact of mean sea surface (MSS) errors were also considered. CMDTs derived from a range of gravity models were compared with model and GPS based CMDT estimates, providing an additional means of validating the formal errors and their relationship with the CMDT omission errors. The MSS was found to be the dominant source of error in the geodetic CMDT, due to the limitations of altimetry in the coastal zone. This error is much greater than that suggested by the formal MSS errors. As the basis for further refinement, a relatively simple two-stage screening and filtering method was shown to dramatically improve the CMDT while preserving some oceanographically significant differences between the observations and the model.
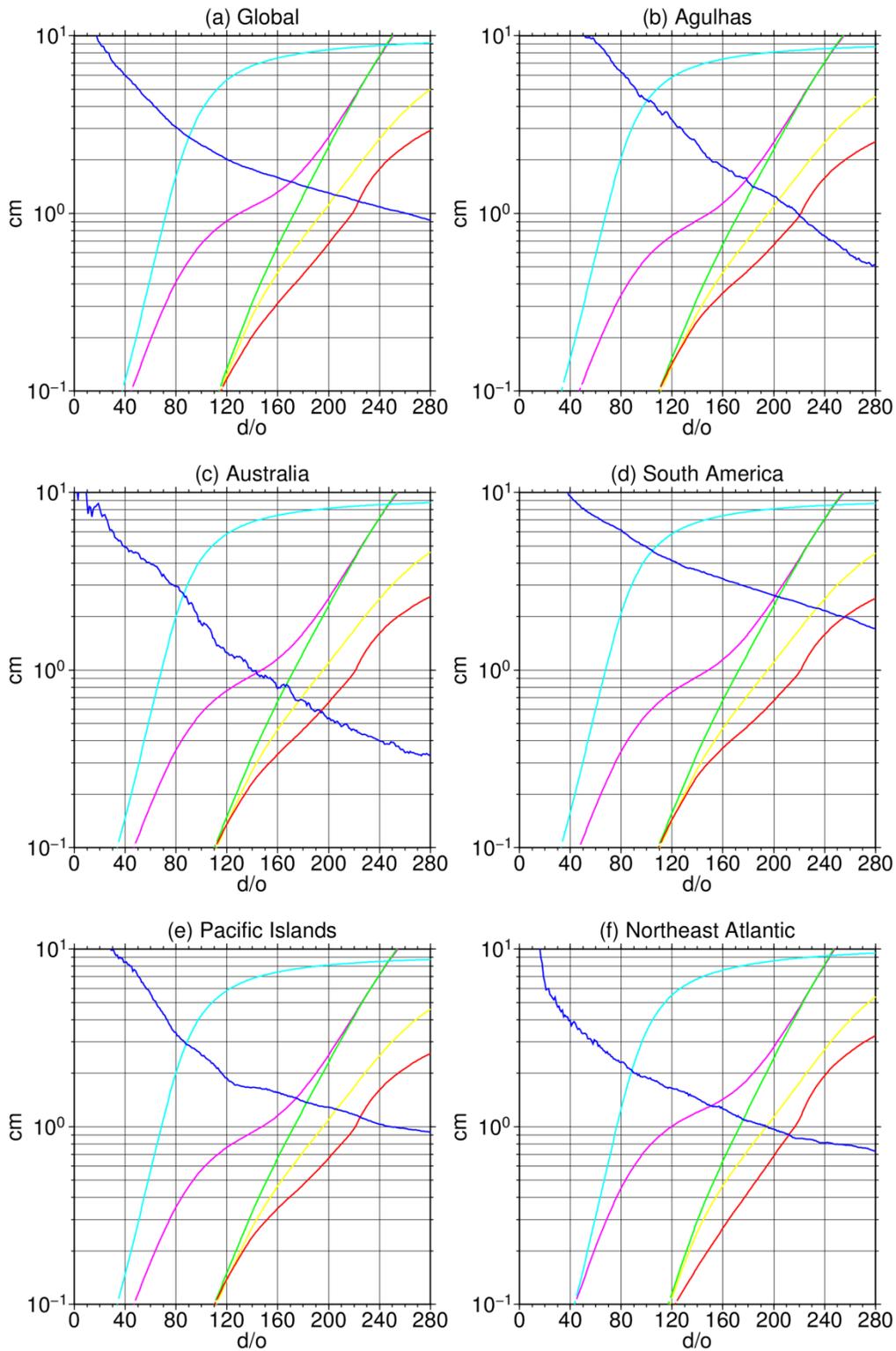
Figure 4: A comparison between MDT omission error (MOE; blue) and formal geoid commission error (GCE) globally and for the five study regions for GTIM5 (magenta), GOCO05S (green), GOCO05C (yellow), EIGEN-6c4 (red) and EGM2008 (cyan).

4.3 WP3300 Coastal Altimetry

Task of WP3300 was to assess the accuracy of current state of the art MSS models in the coastal zone.

A recent study by M. Filmer, C. Hughes et al., demonstrated that the DTU15 MSS was off by around 10 cm when compared with the Port Stanvec tide gauge in Adelaide Australia.

We found out that the problem is here that the ocean tide model applied in DTU15 (GOT4.10) does not have coverage close to the coast and hence the data rejected. This is a fundamental problem to altimetry and particularly SAR altimetry if data are rejected close to the coast. However we found that the new FES2012 and 2014 Elastic ocean tide model was much better and should be used for the updating of the MSS computation using SAR altimetry.
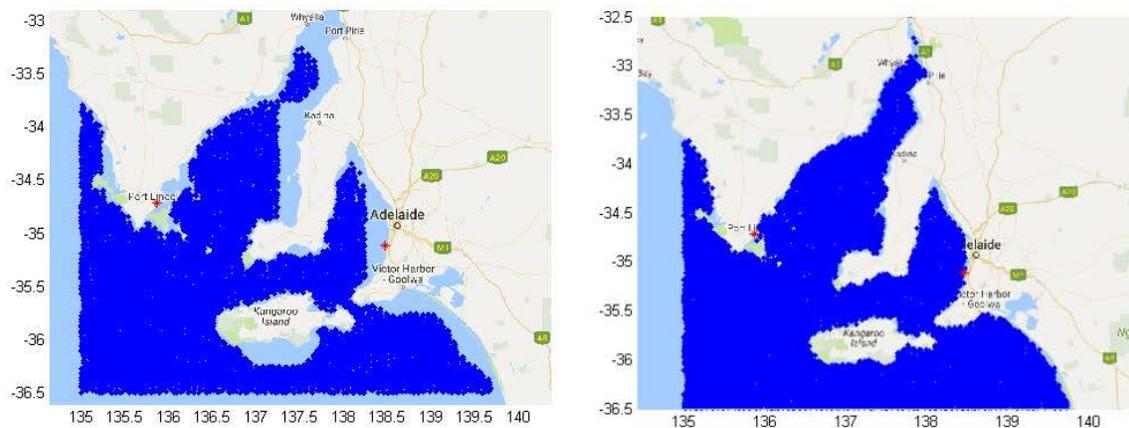
Figure 5: Left panel: The data available (dark blue) in the development of DTU13MSS using the GOT4.8 ocean tide model. Right panel: The data available using the FES2012 ocean tide model.

We studied the performance of SAR- and RDSAR-mode Cryosat-2 data in the North Eastern Atlantic Shelf and evaluated their impact for the dynamic ocean topography [14].Delay Doppler (SAR) Altimetry is found to provide improved sea level in the coastal zone up to is 2-3 km from the coast [12, 13]. A MDT estimated in a grid of 0.25° x 0.25° from 6 years of SAR CryoSat-2 SAMOSA+ (GPOD) sea level heights above the EIGENC4 geoid data (Figure 2, left) is compared to the MDT computed from DTU2015 MSS and EIGENC4 geoid. The good agreement (std 6.4 cm) and higher than or RDSAR-TALES (std 8 cm), suggesting that high-quality SAR coastal data will improve the coastal MSS. Mandatory is to use the data processed with the dedicated SAMOSA+ coastal retracker (GPODC), being the differences between results of SAMOSA+ and SAMOSA2 large in coastal zone, see details in [6].
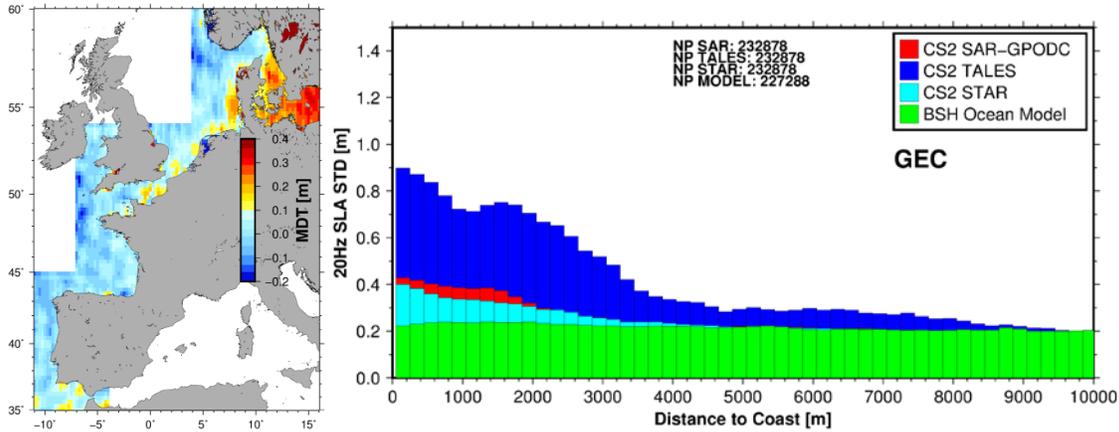
Figure 6: Standard deviation of sea level anomaly SLA from SAR SAMOSA+, PLRM and Model data in the German Bight (right) and MDT from SAR SLA in the Eastern North Atlantic (left)

4.4 WP3400 Connecting tide gauges

Connecting global tide gauges implies expressing their observations in the same global geocentric reference, which space geodesy (and particularly the Global Navigation Satellite System (GNSS) technology) has made possible. Thus, the objective of this task was to build a global network of tide gauges where all the links allowing expressing the sea level observations with respect to the ellipsoid in the ITRF08 are available, using permanent or episodic GNSS stations measurements nearby tide gauges and the corresponding geodetic ties. Information has been recovered from different sources, mainly from the SONEL databank (www.sonel.org).

In the objective of computing precise mean sea level values over these two periods, two methods have been investigated to fill the gaps in the sea level time series: one is using well correlated neighbor tide gauge records, the other is using data from satellite altimetry, both giving similar results for the common stations where the gap could be filled by both methods. The method using satellite altimetry data has been finally selected since it allows to fills the gaps of every station that needed to be.

The combination of these steps finally led to a network of 300 ellipsoidal mean sea level values at tide gauges over [2003-2007] and [2008-2012] (see Figure 7)
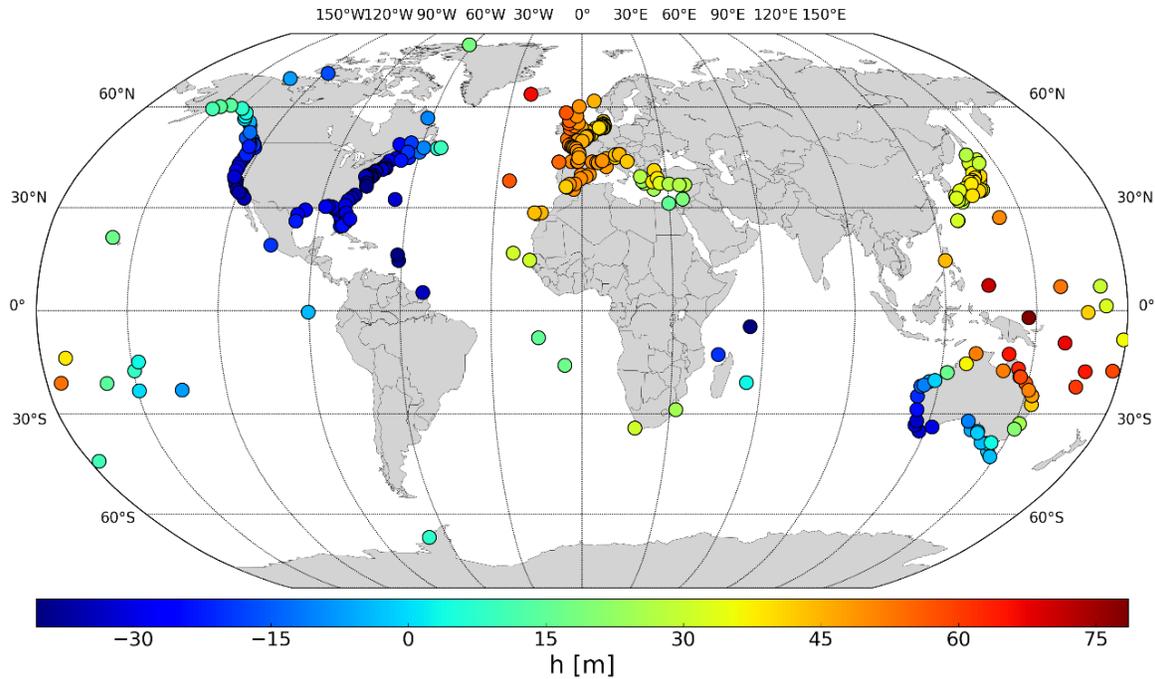
Finally the connection is made by the DT computed by the geodetic method (geoTG) applied to the GPSS@TG stations and, alternatively, to the altimetric locations. The geoid is subtracted in both cases. The difference between the two DTs is for the German stations within few centimetres with mean bias of 2 cm, see [6]. The analysis is part of the Toolbox [4, 5].

4.5   WP3500 Sea level trend

Task of WP3500 was to estimate of the long-term trends in sea-level rise both relative to coast and in absolute sense (relative to the ellipsoid) as well as their difference. This last is an estimate of vertical land motion (VLM), assumed same absolute trends for collocated altimetry and tide gauge sea level.

A trends analysis from tide gauge data has also been studied in this project, particularly the existing datasets and methods used to account for the vertical land movements at a maximum of tide gauge sites: since the tide gauges are grounded on the coast, the vertical land movements (VLM) of the coast can be recorded as well by tide gauges; in order to express the rates of sea level change from tide gauges in a geocentric reference frame (as satellite altimetry), it is necessary to estimate these vertical land movements.

 This trend analysis was performed over three different periods: a long-term period ([1960-2015]) and the two short periods of the MDT analysis ([2003-2007] and [2008-2012]). Over each of these periods, the monthly records from the PSMSL databank with more than 70% of data were selected yielding a number of 352, 748 and 777 RLR records for the respective periods [1960-2015], [2003-2007] and [2008-2012].

To correct the largest number of tide gauges for the VLM, different VLM datasets were used, here listed by "priority":

- The ULR6a GPS solution provides 349 "robust" vertical velocities from permanent GPS stations nearby tide gauges, and expressed in the ITRF2008 reference frame.
- The ALTG solution, published in 2016 by Wöppelmann & Marcos [15], uses a combination of satellite altimetry and tide gauge data to obtain VLM estimates at 478 PSMSL sites.
- The ASG14 dataset, published in 2014 by Santamaria-Gomez, contains estimates of vertical land motions at 86 sites by double-differencing long tide gauge records and satellite altimetry data.
- The MIDAS velocity field, developed at the Nevada Geodetic Laboratory from the processing of more than 10000 permanent GPS stations. The ALTG, ASG14 and MIDAS solution are in agreement with the ULR6a velocities at the level of respectively 1.35 mm/yr, 0.89 mm/yr and 1.89 mm/yr (RMS of differences using the common stations).

The four VLM datasets enabled to correct the 87%, 79% and 74% of the selected RLR tide gauge records over the periods [1960-2015], [2003-2007] and [2008-2012], respectively.

This study confirms that the spread of the tide gauge sea level trends reduces from 3.05 mm/yr (relative) to 1.83 mm/yr (absolute) which can be interpreted as a positive outcome (reducing the spatial noise due to non-climatic signals).

The range of the sea-level trends over the short periods [2003-2007] and [2008-2012] is much larger than over the longest interval, due to multiannual oceanographic oscillations and processes. In these cases, the VLM have a negligible impact in the global estimate of sea-level change from tide gauges, and no significant reduction of the dispersion of the trends is observed.

Finally, we derive for the interval 1993-2015 vertical motion at tide gauges worldwide by using the altimetry minus tide gauge, (al-tg method) for 1993-2015. We compare them to GPS rates and to published results using the al-tg method with different selection criteria for the altimeter time-series. See details in [7]. Figure 8 (left) shows, a reasonable agreement with the GPS rates, correlation and standard deviation of the difference are 0.45 and 3.2 mm/yr for 170 stations. The median of the correlation between altimetry and tide gauges is 0.72. Note that the number of stations considered depends on the allowed difference between GPS and tide gauge location. The agreement with the Wöppelmann and Marcos [15] rates is higher, with correlation 0.8, standard deviation of the difference 2.3 mm/yr with the 462 stations (Figure 8, right).
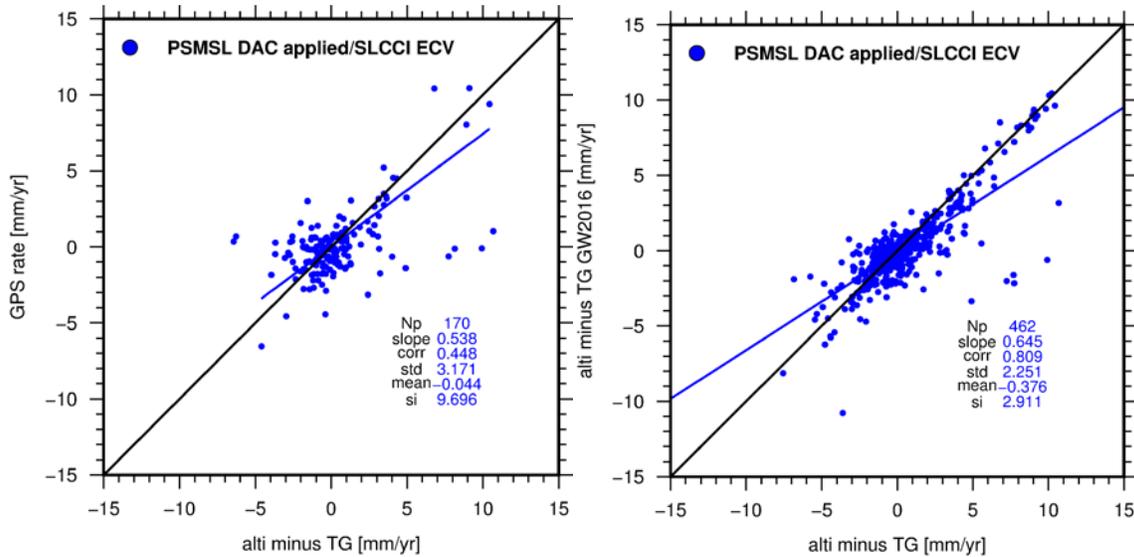
Figure 8: Scatterplot of VLM from altimetry minus tide gauge and the URL6 GPS rates (left). Scatterplot of VLM from altimetry minus tide gauge from this study and from [15] (right).

5 WP4000 Impact and Scientific Roadmap

5.1 WP4100 Impact Assessment

This work packaged assessed the quality of the final Dycot CMDTs against a range of CMDTs produced by ocean models, two additional observational MDTs and the TG based estimates. The analysis was conducted globally and for the five study regions. A particular focus was the impact on the CMDT using the different methods used to extrapolate the MDT to fill land areas. The results are summarized in Table 5. The primary result is that filtering improves the agreement with the model MDTs, globally reducing the mean RMS difference with the models from 32 cm to 19 cm, when using the MDT itself to extrapolate over land. However, which in-fill method to use depends on the region under consideration. For the Northeast Atlantic and Australia, regions with the most tide gauge MDT estimates, the best agreement with the models is obtained when the TG are not used to fill land values. Conversely, for the Agulhas and South America regions, where there are very few tide gauges, the best results are obtained when using the self+TG approach to filling land areas. Only for the Pacific Islands does the TG-only fill approach produce the superior estimate.

Table 5: Assessment of the DYCOT CMDTs against ocean models for all common coastal points. RMS differences are given in m. For each entry four values are given. From top to bottom these are: DYCMDT0 (no filtering), DYCMDTal, DYCMDTtg and DYCMDTbt.

Region	RMSD (mean)	RMSD (min)	RMSD (max)	Model (min)	Model (max)
Global	0.317	0.296	0.329	Nemo12b	LivC
	0.189	0.161	0.206	Nemo12b	Ecco2
	0.258	0.205	0.291	Nemo12a	Ecco2
	*	*	*	*	*
Ne Atlantic	0.142	0.135	0.154	Nemo12a	LivS
	0.081	0.072	0.1	Nemo12a	LivS
	0.095	0.087	0.117	Ecco2	LivS
	0.091	0.082	0.113	EccoG	LivS
Agulhas	0.213	0.21	0.217	Nemo12b	LivC
	0.101	0.091	0.109	Ecco2	Nemo12a
	0.111	0.098	0.123	Ecco2	Nemo12a
	0.082	0.069	0.096	Ecco2	NemoQ
Australia	0.226	0.22	0.234	NemoQ	EccoG
	0.095	0.082	0.115	NemoQ	EccoG
	0.101	0.084	0.128	Nemo12b	EccoG
	0.1	0.086	0.118	Nemo12b	EccoG
South America	0.281	0.266	0.301	Nemo12a	LivC
	0.172	0.149	0.197	Nemo12a	EccoG
	0.155	0.133	0.178	Nemo12a	EccoG
	0.136	0.111	0.159	Nemo12a	EccoG
Pacific Islands	0.386	0.378	0.397	Nemo12b	EccoG
	0.165	0.151	0.184	Nemo12b	EccoG
	0.109	0.085	0.129	Ecco2	EccoG
	0.162	0.148	0.179	Nemo12b	EccoG

5.2   WP4200 Scientific Roadmap

The report included in [8] comprises a synthesis of results from all Work Packages (as briefly summarized throughout this report) and suggested directions for future work on both short (a few years) and long (decadal) time scales. The latter are summarized below.

Recommendations for near-term use of coastal gauge data are to use small-scale spatial variability from closely-spaced tide gauges as a proxy for pointwise MDT errors, and statistics from ocean model data as a model for expected signal size. In combination with satellite derived offshore data, this will permit an optimal combination for the coastal MDT, and a smooth connection to open ocean values. It is also recommended to make as much use as possible of SAR mode altimetry near the coast, as this has been shown to be of good quality, but to take care that limitations are not introduced through the coastal altimetry correction fields. The future SWOT mission is noted as being particularly valuable in this regard.

We also recommend that, in addition to encouraging the continued efforts to improve and document GNSS ties to tide gauges, the potential of direct GNSS measurements of the mean sea surface be investigated as a source of alternative coastal measurements (this could also be a useful technique for future altimeter calibration studies).

The need to use model information to inform the mapping methods highlights the reliance on models which do not contain all the known physics. Accordingly, we also recommend that investigations be undertaken into the impact on MDT of processes not commonly found in global ocean models, in particular wave set-up and residual tidal effects.

On longer time scales we note that the dominant error source is short wavelength geoid error, and that this is unlikely to be resolved by future satellite gravity or gradiometry missions. We encourage the extension of airborne and ground-based gravity measurements, but note that this is unlikely to be a global solution, especially in regions which are currently poorly-surveyed.

On this issue, we note with interest the development of extremely accurate clocks with the capability of directly measuring the geopotential at a single point, with accuracy currently close to 1 cm. We encourage the development of a (probably satellite-based) infrastructure which will allow frequency transfer at the 10^{-18} accuracy level that will be required for this to be realized globally.

6 WP5000 Recommendations

6.1 WP5100 Scientific Paper

A scientific paper with the title: "Improving the coastal Mean dynamic Topography by combining Tide gauges with geodetic Mean dynamic Topography" is currently under preparation for possible submission into Marine Geodesy. During the past 3 months we have had several paper teleconferences to consolidate the material to go into the paper. All project partners as well as Michael Kern will be co-authoring this.

7 References

[1] Hughes, C.W. (2016). State of the Art Review: Ocean dynamic topography determination, WP1100, D1, http://gocehsu.eu/DELIVERABLES/TechReportWP1_Mar2016_v1.pdf

[2] Fenoglio (2017). Description of data and models to be used in subsequent WorkPackages, WP1300 http://gocedt.eu/DELIVERABLES/TechReportWP1300D2_Mar2016_v1.pdf

[3] Fenoglio (2017). Report on selection and justification of test area, WP1300, D3, http://gocedt.eu/DELIVERABLES/TechReportWP1300D3_Mar2016_v4.pdf

[4] Nielsen, K., Knudsen, P., and Andersen O.B. (2017). Selection of approach and description of software for coastal mean dynamic topography, WP2100+WP1200, D4, http://gocehsu.eu/DELIVERABLES/TechReportWP2100D4_Jun2017.pdf

[5] Fenoglio L. (2017). Test and validation report, WP2200, D5, http://gocedt.eu/DELIVERABLES/TechRepWP2200D5_Aug2017.pdf

[6] Andersen O., Bingham R., Fenoglio L. and Hughes C. D6 (2017). Technical Note describing the work performed in WP3000, D6, http://gocedt.eu/DELIVERABLES/TechReport_D6_WP3000_v0.1.pdf

[7] Gravelle M., Fenoglio L., Hughes C., Padilla Polo S., Wöppelmann G. (2017). Connected global tide gauges including trend analysis for selected epochs, D7, http://gocedt.eu/DELIVERABLES/TechReportWP3400D7_Jul2017.pdf

[8] Hughes, C.W. and Bingham, R. (2017), WP4000, D8

[9] Nielsen, K. et al, Package "coastMDT", https://github.com/cavios/coastMDT/blob/master/doc/coastMDT_userManual.pdf

[10] Nielsen, K., Getting started with the coastMDT package, https://github.com/cavios/coastMDT/blob/master/doc/coastMDT_tutorial.pdf

[11] Nielsen, K. et al., Description of data for the coastMDT package, https://github.com/cavios/coastMDT/blob/master/data/data4coastMDT.pdf

[12] Dinardo S., Fenoglio-Marc L., Buchhaupt C., Becker M., Scharroo R., Fernandez J. Benveniste J. (2017). CryoSat-2 performance along the German coasts, AdSR special session CryoSat-2

[13] Fenoglio-Marc, L., Dinardo, S., Scharroo, R., Roland, A., Dutour, M., Lucas, B., Becker, M., Benveniste, J., Weiss, R. (2015). The German Bight: a validation of CryoSat-2 altimeter data in SAR mode, *Advances in Space Research*, doi: http://dx.doi.org/10.1016/j.asr.2015.02.014

[14] Fenoglio-Marc, L., Uebbing et al. (2017). Coastal Sea Level from Delay Doppler Altimetry along the North Eastern Atlantic Shelf The German Bight: a validation of CryoSat-2 altimeter data in SAR mode, poster at the OSTST 2017, Miami

[15] Wöppelmann, G., and M. Marcos (2016), Vertical land motion as a key to understanding sea level change and variability, Rev. Geophys., 54, 64–92, doi:10.1002/2015RG000502.

3   Appendix B, D1   State of the Art Review: Ocean dynamic topography determination.
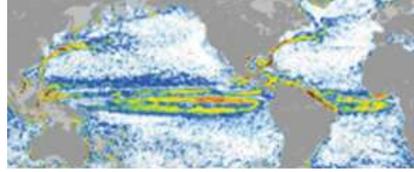
GOCE++ Dynamic Topography at the coast and tide gauge unification
GOCE ++ DYCOT

TITLE. WP1000 Technical Report: State of the Art Review: Ocean dynamic topography determination.

Author Chris W. Hughes

ESTEC Ref: ITT AO/1-8194/15/NL/FF/gp "GOCE++ Dynamic Topography at the coast and tide gauge unification"- Coordinator: Ole B. Andersen (DTU)

DOCUMENT CHANGE LOG				
Rev.	Date	Sections modified	Comments	Changed by
1	11-03-2016	All	Draft	Chris W. Hughes

Review of ocean dynamic topography models.

Introduction

The GRACE and GOCE missions together have dramatically improved our knowledge of the Earth's gravity field, defining the geoid to an accuracy of ~2 cm on length scales (half wavelengths) of ~100 km and larger. However, there is large variability (~30 cm RMS) remaining on shorter, unresolved length scales. The mean sea surface (MSS) is defined to comparable accuracy, and is improving particularly with CryoSat data being added. The Mean Ocean Dynamic Topography (MODT) is the difference between the MSS and the geoid. However, the MSS occurs naturally as a gridded product at high resolution, and the geoid as a spectral model with errors growing at short length scales. Optimal combination of the two is a complicated issue, and is particularly difficult at the coast.

An alternative approach is to use tide gauge measurements. In this case we have a sea level measurement *relative to a land-based datum*, exactly at the coast. To convert this to dynamic topography, we need to know the geopotential at the datum. This requires a knowledge of the geoid including all length scales, and a knowledge from GNSS measurements of the position (including vertical position) of the datum.

In this section we review the state of the art in calculating the MODT (focusing on coastal MODT) by these two methods.

Open Ocean MODT determination

Matching up the mean sea surface with the geoid requires the operation of a filter of some kind. The simplest method in the spherical harmonic domain involves conversion of the MSS (plus an extension over land and missing data, usually taken to be close to the geoid) to spherical harmonics, and then combination with the geoid followed by a (usually smooth) truncation at some chosen degree, followed be reconstitution of the harmonics in the spatial domain. The simplest in the spatial domain is to use the gridded MSS minus a spatial representation of the geoid truncated at some chosen spherical harmonic degree, and then smoothing the resulting noisy MODT using a simple isotropic (often Gaussian) kernel of chosen width.

Both of these methods involve isotropic, homogeneous smoothers (i.e. the smoothing kernel is a function only of distance from the point considered, and doesn't vary with either azimuthal angle or position of the point). However, the characteristics of the ocean circulation are such that the expected statistics of the MODT gradients are far from isotropic and homogeneous. Several recent solutions have used more sophisticated methods with more complex filters.

Rio et al (2011) used an optimal mapping technique, using an a priori ocean model/analysis product to define natural scales of the MODT as a function of region,

allowing for a difference between zonal and meridional scales (i.e. an initially radially-symmetric covariance function of fixed form, stretched to different extents in the meridional and zonal directions). This permits a limited degree of anisotropy and inhomogeneity, and relies on an ocean model to determine the length scales. This satellite information was combined with a wide variety of other sources of ocean data, including surface drifters, to produce the CLS09 MODT (Rio et al., 2011), later updated to the CLS13 MODT (Rio et al., 2014). A similar method is being used in the development of the DTU15 MODT, but using currents from drifters to define the zonal and meridional length scales.

In contrast, Bingham (2010) introduced the nonlinear, anisotropic, diffusive filter. This treats the isotropic Gaussian filter as a smoothing by diffusion of the initial field, and generalises the concept by introducing diffusion coefficients which depend on direction, producing larger diffusion along currents than across them (the current directions being themselves defined by the approximate MODT). This has the effect of allowing for a smoothing of small scales without blurring the sharp gradients across strong, near-rectilinear current features. The results have been shown to have advantages over more conventional filtering in comparison with currents from drifter data (Bingham et al., 2015), though they do not completely avoid smoothing (and hence weakening) of currents. This method allows for the definition of an MODT purely based on the satellite gravity and sea surface measurements, with no additional information required.

More recently, Hughes (2015) has explored the use of a more flexible optimal mapping method based on the Wiener filter. The noise covariance function is defined based on a region known to have little large-scale dynamic variation, and a full two-dimensional signal covariance is estimated regionally (overlapping patches of 10 by 10 degrees latitude and longitude). The covariance function is taken either from a high resolution ocean model, or from a rescaled observed mean sea surface temperature field (only scales shorter than about 300 km are filtered). The two methods were found to give very similar results, and independent tests suggest a similar accuracy in the Southern Ocean to the CLS13 MODT without recourse to the additional ocean information. A significant difference, though, is that Hughes started not with a pure satellite gravity solution, but with a combined solution incorporating in-situ gravity and gravity anomalies determined from satellite altimetry over the ocean field (Fecher et al., 2015).

All of these methods have been implemented with (various releases of) GOCE gravity fields, but detailed assessments are not yet available. A point worth making, though, is that they will all be weaker in coastal regions than elsewhere, for three reasons. 1) altimeter data is poorer close to the coast, and often has gaps (see below). 2) Mapping functions based on covariance information are stronger when there is data surrounding the point in question on all sides, which is not the case at the coast. 3) The coast is special in dynamical terms, as it imposes a constraint on the direction of the flow, meaning the sea level slopes near the coast are not simply related to those nearby. In the case of this last point, it would be possible to explicitly incorporate the special nature of the coast into the anisotropic diffusion equation of Bingham (2010), but it is less straightforward to incorporate in other methods.

There are a variety of mean sea surfaces and geoids available for calculating the MODT. The primary recent MSS estimates are CLS11 (Schaeffer et al., 2012), DTU13 (Andersen et al., 2015), and the new DTU15 (Stenseng et al., 2015). Recent geoids all use the GOCE data, some in combination with GRACE, and some also in combination with in-situ data and altimetry. The GOCE data have led to significant improvements, and clear progress from Release 1 to Release 5 of the dataset – see the review by van der Meijde et al. (2015) for an overview. Rather than describe the details of the many different solutions available, we will focus (for reasons which will become apparent below) on the "combined" solutions in which some form of altimetry is incorporated into the solutions to regularise the small scales and make them compatible with a mean sea surface.

Of these combined models, the most recent are TUM13 (Fecher et al., 2015), GGM05C (Ries et al., 2016) and EIGEN6C4 (Förste et al., 2015), all of which incorporate gravity anomalies consistent with some form of the DTU MSS. TUM13 uses release 3 GOCE data together with a wide variety of in situ data and DTU10 gravity anomalies, and is provided up to degree 720 (approximately equivalent to 0.25 degree resolution). It will shortly be superseded by a model to be called GOCO05C, using the latest release 5 GOCE data and improved relative weighting of the different observations (Thomas Gruber, personal communication). GGM05C uses the DTU13 gravity anomalies (Andersen et al., 2014) and is provided to degree 360, and GGM05C uses DTU10 gravity anomalies as used in the pre-GOCE EGM08 gravity field (Pavlis et al., 2012). It is provided to degree 2190.

The DTU13 MSS has associated with it a DTU13 MODT, which is calculated using the earlier EIGEN-6C3 Geoid which is available to degree 1949 (Förste et al., 2011).

These latest data sources have moved on significantly since the initial comparison of geodetic ocean dynamic topographies demonstrated good general agreement with ocean model predictions (Woodworth et al., 2012). That comparison used Release 1 GOCE solutions with a very simple isotropic smoothing. There is clearly scope to improve on these comparisons now.

The MODT at tide gauges

A quite different methodology is necessary to calculate the MODT at tide gauges. A tide gauge is effectively a point (in space) measurement of the sea surface relative to a given land-based datum. In order to calculate the MODT from such a measurement it is necessary to know the precise position (e.g. from GPS) of the datum, and the geoid at that point (assuming the connection between datum and tide gauge zero is made by levelling). A point value of the geoid is therefore required, with full spectral content. This means that more than just satellite data is required, because geoid variability on scales shorter than those resolved by satellite gravity is typically around 20-30 cm, and can be more than 2 m in some cases (Gruber et al., 2012). The method is also limited to the relatively

small number of tide gauges for which accurate GPS datum positions have been calculated.

Much of the work on this method has taken place under the GOCE+HSU study (see http://www.goceplushsu.eu/). A common approach to accounting for this "omission error" was to use GOCE-derived geoid solutions up to a chosen spherical harmonic degree, and supplement these with coefficients from EGM08 (Pavlis et al., 2012) at higher degrees. In all cases it was found that, although known to be an imperfect methodology, this produced significantly better results than simply using the solutions to low degree (typically in the range 180 to 220).

Using this methodology, Woodworth et al. (2012) showed agreement between tide gauge derived MODT and that from ocean models at the level of 6-10 cm standard deviation in favourable regions, rising to 14 cm on the Pacific coast of the Americas. At that time, this was larger than the disagreement between ocean models, and therefore demonstrated the accuracy possible with the geodetic data available. Similar levels of accuracy were found in studies with the complementary aim of defining continental vertical datums (Gruber et al., 2012; Bolkas et al., 2012).

A significant step forward has been made since then with the improved GOCE data resulting from the longer time series available, and with the emergence of combined solutions which integrate GOCE and GRACE data with in-situ gravity and altimeter-derived gravity. Hayden et al. (2015) use the Release 3 GOCE solutions in comparison with tide gauge data to determine the appropriate datum for Canada, with good consistency. More importantly, the combined solution of Fecher et al. (2015) extends the usable geoid resolution to degree 720, reducing the incompatibility with the shorter scales of EGM08. This, in combination with the collection of new GPS measurements at tide gauges (Hughes et al., 2015; Woodworth et al., 2015), has improved accuracy to the point where it is now possible to distinguish between different ocean models and see useful oceanographic features from tide gauges.

To illustrate this, Figure 1 shows observed and modelled MODT around the coast and islands of the North Atlantic and Mediterranean Sea (Hughes et al., 2015). The broad spatial pattern is in good agreement, and the difference between the two is a joint measure of the accuracy of the geoid used, the tide gauge and GPS data, and the ocean model.

To explore this further (Hughes, Woodworth and Gruber, unpublished work), we have looked at the misfit as a function of geoid and ocean model. This is shown in Figure 2, which clearly shows best agreement when using the most recent ocean models (Nemo12, NemoQ and Ecco2) and the combined geoid TUM13 (though only when extended with EGM08). The extended satellite only solutions show improvement from Release 3 (GOCO03x) to Release 5 (DIR5x). The importance of small scale geoid information is emphasised by the success of EGM08, which is only improved on by TUM2013x (which uses Release 3 GOCE data), and perhaps DIR5x. In these plots, one of the "models" (Aviso2014) is in fact the CLS13 MODT (Rio et al., 2014) which also includes Release 3

GOCE data as well as much more ocean information. The column labelled "NemoAviso" is an average of this with the two Nemo models, which gives the values shown in Figure 1.
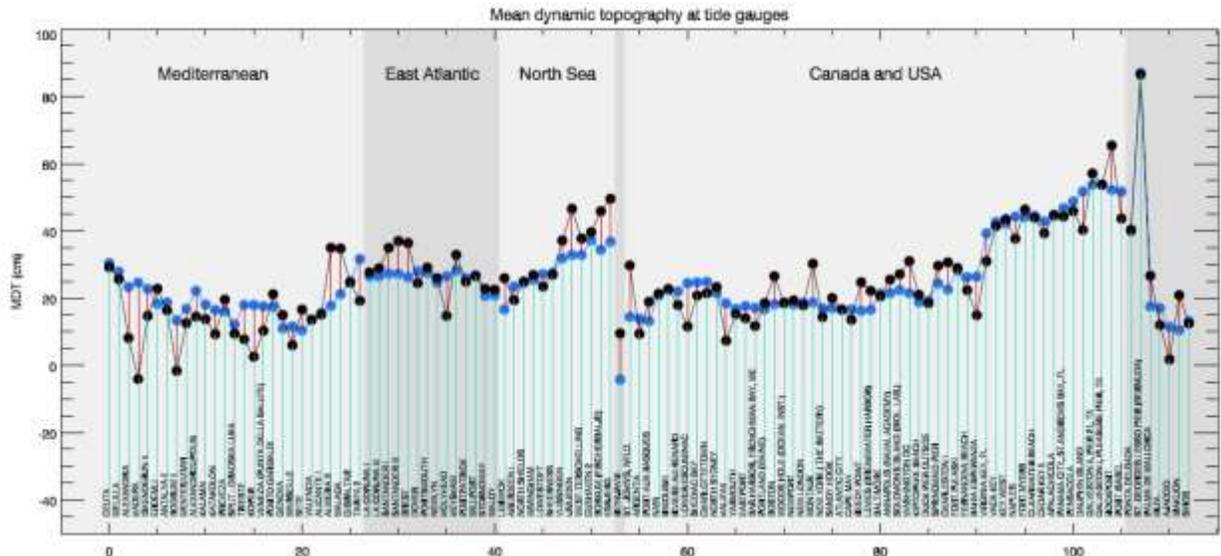

Figure 1: Mean ocean dynamic topography from tide gauges around the North Atlantic and Mediterranean (black), compared with the average of two ocean models and an observational analysis (blue). Means are arbitrary. Taken from Hughes et al. (2015).

We now see that the best combination of geoid and ocean model permits agreement on basin scales of around 8 cm standard deviation, or perhaps 5 cm if we can legitimately exclude a small number of tide gauges from the analysis. The basin scale accuracy is thus as good now as the regional accuracy was in the Woodworth et al. (2012) study. As a result of these studies it is now accepted that there are large errors in levelling over continental scales.

Outside the HSU study, other groups have also been comparing MODT estimates at tide gauges with those from ocean models, with a variety of different aims. Featherstone and Filmer (2012) showed that a large part of the tilt observed in the Australian national datum is due to ocean dynamics, and Filmer (2014) went on to use ocean models to identify levelling errors in the region. Penna et al. (2013) used a similar analysis to identify levelling errors in the UK national network. Lin et al. (2015) focused on the North Pacific, adding more tide gauges from the US, Canada and Japan, and making a partial analysis of the dynamical causes of the observed alongshore slopes. Other analyses making dynamical interpretations include Higginson et al. (2015), who showed that the steep slope along the Florida coast is a robust feature associated with the Gulf Stream, and Hughes et al. (2015) who showed that the Mediterranean inflow has far-reaching effects on the MODT of much of Europe. However, there remain some fundamental questions about how alongshore slopes of the MODT are controlled and maintained on global scales.

In most cases, the GPS measurements used in these analyses are "campaign" measurements, i.e. short duration deployments to fix a position at a single time. Little

attention has been paid to the issue of vertical land motion, which is assumed to be a small factor over the time scales considered.
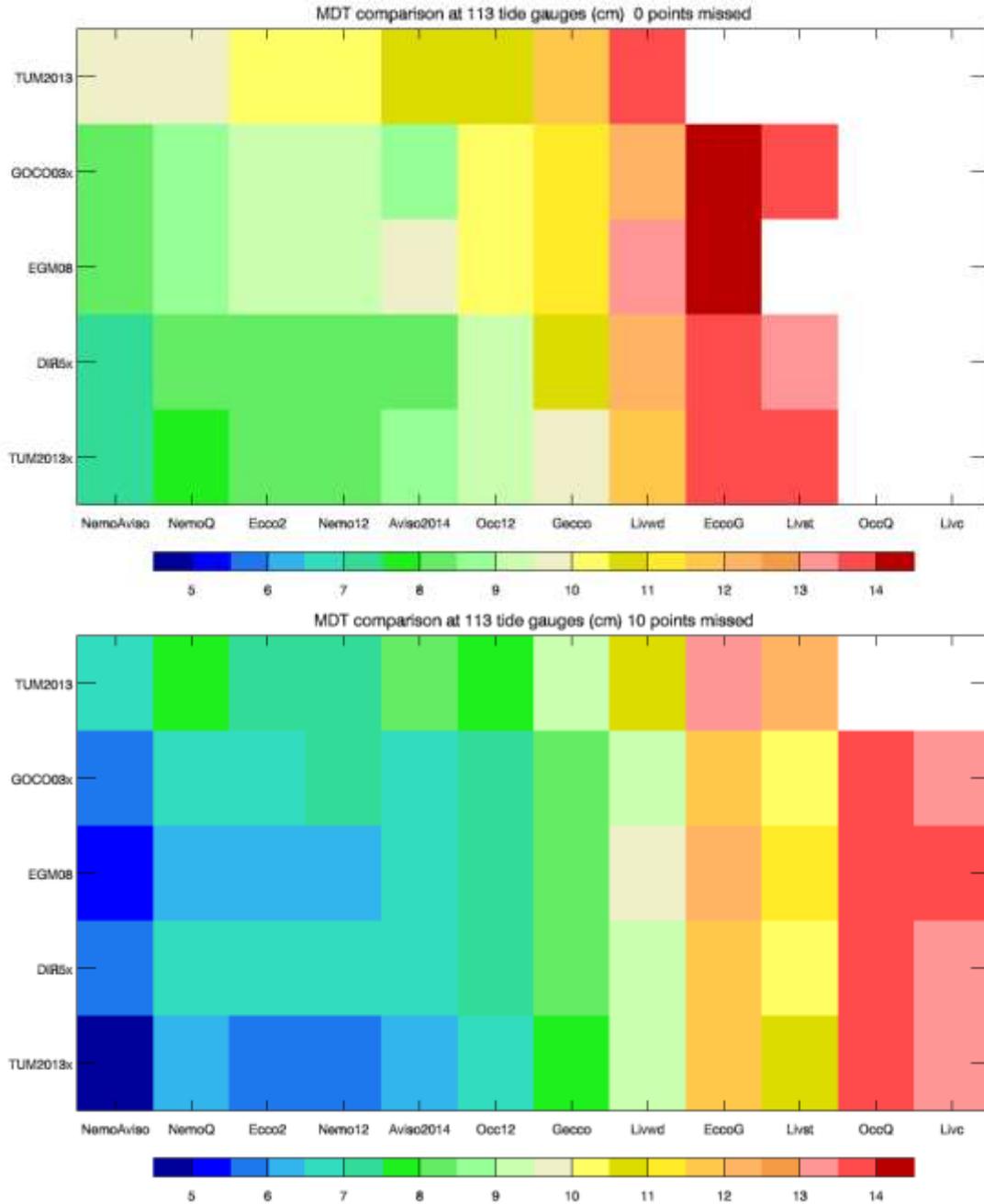
Figure 2: Standard deviation (cm) of the difference between ocean model MODTs (x-axis) and those derived from tide gauges with different geoids (y-axis). Geoids with "x" in the name are extended to higher degree using EGM08. Top uses all 112 tide gauges from Figure 1, bottom uses the "best" 102 gauges. White is off the scale.

An exception is the Lin et al. (2015) study, which used the full time-dependent GPS data. In some regions, particularly tectonically-active regions like Japan, and regions of strong Glacial Isostatic Adjustment like Canada and Scandinavia, this vertical motion can be a

significant issue, and should be accounted for wherever possible. For this reason, the present study aims to use full GPS time series wherever they are available, and at least use a fitted linear trend to adjust those measurements to a common epoch. even outside these obvious regions, vertical land movement rates are observed which could contribute several cm offsets if applied a decade or so away from their measurement epoch (Santamaría-Gómez et al., 2012).

The importance of small-scale geoid structure raises a couple of possibilities which, to this point, have not generally been applied to MODT calculations. First, the dependence on the geoid at a single point can be mitigated if there are levelling connections between the tide gauge and several points rather than just one. Simple statistical averaging then means that the tide gauge level will be better determined if there are GPS coordinates for each of these points. In principle, this could mean the whole of a national levelling network. The difficulty is in working out how to weight the contributions from nearby and distant parts of the network, as it is now established that errors come to dominate the levelling over large scales. This is effectively the approach which has been taken by Ophaug et al. (2015), who have used satellite gravity data to provide a "corrector surface" to the Norwegian levelling network, thus enabling MODT calculation at far more tide gauges than the few which have good local ties to GPS measurements.

The second issue is that of smoothing along the coast. Ocean models tell us that the MODT varies gradually along the coast except in a few special cases (e.g. the Gulf Stream region, and the mouth of the Mediterranean where there is effectively a gap in the coast). Accounting for this expected smoothness could enable a better estimation of the MODT. However, it also means that we would miss any sharp gradients due to processes which are missing from ocean models or are poorly modelled (e.g. effects of river flow).

Summary

It has been shown that the coastal MODT is consistent with ocean model predictions at the 5-10 cm level. However, recent improvements and new geoid data available have not yet been fully exploited. There are two approaches: the open ocean approach using satellite altimetry, for which the next section addresses many of the issues, and the tide gauge approach. For the latter, and to a large extent also for the former approach, the inclusion of small scale gravity information is crucial. Ideally this information is incorporated into a global gravity solution in a consistent way, which is why it has been difficult to demonstrate improvements over the pre-GOCE EGM08 geoid which took this approach. The TUM13 geoid demonstrates that extension of the consistent solution to degree 720 is possible and results in significant improvements over the simple combination with EGM08, but this still requires additional information from EGM08 at higher degrees.

These consistent geoid solutions (TUM13, GGM05C, EIGEN-6C4, and the expected GOCO05C) all use versions of the gravity anomalies associated with the DTU mean sea surface, so should be compatible with that surface when calculating the MODT.

Review of satellite altimetry possibilities.

Introduction

Satellite altimetry has traditionally focused, for a number of reasons, on the open ocean. Recently there have been a number of developments with the aim of improving coastal altimetry (Vignudelli et al., 2011), involving both new techniques for exploiting old and current missions, and new kinds of satellite altimeter. Here we review the current state of understanding and development, and suggest ways in which this can be further advanced with the aim of maximising the return from satellite altimeter measurements in coastal regions, and minimising the distance to the coast from which measurements can be taken.

Traditional altimetry

Traditional, pulse-limited altimetry works by measuring the travel time of a radar pulse between satellite and sea surface, and back. Over the ocean, the reflection is from a circular area of radius typically a few kilometres (depending on wave height – the radius is larger when waves are higher), termed the altimeter footprint. As a function of time, the reflection is initially from the nadir point directly below the satellite, and spreads in concentric circles over time. Typically, data are amalgamated into one measurement per second (1 Hz), giving an along-track resolution of 6-7 km depending on satellite altitude, but higher temporal resolution (10-20 Hz) may be available, at the cost of weaker statistical averaging leading to higher noise values at individual points.

This is the mode of operation for Geosat, ERS-series, TOPEX/POSEIDON, Jason 1-2, Envisat, and other altimeters before the 2010 launch of Cryosat 2.

These altimeters suffer from various problems in coastal waters which limits their ability to measure close to the coast. There has been significant recent progress in addressing these problems, which relate to both the nature of the returned signal (the waveform) when land is included in the altimeter footprint, and also the various corrections which are used to convert travel time to sea surface height. These are the ionosphere, wet tropospheric, dry tropospheric, and sea state bias corrections (we assume a well-determined satellite orbit, though there are also subtleties to this, particularly on long time scales). More detailed descriptions of these corrections and their sizes can be found in Andersen and Scharroo (2011). In addition, there is the important issue of temporal aliasing (including tides), to which we will return below.

Corrections to the sea level measurement.

The ionospheric correction is not especially troublesome at the coast, since the ionosphere does not behave any differently at the coast compared to the open ocean. Ionospheric models are commonly used to make a path-length correction at the level of a around 1 cm accuracy, though in some cases the combination of two radar frequencies (Ku and C band in the case of Topex/Jason) allows an independent ionospheric correction

to be calculated from the difference in inferred sea surface height. In the latter case, the coast is slightly more complicated, but along-track smoothing (about 100 km) is the best approach in open ocean, so extrapolation near the coast is not particularly troublesome. However, using the difference between Ku and C band ranges does make the assumption that other factors which influence the two bands differently (such as sea state and wet tropospheric correction) have been properly accounted for. This is less true in coastal than in open ocean regions, so a degree of coastal deterioration is to be expected. Recent data-based global ionosphere models appear to show sub-centimetre, but dual-frequency corrections remain better at least at distances greater than 10 km from the coast accuracy (Andersen and Scharoo, 2011). The AltiKa altimeter operates at Ka band, which is less sensitive to the ionosphere.

The wet tropospheric correction is more complicated, since it can involve quite short length scales close to the coast. The size of this correction is highly variable around the globe, with standard deviations varying regionally between more than 10 cm and less than 3 cm (e.g. Joana Fernandez et al., 2013). This problem is exacerbated by the large footprint of the radiometer which measures atmospheric column water content. The main return comes from a circle of radius 15-25 km, but points further afield can contribute, and land points can produce a large distortion of the return. For this reason, there can be a margin of as much as 50 km around the coast over which the wet tropospheric correction is not available.

One option is to use atmospheric model analyses, and this does lead to a significant improvement, but the small spatial scales and rapid temporal evolution close to the coast limit the quality of such corrections. Another very promising option is to use land-based GNSS receivers to add information on the land side of the coastal boundary, to complement the offshore radiometer measurements. This is the approach taken by Joana Fernandes et al. (2013), who conclude that total tropospheric delay can be determined at the level of about 0.6 cm, and agreement with atmospheric models (in particular, the ERA-Interim run from ECMWF) is at 1.2 cm RMS. Thus, atmospheric models can be used where GNSS data are sparse, but including GNSS data improves the accuracy to sub-centimetre. This is a similar level if improvement to that found from using the radiometer-derived wet correction rather than a model over the open ocean (Andersen and Scharroo, 2011). It is worth noting that most of this improvement comes from the wet tropospheric delay component, as the dry troposphere corrections agree at the 0.1-0.3 cm level, equivalent to 0.5-1.5 mbar errors in atmospheric pressure. The latter number becomes the relevant one when considering inverse barometer corrected sea surface height.

The last of the "corrections" is the sea state bias (SSB), which accounts for the fact that surface waves reflect radar unevenly, so that the apparent "mean" sea surface is not a true average over the distribution of heights occupied by the range from peak to trough of the waves. This correction is empirically determined (it is typically a few percent of significant wave height, but depends on the nature of the wave field so that empirical fits use both altimeter-derived wave height and wind speed inferred from radar reflection coefficient as inputs). The size of the correction may be more than 15 cm in the mean, in

parts of the Southern Ocean), though typically around 10 cm in coastal regions, with temporal variability of about half that. SSB is complicated by the fact that the bias depends not just on the state of the sea surface, but on the nature of the altimeter tracker response to that state (how the instrument determines where to measure), making its determination a subtle question which must be readdressed any time there is a change in tracking methodology. In addition, it is acknowledged that the bias depends on more parameters than the two which are available from satellite altimeter measurements. Furthermore, waves change their character in shallow water as they start to interact with the sea floor, and as they come closer to a lateral boundary (so that propagation direction becomes more biased). There are good reasons to expect the SSB correction to take a different form in shallow water than in the open ocean (Vandemark et al., 2008).

A promising approach to addressing this issue is the combination of altimeter data with operational wave model analyses to supply the missing information. This method has been used to develop a correction for the Jason 1 and Jason 2 altimeters (Tran et al., 2010), and is also being used to develop a model for the AltiKa altimeter (Valledeau et al., 2015), though little detail is available about how coastal and open ocean regions differ in this correction. This is an area which would benefit from significant extra attention, as it is presently very difficult to evaluate the accuracy of the SSB corrections in coastal regions. Errors of several centimetres are possible in the mean, as well as in time dependent variations.

Improvements due to retracking.

In addition to the improved corrections discussed above, progress has been made on mitigating the polluting effects of land in the altimeter footprint, enabling improved rates and accuracy of returns in coastal regions. This is done by "retracking", which means reanalysing the returned waveform with different software in order to improve the chances of identifying the correct ocean surface amid the noise from land and other reflective surfaces. There are a myriad of proposed and implemented retracking algorithms – see Gommenginger et al. (2011) for a discussion of the issues – but we will focus here on the ALES retracker (Passaro et al., 2014), which has demonstrated clear improvements in coastal regions while remaining consistent with more standard methods in the open ocean, thus avoiding any steps between coast and open ocean.
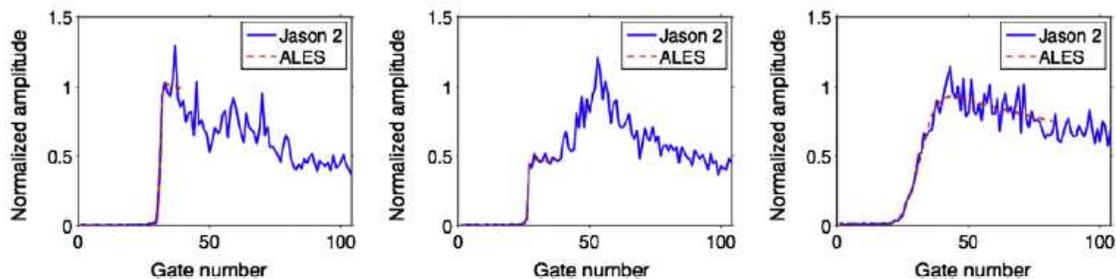
Figure 3: Example waveforms and their fits using the ALES retracker, from Passaro et al. (2014)

ALES combines a simple concept with quite sophisticated statistical methods. The idea is to identify the portion of the waveform which corresponds to the sea surface (the initial

amplitude rise), and to perform a fit of the standard Brown model to this region plus the part of the tail of the waveform which is not contaminated. Figure 3 shows examples of its operation, showing how the land contamination which distorts the tail in the centre panel does not distort the fit (red), which provides the estimate of sea surface and wave height. This retracker has been implementes for Jason-1, Jason-2 and Envisat altimeters, and shows significant improvement in the number of good returns in many coastal areas. An example is shown in Figure 4, where it is compared with the standard retracker (SGDR) and results (CTOH) from an initiative to improve (without retracking) the quality of coastal altimetry by improving models and corrections (Roblou et al., 2011). The CTOH measurements are plotted at 1 Hz sampling.
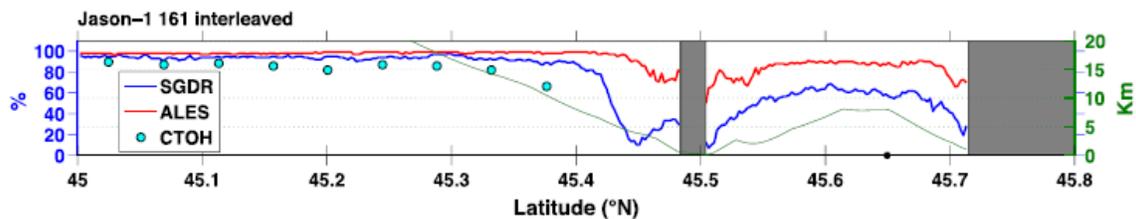
Figure 4: Percentage of returns which can be retained in order for correlation of time series with that at the tide gauge (black dot) to remain above 0.9, using three retrackers, for a Jason-1 track in the north Adriatic Sea. The green line shows distance from the nearest coast (right hand scale). From Passaro et al. (2014).

The 20 Hz sampling displayed in Figure 2 (18 Hz for Envisat) results in significant noise, seen in the point-to-point differences, which are typically 2.5 to 12.5 cm (Passaro et al., 2014). To the extent that this noise is independent at each point, averaging to 1 Hz would reduce the statistical errors to 0.4-2.0 cm.

Retracking cannot solve problems in all coastal regions. A particular exception is in the case of an altimeter moving from land to ocean, which can result in loss of track (the onboard tracker takes some time to reacquire the sea surface). Retracking cannot help in this case, as the required information simply is not recorded. However, improved strategies for onboard trackers, such as the Jason-2 DIODE/DEM tracker (based on a map of expected elevations) can greatly accelerate acquisition of the sea surface. While this is no help for historical data, it means that present and future data returns are significantly improved.

The ALES-retracked Envisat product has demonstrated its value in the complex and narrow straits separating the North Sea from the Baltic. The annual cycle of sea level in this region shows differences between mid-basin and coast (as seen from tide gauge). From the retracked product, it can be seen that the mid-basin cycle does approach that seen in the tide gauge data as the coast is approached (Passaro et al., 2015).

Aliasing of tides and other high frequencies

The above discussion concerns corrections necessary to produce a genuine measurement of the position of the sea surface. However, given the relatively infrequent sampling of altimetry (almost 10 day intervals for Jason, and longer for satellites in other orbits), there is also the question of whether the measurement is representative, or suffers from

temporal aliasing. This question is most acutely felt in the case of tides which, as they have definite periods which are shorter than the sampling Nyquist period, are aliased to a variety of long periods (around 60 days for the dominant semidiurnal tides in Jason, but in many cases much longer).

In the case of tides, this is addressed by using a tide model to remove these effects. The tide models use altimetry and, in some cases, tide gauge data to constrain their predictions, and have developed significantly since the early days of satellite altimetry. For example, a recent review (Stammer et al., 2014) shows that several models now agree to better than 1 cm with open ocean observations, for the sum of 8 major tidal constituents. However, this increases to around 5 cm for shelf sea tides, and larger still for comparisons with coastal tide gauges. The situation in shallow water is not so simple though, for two reasons.

1) The statistics are skewed by small regions with large errors, so typical (median) errors are much smaller than the standard deviation - about 1.5 to 2 cm at tide gauges
2) The number of constituents needed to describe the tidal variability can be much larger in shallow water than in deep water. For example, Ray et al. (2011) shows that tides at around 3, 4, 5 and 6 cycles per day are comparable in amplitude to the diurnal tides at Calais, whereas at a deep water site they have amplitudes below the background "noise" (i.e. non-tidal ocean dynamics) level from Calais.

As a result, although tide models have improved significantly, more work remains to be done to define the nonlinear tides and the large number of constituents which are needed in shallow water. This is highly geographically variable: the relatively small tides in the Baltic region were not a large problem in the ALES retracker study mentioned above. However, around the UK, where tidal amplitudes of many metres occur, and highly nonlinear regimes are observed, errors in tidal models are still a major source of aliased variability for a comparable analysis (Simon Williams, personal communication). Furthermore, care must be taken over the sporadic large errors observed in tide models. Stammer et al. (2014) report that these are quite unpredictable, occurring in different regions of different models, and with no consistent physical cause. There is room for significant improvement, especially using regional tidal solutions, as illustrated by Ray et al. (2011), though a major limitation on such regional solutions is the poor availability of accurate bathymetry, often the limiting factor.

Aside from tides, there is also the issue of other high frequency ocean variability. In early altimeter products, this was partially dealt with via the inverse barometer correction, which serves a dual purpose: it reduces the high frequency variability, and also converts sea level to a proxy for sub-surface pressure, which is the variable of interest for ocean dynamics (for example, geostrophic flow is a result of there being a pressure gradient along a level surface). More recently, an extension to the inverse barometer correction termed the Dynamic Atmosphere Correction (DAC) has been used (Carrère and Lyard, 2003), in which a barotropic ocean model has been used to predict and remove variability at periods shorter than 20 days. This includes the dynamic response (as opposed to

equilibrium inverse barometer response) to atmospheric pressure variations, as well as the response to wind stress. It merges smoothly with a pure inverse barometer correction at longer periods.

The DAC certainly reduces aliased variability. It is one of the few correction changes (in this case in comparison to simple inverse barometer) which noticeably reduces altimeter crossover variability, and it does so particularly in coastal areas (Andersen and Scharroo, 2011). This is to be expected as simple arguments show that the sea level response to a given wind stress is inversely proportional to the water depth. For this reason, aliasing of high frequency variability is a much more important issue in coastal regions than in the bulk of the ocean.

Again, however, there is clearly room for improvement. Just as for tides, improved bathymetry can make an important difference, and the DAC is a pure hydrodynamic simulation with no assimilation of observations – it could be expected that incorporating tide gauge observations would improve the model simulations. Furthermore, the model is purely barotropic (i.e. constant density). High frequency heat flux variations are likely to produce centimetric steric sea level variations in places, and narrow boundary currents have important baroclinic contributions, especially at lower latitudes. This opens up some difficulties, as any baroclinic model with sufficient resolution to simulate these boundary currents would also produce a rich eddy field, which would add noise to the sea level product (primarily a problem in the open ocean). Difficult though it may be, there would certainly be value in exploring more sophisticated modelling methods.

To give a feel for the importance of this aliasing, consider a coastal region in which sea level has a 20 cm standard deviation associated with high frequency wind and pressure driven storm surges, or an occasional 2 m surge (these are large, but not unreasonable values for a shallow, wide shelf sea). In order to remove this high frequency variability at the 1 cm level by simple statistical averaging, the 2 m surge would have to occur only once every 200 cycles (about once every 5.5 years for Jason sampling, 19 years for Envisat), and the 20 cm standard deviation would require 400 cycles (11 years for Jason, 38 for Envisat). For long time series on repeat tracks, this is not a major issue for the mean sea surface, but it means that time dependent changes are very difficult to monitor at periods shorter than a few years. For non-repeat tracks (as in the case of CryoSat-2), this becomes an important issue for the mean sea surface too.

New altimeters

A new era in satellite altimetry began with the launch in April 2010 of CryoSat 2, the first in a series of new altimeters to operate in SAR mode (in the case of CryoSat, several different modes are available). Jason 3 (launched January 2016) is a conventional altimeter, but Sentinel 3A (launched February 2016) has a SAR mode, and the future Jason Continuity Series/Sentinel 6 satellites will also have SAR mode. There are many complications and subtleties to SAR operation but, in its simplest form, Doppler shift is recorded in addition to timing of the return radar pulse. Returns from ahead of the satellite are blue-shifted, and those from behind the satellite are red-shifted, making it

possible to divide the footprint into strips aligned perpendicular to the satellite track, distinguished by the Doppler shift. This enables measurements close to the coast, and in small leads within floating sea ice. SAR mode also enables an improvement in precision, with CryoSat 1 Hz noise reduced from 1.57 to 1.22 cm when SAR processing is used (Cotton, 2014).

Cryosat is not primarily an ocean altimeter, and lacks a radiometer needed for the wet troposphere correction (though alternatives are available). Nonetheless, it has clearly demonstrated the improved precision and along-track resolution expected from SAR, and has shown that good returns can be detected (with favourable orientation) as close as 100 m to the coast (Cotton, 2014). Another issue with CryoSat is that it has a nominal 369-day repeat (though small shifts mean that it can almost be considered a non-repeat orbit). While this is excellent for spatial resolution and determination of the mean sea surface, it brings the question of temporal aliasing to the fore.

Further ahead, the SWOT mission uses full SAR imaging methods to provide swath measurements of sea level to either side of the nadir track. This will provide much more data and higher spatial resolution, and has the potential to greatly improve the information available in coastal regions, including connecting coastal signals to river levels – a dynamical connection which is known to exist but is beyond the capabilities of present altimeter technology to detect. As with each new altimeter, the issue of sea state bias will need to be addressed afresh, for each kind of SAR method. Work on this is beginning with CryoSat, but it will be different again for each new altimeter.

Summary

Improved corrections are pushing to the centimetre level for coastal regions, but there remain important questions about the validity of the sea state bias correction. New techniques involving wave models are addressing part of this issue, but there are additional questions concerning the changing shape of waves in coastal regions which would benefit from further investigation.

Retracking methods are succeeding in providing more data close to the coast, though in some cases the loss of data is due to a failure of the onboard tracker as the instrument crosses from land to ocean, and these data losses are irretrievable. More recent onboard trackers do not suffer from this problem.

New SAR altimetry methods are accurate and have higher spatial resolution, allowing closer approach to the coast, but otherwise suffer the same limitations associated with corrections as traditional altimeters, including the important issue of sea state bias.

All methods suffer from important temporal aliasing effects, leading to a requirement for accurate tidal models as well as models for the high frequency response to atmospheric forcing. These issues become much more acute in coastal regions as both sources of variability increase in amplitude, and tides in particular become more complex, requiring more components than are commonly provided in tide models. This issue is mitigated for

mean sea level given sufficient data (many years) for exact repeat missions, but remains an issue for the slow or no repeat CryoSat mission. The size of the problem is highly dependent on region, being particularly difficult in wide shelf seas and regions of high tides. SWOT should help in this regard, as its swath capability circumvents the classic trade-off between spatial and temporal sampling for a nadir track altimeter.

Concluding Remarks.

This report has summarised the state-of-the-art in calculation of the coastal Mean Ocean Dynamic Topography using satellite gravity in combination with either satellite altimetry or tide gauge data, with other auxiliary datasets, together with an outlook on developments and requirements for coastal satellite altimetry. The references below, together with the GOCE+HSU publication list available at http://www.goceplushsu.eu, and particularly the Tide Gauge Unification Workshop Synthesis Report available here, constitute a summary of the available scientific literature and reports. This may be supplemented for recent developments in satellite altimetry with outputs of the CryoSat+ for Ocean project at http://www.satoc.eu/projects/CP4O/.

It is clear from this report that the project partners possess expertise in all relevant aspects of the project, including development of mean sea surface and gravity products, combination with geoid to produce optimised MODT estimates, expertise in tide gauge data and GPS at tide gauges, with close links to the relevant global databases, and expertise in the synthesis and interpretation of these datasets.

References

Andersen, O. B. and R. Scharroo, 2011: Range and geophysical corrections in coastal regions: and implications for mean sea surface determination. pp 103-145 in, Vignudelli et al. (2011). doi: 10.1007/978-3-642-12796-0_5.

Andersen, O. B., P. Knudsen and L Stenseng, 2015: The DTU13 MSS (Mean Sea Surface) and MDT (Mean Dynamic Topography) from 20 Years of Satellite Altimetry. IAG proceedings, doi: 10.1007/1345_2015_182.

Andersen, O.B., P. Knudsen, S.C. Kenyon, J.K. Factor and S. Holmes, The DTU13 Global marine gravity field – first evaluation. Presentation at OSTST meeting, Boulder, 8-11 October 2013. http://www.aviso.altimetry.fr/fileadmin/documents/OSTST/2013/oral/Andersen_DTU13 GRA.pdf.

Bingham, R. J., 2010: Nonlinear anisotropic diffusive filtering applied to the ocean's mean dynamic topography, Remote Sensing Letters, 1:4, 205-212, doi: 10.1080/01431161003743165.

Bingham, R. J., K. Haines and D. Lea, 2015: A comparison of GOCE and drifter-based estimates of the North Atlantic steady-state surface circulation. Int. J. Appl. Earth Obs. Geoinf. 35, 140-150, doi: 10.1016/j.jag.2014.03.012.

Carrère and Lyard, 2003: Modeling the barotropic response of the global ocean to atmospheric wind and pressure forcing - comparisons with observations. Geophys. Res. Lett. 30, 1275, doi:10.1029/2002GL016473.

Cotton, D. P., 2014: Cryosat Plus for Oceans: CP4O, Final Report, Executive Summary and Abstract (65 pp). http://www.satoc.eu/projects/CP4O/docs/CP4O_FinalReport.pdf

Featherstone, W. E., and M. S. Filmer, 2012: The north-south tilt in the Australian Height Datum is explained by the ocean's mean dynamic topography, J. Geophys. Res., 117, C08035, doi:10.1029/2012JC007974.

Fecher, T. R. Pail and T. Gruber, 2015: Global gravity field modeling based on GOCE and complementary gravity data. Int. J. Appl. Earth Obs. Geoinf. 35, 120-127, doi: 10.1016/j.jag.2013.10.005.

Filmer, M. S., 2014: Using Models of the Ocean's Mean Dynamic Topography to Identify Errors in Coastal Geodetic Levelling, Marine Geodesy, 37:1, 47-64, doi: 10.1080/01490419.2013.868383.

Förste C, Bruinsma S, Shako R, Marty J-C, Flechtner F, Abrikosov O, Dahle C, Lemoine J.-M, Neumayer KH, Biancale R, Barthelmes F, König R, Balmino G (2011) EIGEN-6 – a new combined global gravity field model including GOCE data from the collaboration of GFZ-Potsdam and GRGS-Toulouse. Geophys Res Abstr 13:EGU2011-3242-2, EGU General Assembly. http://meetingorganizer.copernicus.org/EGU2011/EGU2011-3242-2.pdf.

Förste C, Bruinsma SL, Abrikosov O, Lemoine J-M, Schaller T, Götze H-J, Ebbing J, Marty J-C, Flechtner F, Balmino G, Biancale R, 2014: EIGEN-6C4 The latest combined global gravity field model including GOCE data up to degree and order 2190 of GFZ Potsdam and GRGS Toulouse; presented at the 5th GOCE user workshop. Paris, pp 25–28. https://earth.esa.int/documents/10174/1860536/6_Foerste-et-al-EIGEN-6C4-GOCE-Userworkshop-2014

Gommenginger, C., P. Thibaut, L. Fenoglio-Marc, G. Quartly et al., 2011: Retracking altimeter waveforms near the coasts. pp 61-101 in, Vignudelli et al. (2011). doi: 10.1007/978-3-642-12796-0_4.

Gruber, T., C. Gerlach and R. H. N. Haagmans, 2012: Intercontinental height datum connection with GOCE and GPS-levelling data. Journal of Geodetic Science, 2(4), 270–280. doi: 10.2478/v10156-012-0001-y.

Hayden T., Rangelova E., Sideris M.G., Véronneau, M. (2014) Contribution of tide gauges for the determination of Wo in Canada, In: IAG Symposia Vol. 141, Gravity, Geoid and Height Systems Proceedings of the IAG Symposium GGHS2012, October 9-12, 2012, Venice, Italy. Volume 141 of the series International Association of Geodesy Symposia pp 241-248. doi: 10.1007/978-3-319-10837-7_31.

Higginson, S., K. R. Thompson, P. L. Woodworth, and C. W. Hughes, 2015:, The tilt of mean sea level along the east coast of North America, Geophys. Res. Lett., 42, 1471–1479, doi:10.1002/2015GL063186.

Hughes, C. W., R. J. Bingham, V. Roussenov, Joanne Williams and P. L. Woodworth, 2015: The effect of Mediterranean exchange flow on European time mean sea level. Geophys. Res. Lett. 42(2), 466-474. doi: 10.1002/2014GL062654.

Hughes, C. W., C. Wilson and T. Gruber, 2015: Improvements in the oceanic mean dynamic topography as determined using GOCE gravimetry. Geophysical Research Abstracts Vol. 17, EGU2015-11649, 2015. http://meetingorganizer.copernicus.org/EGU2015/EGU2015-11649.pdf (some figures from this presentation can be found at http://marine-climate.uib.es/SLR2015/presentations/Hughes.pdf)

Joana Fernandes, M., N. Pires, C. Lázaro and A. L. Nunes, 2013: Tropospheric delays from GNSS for application in coastal altimetry. Adv. Space Res 51, 1352-1368, doi: 10.1016/j.asr.2012.04.025.

Lin, H., K. R. Thompson, J. Huang, and M. Véronneau, 2015, Tilt of mean sea level along the Pacific coasts of North America and Japan, J. Geophys. Res. Oceans, 120, 6815–6828, doi:10.1002/2015JC010920.

Ophaug, V., K. Breili, and C. Gerlach, 2015: A comparative assessment of coastal mean dynamic topography in Norway by geodetic and ocean approaches, J. Geophys. Res. Oceans, 120, 7807–7826, doi:10.1002/2015JC011145.

Passaro, M., P. Cipollini, S. Vignudelli, G. D. Quartly and H. M. Snaith, 2014: ALES: A multi-mission adaptive subwaveform retracker for coastal and open ocean altimetry. Rem. Sens. Env. 145, 173-189, doi: 10.1016/j.rse.2014.02.008.

Pavlis, N. K., S. A. Holmes, S. C. Kenyon, and J. K. Factor, 2012: The development and evaluation of the Earth Gravitational Model 2008 (EGM2008), J. Geophys. Res., 117, B04406, doi: 10.1029/2011JB008916.

Passaro, M., P. Cipollini and J. Benveniste, 2015: Annual sea level variability of the coastal ocean: The Baltic Sea-North Sea transition zone. J. Geophys. Res. Oceans, 120, 3061–3078, doi: 10.1002/2014JC010510.

Penna, N., W. Featherstone, J. Gazeaux, and R. Bingham (2013), The apparent British sea slope is caused by systematic errors in the leveling-based vertical datum, Geophys. J. Int., 194(2), 772–786. doi: 10.1093/gji/ggt161.

Ray, R. D., G. D. Egbert and S. Y. Erofeeva, 2011: Tide predictions in shelf and coastal waters: status and prospects. pp 191-216 in, Vignudelli et al. (2011). doi: 10.1007/978-3-642-12796-0_8.

Ries, J., S. Bettadpur, R. Eanes, Z. Kang, U. Ko, C. McCullough, P. Nagel, N. Pie, S. Poole, T. Richter, H. Save, and B. Tapley, 2016: The combination global gravity model GGM05C. University of Texas at Austin Technical Memorandum CSR-TM-16-01. ftp://ftp.csr.utexas.edu/pub/grace/GGM05/README_GGM05C.pdf (and dataset at doi: 10.5880/icgem.2016.002).

Rio, M. H., S. Guinehut, and G. Larnicol, 2011: New CNES-CLS09 global mean dynamic topography computed from the combination of GRACE data, altimetry, and in situ measurements, J. Geophys. Res., 116, C07018, doi:10.1029/2010JC006505

Rio, M.-H., S. Mulet, and N. Picot, 2014: Beyond GOCE for the ocean circulation estimate: Synergetic use of altimetry, gravimetry, and in situ data provides new insight into geostrophic and Ekman currents, Geophys. Res. Lett., 41, 8918–8925, doi:10.1002/2014GL061773.

Roblou, L., Lamouroux, J., Bouffard, J., Lyard, F., Le Hénaff, M., Lombard, A. et al., 2011: Post-processing altimeter data toward coastal applications and integration into coastal models. pp. 217–246 in, Vignudelli et al. (2011). doi: 10.1007/978-3-642-12796-0_9.

Santamaría-Gómez, A., M. Gravelle, X. Collilieux, M. Guichard, B. Martín Míguez, P. Tiphaneau and G. Wöppelmann , 2012: Mitigating the effects of vertical land motion in tide gauge records using a state-of-the-art GPS velocity field. Global and Planetary Change 98–99 (2012) 6–17. doi: 10.1016/j.gloplacha.2012.07.007.

Schaeffer , P., Y. Faugére , J. F. Legeais , A. Ollivier , T. Guinle & N. Picot, 2012: The CNES_CLS11 Global Mean Sea Surface Computed from 16 Years of Satellite Altimeter Data, Marine Geodesy, 35:sup1, 3-19, doi: 10.1080/01490419.2012.718231.

Stammer, D., R. D. Ray, O. B. Andersen et al., 2014: Accuracy assessment of global barotropic ocean tide models. Rev. Geophys., 52, 243–282, doi: 10.1002/2014RG000450.

Stenseng, L., G. Piccioni, O. B. Andersen and P. Knudsen, 2015: Sea surface retracking and classification of CryoSat-2 altimetry observations in the Arctic Ocean. AGU Fall meeting, 2015, abstract C41A-0686.
https://ftp.space.dtu.dk/pub/DTU15/DOCUMENTS/MSS/AGU_Steenseng_C41A-0686.pdf

Tran, N., D. Vandemark, S. Labroue, H. Feng, B. Chapron, H. L. Tolman, J. Lambin and N. Picot, 2010: Sea state bias in altimeter sea level estimates determined by combining wave model and satellite data, J. Geophys. Res., 115, C03020, doi: 10.1029/2009JC005534.

Valledeau, G., P. Thibaut, B. Picard, J. C. Poisson, N. Tran, N. Picot and A. Guillot, 2015: Using SARAL/AltiKa to Improve Ka-band Altimeter Measurements for Coastal Zones, Hydrology and Ice: The PEACHI Prototype. Marine Geodesy, 38(S1):124–142, doi: 10.1080/01490419.2015.1020176.

van der Meijde, m., R. Pail, R. Bingham and R. Floberghagen, 2015: GOCE data, models, and applications: A review. Int. J. Appl. Earth Obs. Geoinf. 35, 4-15, doi: 10.1016/j.jag.2013.10.001.

Vandemark, D., S. Labroue, R. Scharroo, V. Zlotnicki, H. Feng, N. Tran, B. Chapron and H. Tolman, 2008: Sea state bias correction in coastal waters. 1st coastal altimetry workshop (http://cioss.coas.oregonstate.edu/CIOSS/altimeter_workshop.html)

Vignudelli, S., A. Kostianoy, P. Cipollini, & J. Benveniste (Eds.), 2011: Coastal altimetry. Berlin Heidelberg: Springer-Verlag, 565pp. doi: 10.1007/978-3-642-12796-0.

Woodworth, P. L., C. W. Hughes, R. J. Bingham and T. Gruber, 2012: Towards worldwide height system unification using ocean information. Journal of Geodetic Science 2(4), 302–318, doi: 10.2478/v10156-012-0004-8.

Woodworth, P. L., M. Gravelle, M. Marcos, G. Wöppelmann and C. W. Hughes, 2015: The status of measurement of the Mediterranean mean dynamic topography by geodetic techniques. J. Geodesy 89(8), 811-82. doi: 10.1007/s00190-015-0817-1.

4 Appendix C, D2: Description of data and models to be used in subsequent Work Packages
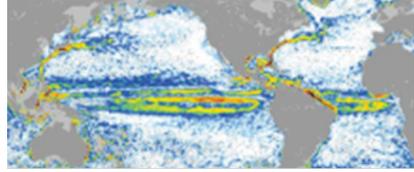
GOCE++ Dynamic Topography at the coast and tide gauge unification
GOCE ++ DYCOT

TITLE. WP1300 Technical Report: Description of data and models to be used in subsequent Work Packages

Author Luciana Fenoglio-Marc

ESTEC Ref: ITT AO/1-8194/15/NL/FF/gp "GOCE++ Dynamic Topography at the coast and tide gauge unification"- Coordinator: Ole B. Andersen (DTU)

DOCUMENT CHANGE LOG				
Rev.	Date	Sections modified	Comments	Changed by
1	11-03-2016	All	Draft	Luciana Fenoglio-Marc
2	16-03-2016	All	Draft	Luciana Fenoglio-Marc
3	16-08-2016	All	Draft	Luciana Fenoglio-Marc

Description of data and models to be used in subsequent Work Packages

Introduction

In this section we review the data that are going to be used in the project. Table 1 summarized the data stored in ftp://skylab.itg.uni-bonn.de/gocedycot. The mean dynamic topography will be estimated from the data over a selected time interval. We have selected the 5 year time interval from beginning 2003 to end of 2007 as the main time interval of analysis, as this interval is common to most of the data. Additionally, annual values will also be computed.

Data Type	Quantity	Name of Products
Altimeter data	Ell. heights	AVISO, RADS, CryoSat-2, Topex/Poseidon, Jason, Envisat
Bathymetry	depth	GEBCO_2014
Geoid	height	TUM2013C, GGM05C, EIGEN6C4, GOCO05C, EGM08, DIR5C
Mean Sea Surface	Ell. height	DTU15MSS, DTU13MSS, CLS
Mean Topography Ocean Dynamic	height	DTU15MDT, DTU13MDT
Ocean Models	11	EccoG, NemoQ, Nemo12, Livc,Livsr, Livwd, Ecco2, CS3X
Tide gauge data	Time-series	PSMSL, local organisation
Tide gauge GPS	Ell. heights	280
Drifter mean velocities	Velocity	UHDTU15MGV

Table 1. Data and models used

1. Altimeter Data

Satellite altimetry provides sea level heights above a reference ellipsoid at 1 Hz and higher temporal sampling along the satellite ground track (Vignudelli et al., 2011). We will use along-tracks and gridded sea level data available from standard altimeter database, e.g AVISO (http://www.aviso.altimetry.fr), CCI (http://www.esa-sealevel-cci.org) and RADS (http://rads.tudelft.nl). In addition we will also consider improved coastal datasets, e.g. CCTOH (Roblou et al., 2011) and ALES (Passaro et al-. 2014). The corrections to the altimeter data will be selected depending on the type of analysis, i.e. comparison with tide gauge or model run, accounting for the need of improved corrections in the coastal zone (Vandemark et al. 2008, Fernandez et al., 2013, Gommerginger et al., 2011, Fenoglio-Marc et al, 2015a). The interval 2003-2007 includes the satellite missions Topex/Poseidon, ERS2, Envisat, Jason-1, GFO (see Figure 1). It is intended to use both the pulse-limited and SAR altimeter data and assess the improvements obtained from the new SAR technique (Fenoglio-Marc et al., 2015).
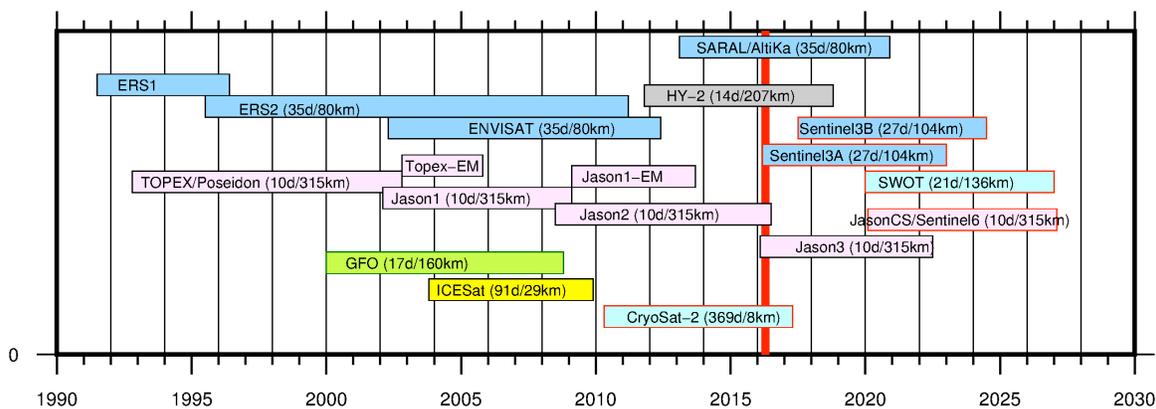
Figure 1. Satellite altimetry missions

2. Bathymetry

The bathymetry **GEBCO_2014** is a 30 arc-second global grid of elevations (1/120° = 0.0083°). (http://www.gebco.net/data_and_products/gridded_bathymetry_data/gebco_30_second_grid).
The complete data set gives global coverage, spanning 89° 59' 45"N, 179° 59' 45"W to 89° 59' 45"S, 179° 59' 45"E. It consists of 21,600 rows x 43,200 columns, giving 933,120,000 data points. The netCDF storage is arranged as contiguous latitudinal bands. The data values are pixel-centre registered i.e. they refer to elevations at the centre of grid cells.
The GEBCO_2014_2D points are generated by combining quality-controlled ship depth soundings with interpolation between sounding points guided by satellite-derived gravity data. Where they improve on the existing grid, data sets developed by other methods are included to create a continuous terrain model for ocean and land. The GEBCO_2014 Grid is accompanied by a **Source Identifier (SID) Grid**. This identifies which cells are based on actual depth values and which contain predicted depth values. Dataset is stored in directory **Data/bathymetry.**
The GEBCO2014 dataset has ben used to create the five land mask files with ones for ocean and zeros for land. Points with height above zero have been labelled as "land", except for 4 points that have been changed to "ocean" in order to connect the Black Sea to the Mediterranean Sea. Point below sea level (negative heights) have been labelled as "land" if they are enclosed by land. Binary data and netcdf files are stored in **Data/Landmasks.**

File name	Format	Res.	Data
GEBCO_2014_2D	netcdf		
landmask8_gebco	binary	1/120	1 ocean; 0 land; modified to allow Marmara and Black Sea to be connected
landmask8.dat	binary	1/8	1 > 50% ocean; 0 < 50% ocean; isolated ocean points removed
landmask8_notcleaned.dat	binary	1/8	As above, but isolated points not removed
landmask8_anyland.dat	binary	1/8	1 if completely ocean; 0 if any land
landmask8_anyocean.dat	binary	1/8	1 if any ocean; 0 if entirely land

Table 2. Land masks

3. Geoid Models

The geoid reference surface is a key parameter on the way to a globally unified height system. In order to exploit the full potential of gravity measurements and to achieve the best gravity field solution, all kinds of complementary gravity field information have to be combined. The combination geoids are therefore most suitable for our application. By combining GRACE and GOCE information, a satellite-only gravity field is available, which is highly accurate very long to medium wavelengths (80-100 km). By adding information from terrestrial/airborne gravimetry and satellite altimetry, which provide short wavelength gravity information, the full gravity field spectrum can be obtained. We will consider the most recent models, which have different degree and order: GOCO05S(280) and GOCO05C (720), GGM05C (360), and finally EIGEN6C4 (2190) and EIGEN6C3STAT (1949) and also EGM2008 (2190).

These geoids have moved on significantly since the initial comparison of geodetic ocean dynamic topographies demonstrated good general agreement with ocean model predictions (Woodworth et al., 2012). That comparison used Release 1 GOCE solutions with a very simple isotropic smoothing. There is clearly scope to improve on these comparisons now. The last geoid EIGEN6C4 and EIGEN6C3stat (Förste et al., 2015, 2012) have been derived using both satellite gravimetry data from GRACE/GOCE and surface gravity information computed from satellite altimetry (DTU10GRA).

We store spherical harmonic coefficients in gfc format in directory **Data/geoid**. The coefficients are given in the reference system tide free (the EIGEN and EGM2008) or in the zero-tide system (see Table 2).

	Geoid Name	Year	Deg	Data	
Mayer-Gürr	GOCO05S	2015	280	S(see model)	zero-tide
Fecher et al., 2016	GOCO05C	2016	720	GOCE Rel5	zero-tide
Ries et al, 2016	GGM05C	2016	360	S(Grace,Goce),G,A	zero-tide
Förste et al, 2012	EIGEN6C3STAT	2014	1949	S(Goce,Grace,Lageos),G,A	tide-free
Förste et al., 2015	EIGEN6C4	2014	2190	S(GOCE, GRACE, Lageos), G, A	tide-free
Pavlis	EGM2008	2008	2190	Grace	tide-free

Table 2. Geoid models

4. Mean Sea Surface

The mean sea surface is the displacement of the sea surface relative to a mathematical model of the earth (the ellipsoid) and closely follows the geoid. Amplitude ranges between +/- 100 meters. The global mean sea surface DTU15MSS (ftp.space.dtu.dk/pub/DTU15) is given as grids of 1 minute, 2 and 5 minutes. Formats are Gravsoft, NETCDF and as XYZ files, as in the previous releases DTU13 and DTU10. New is the interpolation error estimate, contained in the DTU15MSS_ XYZ file. Compared to the DTU13MSS, the DTU15MSS has been derived by including re-tracked CRYOSAT-2 altimetry also, hence, increasing its resolution. Over the TOPEX/JASON time span an improvement with respect to DTU13 is observed, with reduction of the global RMS with the TP-J1-J2 tracks from 1.41 to 1.33 cm. Some issues in the Polar regions

have been solved. Finally, the filtering was re-evaluated by adjusting the quasi-gaussian filter width to optimize the fit to drifter velocities.

The improvement arises from a reduced spatial filtering in DTU15. In several coastal regions (like Borneo) more substantial improvements are observed. The DTU15 MSS is based on multi-mission satellite altimetry from 10 different satellites. The time series have been extended to 23 years from the 20 years used in DTU13MSS. DTU15MSS ingests like DTU13MSS Cryosat-2 LRM and SAR data as well as 1 year of Jason-1 geodetic mission as part as it end-of-life mission between May 2012 and June 2013. The availability of Cryosat-2 SAR altimetry enables the determination of sea level in leads in the ice, which enables to derive an accurate MSS up to 88°N. .In the Artic region the DTU15MSS is an improvement with respect to existing UCL13 product, which merges CLS11 and CryoSat-2 data and is included as the default MSS in the CryoSat-2 Baseline-C products. The UCL13 model is contaminated by striping and errors near the coasts. Biases between UCL13 and DTU15 amount to -20 cm in large parts of the Arctic ocean (Stenseng et al., 2015). Alternatively the CLS13 MDT (Rio et al., 2014) will be used. CLS13 uses an optimal mapping technique and a priori ocean model/analysis product to define natural scales of the MDT as a function of region. Grids are stored in directory **Data/MSS**. Format is indicated in Table 3. The reference system is the mean tide system.

MSS Name	Year	Format	Resolution
DTU2013MSS	2013	netcdf, gravsoft	1/60, 1/30, 1/12, 1/5
DTU2015MSS	2015	netcdf, ascii, gravsoft	1/8
CNES_CLS11	2011	netcdf	1/30

Table 3. MSS models

5. Mean Ocean Dynamic Topography

The global mean dynamic topography model DTU15MDT has been computed using the DTU15MSS mean sea surface model and the gravity model EIGEN-6C4.

The EIGEN-6C4 is derived using the full series of GOCE data which provides a better resolution. The better resolution in EIGEN-6C4 fixes a few problems related to geoid signals in the former models such as DTU13MDT. Slicing in the GOCO05S gravity model up to harmonic degree 150 has solved some issues related to striations. DTU15MDT is a satellite-only mean dynamic ocean topography derived entirely from satellite observation. In DTU15MDT a truncated Gaussian filter with a half-width at half-maximum of about 0.8 spherical degrees was used. This choice is particularly important in regions with strong currents where the half-width was reduced to about 0.6 degrees. Approaching the equator an an-isotropic filter was used to overcome problems with minor north-south geoid stripes. Subsequently, geostrophic surface currents were derived from the DTU15MDT. The results show that geostrophic surface currents associated with the mean circulation have been further improved and that currents having speeds down to below 4 cm/s have been recovered. DTU15MDT is available in Gravsoft format.

MSS Name	Year	Format	Resolution	Other than heights
DTU13MDT	2013	Netcdf	1/60, 1/30, 1/12, 1/5	Error estimate
DTU2015MSS	2015	Gravsoft	1/60, 1/30, 1/12, 1/5	

Table 4. MDT models

6. Ocean models

Mean Ocean Dynamic Topography has been sourced from a variety of ocean models with different configurations and resolutions, as summarised in Table 5. Unlike earlier work (Woodworth et al., 2012), it is the intention to use these model data at native resolution wherever possible, rather than on a common ¼ degree resolution grid. The global models included here do not include tides, and only the OCCAM models have atmospheric pressure forcing, which can be significant at high frequencies. To assess this missing effect, we have also included a regional operational model for the NW European shelf (CS3X, Flather 2000), which includes these effects but excludes others, being purely barotropic. OCCAM was eliminated because not available in interval.

ECCO products support the Global Ocean Data Assimilation Experiment (GODAE), from which the **ECCO-GODAE** MDT is derived. The third version of this model is delivered with a resolution of 1-by-1 degree and covers the time period 1992-2007, Artic is excluded.

Two Nucleus for European Modelling of the Ocean (NEMO) models are available directly for the time span 1996-2000 and differ in resolution: **NEMOQ** is given with ¼×¼ degree grid spacing while **NEMO12** is delivered with a 1/12x1/12 degree resolution [Ophaug et al., 2015]. NEMO12b 1958-now with different forcing . All Nemo models are variable in latitude and distorted north of about 20 N.

L-MIT models are computed at Liverpool University and are based on the global ocean circulation model implemented at the Massachusetts Institute of Technology (MIT). The **L-MITc** coarse version has resolution 1x1 degree, while the fine version **L-MITf** has 1/5×1/6 degree resolution [Ophaug et al. 2015]. Two models exists at this resolution, they are identical except in the strait of Gibraltar (Livst, Livwd).

The ECCO2 - JPL model is computed in the Phase 2 of the Estimating the Circulation and Climate of the Ocean (ECCO) project. The estimated SSH is available with a time range that goes from 1992 to present, with a resolution of ¼ of degree and it is the result of combination of different assimilations, such as altimetric, geodetic and in-situ data [Wunsch and Heimbach, 2007].

We finally consider 7 ocean models. The mean over the interval 2003-2007 as well as annual means will be computed for the model grid and stored in the ftp in directory.

Label	Heritage	Run	Resolution	Grid	Reference	Comment	Interval
EccoG	MITgcm		1°	C, no Arctic	*Köhl et al.* [2007]	Data assimilating model, ECCO-Godae	1993-2007
NemoQ	OPA	N206	¼°	C, tripolar ORCA	*Blaker et al.* [2014]	Free-running, initiated with climatological T&S	1958-2007
Nemo12	OPA	N001	1/12°	C, tripolar ORCA	*Blaker et al.* [2014]	Free-running, initiated with climatological T&S	1979-2011
Nemo12b			1/12°				1958-2012
Livc	MITgcm		1°	C, no Arctic	*Williams et al.* [2014]	Model-based ocean analysis using Hadley Centre temperature and salinity for each year	1950-2010
Livst	MITgcm		1/5 x 1/6°	C, no Arctic	*Woodworth et al.* [2012]	Grid reverts to 1° far from N. Atlantic	1950-2010
Ecco2	MITgcm		~ 18 km	C, Cubed sphere	*Menemenlis et al.* [2005a,b]	Data assimilating model	1992-2007

Table 5. Ocean models with their different configurations and resolutions

7. Tide Gauge data

Established in 1933, the Permanent Service for Mean Sea Level (PSMSL, http://www.psmsl.org) has been responsible for the collection, publication, analysis and interpretation of sea level data from the global network of tide gauges. It is based in Liverpool at the National Oceanography Centre (NOC), which is a component of the UK Natural Environment Research Council (NERC). In order to construct time series of sea level measurements at each station, the monthly and annual means are reduced to a common datum. This reduction is performed by the PSMSL making use of the tide gauge datum history provided by the supplying authority. To date, approximately two thirds of the stations in the PSMSL database have had their data adjusted in this way, forming the 'REVISED LOCAL REFERENCE' (or 'RLR') dataset. In general, only

RLR data should be used for time series analysis. We use addition metric and external to PSMSL data only after a careful check. See in PSMSL_RLR_list_cwhplwmg2lf3_win.txt the list of stations used.

8. GPS data

We are interested in the ellipsoidal height of the zero point of the tide gauge data. This is generally computed as the sum of the ellipsoidal heiht of a GPS marker plus the vertical distance between the GPS marker and the zero point of the tide gauge.

SONEL (http://www.sonel.org) aims at providing high-quality continuous measurements of sea- and land levels at the coast from tide gauges (relative sea levels) and from modern geodetic techniques (vertical land motion and absolute sea levels) for studies on long-term sea level trends, but also the calibration of satellite altimeters, for instance. SONEL serves as the GNSS data assembly centre for the Global Sea Level Observing System (GLOSS), which is developed under the auspices of the IOC/Unesco. It works closely with the PSMSL by developing an integrated global observing system, which is linking both the tide gauge and the GNSS databases for a comprehensive service to the scientific community. It also acts as the interface with the scientific community for the French tide gauge data. SONEL identify the existence of a GPS station nearby a tide gauge, tries to collect, analyse and distribute the observation files (RINEX), the metadata (log file, contact name), the geodetic tie, and, if it has been processed in one of our solution, provides the ellipsoidal height. We will also use ellipsoidal heights not referenced in SONEL if metadata are available to document the procedure used to derive the heights and to give a realistic uncertainty.

File PSMSL_RLR_list_heights_SP_v1.csv contains 280 stations with geodetic tie, i.e. GPS@TG, collected by SONEL (MG) and from other sources (PLW, MG, LFWS, LFRW, Lin). Along the German Bight (coastline 140) three PLRM stations belong to the Revised Local Reference datase (RLR): Cuxhaven2 (TGCU), Borkum Fischenbaje (BORJ) and Wittdün (TGWD). The first two have ellipsoidal heights available both in SONEL and in a regional network including other 15 stations (Table 6). Most of those stations have been processed in one of the SONEL GPS solution, which are aligned to the ITRF08 reference frame. The ellipsoidal heights of the 17 stations in the German Bight are from Weiss and Sudau (2011) and Weiss (2013). Updated GPS ellipsoidal heights solutions were computed at TU Darmstadt in the frame of the ESA CCI project. The PPP Canadian software (http://webapp.geod.nrcan.gc.ca/geod/tools-outils/ ppp.php?locale=en), which gives ellipsoidal heights in the ITRF08 reference and accurate enough for our application could also be used alternatively to estimate the stations coordinates and rates.
Moreover the Bundesamt für Kartographie und Geodäsie (BKG, G. Liebsch personal communication) has made available ellipsoidal height of the tide gauge reference level (tide gauge zero) for four stations in the German Bight (Borkum (BORJ), Helgoland (HELG), Helgoland2 (HEL2), Hörnum (HOE2)). Height differences between SONEL and BKG for the two common stations TGCU and BORJ) are due to the definition of the tide gauge zero in PSMSL (RLR), which does not coincide with the BfG values. See example in Table 6 and also http://www.psmsl.org/data/obtaining/rlr.diagrams/1037.php.

PSMSL	SONEL	BfG	Diff.	RLR20 – Datum20
TGCU	32.399 +/- 0.010	34.351	1.952	1.98
BORJ	33.2040	35.180	1,976	1,98

Table 6. Ellipsoidal heights above WGS84 of tide gauge zero from SONEL and BfG
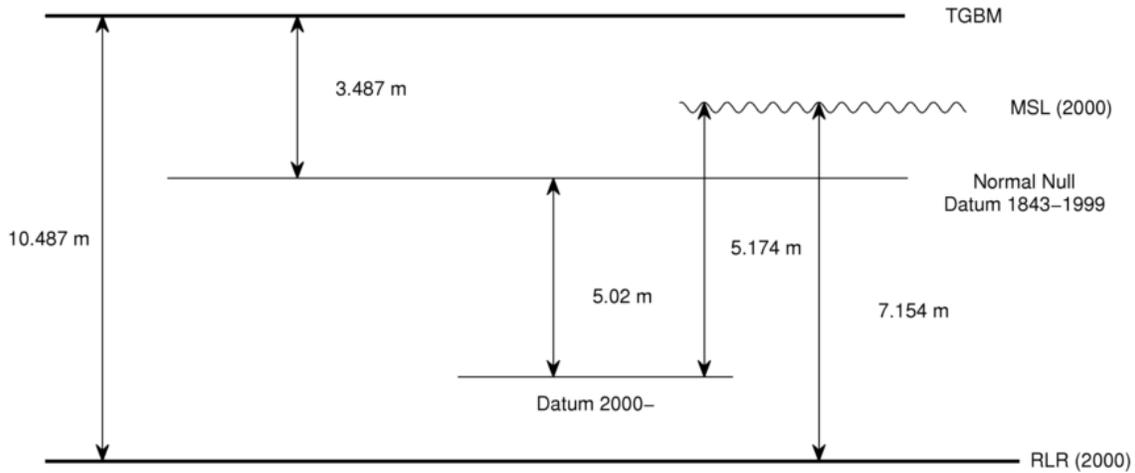
Figure 1. Example : Revised Local Reference (RLR) Diagram for CUXHAVEN 2

Variable Name	Definition
PSMSL ID	column 2 in http://www.psmsl.org/data/obtaining/
Latitude	column 3
Longitude	column 4
Station name	column 1
Coastline	column 8
Station	column 9
QC Flag	this project
GPS Number source	this project
InformationSource	this project (PLW, MG, LFWS, LFRW, Lin)
Ellipsoidal height	this project
Time corresponding to reference height	this project (computation or biblio date)

Table 7. Content of PSMSL_RLR_list_heights_SP_v1.csv in /Data/tg_GPS/

9. Drifter mean velocities

The mean geostrophic surface velocities have been derived using the drifter velocities from both drougued and undrogued buoys from the period 1993-2002. The drifter velocities were corrected for wind driven flows using NCEP winds. The wind driven flows were estimated using empirical correlation analyses where flow components parallel and perpendicular to the wind direction, were estimated in two-degree latitude bands. For the undrogued buoy data an additional flow term was estimated. To reduce the temporal variability the AVISO geostrophic current anomalies estimated from altimetric sea level anomalies were applied. Subsequently the drifter velocities were averaged in cells covering the oceans.

10. Transformations

Current practice is zero for gravity, tide-free for 3-D (e.g., ITRFxx), and mixed (overwhelmingly mean) for potential differences determined with precise levelling. Earth geopotential are generally given in both tide-free and zero-tide as far as the potential coefficients are concerned. The difference is only in the C_{02} term.

For the conversion of ellipsoidal height from the tide-free to the mean-tide system we need to add the effect of the permanent tide to the tide-free values. If the sea surface height is given in the mean tide system (i.e. it is the actual position of the sea surface, the most natural representation), and the gravitational field is given as for GOCO05C in the zero-tide system, then the sea surface height will contain the tidal bulge resulting from direct attraction of the Sun and Moon, but this will be absent from the gravitational field.

To convert zero-tide coefficients to mean tide (http://mitgcm.org/~mlosch/geoidcookbook/node9.htm)

$$C^{mean-tide} - C^{zero-tide} = -1.39 \times 10\text{-}8$$

To convert tide-free coefficients to mean tide:

$$C^{mean-tide} - C^{tide-free} = -(1+k)1.39 \times 10\text{-}8$$

where k is the zero-frequency Love number (k=0.3).

Alternatively the permanent tide correction can be added in the space domain, after computing the geoid height (Rapp 1989; Fenoglio-Marc 1996):

$$N^{mean-tide} - N^{tide-free} = -0.198 \left(3/2 \sin^2 \phi - \tfrac{1}{2} \right)$$

and

$$N^{mean-tide} - N^{tide-free} = -(1+k) \, 0.198 \left(3/2 \sin^2 \phi - \tfrac{1}{2} \right)$$

where ϕ is the geographic latitude.

References

Blaker, A. T., J. J.-M. Hirschi, G. McCarthy, B. Sinha, S. Taws, R. Marsh, A. Coward, B. de Cuevas (2014), Historical analogues of the recent extreme minima observed in the Atlantic meridional overturning circulation at 26°N, Clim. Dyn., 44, 457–473, doi:10.1007/s00382-014-2274-6.

Carrère and Lyard, 2003: Modeling the barotropic response of the global ocean to atmospheric wind and pressure forcing - comparisons with observations. Geophys. Res. Lett. 30, 1275, doi:10.1029/2002GL016473.

Fecher, T. R. Pail and T. Gruber, 2015: Global gravity field modeling based on GOCE and complementary gravity data. Int. J. Appl. Earth Obs. Geoinf. 35, 120-127, doi: 10.1016/j.jag.2013.10.005.

Fenoglio-Marc L. (1996). Sea Surface Determination with Respect to European Vertical Datums, PhD Thesis, Deutsche Geodaetische Kommission, Heft Nr. 464, München

Fenoglio-Marc, L., R. Scharroo, A. Annunziato, L. Mendoza, M. Becker, and J. Lillibridge (2015a), Cyclone Xaver seen by geodetic observations, Geophys. Res. Lett., 42, doi:10.1002/2015GL065989.

Fenoglio-Marc, L., Dinardo, S., Scharroo, R., Roland, A., Dutour, M., Lucas, B., Becker, M., Benveniste, J., Weiss, R. (2015a). The German Bight: a validation of CryoSat-2 altimeter data in SAR mode, *Advances in Space Research*, doi: http://dx.doi.org/10.1016/j.asr.2015.02.014

Fernandes J., M., N. Pires, C. Lázaro and A. L. Nunes, 2013: Tropospheric delays from GNSS for application in coastal altimetry. Adv. Space Res 51, 1352-1368, doi: 10.1016/j.asr.2012.04.025.

Flather, R., 2000: Existing operational oceanography. Coastal Engineering 41 2000. 13–40. doi: 10.1016/S0378-3839(00)00025-9.

Förste C, Bruinsma SL, Abrikosov O, Lemoine J-M, Schaller T, Götze H-J, Ebbing J, Marty J-C, Flechtner F, Balmino G, Biancale R, 2014: EIGEN-6C4 The latest combined global gravity field model including GOCE data up to degree and order 2190 of GFZ Potsdam and GRGS Toulouse; presented at the 5th GOCE user workshop. Paris, pp. 25–28. https://earth.esa.int/documents/10174/1860536/6_Foerste-et-al-EIGEN-6C4-GOCE-Userworkshop-2014

Gommenginger, C., P. Thibaut, L. Fenoglio-Marc, G. Quartly et al., 2011: Retracking altimeter waveforms near the coasts. pp 61-101 in, Vignudelli et al. (2011). doi: 10.1007/978-3-642-12796-0_4.

Hughes, C. W., R. J. Bingham, V. Roussenov, Joanne Williams and P. L. Woodworth, 2015: The effect of Mediterranean exchange flow on European time mean sea level. Geophys. Res. Lett. 42(2), 466-474. doi: 10.1002/2014GL062654.

Köhl, A., and D. Stammer, 2008: Variability of the meridional overturning in the North Atlantic from the 50 years GECCO state estimation, J. Phys. Oceanogr., 38, 1913–1930, doi:10.1175/2008JPO3775.1.

Köhl, A., Stammer, D., Cornuelle, B., 2007: Interannual to decadal changes in the ECCO global synthesis, J. Phys. Oceanogr., 37, 313–337, doi: 10.1175/JPO3014.1.

Marsh, R., S. A. Josey, B. A. de Cuevas, L. J. Redbourn, and G. D. Quartly, 2008: Mechanisms for recent warming of the North Atlantic: Insights gained with an eddy-permitting model, J. Geophys. Res., 113, C04031, doi:10.1029/2007JC004096.

Marsh, R., B. A. de Cuevas, A. C. Coward, J. Jacquin, J. J. M. Hirschi, Y. Aksenov, A. J. G. Nurser, and S. A. Josey, 2009: Recent changes in the North Atlantic circulation simulated with eddy-permitting and eddy-resolving ocean models, Ocean Modell., 28(4), 226–239, doi:10.1016/j.ocemod.2009.02.007.

Menemenlis, D., Fukumori, I., and Lee, T., 2005a: Using Green's functions to calibrate an ocean general circulation model, Mon. Weather Rev., 133, 1224–1240, doi:10.1175/MWR2912.1.

Menemenlis, D., C. Hill, A. Adcroft, J. –M. Campin, B. Cheng, B. Ciotti, I. Fukumori, P. Heimback, C. Henze, A. Köhl, T. Lee, D. Stammer, J. Taft and J. Zhang, 2005b: NASA Supercomputer Improves Prospects for Ocean Climate Research. EOS 86 (9), 89-96. doi: 10.1029/2005EO090002.

Passaro, M., P. Cipollini, S. Vignudelli, G. D. Quartly and H. M. Snaith, 2014: ALES: A multi-mission adaptive subwaveform retracker for coastal and open ocean altimetry. Rem. Sens. Env. 145, 173-189, doi: 10.1016/j.rse.2014.02.008.

Pavlis, N. K., S. A. Holmes, S. C. Kenyon, and J. K. Factor, 2012: The development and evaluation of the Earth Gravitational Model 2008 (EGM2008), J. Geophys. Res., 117, B04406, doi: 10.1029/2011JB008916.

Rapp, R. H., 1989. The treatment of permanent tidal effects in the analysis of satellite altimeter data for sea surface topography. *manuscripta geodaetica*, 14(6), pp. 368-372.

Ries, J., S. Bettadpur, R. Eanes, Z. Kang, U. Ko, C. McCullough, P. Nagel, N. Pie, S. Poole, T. Richter, H. Save, and B. Tapley, 2016: The combination global gravity model GGM05C. University of Texas at Austin Technical Memorandum CSR-TM-16-01. ftp://ftp.csr.utexas.edu/pub/grace/GGM05/README_ GGM05C.pdf (and dataset at doi: 10.5880/icgem.2016.002).

Roblou, L., Lamouroux, J., Bouffard, J., Lyard, F., Le Hénaff, M., Lombard, A. et al., 2011: Post-processing altimeter data toward coastal applications and integration into coastal models. pp. 217–246 in, Vignudelli et al. (2011). doi: 10.1007/978-3-642-12796-0_9.

Stenseng, L., G. Piccioni, O. B. Andersen and P. Knudsen, 2015: Sea surface retracking and classification of CryoSat-2 altimetry observations in the Arctic Ocean. AGU Fall meeting, 2015, https://ftp.space.dtu.dk/pub/DTU15/DOCUMENTS/MSS/AGU_Steenseng_C41A-0686.pdf

Vandemark, D., S. Labroue, R. Scharroo, V. Zlotnicki, H. Feng, N. Tran, B. Chapron and H. Tolman, 2008: Sea state bias correction in coastal waters. 1st coastal altimetry workshop (http://cioss.coas.oregonstate.edu/CIOSS/altimeter_workshop.html)

Vignudelli, S., A. Kostianoy, P. Cipollini, & J. Benveniste (Eds.), 2011: Coastal altimetry. Berlin Heidelberg: Springer-Verlag, 565pp. doi: 10.1007/978-3-642-12796-0.

Weiss R. and A. Sudau (2011). Satellitengestützte Überwachung der Pegelnullpunkthöhe

in der Deutschen Bucht, Die Küste, 78 (2011), 1- 32

Weiss, R. (2013). Erfassung und Beschreibung des Meeresspiegels und seiner Veränderungen im Bereich der Deutschen Bucht Heft, PhD, Technische Universität Darmstadt, ISBN 978-3-935631-29-7, http://tuprints.ulb.tu-darmstadt.de

Williams, R. G., V. Roussenov, D. Smith, and M. S. Lozier, 2014: Decadal evolution of ocean thermal anomalies in the North Atlantic: The effects of Ekman, overturning, and horizontal transport, J. Clim., 47, 698–719, doi:10.1175/JCLI-D-12-00234.1.

Woodworth, P. L., C. W. Hughes, R. J. Bingham, and T. Gruber, 2012: Towards worldwide height system unification using ocean information, J. Geodetic Sci., 2(4), 302–318, doi:10.2478/v10156-012-0004-8.

5 Appendix D, D3: Report on selection and justification of test area
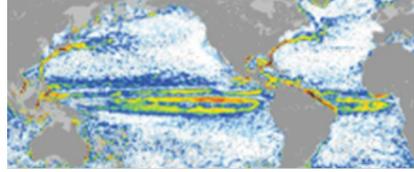
GOCE++ Dynamic Topography at the coast and tide gauge unification
GOCE ++ DYCOT

TITLE. WP1300 Technical Report: report on selection and justification of test area

Author Luciana Fenoglio-Marc

ESTEC Ref: ITT AO/1-8194/15/NL/FF/gp "GOCE++ Dynamic Topography at the coast and tide gauge unification"- Coordinator: Ole B. Andersen (DTU)

DOCUMENT CHANGE LOG				
Rev.	Date	Sections modified	Comments	Changed by
1	11-03-2016	All	Draft	Luciana Fenoglio-Marc
2	16-08-2116	All	Draft	Luciana Fenoglio-Marc

Report on selection and justification of test areas

Introduction

Tasks of this report are two: first to perform an initial screening of the data and select few test regions and second to establish a database of relevant data for the project (see also Technical Report WP1300D2).

The areas will be used in the validation of in WP2200, further on will be considered in WP3000.

We make a distinction between well-surveyed and poorly-surveyed areas based on the availability of in-situ data. We consider "well-surveyed" a region where in-situ data at many stations in the region are available, that is when both the PSMSL tide gauge time-series and the ellipsoidal heights of the zero of the tide gauges exist. "Poor-surveyed" is a region where one or both types of in-situ data are very few. We select regions for each of the two groups (well surveyed and poor surveyed regions).

We select an interval of time corresponding to many in-situ data available in the "well-surveyed" regions. We also account for the availability of the space-based altimetry data.

FTP access is made available at the University of Bonn and at the partners' managed servers to provide all data required for WP2000 and for part of the data used in WP3000 activities. The database includes supporting information, as description and format specification.

1. Regional selection and data

A list of tide gauges includes a total of 1453 tide gauge stations has been prepared. Most of the stations, 1436 in number, belong to the REVISED LOCAL REFERENCE' (or 'RLR') dataset of the Permanent Service for Mean Sea Level (**PSMSL**) (**www.psmsl.org/data/**), one is a PLRM metric station (Helgoland) and 13 tide gauges are not in the PLRM database and are made available by the Bundesanstalt für Gewässerkunde (BSH). File **PSMSL_RLR_list_heights_SP_v1.csv** gives the complete list.

Organisation	N. of stations	N. of GPS@TG	GPS@tG
PLRM RLR	1436	280 +	280
PLRM metric, GPS BfG	1	1 (Helgoland) not in 280	1
no PSMSL, GPS in BfG	13	13 not in 280	13
RLR GPS BfG & SONEL	In 280	TGBF, TGCU, in 280	
RLR no GPS (BfG)	1, Not in 280	1 (Amrun, TGWD), not in 280	1

Table 1. Tide gauge stations

To evaluate ellipsoidal height of sea level at the tide gauge stations the ellipsoidal height of the zero point of the tide gauge need to be computed from GPS (hGPS0) and from levelling measurements, which give the vertical distance between tide gauge zero point and GPS zero point (dh0=TG0 – GPS0). Of the set of 1453 stations only 295 are co-located with a GPS. This leaves 1158 tide gauge stations without GPS. Figure 1 shows the set of tide gauge (black) and GPS stations (red) available over the selected interval. For the validation of the method in WP2000 we have selected the interval 2003-2007. We have first investigated which of the tide gauge stations are available at least 70% of the time over the interval 2003-2007. As an example, of the 736 stations with data available for more than 70% of the time 265 are co-located with a GPS (Table 3). The pink dots in Figure 2 are the GPS stations with co-located tide gauge data not available over 2003-2007. Figure 3 shows the final set of tide gauge (green) and GPS stations (red) that could be considered.

Organisation	Number of stations
SONEL	280
BfG	15 (13 not PSMSL + 1 not RLR + 1 RLR)

Table 2. GPS@TG stations available

Interval	PSMSL > 1%	PSMSL >70%	PSMSL > 99%
2003-2007	850/286	736/265	454/186
2008-2012	865/290	724/263	401/155

Table 3. PSMSL stations available for more than x% (x=1,70,99) of the selected interval and number of GPS@TG stations out of total number of 298.
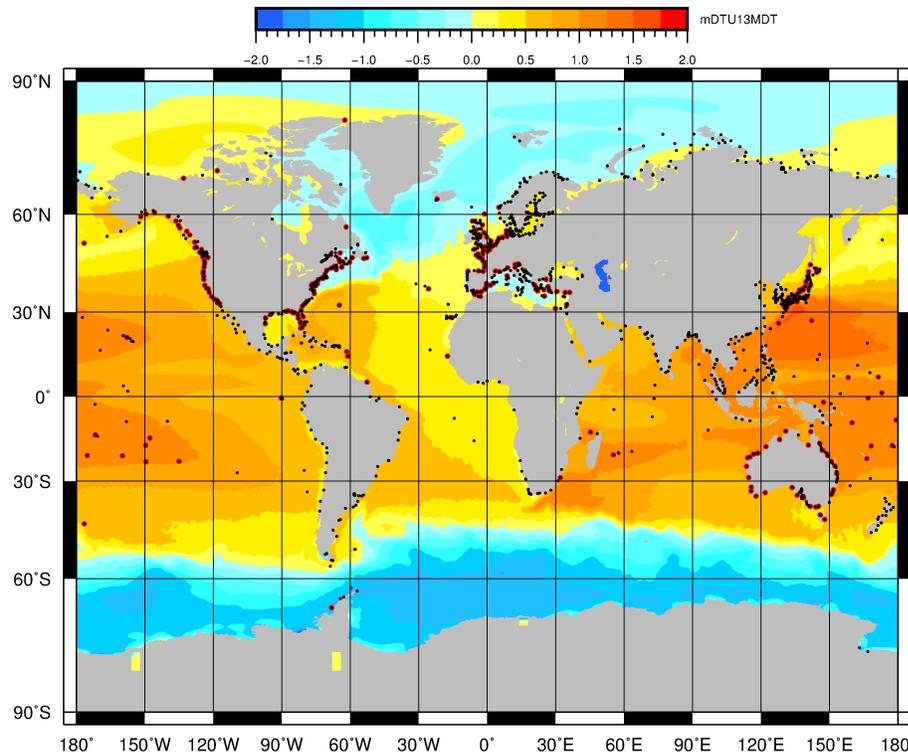
Figure 1. Complete database of tide gauge stations (black) and GPS stations (red).

4
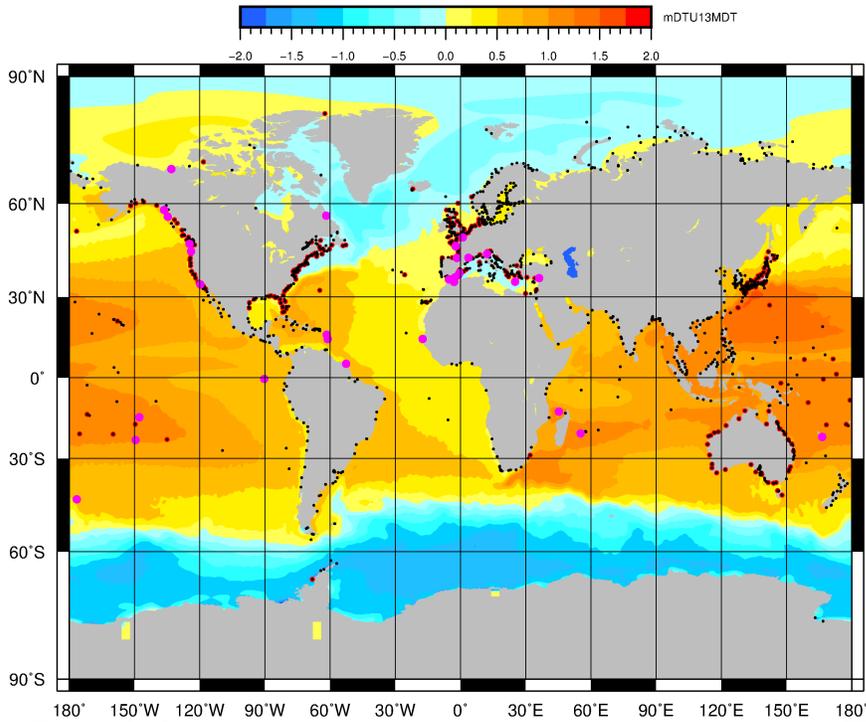
Figure 2. Complete database of tide gauge stations (black) and GPS stations (red) with GPS@TG stations without tide gauge data in 2003-2007.
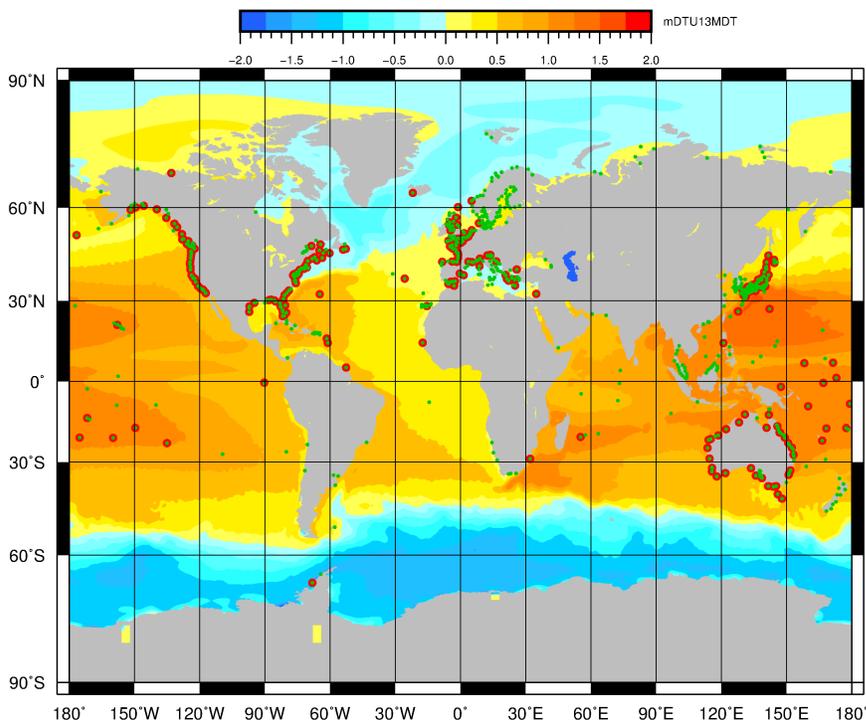
Figure 3. Dataset of tide gauge stations (green) available in 2003-2007 and corresponding and GPS stations (red).

We consider six world regions: the North-Eastern Atlantic coast including the North Sea and the Baltic Sea, Australia, the Pacific Islands, the South-Eastern African coast, South America, South-Eastern Asia. Table 4 gives the number of PSMSL time-series in the interval 2003-2007 and the GPS stations providing the corresponding ellipsoidal heights of the reference point of the tide gauges.

Based on the availability of in-situ time-series and ellipsoidal heights, the North-Eastern Atlantic coast and Australia are the most well surveyed regions. Of the less well surveyed regions we finally select three of the four investigated regions, excluding South Eastern Asia that has only one GPS station Linking the regions to each others will enable investigation of long distance connections. In the following sections we describe in details the regions analysed.

Region	GPS Stations	PSMSL	
North-Eastern North Atlantic	51	107	WS1
Australia	35	62	WS2
Pacific Islands	20	35	BS1
South Eastern African Coast Angulhas	3	7	BS2
South America	3	15	BS3
South Eastern Asia	1	20	BS4

Table 4: Number of stations with PSMSL time-series in 2003-2007 and TG@GPS

2. Well surveyed regions

2.1 North-Eastern Atlantic coast

As first well surveyed areas we select the North Atlantic Ocean. Figure 4 shows a large number of PSMSL tide gauge stations co-located and not with GPS stations.

Figure 5 shows additional tide gauges in the German Bight which are not yet included in the PSMSL. The GPS heights for the time interval 2008-2010 and levelling values are available (Table 11 in Weiss and Sudau, 2011). Values from Weiss (2013) have been used in the validation of CryoSat-2 data (Fenoglio-Marc et al., 2015). Updated GPS positions and velocities are being computed at TUDa in the frame of the SLCCI project for 19 Stations, 15 of them are in common with WS11 (Mendoza et al., 2015). Note that in CCI the stations TGF3, TGD2, TGEM, TGLE and HELG2 are not used for sea level studies.

For the CCI stations we have updated GPS coordinates and velocities, for other stations we will use results published in Weiss and Sudau (2011) and in Weiss (2013). The levelling information is missing for some of the GPS stations we are analysing in the CCI project. For example, the TUDa CCI GPS solutions include 4 stations which are not given in Weiss and Sudau 2011 (TGD2, TGLE, TGWD, HEL2). As dh0 and hTG0 are unknown for those four stations, the ellipsoidal heights are not available. Moreover, we can use here stations which are not processed in CCI. For example, for the four stations TGPA, TGPO, TGTE, TGWE, which are not included in CCI, WS11 give the necessary information. In this case the ellipsoidal height are available, but the GPS coordinates cannot be updated at TUDa. Figure 5 shows the 17 stations finally included in the project (15 are used in CCI + 2 from Weiss (2013)). See also in file **PSMSL_RLR_list_heights_SP_v1.csv**. For TGWD, TGLA and TGPE ellipsoidal height information is provided by Weiss 2013, for the other stations the information is given in Weiss and Sudau (2011) as GPS height and levelling information separately.
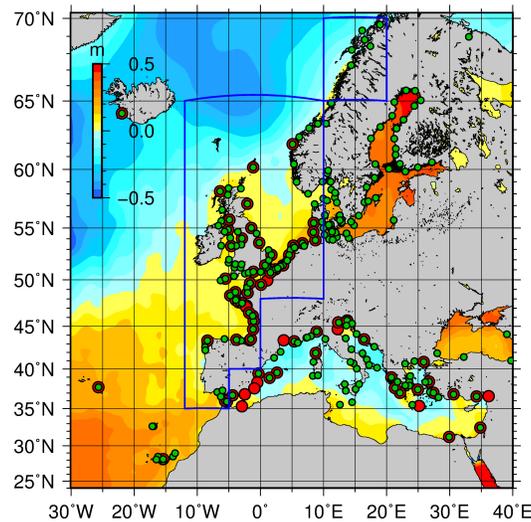
Figure 4. North-Eastern Atlantic : Dataset of tide gauge stations (green) available in 2003-2007 and corresponding and GPS stations (red). Region considered is in blue.

Data	Source/Agency	Stations
GNSS data at 12 TGs	BfG, BKG	FLDW, LHAW, TGBU, TGBF, TGBH, TGCU, TGDA, TGEM, TGKN, TGME, TGWD (W13), TGWH
GNSS at 3 TGs	EUREF	BORJ, HELG, HOE2
Levelling	BfG	TGLA, TGPE (W13)
sea level In-situ data (SL)	BfG, WSV, PSMSL	FLDW, LHAW, TGBU, TGBF, TGBH, TGCU, TGDA, TGEM, TGKN, TGME, TGWD, TGWH, BORJ, HELG, HOE2 TGLA, TGPE

Table 5: GPS and tide gauge stations used in the German Bight. In bold are the stations which are not part of the CCI project. Data input are sorted by agency and name

Figure 5. North-Eastern Atlantic/German Bight : stations with ellipsoidal heights and DTU2013. PSMSL tide gauge stations available in 2003-2007 (green), stations connected by levelling (violet), IGS stations (green), local BfG stations (yellow)

2.2 Australia

Australia is the second selected well surveyed areas. Figure 6 shows that a large number of PSMSL tide gauge stations is co-located with GPS stations. The East Australian and the Leuwin Currents are well-monitored areas with good ocean modelling. The use of drifter has shown strong impacts in the determination of the MDT (Rio, 2013).

Figure 6. Tide gauge and GPS@TG in Australia and DTU2013 Mean Dynamic Topography

3. Poorly surveyed areas

With exception of the North-America, Europe, Australia and Japan, the areas are poorly surveyed.

3.1 Pacific Islands

A large number of tide gauges in the Western Tropical Pacific are co-located to GPS. It is well know that geoid is on island problematic, therefore the determination of the mean dynamic topography near to the coast is expected to be here particularly challenging. The SAR altimetry covers part of this region.
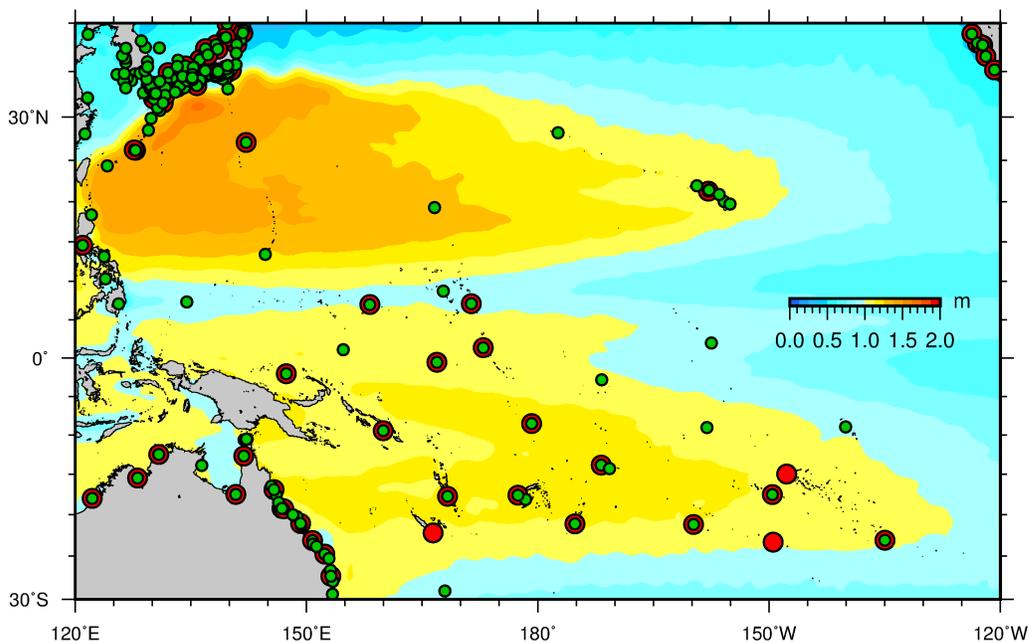
Figure 7. Tide gauge and GPS@TG in the Western Pacific and Mean Dynamic Topography DTU2013.

3.2 South Eastern African Coast Angulhas Current and Madagascar strait Pacific Islands

The Agulhas Current and the Madagascar Strait are very interesting for the currents and for the steep slope of their mean dynamic topography. The regions benefits from some good tide gauges and from CryoSat-2 SAR model altimetry since 2010, which covers part of the region. The Madagascar strait is a challenging region for gravity due to has a very poor geoid.

9
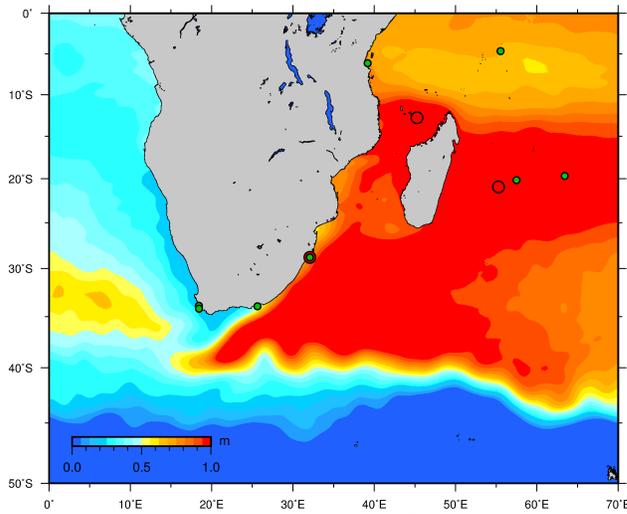
Figure 8. Tide gauge and GPS@TG in South-Eastern Africa and Mean Dynamic Topography DTU2013.
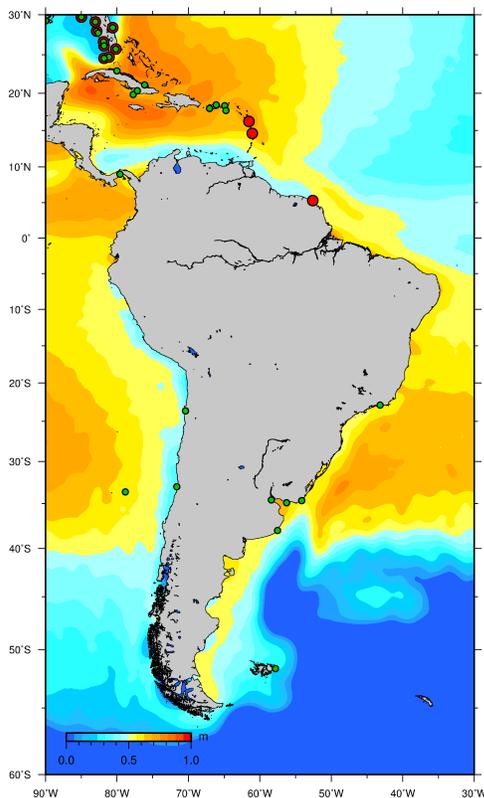
Figure 9. Tide gauge and GPS@TG in South-America and Mean Dynamic Topography DTU2013.

3.3 South-America

The South Chilean Coasts has very rapid elevation change in the coastal strip and is therefore an extremely challenging region for gravity.

Unfortunately GPS@TG stations are only available in the Northern part of South-America continent. This part presents a steep mean dynamic topography generated by the current between the Golf of Mexico and the Atlantic.

3.4 South-Eastern Asia

South-Eastern Asia is a very challenging region for many reasons, firstly for satellite coastal altimetry and for geoid determination due to the many islands, secondly for the high vertical motion due to the strong seismic activity. CryoSat-2 covers the complete region since 2010.

Unfortunately only one GPS stations is available in our datasets, other stations exist but are not publicly available (Fenoglio-Marc et al., 2012). Therefore it is less suitable that the others for our study. We will consider the region if additional GPS data are made available.
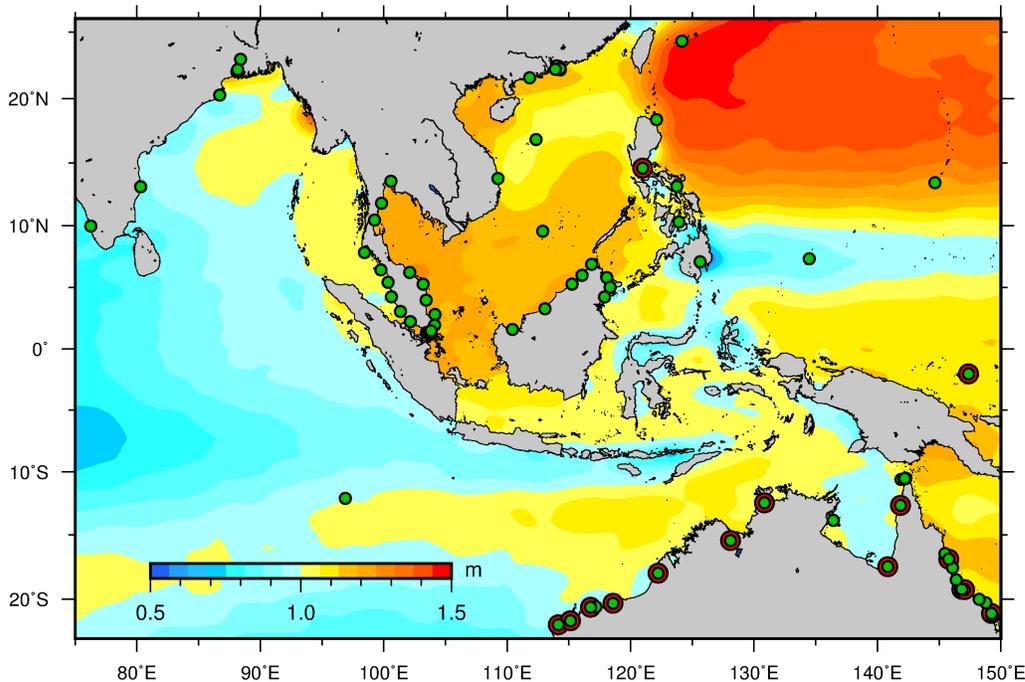
Figure 10. Tide gauge and GPS@TG in South-Eastern Asia and Mean Dynamic Topography DTU2013.

4. Concluding remarks

We have identified two well-surveyed and three poor-surveyed areas. The two well surveyed areas are the North-Eastern Atlantic and Australia coasts. We poor-surveyed areas are the Pacific Islands, the South Eastern African Coast (near Madagascar) and the North-Eastern coast of South-America (Brazil).

The first will be used for the validation in WP2200, the others will be considered in WP3000.

Thus we keep one additional survey region compared with the original plan. This is because the availability of tide gauges is still under investigation and more will appear constantly, so we do not want to rule out any stations. However we will base the work on the current available choice of regions and stations.

FTP access is made available at the University of Bonn and at the partners' managed servers to provide all data required for WP2000 and for part of the data used in WP3000 activities. The database includes supporting information, as description and format specification. The ftp address/password at the University of Bonn has been sent per e-mail.

References

Andersen, O. B. and R. Scharroo, 2011: Range and geophysical corrections in coastal regions: and implications for mean sea surface determination. pp 103-145 in, Vignudelli et al. (2011). doi: 10.1007/978-3-642-12796-0_5.

Fenoglio-Marc L., Dinardo, S., Scharroo, R., Roland, A., Dutour, M., Lucas, B., Becker, M., Benveniste, J., Weiss, R. (2015). The German Bight: a validation of CryoSat-2 altimeter data in SAR mode, *Advances in Space Research*, doi: http://dx.doi.org/10.1016/j.asr.2015.02.014

Fenoglio-Marc L., T. Schöne , J. Illigner , M. Becker , P. Manurung & Khafid, (2012): Sea Level Change and Vertical Motion from Satellite Altimetry, Tide Gauges and GPS in the Indonesian Region, Marine Geodesy, 35:sup1, 137-150T. http://dx.doi.org/10.1080/01490419.2012.718682

Lin, H., K. R. Thompson, J. Huang, and M. Véronneau (2015), Tilt of mean sea level along the Pacific coasts of North America and Japan, J. Geophys. Res. Oceans, 120, 6815–6828, doi:10.1002/2015JC010920.

Mendoza L.,Becker M. and Fenoglio-Marc L. (2015). GNSS Station coordinates and trend of the vertical component, Zenith Total Delay. Report SLCCI-D5-GPD DataAnalysis-v1.0, CCI project, SLCCI, ESA, May 2015.

Weiss R. and A. Sudau (2011). Satellitengestützte Überwachung der Pegelnullpunkthöhe in der Deutschen Bucht, Die Küste, 78 (2011), 1- 32

Weiss, R. (2013). Erfassung und Beschreibung des Meeresspiegels und seiner Veränderungen im Bereich der Deutschen Bucht Heft, PhD, Technische Universität Darmstadt, ISBN 978-3-935631-29-7, http://tuprints.ulb.tu-darmstadt.de

Woodworth et al. The MDT of the Mediterranean Sea, JOGE

Woodworth et al. (2012) Towards worldwide height system Unification using ocean information, J. of Geod. Science

6 Appendix E, D4: Selection of Approach and description of software for coastal mean dynamic topography
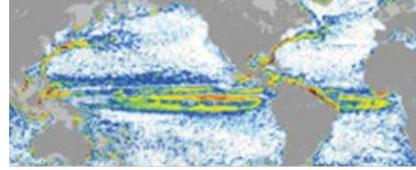
GOCE++ Dynamic Topography at the coast and tide gauge unification
GOCE ++ DYCOT

TITLE. WP 2100-D4 Technical Note: Selection of Approach and description of software for coastal mean dynamic topography

Authors: Karina Nielsen, Per Knudsen, Ole B. Andersen

ESTEC Ref: ITT AO/1-8194/15/NL/FF/gp "GOCE++ Dynamic Topography at the coast and tide gauge unification"- Coordinator: Ole B. Andersen (DTU)

DOCUMENT CHANGE LOG				
Rev.	Date	Sections modified	Comments	Changed by
1	08-11-2016	All	Draft	Karina Nielsen and Ole B. Andersen
2	03-03-2017			Karina

Table of Contents

1 Introduction

This deliverable is a combination of a description of the approach (Section 2) and a description of the prototype software (Section 3).

2 Selection of approach

The following sections describe the selection of approach in the GOCE++ project.

2.1 Mean dynamic topography

The mean dynamic topography is estimated using the geodetic approach,

$$MDT = MSS - N, \tag{1}$$

where MSS is the mean sea surface and N is the geoid height. The quality of the MDT depends on the quality of the MSS and the geoid model. The quality of the MSS is generally less good close to the coast, due to lower data coverage both spatially and temporally. Figure 1 shows the track coverage based on TOPEX Poseidon and Jason 1 and 2 around Scandinavia. It is clear that the coverage is sparse close to the coast.
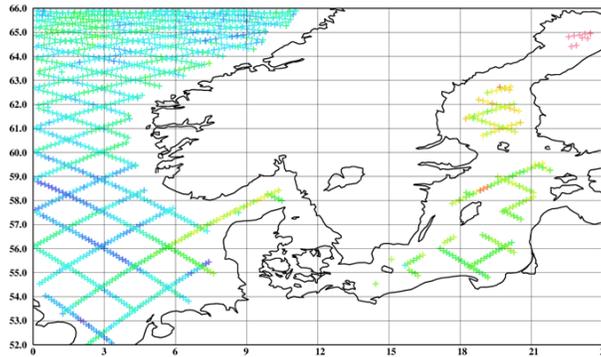
Figure 1: Illustrate the joint T/P-J1-J2 time series with more than 10 years of data (360 repeats).

The MDT may also be derived at tide gauges using a similar approach as (1). These MDT estimates will provide additional information in the coastal region, where the altimetry based estimates are sparse. Hence to improve the MDT in the coastal regions MDT values based on tide gauges are used as constraints. The final MDT is thus a combination of contributions from both altimetry and tide gauges.

To minimize the residue errors in the final MDT it is recommended to uses the same geoid as applied in the altimetric mean sea surface.

2.1.1 MDT gradient along the coast

The geodetic MDT is generally not well constraint in the coastal region, where the MDT contours in some cases crosses the coastline. This is mainly due to the sparse data coverage and that the filter is unconstrained. An example of this is demonstrated in Figure 2 (left) for the east coast of the US.

In the GOCE++ project this is partly accounted for by inserting MDT values over land. After filtering the land values are smoothed into the coastal region and hence aligning the gradients along the coast as demonstrated in Figure 2 (right). It is however crucial to select appropriate values. If the difference between the coastal MDT values and the inserted land values are too large, artificial MDT gradient may be created in the process (see *Figure 7*). In the GOCE++ project tide gauge based MDT values are used as land values.
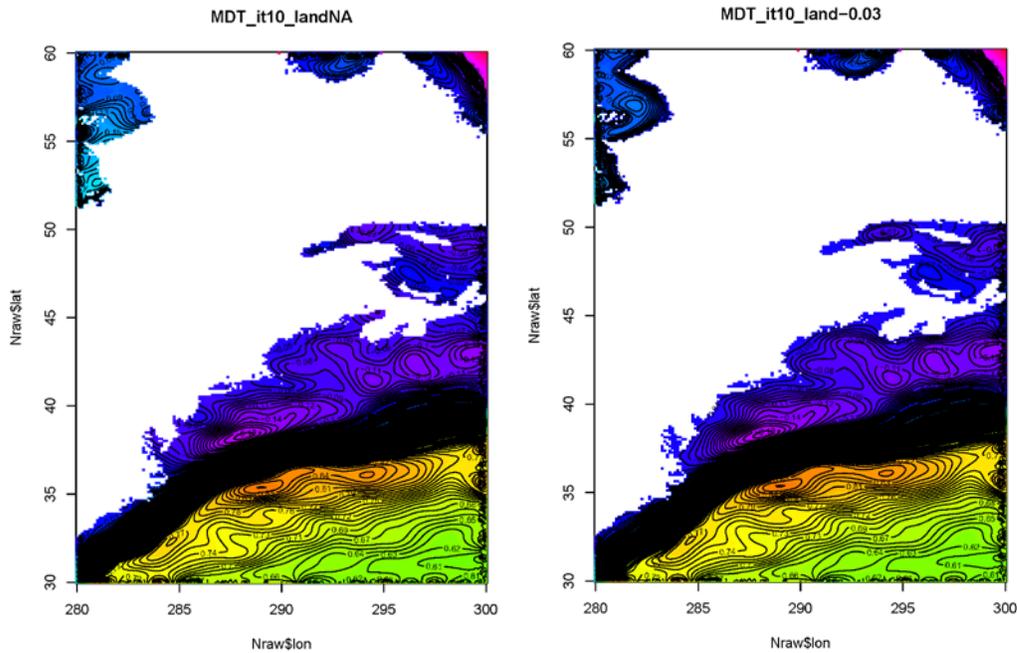
Figure 2: Land value effect. Left: The land values are ignored in the filtering. Right: The land values are set to -0.03 m in the filtering.

2.2 Period issue

Deriving a MDT from either the geodetic method or the oceanographic method entails the use of a reference period. For the oceanographic method the Any Mean sea surface and the reference period used in the project is 2003-2007. To change the reference period of the altimetry based MSS from a period P2 to another period P1 anomalies relative to the period P2 are needed. The expression for the conversion is given by

$$MSS_{P1} = \langle \eta \rangle_{P1} = \langle G+h \rangle_{P1} = G + \langle \overline{h}_{P2} + h'_{P2} \rangle_{P1} = \langle G+h \rangle_{P2} + \langle h'_{P2} \rangle_{P1} = MSS_{P2} + \langle h'_{P2} \rangle_{P1} \ (2)$$

For instance, let us consider the altimetric Sea Level Anomalies distributed by DTU (DTU15), which are referenced to the period 1993-2012. To compute the DTU15 MSS over a different averaging period e.g. 2003-2007, the SLA averaged over 2003-2007 must be added to the DTU15 initial field.

2.2.1 GOCE ++ Approach:

In the GOCE ++ project we have chosen the 2003-2007 averaging period as this was the period giving the highest amount of tide gauges and an adequately long averaging period to obtain a stable average.
We have provided annual averages for each year in the 20 year averaging period as well as an average over the 20 years period relative to the DTU15MSS.

2.3 Filtering

A spatial filter is used to smooth the raw MDT to minimize omission and commission errors from the geoid. The filter is a simple average filter, where the kernel is an average of the nearest neighbors in each direction. Hence the kernel is a nx times ny matrix, where each weight is given by $1/(nx * ny)$. The filter radius is specified in degrees, and subsequently converted to kernel points in the north-south direction by

$$ny = floor \left(\frac{radius}{grid\ resolution} \right) * 2 + 1. \qquad (3)$$

In the east-west direction the number of kernel points nx are scaled by the latitude.

The filter is applied over both the ocean and land. The tide gauge based MDT values are filed in as land values in the altimetric MDT by linear interpolation. Applying the filter with a relative small radius has the effect of smoothing the tide gauge based MDT values in to the coastal regions, without severely affecting the MDT values in the open ocean. The filter is applied iteratively. Under each iteration the land values are reset to their original values. This enhances the effect of transferring the tide gauge based MDT values to the coastal region and the effect of the filter approaches a Gaussian filter. Improved filtering approaches are described in the technical note D6, which will be available from the project webpage http://gocehsu.eu/.

2.4 Error estimate

To derive analytic uncertainty estimates of the filtered MDT is challenging and probably impossible do to correlations in the field. Another approach to derive uncertainty estimates is by using the bootstrap method. A first strategy is to divide the raw MDT of the selected region into blocks. To create new bootstrap data sets we:

1. Sample with replacement between the different blocks of data
2. Derive the filtered MDT for the bootstrap data set
3. Repeat step 1 and 2 N times
4. We can now derive e.g. the standard deviation of the N MDT solutions in each grid cell

The size of the data blocks is specified by the user. The block size should be chosen large enough to ensure that data is independent but not much larger than the size of the filter. If the blocks are too large there will be large gabs in the filtered MDT and the error will be overestimated.

2.5 Height system consistencies

Since different data types are combined; altimetry and gauge based MDTs, special attention must be given to the height reference system. Hence, to minimize biases between the altimetry and tide gauge based MDTs, the following conditions should preferable be met:

- The altimetric and tide gauge based MSS should be referenced to the same reference ellipsoid and be in the same permanent tide system.
- The two MDTs (altimetry and tide gauge) should be based on the same geoid. Hereunder it is important that
    o the geoids are with respect to the same reference ellipsoid and in the same permanent tide systems.

Altimetric heights are defined relative to a reference ellipsoid and relative to a tide system. Furthermore, geophysical and environmental corrections are applied to the individual altimetric heights observations. In some cases, a choice of model or algorithm for the correction must be made. In the following section, we list all the different possibilities, in terms of tidal system, reference ellipsoid and altimetric corrections that will impact the final MSS.

2.5.1 Reference ellipsoid issue

Both altimetric MSS heights and geoid heights are given relative to a reference ellipsoid, which corresponds to a theoretical shape of the Earth. The characteristics of different, currently used, reference ellipsoids are given in Table 1. Before subtracting a geoid from a MSSH, both fields have to be expressed relative to the same reference ellipsoid. If not, the impact on the resulting MDT is large: Figure 3 shows the height differences between the GRIM and TOPEX ellipsoids on a global grid.
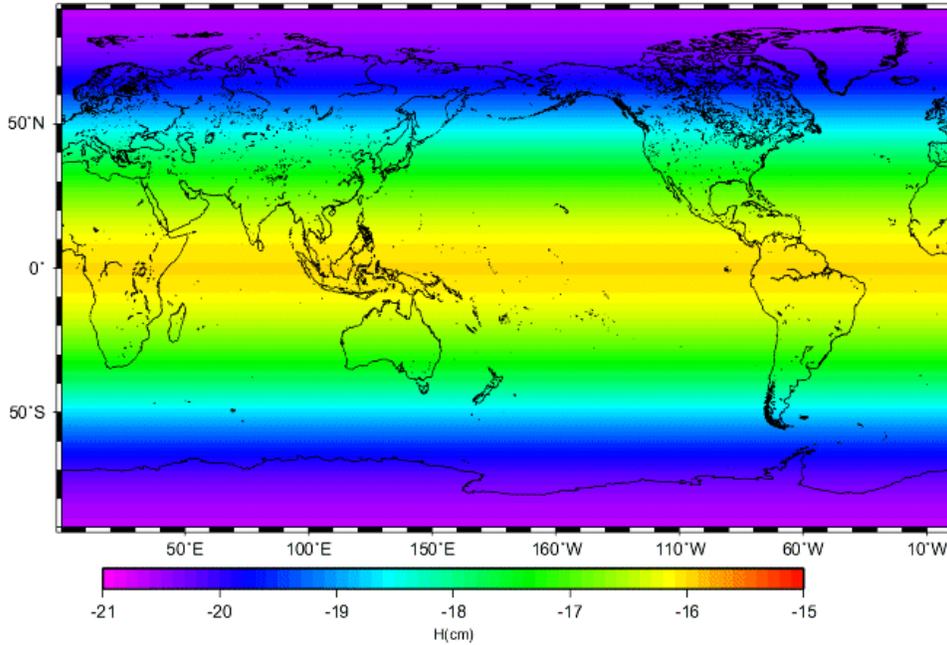
Figure 3: *Height difference between the TOPEX and the GRIM ellipsoids.*

Table 1: *The different reference ellipsoids and their characteristics (semi grand axe a, flattening 1/f and coefficient Gm.*

Ellipsoid name	a (m)	1/f	Gm (m3/s)
"GRIM"	6378136.46	298.25765	398600.4369e9
"TOPEX"	6378136.3	298.257	398600.4415e9
"GRS80"	6378137.0	298.257222101	398600.5e9
"WGS84"	6378137.0	298.257223563	398600.5e9
WGS84 rev 1	6378137.0	298.257223563	398600.4418e9

Altimetric MSS heights are most commonly computed relative to the TOPEX ellipsoid, while the tide gauge MSS heights are relative to the WGS84 ellipsoid. The differences in latitude between these two reference ellipsoids are relatively small. Hence, the following approximate expression can be used to convert the WGS84 to the TOPEX reference ellipsoid.

$$Ellipsoid_{TOPEX} = Ellipsoid_{WGS84} + \Delta h.$$
$$\Delta h = -\big((aTop) - aWGS\big)\cos(\varphi)^2 + (bTop - bWGS)\sin\varphi^2\big). \quad (4)$$

Here $aTop$ and $aWGS$ is the equatorial radius of TOPEX and WGS84, respectively, and $bTop$ and $bWGS$ is the polar radius of TOPEX and WGS84, respectively.

2.5.2   Permanent tide system issue

The geoid can be defined in three different permanent tide systems (Ekman, 1989):
1. **Tide-free:** In this case the effect of the sun and moon is removed.
2. **Mean:** In this case the permanent tidal effect of the sun and moon is considered

3. **Zero:** In this case only the indirect effect of the sun and moon is considered, hence, the effect related to the elastic deformation of the Earth.
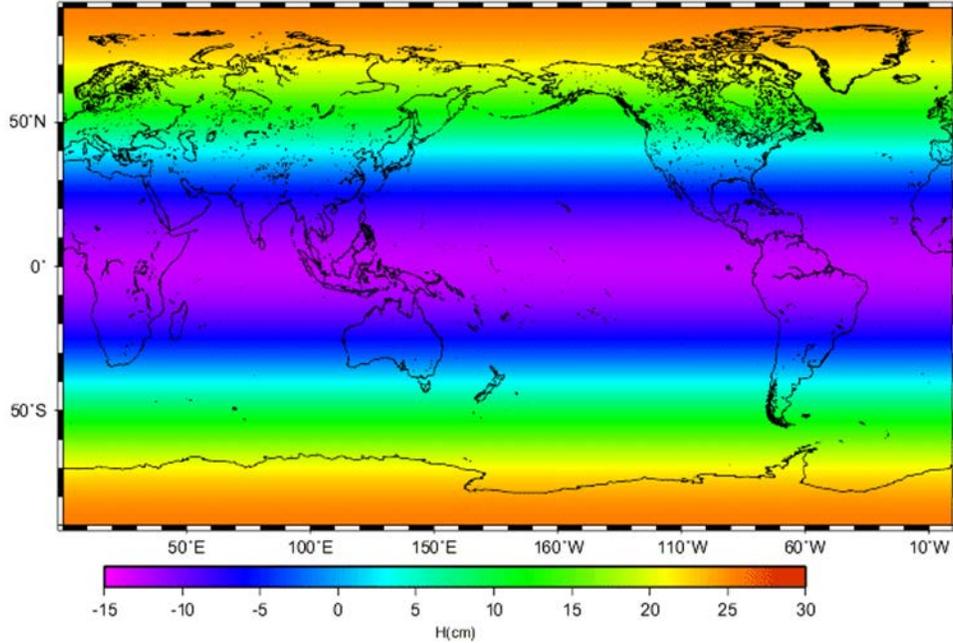
Figure 4: Height difference between the TIDE FREE and the MEAN TIDE reference systems.

Traditionally, altimetry products are given in the mean tide system, while gauge data connected with GPS is given in the tide-free system. An equations to convert between geoids in the two systems (Ekman, 1989) is presented below

$$N_m - N_f = (1 + k)(0.099 - 0.296 * (\sin \varphi)^2)[\text{in m}] \qquad (5)$$

Here N_m and N_f are the geoid undulations in the mean and free-tide system, respectively, φ is the latitude, and k is a Love number, which is usually 0.3. A similar expression exists for converting ellipsoidal height

$$h_m - h_f = h_2(0.099 - 0.296 * (\sin \varphi)^2)[\text{in m}]. \qquad (6)$$

Here, h_m and h_f are the ellipsoidal height in the mean tide and tide free system, respectively. φ is the latitude and the constant $h_2 = 0.62$.

Tide gauge based MSL, which is references with GPS is naturally given in WGS84 ellipsoid height in the tide free system. To synchronize the tide gauge MSL to the altimetry MSL, expression (4) and (6) can be applied. Further issues with respect to the tide system can be solved by applying the same geoid in the derivation of the MDT for both the altimetry and tide gauge based solutions.

GOCE ++ Approach:

In the GOCE ++ approach we have included global grids to enable the transformation from the tide free to the mean tide system. Furthermore, transformation functionality is provided in the software.

2.6 Inverse barometer correction

The ocean reacts roughly as a huge inverted barometer coming up when atmospheric pressure is low and down when pressure rises. For several reasons it has traditionally been an advantage to apply this correction. Its lowers the standard deviation of the sea level anomalies and it eases the comparison with oceanographic models which do not include an atmosphere.

The mean dynamic atmosphere correction from the MOG2D_IB correction over 20 years are shown in Figure 5. The values are ranging from -10 to 10 cm in the global ocean.

Tide gauges measures the physical variation of sea level. This includes the effect of the inverse barometer. Consequently, when integrating with tide gauges we either need to apply the IB correction to the tide gauges or remove the IB correction from the altimetric models in order to make the two MDT quantities consistent.
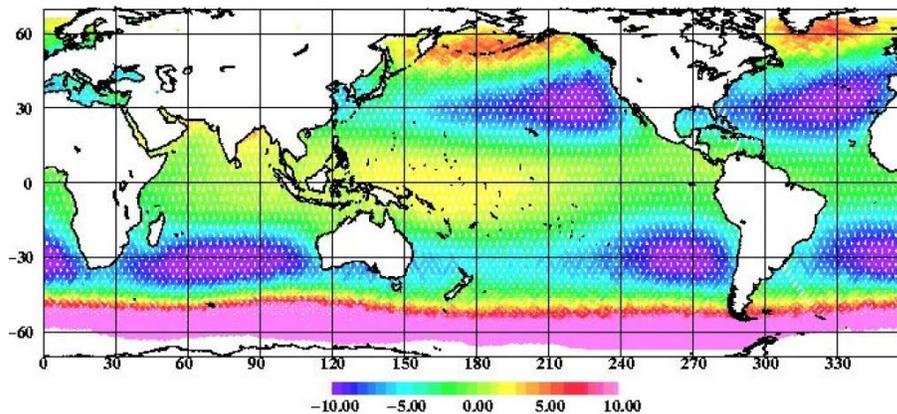
Figure 5: Mean dynamic atmosphere correction from the MOG2D_IB correction over 20 years in centimeters.

2.6.1 GOCE ++ recommendation:

For the computation in GOCE ++ where a certain averaging period is used the averaged MOG2D_IB correction of the chosen period must be computed and re-added to the altimetric MSS/MDT in order to make it consistent with the Tide gauge derived MSS. The quantity must be ADDED to the altimetric MSS.

3 Description of prototype software

This section describes the prototype software for computation of the coastal MDT. Section 3.1 describes the architecture of the software, and section 3.2 gives a short description of the software. A detailed user manual and tutorial is found in Appendix A and B. Appendix C describes the data.

3.1 Architecture

The software architecture is outlined in Figure 6. Data input is shown with green boxes, while purple boxes indicate actions/functions.

- At the zero'th level: If necessary the reference ellipsoid of tide gauge MSS is converted to the reference ellipsoid of the altimetric MSS.
- At the first level the raw altimetric and the tide gauge MDTS are created. If the same geoid model is used, the two MDTs will automatically be in the same permanent tide system.
- At the second level the region of interest is selected.
- At the third level the land/coastal MDT values are estimated based on the selected input data (tide gauge MDT, altimetric MDT or both).
- At the fourth level the raw MDT is filtered, where the ocean values are based on altimetry and the land values are based on input defined at level 3. The filter is applied iteratively N number of times. After each run the land values are reset to the values defined at level 3.
- At the fifth level the final MDT may be displayed and compared with tide gauge estimates. At the level the MDT may also be saved as a NetCDF file.

The output is a MDT which is based on both altimetry and tide gauge data for the selected region.
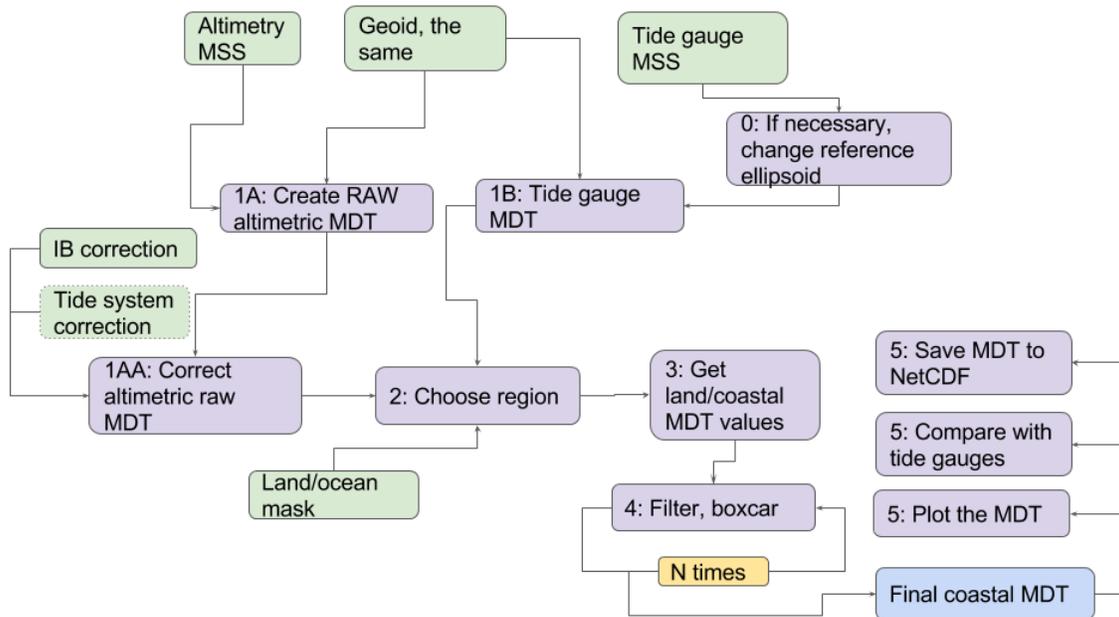
Figure 6: Flowchart of the software architecture. Boxes with a green color indicate data input, while boxes in purple indicate actions/functions.

3.2 Description of software elements

The software "coastMDT" is implemented in the open source programming language "R" https://www.r-project.org/. The software is constructed as an R-package, which works as an R library. The package is available from https://github.com/cavios/coastMDT, where

installation instructions also are found. Installation instructions are also found in Appendix B.

The package "coastMDT" consists of a set of main functions, which are listed and briefly described in Table 2.

Table 2: *Overview of core functions*

Function	Description
compareWithTG	Function to compare altimetric and tide gauge based MDT values at tide gauge stations.
ellipsoidTF2MT	Get correction to go from a tide free to a mean tide ellipsoid.
getData	Function that downloads the data used for constructing the coastal MDT.
getError	Function to estimate the Error of the MDT via the bootstrap approach
getLandVal	Function to estimate MDT values over land/coast.
getSubGrid	Function to extract a regional grid from a global grid.
getSubTG	Function to extract a subset of the tide gauge MDT values.
Grid2file	Function to save the MDT grid to a NetCDF file.
iterativeAveSmoother	Iterative average filter.
plotMDT	Function for plotting the MDT.
readncdf1var	Function to read NetCDF file with one variable.
readRegGridBin	Function to read a regular gridded binary file
tideConvert	Function to convert between different permanent tidal systems.
Wgs2topCorr	Function that estimates the height difference between WGS84 and TOPEX ellipsoids.

The available data, which can be downloaded with the function getData

Data	Description
landmask8	Land/ocean mask on 1/8 degree (0-360 degree) grid.
dDTU15MSS_ref2003_2007	Grid to transform the DTU15 MSS (DTU15MSS)

	to the MSS of the reference period 2003-2007. The grid is defined on 1/8 degree (0-360 degree) grid.
eigen6c4r	Geoid model based on EIGEN-6C4 on 1/8 degree (0-360 degree) grid.
dacCor5Y_2003_2007	Dynamic atmosphere correction for the 5-year reference period 2003-2007 on 1/8 degree (0-360 degree) grid.
ibCor5Y_2003_2007	Inverse barometer corrections for the 5-year reference period 2003-2007 on 1/8 degree (0-360 degree) grid.
TG	Tide gauge based MSL relative to WGS 84 (tide free) ellipsoid heights. The file also contains geoid height based on eigen6c4r.
mean2TF_addThis	Conversion from mean tide to tide-free system on 1/8 degree (0-360 degree) grid.
TF2mean_AddThis	Conversion from tide-free to mean tide system on 1/8 degree (0-360 degree) grid.
difmss15eig6c4r	Raw MDT based on the mean sea surface DTU15MSS and the geoid model eigen6c4r.

3.2.1 Limitations and issues

In the software it is possible to combine altimetry and tide gauge based MDTs to improve the MDT at the coast. However, biases related to different reference systems or other issues may cause non intentional artificial MDT gradients. This is partly accounted for in the software. In the region of interest the difference between the altimetry and gauge based MDT values are estimated. The bias is hereafter estimated as the median of the all differences. *Figure 7* gives an example of unintended MDT gradients around Madagascar, which has arisen due to a bias between the selected land values and the MDT values in the vicinity of the coast.
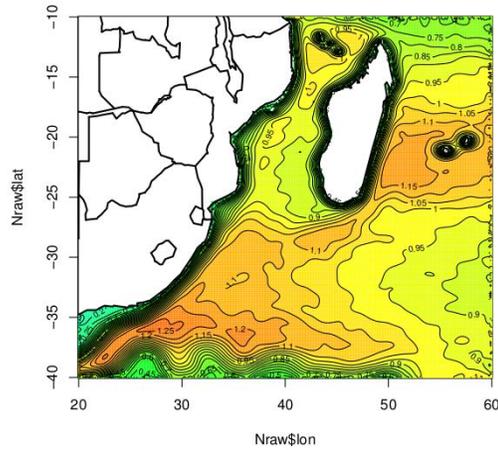
Figure 7: Example of artificial MDT gradient due to bias between land and ocean MDT values.

3.3 Improvements

This section lists various improvements which can be implemented in future versions of the software "coastMDT".

- The distribution of land values: Currently the land values of the MDT are distributed by simple linear or nearest neighbor interpolation. However, a careful evaluations of the MDT length scales in the coastal regions from e.g. ocean model MDTS would be helpful in order to distribute the land values in a more realistic manner.
- Error estimates of the input data e.g. the MSS and tide gauge data will help to improve the final MDT.
- To improve the coastal MDT in poorly surveyed areas. Knowledge of the MDT gradient would be helpful in order to align the MDT contours along the coast.
- Finally other data could be included such as ocean models and drifter data.

4 References

Ekman, M., Impacts of Geodynamic Phenomena on system Heights and Gravity, *Bulletin Geodesique, 63(3), 281-296,1989.*

5 Appendix A: User manual

6 Appendix B: User Tutorial

7 Appendix C: Data manual

Package 'coastMDT'

June 15, 2017

Title Estimate a Coastal MDT Based on Various Input Files

Version 0.0.1

Date 2017-03-01

Author Karina Nielsen, Ole B. Andersen, Per Knudsen, Christopher W. Hughes, Mederic Gravelle and Luciana Fenoglio-Marc.

Maintainer Karina Nielsen <karni@space.dtu.dk>

Description Estimate the coastal MDT. Altimetry data and tidegauge data is combined to form an improved coastal MDT. The software package coastMDT was developed as part of the deliverable D4 in the ESA STSE project ``GOCE++ Dynamic Topography at the coast and tide gauge unification (DYCOT)''. More information regarding the projects are found in the project deliverables D1-D12 which are (or will be) available from the project web page http://gocehsu.eu/. Installation instructions are found in the tutorial ``coastMDT_tutorial.pdf'' available from https://github.com/cavios/coastMDT/tree/master/doc.

License GPL-2

Imports ncdf4,
fields,
FNN,
raster,
sp,
akima,
parallel

URL https://github.com/cavios/coastMDT

LazyData TRUE

BugReports https://github.com/cavios/coastMDT/issues

RoxygenNote 6.0.1

R topics documented:

compareWithTG   *Extract MDT values at TG positions*

Description

The function extracts MDT values at the position of the tide gauges, and compares the MDT values
of the field with MDT values based on the tide gauges.

Usage

```
compareWithTG(TG, dat, lonlim, latlim, boxlon = 3, boxlat = 3,
  export = FALSE, tgfile = "TGcompare.csv")
```

Arguments

TG	Data frame or matrix with tide gauge information. TG should contain at least the columns with the names 'Longitude', 'Latitude', and 'TGMDT'. 'TGMDT' should contain MDT values at the tide gauge positions.
dat	An object as returned by the function 'getSubGrid' or 'iterativeAveSmoother', which includes a list containing a matrix g[lon,lat], a vector lon (longitudes) and a vector lat (latitudes).

`lonlim`	Vector of length 2 with the longitude data grid limits, c(lonlim[1],lonlim[2]). The limits must be given in whole degrees.
`latlim`	Vector of length 2 with the longitude data grid limits, c(lonlim[1],lonlim[2]). The limits must be given in whole degrees.
`boxlon`	The number ((2 x boxlon) +1) of grid cells in the longitude direction, that is used to estimate the altimetry based MDT value at the coast.
`boxlat`	The number ((2 x boxlat) +1) of grid cells in the latitude direction, that is used to estimate the altimetry based MDT value at the coast.
`export`	If true the information estimated in the function is saved in a csv file. The default name is "TGcompare.csv". The file contains; All columns in the data frame TG,Alt_mean MDT,MDT_Alt_sd,bias corrected difference (alt-TG_bias_corr).
`tgfile`	a character string giving the name of the file.

Details

Besides the list, that is returned. A plot of the difference between the altimetry and the tide gauges MDT values is automatically generated

Value

A list that includes: mean: The mean values of the field in the box, defined by boxlon and boxlat at each tide gauge position. sd: The standard deviation of the field in the box, defined by boxlon and boxlat at each tide gauge position. bias: The bias between the mean field values and the tide gauge MDT values. diff: The difference between the mean field values and the bias corrected tide gauge MDT values RMS: The RMS of the mean field values and the tide gauge MDT values

---

`ellipsoidTF2MT`	*Function that estimates the correction to go from a tide free ellipsoid to a mean tide ellipsoid.*

Description

Function that estimates the correction to go from a tide free ellipsoid to a mean tide ellipsoid.

Usage

```
ellipsoidTF2MT(phi, h2 = 0.62)
```

Arguments

`phi`	The latitude in degrees.
`h2`	Love number, the default value is h2=0.62

Details

...

Value

An array with the height differences in meter.

---

getBoxMean   *Helper function: Find mean value in a box*

Description

Helper function: Find mean value in a box

Usage

```
getBoxMean(dat, id, boxlon = 4, boxlat = 4)
```

Arguments

dat	Matrix[lon,lat] with MDT values
id	Matrix[N,2] with row and column id, reprecenting the center of the box
boxlon	Integer. The number ((2 x boxlon) +1) of grid cells in the longitude direction, that is used to estimate the altimetry based MDT value at the coast.
boxlat	Integer. The number ((2 x boxlat) +1) of grid cells in the latitude direction, that is used to estimate the altimetry based MDT value at the coast.

Details

...

Value

list with mean and sd values

---

getCoastLine   *Helper function to getLandVal: Extract the coast line from the land*
                                     mask

Description

Helper function to getLandVal: Extract the coast line from the land mask

Usage

```
getCoastLine(mask, land = 0, water = 1)
```

Arguments

`mask`	Matrix[lon,lat] with land mask values.
`land`	Integer value for land. Default is 0.
`water`	Integer value for land. Default is 1.

Details

...

Value

List with the elements; matrix g[lon,lat], which contains the location of the land value which has a water neighbor. Matrix id which contains two columns; row no and col no of the matrix g where a land value is identified as coast.

`getCount`	*Helper function for the bootstrap function getError*

Description

This function returns a matrix with the number of times each element must be counted.

Usage

```
getCount(IMat, nr, nc)
```

Arguments

`IMat`	a matrix that divides the area into sub areas. It is the output of the function getIdMat.
`nr`	the number of rows in the data matrix (the raw MDT).
`nc`	the number of columns in the data matrix (the raw MDT)

Details

...

Value

matrix[lon,lat] where each element represents the number of times each elements should be counted in the iterative filter, when the sd is estimated for the filtered MDT, by the use of bootstrap.

---

getData   *Function to download data from the web*

Description

Function to download data from the web

Usage

```
getData(localdir = tempdir(), files = NULL,
  url = "https://raw.githubusercontent.com/cavios/coastMDT/master/data/files/")
```

Arguments

localdir	A character string with the name of the directory where the data will be stored. If no name is given the data is automatically stored in a temporal directory.
files	A character vector with the names of the files to be downloaded. If not specified all data for the coastMDT package is downloaded.
url	A character string with the url, that specifies where the data is located. If not specified, the url is where the data for the coastMDT package is located.

Details

...

---

getError   *Estimate a MDT error field via bootstrap*

Description

With the function getError it is possible to estimate an MDT error field via the bootstrap approach.

Usage

```
getError(dat, land, mask, bootNr = 100, nnx = 3, nny = 3,
  ncores = detectCores())
```

Arguments

dat	An object as returned by the function 'getSubGrid' or 'iterativeAveSmoother', which includes a list containing a matrix g[lon,lat], a vector lon (longitudes) and a vector lat (latitudes).
land	Matrix[lon,lat] containing land values

mask	An object as returned by the function 'getSubGrid', which includes a list containing a matrix g[lon,lat], a vector lon (longitudes) and a vector lat (latitudes). mask$g is a Matrix[lon,lat] representing the land mask, where land=0 and water=1.
bootNr	Number of bootstap data sets
nnx	number of grid cells in the east-west direction
nny	number of grid cells in the north-south direction
ncores	Number of available cores
dat	An object as returned by the function 'getSubGrid', which includes a list containing a matrix g[lon,lat], a vector lon (longitudes) and a vector lat (latitudes). The matrix dat$g[lon,lat] containes the values to be filtered.

Details

The data is sampled in blocks, which size is specified by the user in the arguments nnx and nny. nnx and nny should be chosen carefully. If nnx and nny are too small the data will not be independent and the error will be underestimated. If too large, there will be data gabs and the errors will not be representative.

---

getIdMat	*Helper function for getError*

Description

The function getIdMat divides a matrix into sub matrices specified by the arguments nnx and nny .

Usage

```
getIdMat(mask, nnx, nny, nr, nc)
```

Arguments

mask	An object as returned by the function 'getSubGrid', which includes a list containing a matrix g[lon,lat], a vector lon (longitudes) and a vector lat (latitudes). mask$g is a Matrix[lon,lat] representing the land mask, where land=0 and water=1.
nnx	number of grid cells in the east-west direction
nny	number of grid cells in the north-south direction
nr	number of rows in the data matrix
nc	number of columns in the data matrix

Value

List with the elements; matrix[lon,lat] Mat (ids of the submatrices), vector mysamples (the values of the ids), and nrSam (the length of mysamples).

---

getLandComb	*Helper funtion to getLandVal: Finds land values based on tide gauges and altimetry*

Description

Helper funtion to getLandVal: Finds land values based on tide gauges and altimetry

Usage

```
getLandComb(polyCoast, TG, TGcorr, dat, lonlim, latlim, boxlon = 4,
  boxlat = 4)
```

Arguments

polyCoast	Matrix[lon,lat], the out put of the function polygonizeCoast. The matrix contains the coastlines of the region defined by lonlim and latlim, where the integer values represents the coast id.
TG	Data frame or matrix with tide gauge information. TG should contain at least the columns with the names 'Longitude', 'Latitude', and 'TGMDT'. 'TGMDT' should contain MDT values at the tide gauge positions.
TGcorr	Vector with bias corrected tide gauge values. Obtained from the helper function getTGVal.
dat	Matrix[lon,lat] with MDT values
lonlim	Vector of length 2 with the longitude data grid limits, c(lonlim[1],lonlim[2]). The limits must be given in whole degrees.
latlim	Vector of length 2 with the longitude data grid limits, c(lonlim[1],lonlim[2]). The limits must be given in whole degrees.
boxlon	Integer. The number ((2 x boxlon) +1) of grid cells in the longitude direction, that is used to estimate the altimetry based MDT value at the coast.
boxlat	Integer. The number ((2 x boxlat) +1) of grid cells in the latitude direction, that is used to estimate the altimetry based MDT value at the coast.

Details

...

Value

Matrix[lon,lat] with MDT land values at the coast line, defined by polyCoast

---

getLandInfo	*Helper function to getLandVal: Estimate land MDT values at the coastline based on altimetry*

Description

Helper function to getLandVal: Estimate land MDT values at the coastline based on altimetry

Usage

```
getLandInfo(mycoast, mask, dat, boxlon = 4, boxlat = 4)
```

Arguments

mycoast	Matrix[N,2] with row and column values of the coast line. mycoast is the out put of helper function getCoastLine
mask	Matrix[lon,lat] representing the land mask, where land=0 and water=1
dat	Matrix[lon,lat] with MDT values
boxlon	Integer. The number ((2 x boxlon) +1) of grid cells in the longitude direction, that is used to estimate the altimetry based MDT value at the coast.
boxlat	Integer. The number ((2 x boxlat) +1) of grid cells in the latitude direction, that is used to estimate the altimetry based MDT value at the coast.

Details

...

Value

Matrix[N,4]; row id, col id, mean MDT value, sd of MDT

---

getLandVal	*Estimates MDT land values based based on altimetry, tide gauges of both*

Description

Estimates MDT land values based based on altimetry, tide gauges of both

Usage

```
getLandVal(dat, mask, lonlim, latlim, TG = NULL, type = "alt",
  intMethod = "lin", boxlon = 4, boxlat = 4)
```

Arguments

`dat`	An object as returned by the function 'getSubGrid', which includes a list containing a matrix g[lon,lat], a vector lon (longitudes) and a vector lat (latitudes).
`mask`	An object as returned by the function 'getSubGrid', which includes a list containing a matrix g[lon,lat], a vector lon (longitudes) and a vector lat (latitudes). mask$g is a Matrix[lon,lat] representing the land mask, where land=0 and water=1.
`lonlim`	Vector of length 2 with the longitude data grid limits, c(lonlim[1],lonlim[2]). The limits must be given in whole degrees
`latlim`	Vector of length 2 with the longitude data grid limits, c(lonlim[1],lonlim[2]). The limits must be given in whole degrees
`TG`	Data frame or matrix with tide gauge information. TG should contain at least the columns with the names 'Longitude', 'Latitude', and 'TGMDT'. 'TGMDT' should contain MDT values at the tide gauge positions.
`type`	Character string representing the data to be used when the land values are estimated. type="tg": tide gauge data is used to estimate the MDT land values, type="alt": altimetry data is used, and type="both": both altimetry and tide gauge data is used.
`intMethod`	Character string describing the interpolation method used. "lin": linear interpolation and "nn": nearest neighbor interpolation
`boxlon`	Integer. The number ((2 x boxlon) +1) of grid cells in the longitude direction, that is used to estimate the altimetry based MDT value at the coast.
`boxlat`	Integer. The number ((2 x boxlat) +1) of grid cells in the latitude direction, that is used to estimate the altimetry based MDT value at the coast.

Details

...

Value

Matrix[lon,lat] with land values

`getSubGrid`	*Extract sub grid*

Description

Extract sub grid

Usage

```
getSubGrid(grid, lonlim, latlim, res = 0.125, glonlim = c(0 + (res/2), 360 -
    (res/2)), glatlim = c(-90 + (res/2), 90 - (res/2)))
```

Arguments

grid	Input grid[longitude,latitude] of type matrix.
lonlim	Vector of length two containing the longitude limits of the sub grid. The limits must be given with the smallest longitude first for example c(270,300), except when the 0 longitude id crossed. In this case for example c(355,10). Acceptable values are between 0 and 360.
latlim	Vector of length two containing the latitude limits of the sub grid.
res	The resolution of the input grid in decimal degrees.
glonlim	Vector of length two containing the longitude limits of the input grid. The default is c(0,360).
glatlim	Vector of length two containing the latitude limits of the input grid. The default is c(-90,90).

Value

List with the elements; matrix g (sub grid), vector lon (longitudes), vector lat (latitudes) ##' @details ...

Examples

```
## Not run: data(landmask8)
out<-getSubGrid(landmask8,c(280,300),c(30,60))
image(out$lon,out$lat,out$g)
## End(Not run)
```

---

getSubTG   *Find subset of tide gauges*

Description

Find subset of tide gauges

Usage

```
getSubTG(TG, lonlim, latlim)
```

Arguments

TG	Data frame or matrix with tide gauge information. TG should contain at least the columns with the names 'Longitude' and 'Latitude'.
lonlim	Vector of length 2 with the longitude data grid limits, c(lonlim[1],lonlim[2]). The limits must be given in whole degrees.
latlim	Vector of length 2 with the longitude data grid limits, c(lonlim[1],lonlim[2]). The limits must be given in whole degrees.

Value

subset of TG

---

getTGCoast	*Helper function to getLandVal: Identify Coast lines with tide gauges*

Description

Helper function to getLandVal: Identify Coast lines with tide gauges

Usage

```
getTGCoast(polyCoast, TG, lonlim, latlim)
```

Arguments

polyCoast   Matrix[lon,lat], the out put of the function polygonizeCoast. The matrix contains the coastlines of the region defined by lonlim and latlim, where the integer values represents the coast id.

TG   Data frame or matrix with tide gauge information. TG should contain at least the columns with the names 'Longitude', 'Latitude', and 'TGMDT'. 'TGMDT' should contain MDT values at the tide gauge positions.

lonlim   Vector of length 2 with the longitude data grid limits, c(lonlim[1],lonlim[2]). The limits must be given in whole degrees.

latlim   Vector of length 2 with the longitude data grid limits, c(lonlim[1],lonlim[2]). The limits must be given in whole degrees

Details

...

Value

Vector with coast id for the tide gauges.

---

getTGid	*Helper function: Finds row and col id of Tide gauges*

Description

Helper function: Finds row and col id of Tide gauges

Usage

```
getTGid(TG, lonlim, latlim)
```

Arguments

TG	Data frame or matrix with tide gauge information. TG should contain at least the columns with the names 'Longitude', 'Latitude', and 'TGMDT'. 'TGMDT' should contain MDT values at the tide gauge positions.
lonlim	Vector of length 2 with the longitude data grid limits, c(lonlim[1],lonlim[2]). The limits must be given in whole degrees.
latlim	Vector of length 2 with the longitude data grid limits, c(lonlim[1],lonlim[2]). The limits must be given in whole degrees.

Value

Matrix[N,2] with row and coulmn id for the tide gauges

---

getTGVal	*Helper function to getLandVal:*

Description

Extract MDT values at TG positions and estimates a potential bias between the tide gauges and the model based MDT.

Usage

```
getTGVal(TG, dat, mask, lonlim, latlim, boxlon = 4, boxlat = 4)
```

Arguments

TG	Data frame or matrix with tide gauge information. TG should contain at least the columns with the names 'Longitude', 'Latitude', and 'TGMDT'. 'TGMDT' should contain MDT values at the tide gauge positions.
dat	Matrix[lon,lat] with MDT values
mask	An object as returned by the function 'getSubGrid', which includes a list containing a matrix g[lon,lat], a vector lon (longitudes) and a vector lat (latitudes). mask$g is a Matrix[lon,lat] representing the land mask, where land=0 and water=1.
lonlim	Vector of length 2 with the longitude data grid limits, c(lonlim[1],lonlim[2]). The limits must be given in whole degrees.
latlim	Vector of length 2 with the longitude data grid limits, c(lonlim[1],lonlim[2]). The limits must be given in whole degrees.
boxlon	Integer. The number ((2 x boxlon) +1) of grid cells in the longitude direction, that is used to estimate the altimetry based MDT value at the coast.
boxlat	Integer. The number ((2 x boxlat) +1) of grid cells in the latitude direction, that is used to estimate the altimetry based MDT value at the coast.

Details

...

Value

list(TGland=out,bias=bias). TGland is data frame with 4 columns; row id, col id, corrected tide gauge value, sd of boxmean value of modeled MDT

---

grid2file   *Write a grid[lon,lat] to a netcdf file*

Description

This function grid2file saves a grid[lon,lat] to a netcdf file.

Usage

```
grid2file(grid, varname = "MDT", filename = "grid.nc")
```

Arguments

grid   An object as returned by the function 'iterativeAveSmoother', which includes
              a list containing a matrix g[lon,lat], a vector lon (longitudes) and a vector lat
              (latitudes).

varname   A string containing the name of the variable, the default is 'MDT'

filename   A string containing the file name, the default is 'grid.nc'

Details

...

Examples

```
## Not run:
grid2file(boxTG_ALT,filename='MDT_filtered.nc')

## End(Not run)
```

```
iterativeAveSmoother
```
                        Iterative box filter

Description

The function `iterativeAveSmoother` is a simple average filter applied nit number of times.
The size of the filter in the E-W direction is scaled according to the latitude.

Usage

```
iterativeAveSmoother(dat, mask, land, radius = 0.15/0.83, nit = 10,
  res = 0.125)
```

Arguments

dat   An object as returned by the function 'getSubGrid', which includes a list con-
                taining a matrix g[lon,lat], a vector lon (longitudes) and a vector lat (latitudes).
                The matrix dat$g[lon,lat] containes the values to be filtered.

mask   An object as returned by the function 'getSubGrid', which includes a list con-
                taining a matrix g[lon,lat], a vector lon (longitudes) and a vector lat (latitudes).
                mask$g is a Matrix[lon,lat] representing the land mask, where land=0 and wa-
                ter=1.

land   Matrix[lon,lat] containing land values

radius   Filter radius. Default is radius=0.15/0.83

nit   Number of iterations of the box filter. Default is nit=10

res   Grid spacing of the matrix dat. Default is dlat=0.125

Details

...

Value

List with the elements; matrix[lon,lat] g (grid), vector lon (longitudes), vector lat (latitudes).

```
iterativeAveSmootherBoot
```
Iterative box filter

Description

The function `iterativeAveSmoother` is a simple average filter applied nit number of times. The size of the filter in the E-W direction is scaled according to the latitude.

Usage

```
iterativeAveSmootherBoot(dat, mask, land, radius = 0.15/0.83, nit = 10,
   res = 0.125, countMat = NULL)
```

Arguments

dat	An object as returned by the function 'getSubGrid', which includes a list containing a matrix g[lon,lat], a vector lon (longitudes) and a vector lat (latitudes). The matrix dat$g[lon,lat] containes the values to be filtered.
mask	An object as returned by the function 'getSubGrid', which includes a list containing a matrix g[lon,lat], a vector lon (longitudes) and a vector lat (latitudes). mask$g is a Matrix[lon,lat] representing the land mask, where land=0 and water=1.
land	Matrix[lon,lat] containing land values
radius	Filter radius. Default is radius=0.15/0.83
nit	Number of iterations of the box filter. Default is nit=10
res	Grid spacing of the matrix dat. Default is dlat=0.125
countMat	A matrix where each element represent the number of times each element i the data matrix "dat" should be counted.

Details

...

Value

List with the elements; matrix[lon,lat] g (grid), vector lon (longitudes), vector lat (latitudes).

---

plotMDT	*Plot MDT grid*

Description

Plot MDT grid

Usage

```
plotMDT(dat, zlim, addContour = TRUE, conlev = 0.05, TGdat = NULL,
   legendUnit = "m", ...)
```

Arguments

dat	An object as returned by the function 'getSubGrid' or 'iterativeAveSmoother', which includes a list containing a matrix g[lon,lat], a vector lon (longitudes) and a vector lat (latitudes).
zlim	Range of the MDT values given as a Vector of length 2.
addContour	Bolean; To add a contour plot. Default is TRUE
conlev	The spacing between contour lines given in meters. The default is 0.05.
TGdat	MDT tide gauge data file. The file TGdat must contain at least the columns; Longitude, Latitude, TGMDT. The default is NULL.
...	Additional arguments to image.plot from fields

Details

...

---

polygonizeCoast	*Helper function to getLandVal: Turns land mask matrix into polygons*

Description

Helper function to getLandVal: Turns land mask matrix into polygons

Usage

```
polygonizeCoast(mask, landVal = 0)
```

Arguments

mask	Matrix[lon,lat] with land mask. Land=0 (default) and water=1.
landVal	integeer representing the land value in the mask

Value

Matrix[lon,lat] whith coast line ids ##' @details ...

---

readncdf1var   *Read net cdf file with one variable*

Description

This function `readncdf1var` ....

Usage

```
readncdf1var(filename)
```

Arguments

`filename`   String containing the filename

Value

Matrix var[longitude,latitude] ##' @details ...

Examples

```
## Not run:
mydat<-readncdf1var('landmask8.nc')

## End(Not run)
```

---

readRegGridBin   *Function that reads a regular global binary grid.*

Description

Function that reads a regular global binary grid.

Usage

```
readRegGridBin(filename, nx = 2880, ny = 1440, res = 0.125, ...)
```

Arguments

`filename`   A character string with the file name.

`nx`   Number of rows in the grid (longitude). Deafault is nx=2880.

`ny`   Number of columns in the grid (latitude). Deafault is ny=1440.

`res`   The grid spacing in degrees. Default is res=0.125.

`...`   Additional arguments to readBin.

Details

The default is grid is a 1/8 degree grid which is 2880 longitudes by 1440 latitudes: longitudes (0.5,1.5,2.5 .... 2879.5)/8 degrees, latitudes -90 + (0.5,1.5,2.5 .... 1439.5)/8 degrees. The type is real*4, hence the length of the file i 4*nx*ny. The unit is meter.

Value

An object of the type coastMDT; a list containing a matrix g[lon,lat], a vector lon (longitudes) and a vector lat (latitudes).

---

tideConvert   *Function for converting between different permanent tide systems.*

Description

Function for converting between different permanent tide systems.

Usage

```
tideConvert(phi, convtype, k = 0.3)
```

Arguments

phi	The latitude in degrees.
convtype	A character string giving the type of conversion. The legal strings are; 'MT2ZT', 'ZT2MT', 'ZT2TF', 'TF2ZT', 'MT2TF', and 'TF2MT'. Here, MT is mean tide, ZT is zero tide and TF is tide free (or nontidal)
k	is a love number, the default value is k=0.3

Details

The conversion expressions are based on Ekman, 1989. The correction must be added.

Value

The conversion correction; An array of height differences in meters.

wgs2topCorr	*Function that estiamtes the height difference between WGS84 and Topex ellipsoids*

Description

Function that estiamtes the height difference between WGS84 and Topex ellipsoids

Usage

```
wgs2topCorr(phi)
```

Arguments

phi   The latitude in degrees.

Details

...

Value

An array with the height differences.

Index

Getting started with the coastMDT package

Karina Nielsen

2017-06-15

Contents

Preface

The software package coastMDT was developed as part of the deliverable D4 in the ESA STSE project "GOCE++ Dynamic Topography at the coast and tide gauge unification (DYCOT)". More information regarding the projects are found in the project deliverables D1-D12 which are (or will be) available from the project web page http://gocehsu.eu/.

Installation

The software is implemented in the open source language "R" which can be found at https://www.r-project.org/. The source code to the "R" software package coastMDT is located at GitHub at https://github.com/cavios/coastMDT

From GitHub

The easiest way to install the package is directly from Github by using the R devtools package. The R-version should be 3.2.2 or higher.

1. Open R
2. Install the devtools library by typing

```r
install.packages('devtools')
```

3. Install the coastMDT package

```r
devtools::install_github("cavios/coastMDT/coastMDT")
```

4. Without devtools

```r
install.packages("https://raw.githubusercontent.com/cavios/coastMDT/master/coastMDT_0.0.1.tar.gz")
```

Dependencies

The packages depends on the following R libraries which can be installed from R with the function `install.packages`. Hence, to install the package "ncdf4" use the following command for the R window:

```r
install.packages("ncdf4")
```

- ncdf4
- smoothie
- fields
- FNN
- raster
- sp
- akima

Getting started with R

The section gives a short introduction to R, which is useful to new R users.

R tutorials can be found at the r-project web side https://cran.r-project.org/manuals.html

Help pages can be accessed by typing "?" in front of a given function. If we want to access the help for the function `plot` we write

```
?plot
```

To start the web based help interface

```
help.start()
```

To exit R write

```
q()
```

Introduction to the package "coastMDT"

coastMDT is an R package built to improve the estimate of the coastal mean dynamic topography (MDT). The package combine altimetry and tide gauge based MDT values. The tide gauge based MDT values are used to constrain the MDT values at the coastline and on land. An iterative average filter is used to smooth the raw MDT. Under each iteration the land values are reset. In this introduction, examples are given to illustrate how to use the package.

Different height systems

The geodetic MDT

The geodetic MDT ξ is constructed from the MSS and the geoid.

$$\xi = MSS - N, \tag{1}$$

where N is the geoid.

To load the package simply write:

```
library(coastMDT)
```

Using the package "coastMDT", an example

This section gives a step by step guide on estimating the coastal MDT.

Download and Load data

The test data sets are kept separate from the package but can be downloaded via the function getData. The data can be saved to a directory. In the example below the data and save in the folder "MDTdat". In the example below it is assumed that the folder "MDTdat" exists. If not it must be created before. If a data directory is not specified, data is saved in a temporary directory.

```
getData() # Data is stored in a temporary directory
getData(localdir="MDTdat") # Data is stored in the directory "MDTdat"
```

A manual, "data4coastMDT.pdf", describing the available data sets are available from Github https://github.com/cavios/coastMDT/tree/master/data

The available data sets are listed below. All the grid data sets in the package are given on an 1/8 degree grid. The first cell is longitude 0 to 1/8 degree, latitude -90 to -90+1/8 degree and the order is east to west, then south to north. The data set "TG" contains information regarding the tide gauge data among other the MSL.

- **DTU15MSS**: DTU15 mean sea surface on 1/8 degree grid (0-360 degree).
- **eigen6c4r**:Geoid model based on EIGEN-6C4 on 1/8 degree grid (0-360 degree).
- **landmask8**:Land/ocean mask on 1/8 degree grid (0-360 degree).
- **difmss15eig6c4r**: Raw MDT based on the mean sea surface DTU15MSS and the geoid model eigen6c4r.
- **dDTU15MSS__ref2003__2007**: Grid to transform the DTU15 MSS (DTU15MSS) to the MSS of the reference period 2003-2007. The grid is defined on 1/8 degree grid (0-360 degree).
- **ibCor5Y__2003__2007**: Inverse barometer corrections for the 5-year reference period 2003-2007 on 1/8 degree grid (0-360 degree).
- **dacCor5Y__2003__2007**: Dynamic atmosphere correction for the 5-year reference period 2003-2007 on 1/8 degree grid (0-360 degree).
- **mean2TF__AddThis**: Grid to go from the mean tide system to the tide free system. The grid is defined on 1/8 degree grid (0-360 degree).
- **TF2mean__AddThis**: Grid to go from the tide free system to the mean tide system. The grid is defined on 1/8 degree grid (0-360 degree).
- **TG**: Tide gauge data. Please, see the data description manual "data4coastMDT.pdf" (https://github.com/cavios/coastMDT/blob/master/data/data4coastMDT.pdf) for a complete description.

The downloaded data sets can easily be loaded into R as demonstrated in the example below. It is here assumed that R is run from the directory, where the data is located.

```
load('DTU15MSS.rda')
```

The users can also import their own data in which case other appropriate R functions should be used depending on the format of the data. The package has a simple function `readncdf1var` to read one-variable NetCDF files.

Further, there is a function `readRegGridBin` that allows the user to read regular binary grids of type real4. The following example demonstrates how to use the function for the ocean MDT model "livc_5yr_p125grid.dat". Here `nx` and `ny` are the dimension of the grid

```
livc5Y<-readRegGridBin('livc_5yr_p125grid.dat', nx = 2880, ny = 1440, res = 0.125)
```

Data for constructing the MDT

The data needed to construct the coastal MDT are listed below. It is here assumed that R is run from the directory, where the data is located.

```
load('DTU15MSS.rda') # MSS
load('eigen6c4r.rda')# Geoid model
load('landmask8.rda')# land/ocean mask
load('dDTU15MSS_ref2003_2007.rda') # grid to correct the MSS to the reference period.
load('ibCor5Y_2003_2007.rda')# Inverse barometer correction
load('TG.rda')# Tide gauge MDT
```

Constructing the raw MDT in the mean tide system, altimetry

The geodetic MDT ξ is constructed from the MSS and the geoid.

$$\xi = MSS - N, \tag{2}$$

where N is the geoid. In R the two grids are simply subtracted.

```
MDTraw<-DTU15MSS-eigen6c4r
```

The data sets DTU15MSS and eigen6c4r are referenced to the TOPEX ellipsoid and are in the mean tide system.

When working with different data types such as altimetry and tide gauge data it is important to make sure that the data are in the same height reference system, time period and that the same corrections has been applied. In this example we will work with tide gauge data in covering the period 2003-2007. Hence the DTU15 MSS needs to be converted to the same reference period.

The inverse barometer correction is applied to the MSS. Hence it must be re-added to the MSS in case the tide gauge data are not IB corrected. In the example below the MSS is corrected for the reference period and the IB effect is re-added to the MSS.

```
MDTraw<-DTU15MSS+dDTU15MSS_ref2003_2007+ibCor5Y_2003_2007-eigen6c4r
```

Constructing the tide gauge MDT in the mean tide system relative to the TOPEX ellipsoid.

Altimetry products are normally given in the mean tide system, while tide gauge products are given in a tide free system. The height difference between the mean tide and the tide free ellipsoid height is given by (Ekman 1989)

$$h_m - h_f = h_2(0.099 - 0.296 * \sin(\phi)^2). \tag{3}$$

Here ϕ is the latitude and $h_2 = 0.62$. This expression is implemented in the function `ellipsoidTF2MT`

The altimetry MSS is referenced relative to the TOPEX ellipsoid, while the tide gauge data is referenced relative to WGS84. Hence we convert the tide gauge data to the TOPEX reference ellipsoid. The following expression approximates the height difference Δh assuming that the difference in latitude is very small.

$$\Delta h = -((aTop - aWGS)cos(\phi)^2 + (bTop - bWGS)sin(\phi)^2). \tag{4}$$

Here ϕ is the latitude, $aTop$ and $aWGS$ is the equatorial radius of TOPEX and WGS84, respectively, and $bTop$ and $bWGS$ is the polar radius of TOPEX and WGS84, respectively.

Finally, the tide gauge based MDT can be calculated as

```
# TG$RLR_ell_2005.5+TG$MSL_2003_2007, MSL above WGS84
# ellipsoidTF2MT(TG$Latitude), conversion of tide free to mean tide ellipsoid
# wgs2topCorr(TG$Latitude),  conversion of WGS84 to TOPEX ellipsoid
TGMDT<-TG$RLR_ell_2005.5+TG$MSL_2003_2007+ ellipsoidTF2MT(TG$Latitude)+
      wgs2topCorr(TG$Latitude)-TG$eigen6c4rC
TG<-cbind(TG,TGMDT) # Attaching the MDT values to the rest of the TG data set.
```

The altimetry and tide gauge MDTs should now be given in the same height reference system, in the same reference period, and the same correction should be applied.
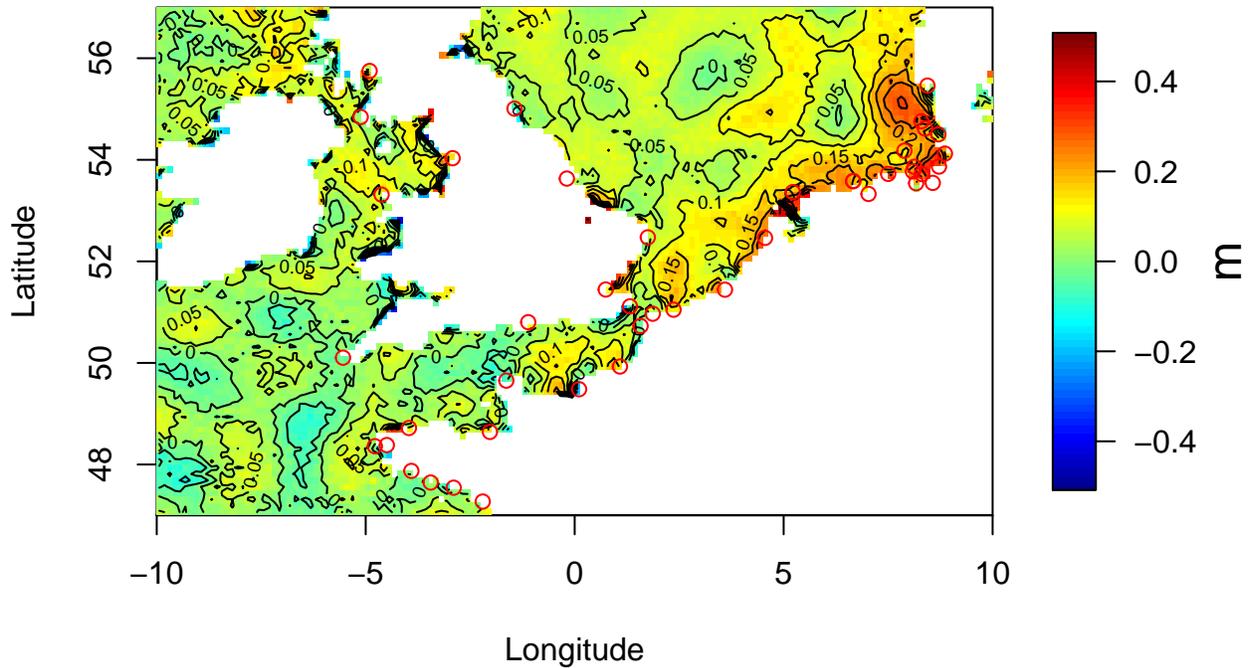
Figure 1: The raw MDT and the location of tide gauges

Extraction a subsection

The available data sets are global,but the user has the possibility to extract regional grids with the function `getSubGrid`. In the example below the coast of Northern Europe is extracted from the raw MDT and the land/ocean mask. The tide gauge data can be extracted with the function `getSubTG`.

```
#Region of interest; here the Northern Europe
lonlim<-c(350,10)
latlim<-c(47,57)
#sub grids and data
rawSub<-getSubGrid(MDTraw,lonlim,latlim)
mask<-getSubGrid(landmask8,lonlim,latlim)
TGsub<-getSubTG(TG,lonlim,latlim)
```

Defining the land values

MDT Land values are estimated with the function `getLandVal`. The land values may be based on tide gauge MDT values, the altimetry alone, or a combination of both. This option is specified with the parameter `type=("tg","alt", or "both")`. In the example below both tige gauge values and altimetry is used to contrain the land MDT values, see figure 2.

```
mylandTG_ALT <- getLandVal(rawSub, mask, lonlim, latlim, TG = TGsub, type = "both",
    intMethod = "lin")
```
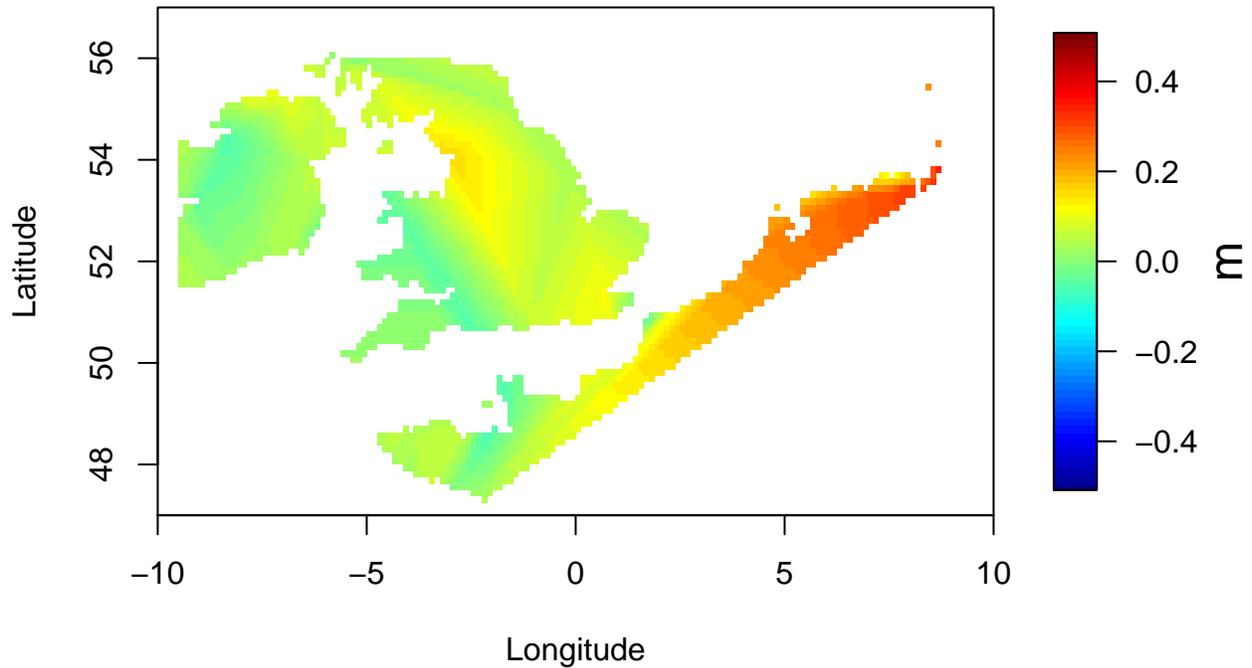
Figure 2: Land values based on tide gauge and altimetry data

```
plotMDT(mylandTG_ALT, c(-0.5, 0.5), addContour = FALSE)
```

Filtering

After the land values are estimated we can start to filter the raw MDT. The package applies an iterative average filter. After each iteration the land values are reset to the original values. It is possible to vary the radius of the filter and the number of iterations that is used. In the example below the default values are used.

```
boxTG_ALT <- iterativeAveSmoother(rawSub, mask, mylandTG_ALT)
```

Error estimate

Due to the complexity of estimating the MDT it is not straight forward to estimate the corresponding error field of the MDT. However, the package allows to user to estimate an error field by using the bootstrap approach. The raw MDT of the selected region is divided into blocks. To create new bootstrap data sets we sample with replacement between the different blocks of data. Each bootstrap data set is filtered. This gives us N different estimates of the MDT in each grid cell from which the standard deviation can be estimated. The size of the data blocks is specified by the user. The block size should be chosen large enough to ensure data independence but not much larger than the size of the filter. If the blocks are to large there will be too
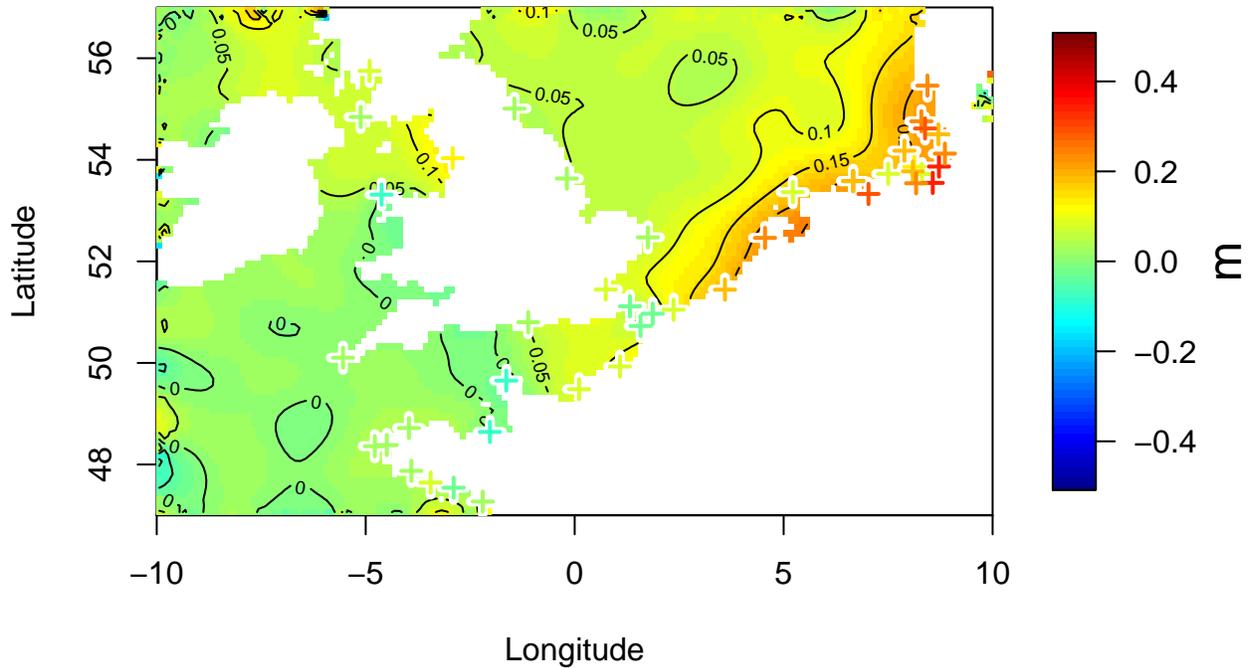
Figure 3: The filtered MDT. The red crosses displays the positions of the tide gauges

large gabs in the filtered MDT and the error will be over estimated. The example below illustrates how to use the function `getError`.

```
sdMDT <- getError(rawSub, mylandTG_ALT, mask, bootNr = 50, nnx = 3, nny = 3)
```

Plotting

The package includes a simple plotting function, so the output MDT can easily be displayed. In this function it is also possible to plot the tide gauge MDT values in the same color scale defined by the option `zlim`, by adding the argument `TGdat`. The example below displays the MDT for the recurring example

```
plotMDT(boxTG_ALT, zlim = c(-0.5, 0.5), conlev = 0.05, TGdat = TGsub)
```

Save output

The filtered MDT can be saved to a NetCDF file with the function `grid2file`

```
grid2file(boxTG_ALT, filename = "MDT_TG_Alt_NEurope.nc")
```

Compare with tide gauge data

The function `compareWithTG` allows to compare the Altimetry based MDT with the tide gauge data. The comparison can be saved to a file with the following command.

```
outTG <- compareWithTG(TGsub, boxTG_ALT, lonlim, latlim, export = TRUE, tgfile = "myfile.csv")
```

Save plot to a pdf file

The MDT plot can be saved to a pdf file with the function `pdf`, see `?pdf` for help

```
pdf("myMDT.pdf")
plotMDT(boxTG_ALT, c(-0.5, 0.5), conlev = 0.05)
points(TGsub$Longitude, TGsub$Latitude, col = "red", pch = 3)
dev.off()
```

Summary

The compleete example is summarized below

```
library(coastMDT)
# download data
getData()
# load data
load("DTU15MSS.rda")
load("dDTU15MSS_ref2003_2007.rda")
load("eigen6c4r.rda")
load("ibCor5Y_2003_2007.rda")
load("landmask8.rda")
load("TG.rda")
# construct the raw altimetry MDT
raw <- DTU15MSS + dDTU15MSS_ref2003_2007 + ibCor5Y_2003_2007 - eigen6c4r
# construct tide gauge MDT
TGMDT <- TG$RLR_ell_2005.5 + TG$MSL_2003_2007 + ellipsoidTF2MT(TG$Latitude) +
    wgs2topCorr(TG$Latitude) - TG$eigen6c4rC
TG <- cbind(TG, TGMDT)  # Attaching the MDT values to the rest of the TG data set.
# define sub region
lonlim <- c(350, 10)
latlim <- c(47, 57)
# extract sub grids
mask <- getSubGrid(landmask8, lonlim, latlim)
rawSub <- getSubGrid(raw, lonlim, latlim)
TGsub <- getSubTG(TG, lonlim, latlim)
# define land values
mylandTG_ALT <- getLandVal(rawSub, mask, lonlim, latlim, TG = TGsub, type = "both",
    intMethod = "lin")
# filter MDT
boxTG_ALT <- iterativeAveSmoother(rawSub, mask, mylandTG_ALT)
# plotting
plotMDT(boxTG_ALT, c(-0.5, 0.5), conlev = 0.05, TGdat = TGsub)
```

References

Ekman, Martin. 1989. "Impacts of geodynamic phenomena on systems for height and gravity." *Bulletin Géodésique* 63 (3). Springer-Verlag: 281–96. doi:10.1007/BF02520477.

Description of data for the coastMDT package

February 9, 2017

DTU15MSS   *DTU15MSS*

Description

DTU15MSS is the DTU15 mean sea surface (MSS). DTU15MSS is a 2880 x 1440 matrix. The first cell is longitude 0 to 1/8 degree, latitude -90 to -90+1/8 degree cells are all 1/8 by 1/8 degree order is east to west, then south to north

The MSS is in meters and are referenced to the TOPEX ellipsoid. The grid is in the permanent mean tide system.

Usage

```
data("DTU15MSS")
```

Format

A matrix[lon,lat] of dimension 2880 x 1440

Details

...

Source

...

References

Created by Ole B. Andersen `<oa@space.dtu.dk>`

Examples

```
data(DTU15MSS)
```

`TF2mean_AddThis` *TF2mean_AddThis*

Description

Grid to go from tide free to mean tide. The grid should be added. TF2mean_AddThis is a 2880 x 1440 matrix.

Usage

```
data("TF2mean_AddThis")
```

Format

A matrix[lon,lat] of dimension 2880 x 1440

Details

...

Source

...

References

Created by Ole B. Andersen <oa@space.dtu.dk>

Examples

```
data(TF2mean_AddThis)
```

`TG` *TG*

Description

Tide gauge information and data: MSL estimates relative to WGS84 must be created by adding the RLR heights to the MSL estimates for the respective reference periods.

Usage

```
data(tideGauge)
```

Format

A data frame with 302 observations of the following variables.

PSMSL_ID a numeric vector

Latitude a numeric vector

Longitude a numeric vector

Station_Name a factor vector

Coastline a numeric vector

Station a numeric vector

QC_Flag a factor vector

GPS_type a factor vector

GPS_code a factor vector

RLR_ell_2005.5 a numeric vector

Uncertainty_2005.5 a numeric vector

MSL_2003_2007 a numeric vector

RLR_ell_2010.5 a numeric vector

Uncertainty_2010.5 a numeric vector

MSL_2008_2012 a numeric vector

IB_2003_2007 a numeric vector

IB_2008_2012 a numeric vector

DAC_2003_2007 a numeric vector

DAC_2008_2012 a numeric vector

egm08C a numeric vector, EGM2008 geoid height above TOPEX ellipsoid. The values have been extracted the high resolution EGM2008

egm08H a numeric vector, EGM2008 geoid height above TOPEX ellipsoid. The values have been extracted a 1/8 degree version of EGM2008

eigen6c4rC a numeric vector, Eigen6c4r geoid height above TOPEX ellipsoid. The values have been extracted a 1/8 degree version of Eigen6c4r

Details

To construct MSL values above WGS84 for the reference period 2003-2007; MSLWGS84=RLR_ell_2005.5+ MSL_2003_2007. MSLWGS84 will be in the tide free system.

Source

...

References

Create by Mederic Gravelle and Karina Nielsen

Examples

```
data(TG)
```

```
dDTU15MSS_ref2003_2007
```
dDTU15MSS_ref2003_2007

Description

Grid to transform the DTU15 MSS (DTU15MSS) to the MSS of the period 2003-2007. The grid should be added. dDTU15MSS_ref2003_2007 is a 2880 x 1440 matrix. The unit is meter.

The first cell is longitude 0 to 1/8 degree, latitude -90 to -90+1/8 degree cells are all 1/8 by 1/8 degree order is east to west, then south to north

Usage

```
data("dDTU15MSS_ref2003_2007")
```

Format

A matrix[lon,lat] of dimension 2880 x 1440

Details

...

Source

...

References

Created by Ole B. Andersen <oa@space.dtu.dk>

Examples

```
data(dDTU15MSS_ref2003_2007)
```

```
dacCor5Y_2003_2007
```
dacCor5Y_2003_2007

Description

Dynamic atmosphere corrections for the reference period 2003-2007. The corrections are given on the following grid:

2880 = longitudes (0.5+(0,1,2....2879))/8. degrees 1440 = latitudes (0.5+(0,1,2....1439))/8. -90 degrees

These numbers should be added to ssh in metres to give ib-corrected ssh

They are derived from the DAC, as provided by aviso at 6-hour and 1/4 degree resolution.

dacCor5Y_2003_2007 represents the 5-year average of the period 2003 to 2007.

Usage

```
data("dacCor5Y_2003_2007")
```

Format

A matrix[lon,lat] of dimension 2880 x 1440

Details

...

Source

...

References

Created by Christopher W. Hughes <cwh@noc.ac.uk>

Examples

```
data(dacCor5Y_2003_2007)
```

```
difmss15eig6c4r          difmss15eig6c4r
```

Description

difmss15eig6c4r is an unfiltered MDT based on the MSS DTU15 and the geoid model Eigen6c4r. difmss15eig6c4r is a 2880 x 1440 matrix. The first cell is longitude 0 to 1/8 degree, latitude -90 to -90+1/8 degree cells are all 1/8 by 1/8 degree order is east to west, then south to north. The MDT values a in meters and are referenced to the TOPEX ellipsoid. The grid is in the permanent mean tide system.

Usage

```
data("difmss15eig6c4r")
```

Format

A matrix[lon,lat] of dimension 2880 x 1440

Details

...

Source

...

References

Created by Per Knudsen

Examples

```
data(difmss15eig6c4r)
```

---

eigen6c4r   *eigen6c4r*

Description

eigen6c4r is a geoid model based on EIGEN-6C4. Eigen6c4r is a 2880 x 1440 matrix. The first cell is longitude 0 to 1/8 degree, latitude -90 to -90+1/8 degree cells are all 1/8 by 1/8 degree order is east to west, then south to north.

The unit is in meters. The geoid is referenced to the TOPEX ellipsoid and is given in the permanent mean tide system.

Usage

```
data("eigen6c4r")
```

Format

A matrix[lon,lat] of dimension 2880 x 1440

Details

...

Source

...

References

F\"orste, Christoph; Bruinsma, Sean.L.; Abrikosov, Oleg; Lemoine, Jean-Michel; Marty, Jean Charles; Flechtner, Frank; Balmino, G.; Barthelmes, F.; Biancale, R. (2014): EIGEN-6C4 The latest combined global gravity field model including GOCE data up to degree and order 2190 of GFZ Potsdam and GRGS Toulouse. GFZ Data Services. http://doi.org/10.5880/icgem.2015.1

Examples

```
data(eigen6c4r)
```

`ibCor5Y_2003_2007` *ibCor5Y_2003_2007*

Description

Inverse barometer correction for the 5 year reference period given on the following grid:

2880 = longitudes (0.5+(0,1,2....2879))/8. degrees 1440 = latitudes (0.5+(0,1,2....1439))/8. -90 degrees

These numbers should be added to ssh in metres to give ib-corrected ssh

They are derived from monthly-mean sea-level pressure from the era-interim analysis, as provided by ECMWF at 1/4 degree resolution. The conversion from pressure in Pa to sea level correction in m is given by correction = -1.e-4*(0.99*(p-101100.)-0.974*(pglob-101100.)) where p is pressure and pglob is global-ocean-average pressure at the same time.

(the reason for the different coefficients, 0.99 and 0.974, is that global ocean average pressure does produce a small sea level change due to compressibility of seawater - without this effect, the formula would reduce to -1.e-4*0.99*(p-pglob))

ibCor5Y_2003_2007 represents the 5-year average of the period 2003 to 2007.

NOTE: Gibbs fringes can be seen in both these products, slightly larger in the ib than the dac, but are typically at the 1 mm level or less (the largest ocean values occur by the Pacific South American coast).

Usage

```
data("ibCor5Y_2003_2007")
```

Format

A matrix[lon,lat] of dimension 2880 x 1440

Details

...

Source

...

References

Created by Christopher W. Hughes <cwh@noc.ac.uk>

Examples

```
data(ibCor5Y_2003_2007)
```

---

landmask8	*landmask8*

Description

landmasks from GEBCO2014, on a 1/8 degree grid.

landmask8 is a 2880 x 1440 matrix

first cell is longitude 0 to 1/8 degree, latitude -90 to -90+1/8 degree cells are all 1/8 by 1/8 degree order is east to west, then south to north

value is 1 for any cell which is 50 0 for any cell which is less than 50

isolated ocean points have been removed (excluding Black Sea and Sea of Marmara)

Usage

```
data(landmask8)
```

Format

A matrix of dimension 2880 x 1440

Details

points below sea level, but enclosed by land (e.g. Caspian Sea, Dead Sea) are here classed as land.

GEBCO2014 original data have been modified by hand to allow the Sea of Marmara and the Black Sea to be connected. This involved converting 1 point in the Dardanelles (strait connecting Sea of Marmara to the Mediterranean), and 3 points in the Bosphorus (strait connecting Sea of Marmara to the Black Sea), from land to ocean. For reference, these points are:

i values (counting in range 1 to 43200) = 3167, 3484, 3486, 3486 j values (counting in range 1 to 21600) = 15618,15725,15726,15729

Source

...

References

Create from GEBCO2014 by Chris Hughes

Examples

```
data(landmask8)
```

```
mean2TF_AddThis        mean2TF_AddThis
```

Description

Grid to go from mean tide to tide free. The grid should be added. mean2TF_AddThis is a 2880 x 1440 matrix.

Usage

```
data("mean2TF_AddThis")
```

Format

A matrix[lon,lat] of dimension 2880 x 1440

Details

...

Source

...

References

Created by Ole B. Andersen <oa@space.dtu.dk>

Examples

```
data(mean2TF_AddThis)
```

Index

7 Appendix F, D5: Test and Validation Report
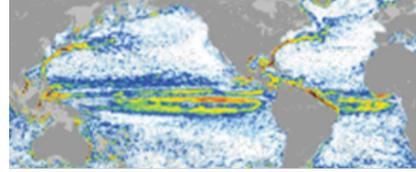
GOCE++ Dynamic Topography at the coast and tide gauge unification
GOCE ++ DYCOT

TITLE.

D5 - WP2200 Technical Report: Test and Validation Report

Author

Luciana Fenoglio

ESTEC Ref: ITT AO/1-8194/15/NL/FF/gp "GOCE++ Dynamic Topography at the coast and tide gauge unification"- Coordinator: Ole B. Andersen (DTU)

DOCUMENT CHANGE LOG				
Rev.	Date	Sections modified	Comments	Changed by
1	11-01-2017	All	Draft	Luciana Fenoglio
2	29-05-2017	All	Draft	Luciana Fenoglio
3	19-08-2017	All	Draft	Luciana Fenoglio

Contents

1. Introduction

Aim of the report is to test and validate the software described in D4 and to present results for some test cases. We distinguish two parts: test software capability and validate the approach in two well-surveyed areas. The first section deals with tests of the software capability. In the second section the approach is validated in two well surveyed areas. The software used here is dated 15 June 2017, the downloaded tarred gzipped file is named coastMDT_0.0.1.tar.gz

2. Test software capabilities

2.1. Installation of the software under Linux SUSE and macOS

Both in Linux and in macOS Sierra V10.12.2 the commands described in Document 1 Tutorial (Getting started) do not fully work. We install from Github successfully from Github without devtools as following described. We use wget from https://github.com/cavios/cooastMDT and store in Downloads coastMDT_0.0.1.tar.gz. Finally, we run R and from there we use the command to install the package: Install.packages("coastMDT_0.0.1.tar.gz")

2.2. Software documentation

The software documentation consists of four documents available for download in http://gocehsu.eu under Deliverables. The main document is the technical note in delivery D4 (Nielsen at al., 2017d) together with its three appendices A (User Manual), B (User tutorial) and C (Data manual) (Nielsen 2017a,b,c).

It has been recommended in previous version of this document to add version number, which is useful for referencing purposes, however the version is here still the same, i.e. 0.0.1, as the tarred file name says.

2.2.1 Document Number 1: Tutorial (Getting started)
Version number and datum were both missing in previous versions. The actual version is dated June 15 2017.

2.2.1.1 Section "Getting started with R" includes only 3 commands. Few basic commands could be added, for example:
source('Test_NSE.R')
setwd()
setwd("..")   go back of one directory
setwd('..')
getwd()   show working directory
list.files()   list files in the actual R directory
vi(file="AUS_v2.R")   use vi command to edit files
attributes(livc5Y)   see content of variable
min(livc5Y$lon)

The reader should know that, when data have been downloaded, the command getdata() need to be commented in the scripts and the data loaded from the directory where they are. We have the data stored in the working directory.

2.2.1.2 Results of compareWithTG need small changes.
Firstly, the numbers output of this function (see Figure 1) are not fully readable in Figure 2 because the text "Bias corrected RMS" is too long. This happens in each of the following figures (2, 4 to 12).

Secondly, the correspondence between the results of the program in Figure 1 and the values written in the Figure 2 is not clear. Also, the order of the variables is not the same in the User manual and in the output itself, which is confusing for the reader. We suggest to keep the same order in description and software realisation, and to clearly define what RMS and bias is (see point below, Thirdly…)

*Value :A list that includes: **mean:** The mean values of the field in the box, defined by boxlon and boxlat at each tide gauge position. **sd:** The standard deviation of the field in the box, defined by boxlon and boxlat at each tide gauge position. bias: The **bias** between the mean field values and the tide gauge MDT values. **diff:** The difference between the mean field values and the bias corrected tide gauge MDT values **RMS**: The RMS of the mean field values and the tide gauge MDT values*

Thirdly, the definition itself of RMS and bias needs a reformulation. See below:

RMS *= root mean square of the differences between the TG_ MDT at a given tide gauge and the mean of the altimeter values in each of the boxes corresponding to the tide gauge (for example for 17 TGs we have 17 differences and the RMS is computed).*

 bias *= the median of the differences between the TG_ MDT at a given tide gauge and the mean of the altimeter values in each of the boxes corresponding to the tide gauge (for example for 17 TGs we have 17 differences and the median is computed).*

In cross-validation analysis (Fenoglio-Marc et al. 2015) we do not use for the statistic metrics mean and RMS, but mean and Standard deviatuion, because meanand RMS are still related! I therefore strongly suggest to substitute RMS with STD. This was already suggested in the previous version of this document. Note that numbers in columns 4 to 7 of Table 3 are the variabiles §RMS and $bias reported in the example in Figure 1.

Finally, the cvs file output of compareWithTG is not directly recognized by excel. The programmer is invited to run the script available as appendix, check, change and report when necessary.

```
$mean
 [1] 0.2047013 0.1802421 0.2418554 0.2266128 0.2110984 0.2205870 0.2385085
 [8] 0.2025666 0.2239497 0.2322080 0.2183864 0.2449474 0.2303147 0.1824470
[15] 0.1883144 0.1802421 0.2167141

$sd
 [1] 0.0021629119 0.0029219745 0.0026872267 0.0119917492 0.0009215841
 [6] 0.0013476628 0.0029354656 0.0021689534 0.0033666095 0.0034806607
[11] 0.0036938466 0.0031452061 0.0047174717 0.0026480981 0.0032830889
[16] 0.0029219745 0.0012543727

$diff
 [1] -0.022567906 -0.055886890 -0.094372361  0.120759213 -0.014425409
 [6]  0.025443501  0.000000000  0.021018907  0.075912209  0.131662015
[11]  0.016090399 -0.071890247  0.009058008  0.095213969 -0.093341059
[16] -0.004005197 -0.048905194

$RMS
[1] 0.0673933

$bias
[1] -0.009632008
```

Figure 1. Output of function compareWithTG
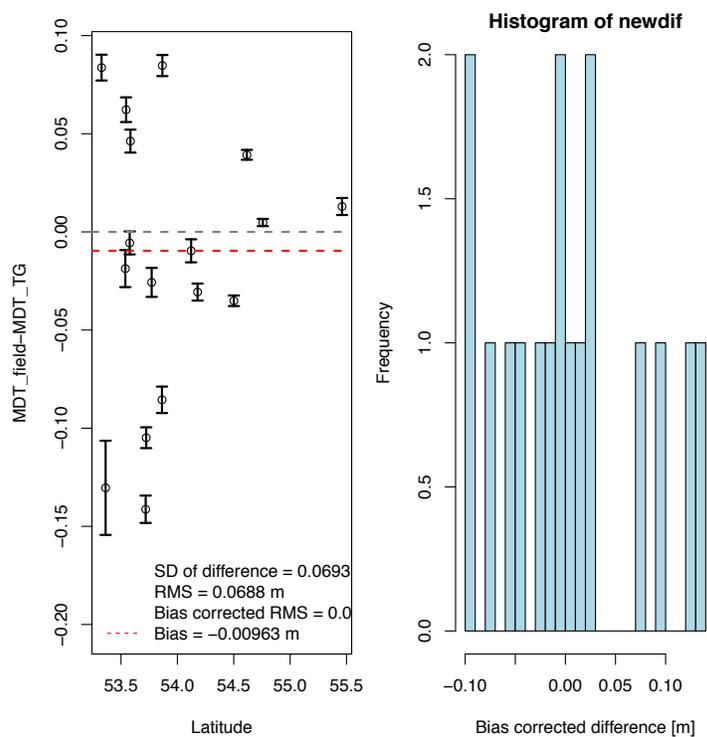
Figure 2. Figure corresponding to output of function compareWithTG in Figure 1. See appendix to this document for script.

2.2.1.3 Description on use of a binary file, missing in previous versions, is present in latest version. Useful functions are:
    "ReadRegGridBin" which transform in dat file
    "grid2file" which transfom in nc file
    "getSubGrid" to make a subgrid
    "subgrid" (3 elements) can be input to compareWithTG

2.2.1.5 An example for the script is given in "Summary". Another example including more commands is found in the appendix to this document.

2.2.1.6 Error estimation is obtained by calling:

mySD<-getError(rawSub,mylandTG_ALT,mask,bootNr=100,nnx=3,nny=3)

The command allows selection of nnx and nny. Figure 1 shows results for different values of nnx and nnx, here respectivedy 3,2 and 1. As expected the higher error is found in coastal region. Values of nnx/nny near to 3 is realistic.
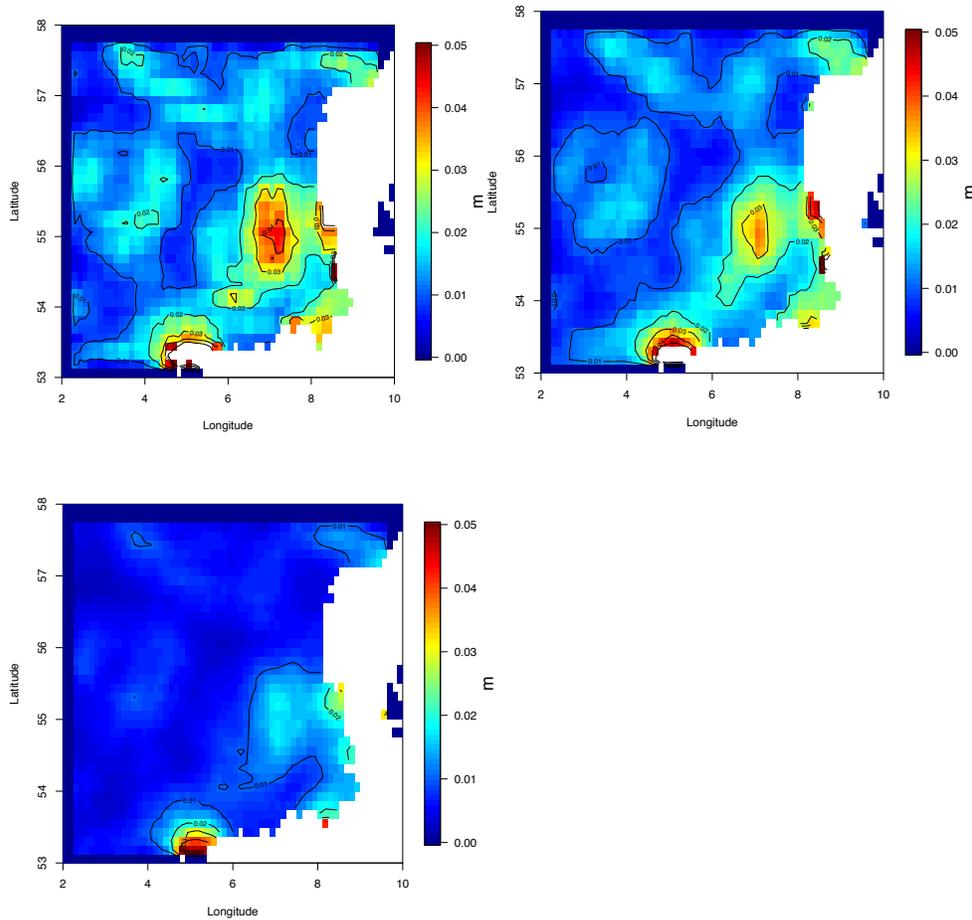
Figure 3. Map of errors for nnx/nny equal to 3 (a), 2 (b) and 1(c).

2.2.2 Document Number 2: User Manual (Package 'coastMDT') Nielsen (2017b).
Version number and datum were both missing in previous releases. The actual version is dated June 15 June. Version Number is not given.

2.2.2.1 The routines in the downloaded directory coastMDT-master/coastMDT/R are 23 and 25 are the functions listed in the User Manual. More information on the correspondence between the package and the description would be helpful to the reader, as already suggested.
The function helper.R includes getBoxMean, getIdMat and getSubTG. TideConvert.R is not in the R directory mentioned above. Needs clarification.

2.2.3 Document Number 3: Data description Nielsen K. (2017c).
Version number and datum were both missing in previous releases. The actual version is dated February 9. Version Number is not given.

The inclusion of ocean model was agreed at the MTR and still missing in the documentation and figures. A script including use of models is available in the appendix. The availability of further input data, stored at Uni Bonn, need to be specified as well. Few datasets, which were not listed in Delivery D2, are now included in the Bonn database.
1) the inverse barometer correction, as gridded yearly and monthly means over the time of availability of data including the interval 1993-2016. We have selected the 5-year time interval from start 2003 to end 2007 as interval of analysis, as common to most of data.
2) the nine ocean models, delivered on October 2016, are slightly different from D3.
3) The tide gauge with ellipsoidal height are now 300.

Drifters and ocean model data not used in the software. The output of the package are MDT evaluated from TG, altimetry and model data over a time interval. Maps of MDT and single values at the tide gauge stations are color-coded. Statistics are available from the figures or extractable when the program is run, for example from the output of Routine "compareWithTG".

Data Type	Quantity	Name of Products	In server
Altimeter data	Ell. heights	AVISO, RADS,CryoSat-2, Topex/Poseidon, Jason, Envisat	
Bathymetry	depth	GEBCO_2014	
Geoid	height	TUM2013C, GGM05C, EIGEN6C4, GOCO05C, EGM08, DIR5C	
Mean Sea Surface	Ell. height	DTU15MSS, DTU13MSS, CLS	
Mean dynamic Topography	height	DTU15MDT, DTU13MDT	
Ocean Models Model grids	11 / 9	EccoG, NemoQ, Nemo12, Livc, Livsr, Livwd, Ecco2, CS3X	Aviso, ecco2, eccog, livc,livs,nemo12a,nemo12b, nemoq,tum13
Tide gauge data	Time-series	PSMSL, local organisation	300 stations
Tide gauge GPS	Ell. heights	300	
Drifter mean velocities	Velocity	UHDTU15MGV	
Inverse Barometer		Dac, Ib to be added to ssh (m)	Yearly averages and average over 2003-2007

Table 1. Data and models used (status May 2017)

Variable Name	Definition
PSMSL ID	column 2 in http://www.psmsl.org/data/obtaining/
Latitude	column 3
Longitude	column 4
Station name	column 1
Coastline	column 8
Station	column 9
QC Flag	this project
GPS Number source (GPS code)	this project
InformationSource	this project (PLW, MG, LFWS, LFRW, Lin)
Ellipsoidal height (RLR or TG0) 2005.5	this project
Ellipsoidal height (RLR or TG0) 2010.5	this project
MSL [2003-2007] [m]	this project
MSL [2008-2012] [m]	this project
IB [2003-2007]	this project
IB [2008-2012] [m]	this project
DAC [2003-2007] [m]	this project
DAC [2008-2012] [m]	this project

Table 2. Update of Content of PSMSL_RLR_list_heights_SP_v1.csv in /Data/tg_GPS/ (compare to deliverable D2)

Note : Original ellipsoidal height and reference time was made available in previous release

2.3. Software capability

Final goal of the software is to compute the MDT. The software evaluates the different types of MDT values and then compare them statistically. Therefore, the software should be able to:
- -Extract data
- -Interpolate data
- -Apply corrections to homogenize the datasets, as environmental Corrections and transformation to the same tidal system
- -Correct for difference in time (MSS)
- -improve DT at coast using TG MSL as constraint
- -Compare geodetic MDT from tide gauges and from satellite altimetry
- -Compare geodetic MDT to MDT from ocean models
- -Estimate Errors of the estimated MDT

The above expected functionalities exist and have been tested. The core functions for each task are listed in the table below.
- -Read data netcdf 1 Var (Netcdf1va)
- -data extraction (getSubGrid, getSubTG)
- -Smoother (iterativeAveSmoother)
- -Interpolation for DT at coast using TG MSL (getLandVal)
- -Correction files (dTU15, ibCor5, dacCor5, mean2TF, TF2mean)
- -Correction for difference in time (MSS)
- -Comparison of geodetic MDTs (compareWithTG)
- -Comparison of geodetic MDT with ocean models
- -Error estimation (gerError)
- -Plotting

With respect to previous version discussed at the MTR, the following improvements have been made by the software developers:

1. The function "compareWithTG" has unclear description and text in figure needs improvement.

2. The ellipsoidal height measured by GPS in tide-free system are transformed to mean tide system.

3. The raw MDT is computed just subtracting the different models and adding corrections. Then the MDT is filtered with an Iterative smoothing filter. The agreement we obtain between MDT from TG and from altimetry confirms that this procedure is promising and needs to be considered extensively.

3. Validation

We compare first the MDT derived from tide gauges and from altimetry. Then we compare the MDT delivered by tide gauges and the MDT from models.

The function "compareWithTG" is used. The agreement is evaluated using the metric given by bias and root mean square differences defined as following: a box around each station and the mean of the differences between altimetry and TG is computed within each box. Then a global average of this mean over all the tide gauge stations is called **bias**. The TG stations are corrected for this common bias and the **RMS** of the difference at each TG between the TG corrected for the bias and the mean in the box is evaluated. A spatial filter can be used to smooth the raw MDT. In Table 3 bias and RMS without smoothing are bias1 and RMS1. Bias and RMS with smoothing are bias2 and RMS2.

Region	lo1/lo2	la1/la2	Bias1	RMS1	Bias2	RMS2	N	Bias oc	RMS oc
NSEAs1	350/10	47/57	-0.0198	0.0589	-0.0196	0.0506	45	0.526	0.121
NSE	360/16	30/70	-0.0177	0.0767	-0.0138	0.0501	84	0.449	0.126
AUS	100/160	-45/-5	-0.0298	0.1353	-0.0283	0.0583	35	0.343	0.147
PAC	160/240	-30/10	0.07686	0.1601	0.0899	0.1503	15	0.566	0.187
SAM	270/330	-10/20	-0.0534	0.0781	-0.0439	0.0768	3	0.384	0.165
MAM	260/285	24/32	0.03829	0.0793	0.02620	0.0966	18	0.129	0.150
SEAfr	10/70	-40/10	-0.0433	0.0341	-0.0623	0.0523	5	0.4395	0.0947
SEAind	80/160	-20/10	0.03541	0.0	-0.0356	0.0	1	0.293	0.0

Table 3. Regions with limits of the region in lon/lat, bias and RMS of the difference before (bias1 and RMS1) and after smoothing (bias2 and RMS2), Number of points considered (N), Bias and RMS of difference between TG_MDT and ocean MDT without smoothing (raw MDT).

3.1 Validation in the two good performing areas

The two good performing areas are the North Eastern Atlantic (Figure 6) and Australia (Figure 7), see Delivery D3 (Fenoglio-Marc, 2016). The number of available stations is quite large in the two regions, with 84 in NEA and 35 in Australia. In Table 3 the RMS after smoothing is about 5 cm, bias is 1-2 cm. The filtering causes a reduction of the STDD, the stronger reduction occurs in Australia, where the unfiltered RMS is 14 cm.

Considering only the subset of the NEA stations in Figure 4 the RMS is the same for smoothed and unsmoothed MDT. The original MDT (Figure 4 top) is filtered in Figure 4 bottom. The MDT from tide gauge compared to ocean models show a bias of 53 cm.
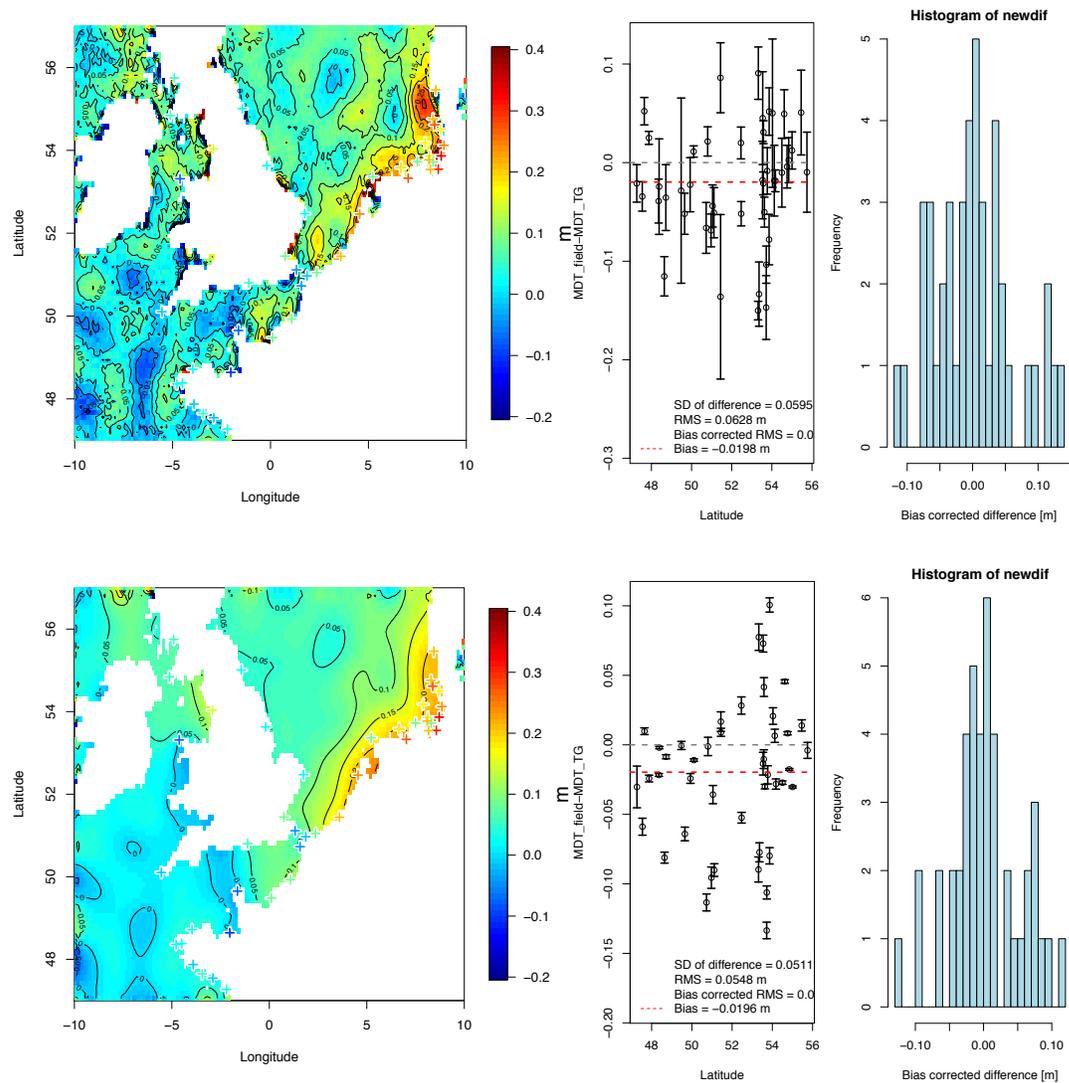
Figure 4. NEAsmall: Part of North-Eastern Atlantic. Mean Dynamic Topography derived applying the geodetic method regionally and at the tide gauge location (l), differences (middle) and histogram of the differences (r). Smoothing not applied (Top) and applied (Bottom).
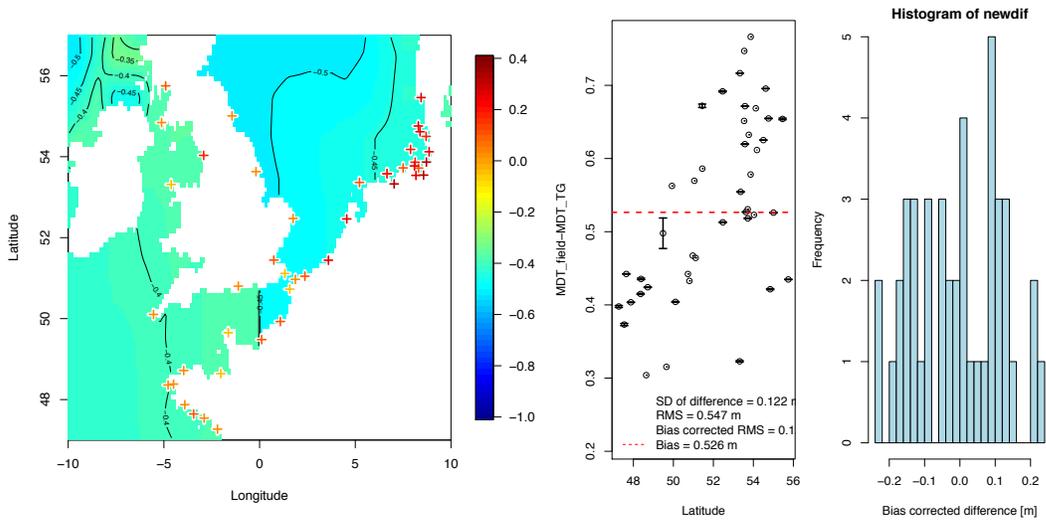
Figure 5. NEAsmall: Part of North-Eastern Atlantic. Mean Dynamic Topography from ocean models and at the tide gauge (l), differences (middle) and histogram of the differences (r). Smoothing is not applied (Top), it is applied (Bottom). Bias is not shown, it should.
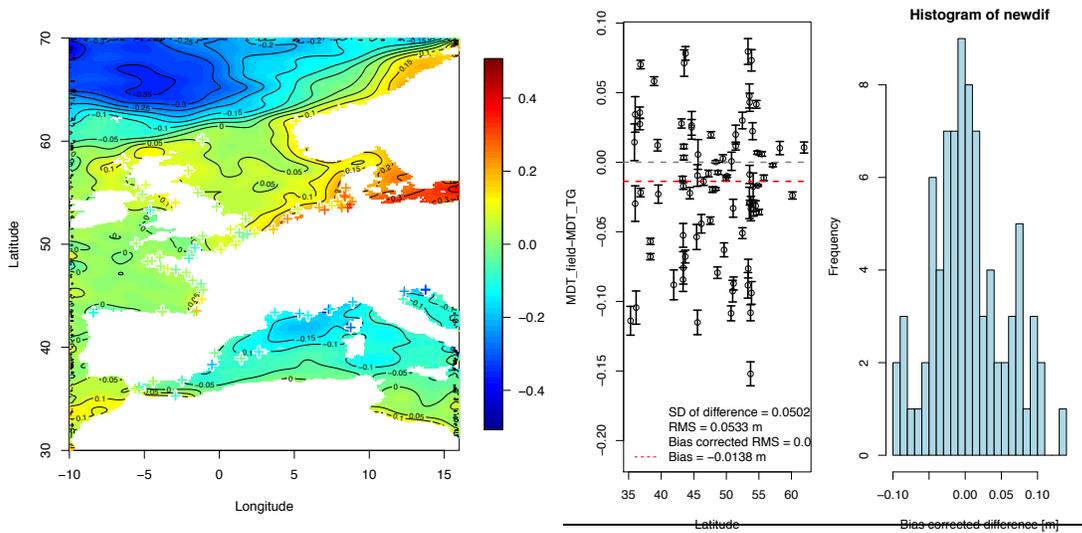
Figure 6. NEA: North-Eastern Atlantic. Mean Dynamic Topography from geodetic method in ocean and at the tide gauge (l), differences (middle) and histogram of differences (r)
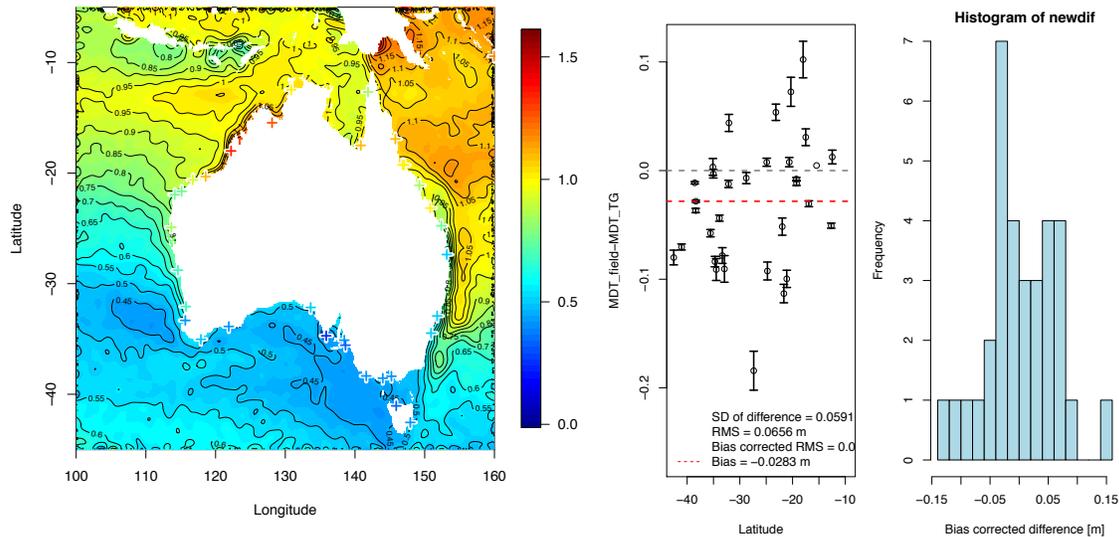
Figure 7. Australia. Mean Dynamic Topography from geodetic method in ocean and at the tide gauge (l), differences (middle) and histogram of differences (r)

3.2 Validation in the poorly surveyed areas

We consider the poorly surveyed areas according to Technical Report for WP 1300 (D3) of this project. The highest RMS differences between MDT from tide gauge and the geodetic MDT is found in the Pacific Islands (15 and 16 cm with and without filtering applied). The bias is smaller than 10 cm in all cases.

For filtered MDT, the best agreement is found in South Africa (SEAfr), with five stations and RMS and bias of 5 cm and -6 cm respectively. In the Pacific Islands we have 15 stations, bias is 9 cm and RMS is 15 cm. In South America the stations are three and the RMS is about 8 cm. In Indonesia (SEAind) there is only one station. Finally we have considered also the Golf of Mexico with 18 stations and RMS and bais of 10 cm and 3 cm respectively.
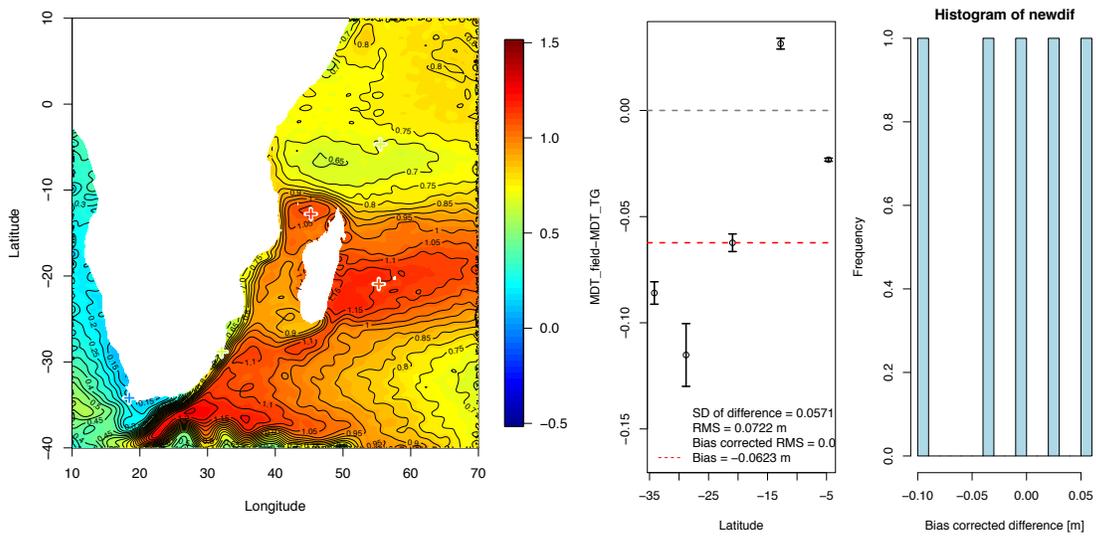
Figure 8. SEAfr: South Africa. Mean Dynamic Topography from geodetic method in ocean and at the tide gauge (l), differences (middle) and histogram of the differences (r)
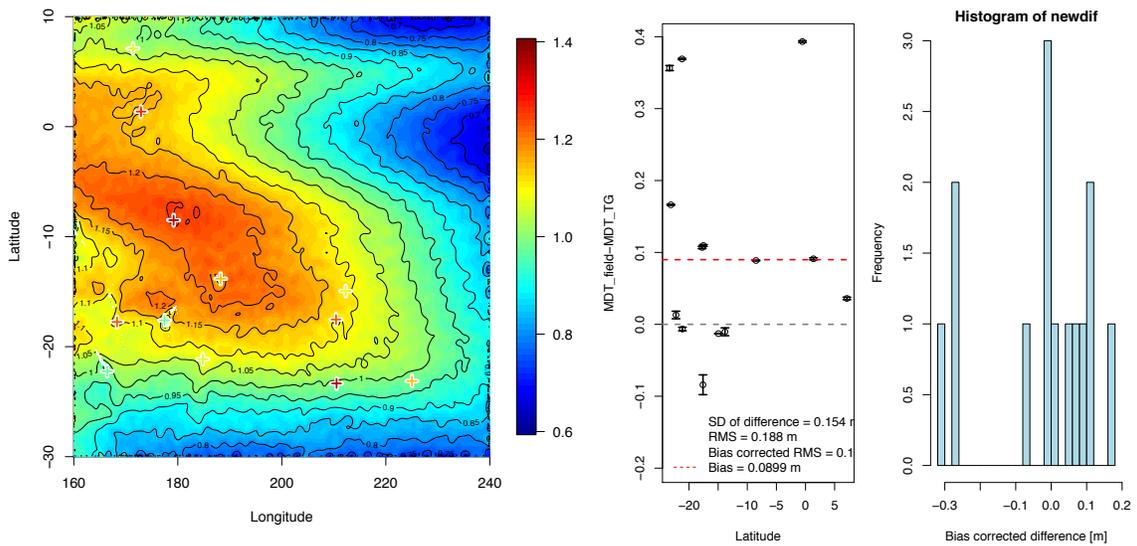
Figure 9. PAC : Pacific Islands. Mean Dynamic Topography from geodetic method in ocean and at the tide gauge (l), differences (middle) and histogram of the differences (r)

13
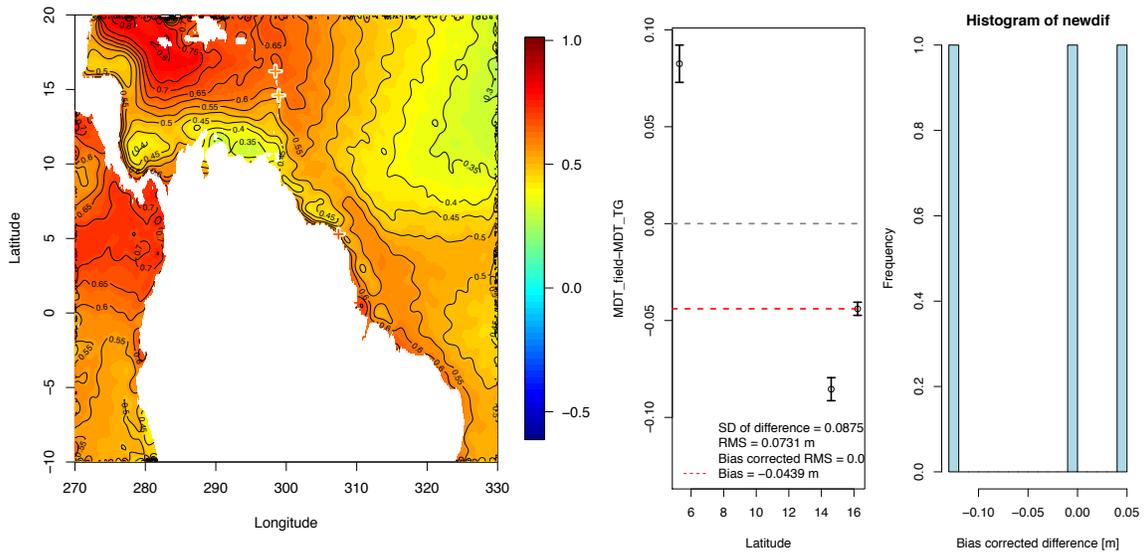
Figure 10. SAM: South America. Mean Dynamic Topography from geodetic method in ocean and at the tide gauge (l), differences (middle) and histogram of the differences (r)
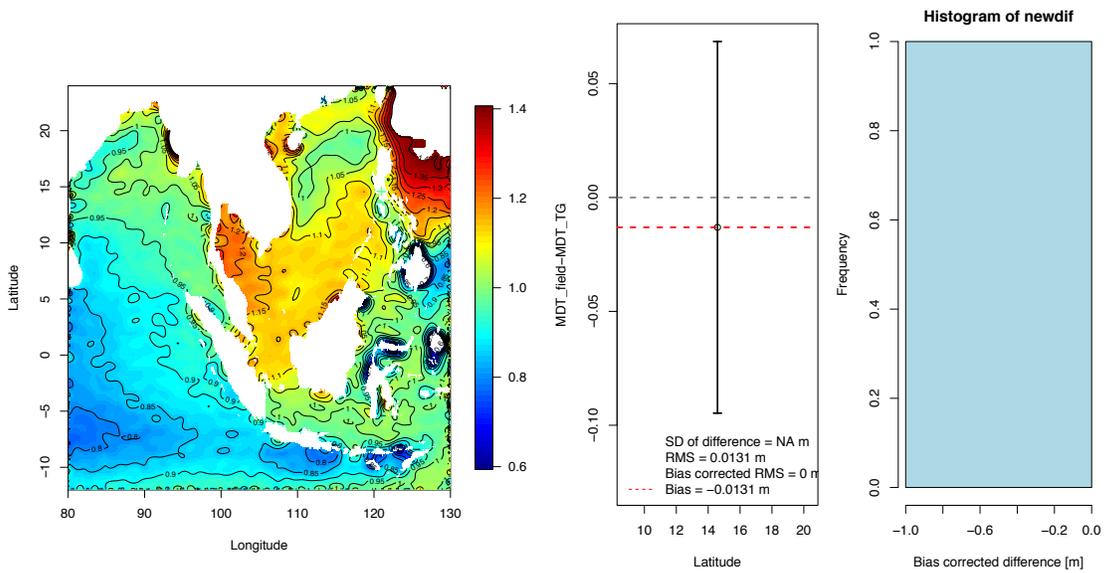
Figure 11. IND: Indonesia. Mean Dynamic Topography from geodetic method in ocean and at the tide gauge (l), differences (middle) and histogram of the differences (r)
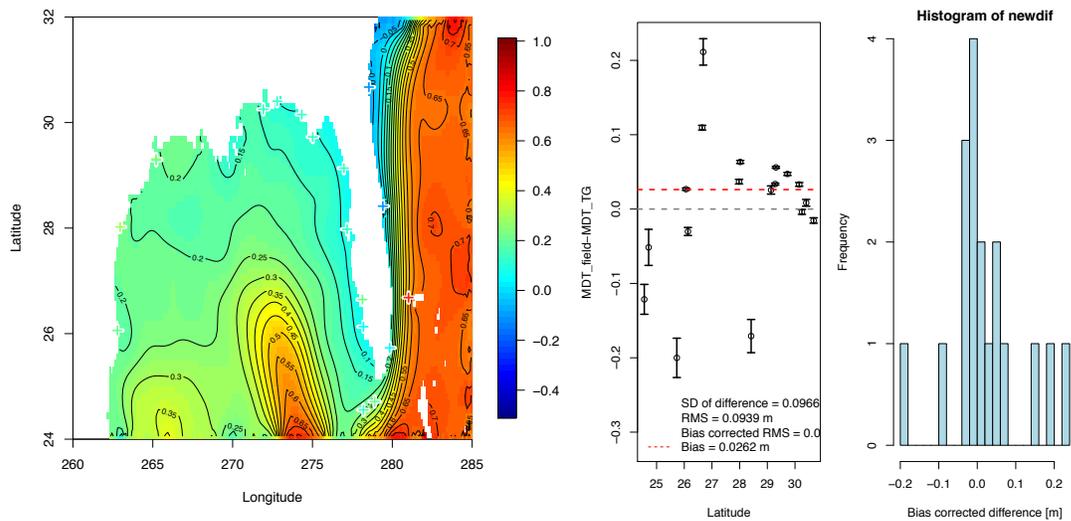
Figure 12. MAM: Golf of Mexico. Mean Dynamic Topography from geodetic method in ocean and at the tide gauge (l), differences (middle) and histogram of the differences (r)

4. Conclusions

The software tool for first computation and visualisation of the different mean Dynamic Topography results has been validated. We have evaluated both the software capability and the results. The comparisons have been presented for a selected geoid (EIGEN6c4) and for one ocean model (Livc).

The documentation of the software offers a basis description. The software is capable of performing comparison of Mean Dynamic Topography pointwise at tide gauge location and over a specified area.

We have validated the approach in two well-surveyed area comparison of the Mean Dynamic Topography pointwise at tide gauge location and over a specified area. All planned comparisons have been done and presented for a selected geoid and ocean model. Results are in agreement with expectations.

Few small modification in documentation and software in function compareWithTG is still needed and should be carefully tested by developer following the given recommendation and documented by replies to each point of this document.

Further work in validation part could include extension to alternative datasets, as ocean models or geoids which are already available in the project database. Comparison with different methodology for filtering and merging of data could be tested (CCN extension).

Here the list of the few points that still need improvement:

1) Improved description of routines and output parameters, e.g. in "compareWithTG".
2) Metrics of comparison, e.g. use for Bias and SD instead of bias and RMS, check definition and allow space in figures.
3) Check warning messages
4) Check particular case of one station only for metrics
5) Check and compare number of described routines and functions in install, discuss differences in manual
6) Use usual short names and simpler structure

5. Example of script

```
#coastMDT test script
# L,.Fenoglio 10.08.2017
library(coastMDT)
#get data from web site and save in local folder
# once downloaded data just load data (data are in sme directory as script)
#getData(localdir='datMDT')
#getData(localdir='MDTdat')

#load
load('DTU15MSS.rda')
load('dDTU15MSS_ref2003_2007.rda')
load('eigen6c4r.rda')
load('ibCor5Y_2003_2007.rda')
load('landmask8.rda')
load('TG.rda')

#the raw MDT
raw<-DTU15MSS+dDTU15MSS_ref2003_2007+ibCor5Y_2003_2007-eigen6c4r

#TGMDT
TGMDT<-TG$RLR_ell_2005.5+TG$MSL_2003_2007+
ellipsoidTF2MT(TG$Latitude)+wgs2topCorr(TG$Latitude)-TG$eigen6c4rC

TG<-cbind(TG,TGMDT)

#Region
lonlim<-c(100,160)
latlim<-c(-45,-5)

#sub grids
mask<-getSubGrid(landmask8,lonlim,latlim)

rawSub<-getSubGrid(raw,lonlim,latlim)
idraw<-which(mask$g==0,arr.ind=TRUE)
rawSub$g[idraw]<-NA
TGsub<-getSubTG(TG,lonlim,latlim)

#land value
mylandTG_ALT<-getLandVal(rawSub,mask,lonlim,latlim,TG=TGsub,type="both",intMethod="lin")
mySD<-getError(rawSub,mylandTG_ALT,mask,bootNr=100,nnx=3,nny=3)
pdf("Tutorial_error.pdf")
plotMDT(mySD,c(0.,0.05),conlev=0.01,TGdat=TGsub)
dev.off()

#Filtering
boxTG_ALT<-iterativeAveSmoother(rawSub,mask,mylandTG_ALT)

#plot
pdf("Tutorial_Fig1.pdf")
plotMDT(rawSub,c(0,1.6),conlev=0.05)
points(TGsub$Longitude,TGsub$Latitude,col='red',pch=1)
dev.off()
```

```
pdf("Tutorial_Fig2.pdf")
plotMDT(mylandTG_ALT,c(0,1.6),conlev=0.05,TGdat=TGsub)
dev.off()

pdf("Tutorial_Fig3.pdf")
plotMDT(boxTG_ALT,c(0,1.6),conlev=0.05,TGdat=TGsub)
#points(TGsub$Longitude,TGsub$Latitude,col='red',pch=3)
dev.off()

#compare with tide gauge the raw values
pdf("Tutorial_add_comparewithTG_raw.pdf")
outTGraw<-compareWithTG(TGsub, rawSub, lonlim, latlim,export=TRUE,tgfile="myfile_raw.csv")
dev.off()

#compare with tide gauge
pdf("Tutorial_add_comparewithTG.pdf")
outTG<-compareWithTG(TGsub, boxTG_ALT, lonlim, latlim,export=TRUE,tgfile="myfile.csv")
dev.off()

#save grid
grid2file(boxTG_ALT,filename='MDT_TG_Alt_AUS.nc')
#dev.off()


#extract ocean MDT
livc5Y<-readRegGridBin("livc_5yr_p125grid.dat",nx=2880,ny=1440,res=0.125)
#save grid
grid2file(livc5Y,filename='MDT_livc5Y.nc')

pdf("Tutorial_Fig3ocW.pdf")
plotMDT(livc5Y,c(-1.,1.),conlev=0.05, TGdat=TGsub)
dev.off()

#sub grids of the first attribute, which is $g (a grid)
livc5YSub<-getSubGrid(livc5Y$g,lonlim,latlim)

pdf("Tutorial_Fig3ocSub.pdf")
plotMDT(livc5YSub,c(0,1.6),conlev=0.05, TGdat=TGsub)
dev.off()

#compare with tide gauge
pdf("Tutorial_add_OCcomparewithTG.pdf")
outTGoc<-compareWithTG(TGsub, livc5YSub, lonlim, latlim,export=TRUE,tgfile="myfile_rawoc.csv")
dev.off()
```

6. References

Dinardo S., Fenoglio-Marc L. Buchhaupt C., Becker M., Scharroo R., Fernandez J., Benveniste J. CryoSat-2 performance along the german coasts, AdSR special session CryoSat-2, submitted January 2017

Egbert G. and Erofeeva S. (2002). Efficient Inverse Modeling of Barotropic Ocean Tides. J. Atmos. Oceanic Technol., 19, 183204

Featherstone, W. E., J. F. Kirby, C. Hirt, M. S. Filmer, S. J. Claessens, N. J. Brown, G. Hu, and G. M. Johnston (2011), The AUSGeoid09 model of the Australian Height Datum, J. Geod., 85(3), 133-150, doi: 870 10.1007/s00190-010-0422-2.

Fecher. T., R. Pail, and T. Gruber (2015), Global gravity field modeling based on GOCE and complementary gravity data, Int. J. Appl. Earth. Obs. Geoinf., 35, 120–127. doi:10.1016/j.jag.2013.10.005

Fenoglio-Marc, L., (2016). Technical report on selection and justification of test area WP1300. Delivery D3, GOCE++dycot ESA Project

Fenoglio-Marc, L., S. Dinardo, R. Scharroo, A. Roland, M. Dutour Sikiric, B. Lucas, M. Becker, J. Benveniste, R. Weiss (2015). The German Bight: A validation of CryoSat-2 altimeter data in SAR mode, Advances in Space Research, 55, 11, 2641-2656, 2015. http://dx.doi.org/10.1016/j.asr.2015.02.014

Nielsen K. (2017a). Getting started with the coastMDT package, 15 June 2017

Nielsen K. (2017b). Package 'coastMDT', June 15 2017

Nielsen K. (2017c). Description of the data for the coastMDT package, February 9, 2017

Nielsen K., P. Knudsen and O. Andersen (2017d). GOCE++ Dynamic Topography at the coast and tide gauge unification, GOCE++DYCOT, March 3, 2017

8 Appendix G, D6: Technical Note describing the work performed in WP3000
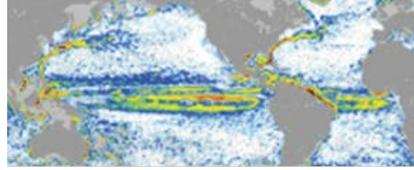
GOCE++ Dynamic Topography at the coast and tide gauge unification
GOCE ++ DYCOT

TITLE.

D6 – Technical Note describing the work performed in WP3000.

Authors

Ole B. Andersen,
Rory Bingham
Luciana Fenoglio
Chris W Hughes

ESTEC Ref: ITT AO/1-8194/15/NL/FF/gp "GOCE++ Dynamic Topography at the coast and tide gauge unification"- Coordinator: Ole B. Andersen (DTU)

DOCUMENT CHANGE LOG				
Rev.	Date	Sections modified	Comments	Changed by
1	23-02-2017	All	Draft	Ole B. Andersen
2	26-02-2017	WP3100 References		Chris W. Hughes
3	07-03-2017	WP3300		Luciana Fenoglio

Contents

Dynamic Topography along the coast Introduction

This technical report summarizes the work on Work package 3 within GOCE+++ and report on determination of Dynamic Topography along the coast and at global tide gauges.

A novel method based on the ESA GUT project to determine MDT along the coast from the newest GOCE release will be tested, and compared with strategies using combined GOCE/GRACE/in-situ gravity. An investigation into the MSS error along the coast from altimetry will be performed. Relative offsets between tide gauge records will be sought

   WP3100 DT along coast
   WP3200 MDT and GOCE
   WP3300 Coastal altimetry

The work performed within WP3400 (Connecting Tide Gauges) and WP3500 (Sea Level Trend) will be reported in Deliverable D7.

WP3100 Dynamic Topography along the coast

The aim of this work package is to use a combination of ocean model analyses and comparisons between tide gauge and satellite altimeter data to assess the nature of coastal dynamic topography variations and make recommendations concerning how to incorporate tide gauge measurements into a global mean dynamic topography estimate. We also make tide gauge estimates for one of our chosen areas (Australia) using a variety of geoids, and an initial global estimate using a single geoid. Finally, we produce a recommended methodology to apply once the parallel developments are complete.

The work undertaken in this work package falls into four subsections, described in more detail below. These are
1) Tide gauge variations and comparison with altimetry.
2) Ocean model mean dynamic topography characterization.
3) Case study of MDT derived from tide gauges in Australia.
4) Initial results for a global tide gauge MDT calculation.

Following these subsections we end with a synthesis subsection in which we summarize what has been learnt and make recommendations for the final stage of the project.

3.1.1 Tide gauge variations and comparison with altimetry.

In this subsection we focus not on the MDT but on the time-dependent variations. There are two reasons for looking at these. First, we need to know whether the tide gauge dynamic topography is representative of a large region or is a purely local measurement (this can be as a result of the position of the tide gauge, for example up a river or in a semi-enclosed bay, or it may simply be that the tide gauge data are poor quality). Second, as an alternative to using ocean models, we can use long-term variations at tide gauges as a proxy for the mean dynamic topography in order to investigate natural scales of variability along the coast. This is imperfect, as it is not clear that the nature of the variability at accessible time scales (in practice interannual to just about decadal) represents the same physics as that which is responsible for spatial variations in MDT, but it is nonetheless a useful guide.

In order to assess the relationship between tide gauges and altimetry we consider all tide gauges in the Permanent Service for Mean Sea Level (PSMSL) Revised Local Reference (RLR) dataset (http://www.psmsl.org). We identify all tide gauges (a total of 1007 sites) with data overlapping the precise satellite altimetry period 1993 to present (in practice to the end of 2015). Using monthly mean values, we apply an inverse barometer correction to make the resulting time series compatible with satellite altimetry. This is determined either from the ERA-Interim reanalysis product (http://www.ecmwf.int/en/elibrary/8174-era-interim-archive-version-20), monthly mean sea level pressure on a ¼ degree grid, interpolated to tide gauge locations, or the Dynamic Atmosphere Correction (DAC), which is a barotropic ocean model forced by atmospheric pressure and wind stress from the same meteorological analysis, reverting to simple inverse barometer correction at periods longer than 20 days. Although this does not mean that monthly mean values in the DAC are precisely equivalent to the simple IB correction, we find that they are

extremely similar (standard deviation of difference < 5 mm, reducing to 1 mm for 5-year means) with both DAC and IB analyses explaining very similar fractions of the variance of the tide gauge data. For this reason, we will focus only on the DAC-corrected product, which is also the product used to correct the altimetry data.

For each tide gauge we seek the altimeter record (from the AVISO gridded absolute dynamic topography) within 300 km which, when supplemented by a trend, annual and semiannual cycle, explains the largest fraction of variance in the tide gauge record. All subsequent diagnostics are shown with DAC correction applied, seasonal cycle removed, and a trend added to the altimetry to make it match the tide gauge trend. Plotting the tide gauge and altimetry data together gives a good feel for the variability and its representativeness of the open ocean. Clearly it is not practical to show all these plots (though all have been inspected), but a few are shown here as examples.
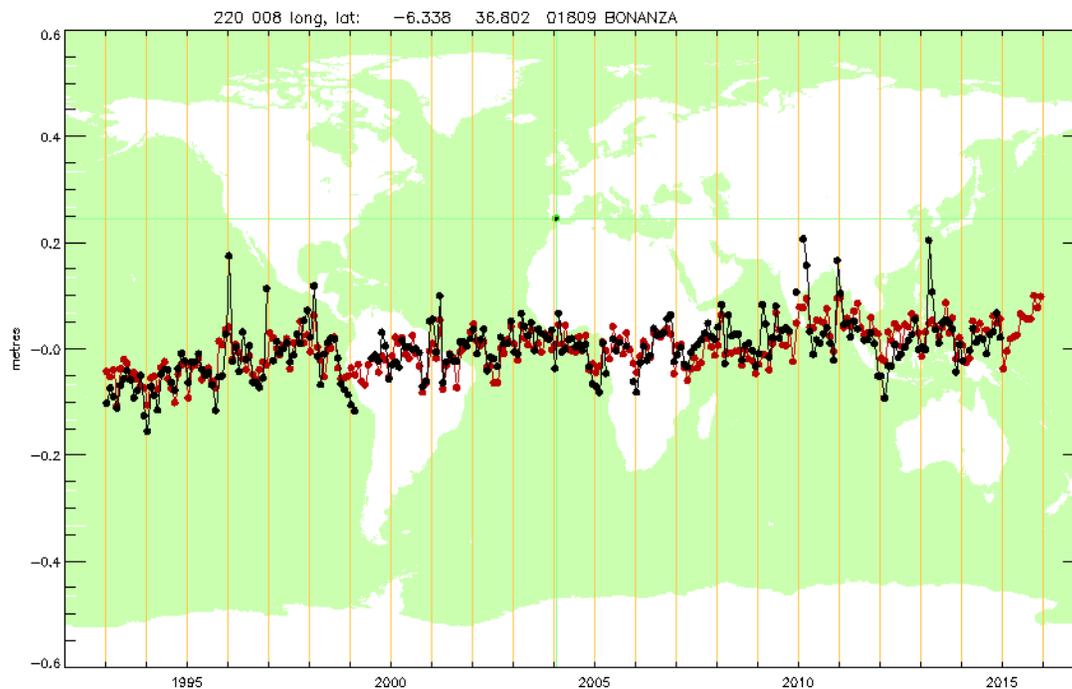
Figure 1: Monthly mean sea level record from tide gauge (black) and from altimetry (red), after removing DAC correction and seasonal cycle, and adding a trend to the altimetry to match the tide gauge trend. The tide gauge name (PSMSL) is Bonanza, shown as a green dot on the map, and altimetry is taken from the point marked by the black spot.

The Bonanza tide gauge (Fig. 1) shows a typical example, with good but not excellent agreement with the altimetry. In contrast, the next tide gauge in the list (Sevilla-Esclusa) shown in Fig. 2 shows much higher variability, and much poorer agreement with satellite altimetry. On closer inspection the reason becomes obvious: the gauge is more than 70 km from the sea along a rather narrow river, so is unlikely to be representative of the open ocean (Bonanza is at the mouth of the same river).
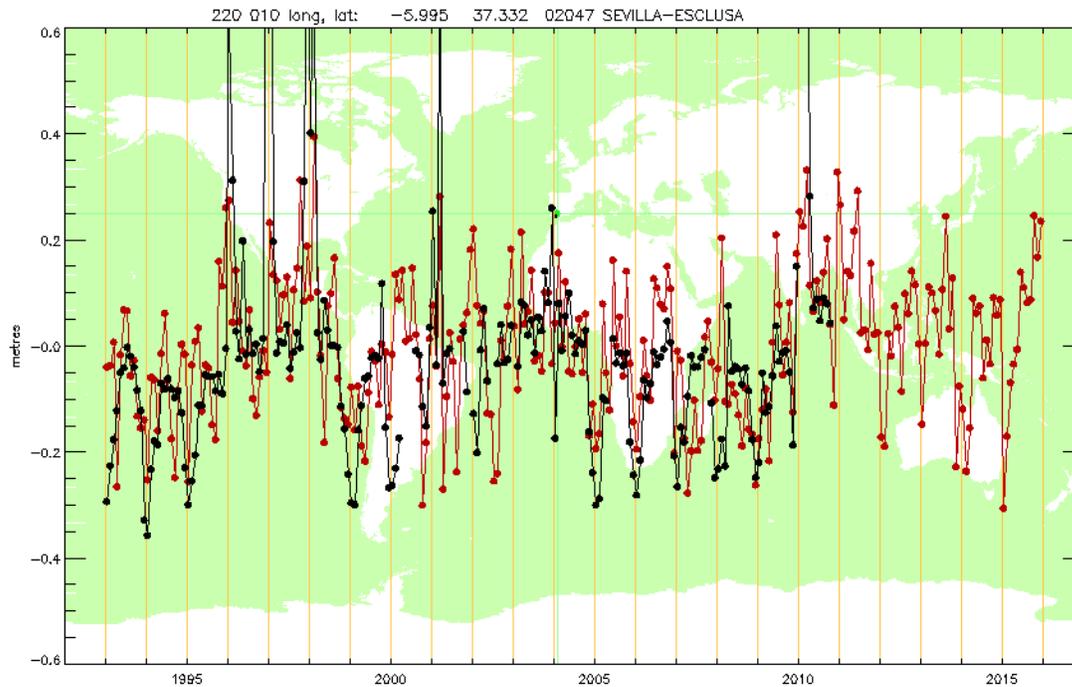
Figure 2: Same as Figure 1, but showing the Sevilla-Esclusa tide gauge and best correlated altimetry (scaled).

Another, rather different example is found in Japan. A series of gauges along the east coast of Japan show rather similar and small variability, the last in this sequence being Aburatsubo (Figure 3). The next tide gauge, Kaminato II (Figure 4) shows much greater variability. Unlike Sevilla-Esclusa, however, Kaminato II agrees well with the altimetry dataset. Again, closer inspection reveals the reason. Kaminato II is on a small island which is sufficiently far offshore that the Kuroshio current meanders to either side of the island, producing very large sea level jumps (around 0.8 m) as it crosses the island. Some other islands show related behaviour, whereas others are sufficiently close to the mainland coast that they behave almost as if they were part of the mainland.

These comparisons highlight the value of comparing with altimetry, and this is certainly valuable qualitative information to help understand particular cases. However, if we are to incorporate tide gauge data into an MDT estimate, we need a quantitative overview of the tide gauge/altimetry comparison. To this end, we calculate two quantities for each tide gauge: percent variance explained by altimetry (Figure 5), and standard deviation of the residual after the altimetry has been subtracted from the tide gauge (Figure 6). The former is a measure of how representative the tide gauge record is of nearby ocean (though it should be borne in mind that disagreement can in some places be a result of poor altimetry data in the coastal zone). The latter is an upper limit on the tide gauge error for a single month of measurement (one standard deviation), with 5-year mean values expected to be better by an amount that depends on the spectral content of the variability (the best possible would be a factor of $\sqrt{60} \approx 7.75$).
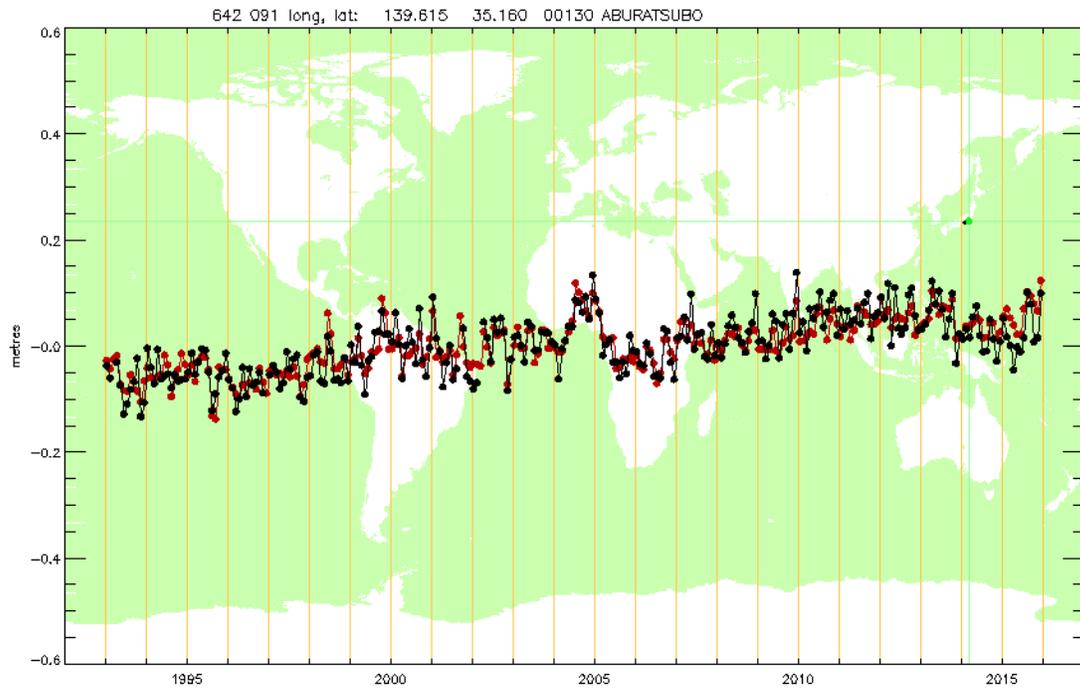
Figure 3: Same as Figure 1, but for Aburatsubo tide gauge in Japan.
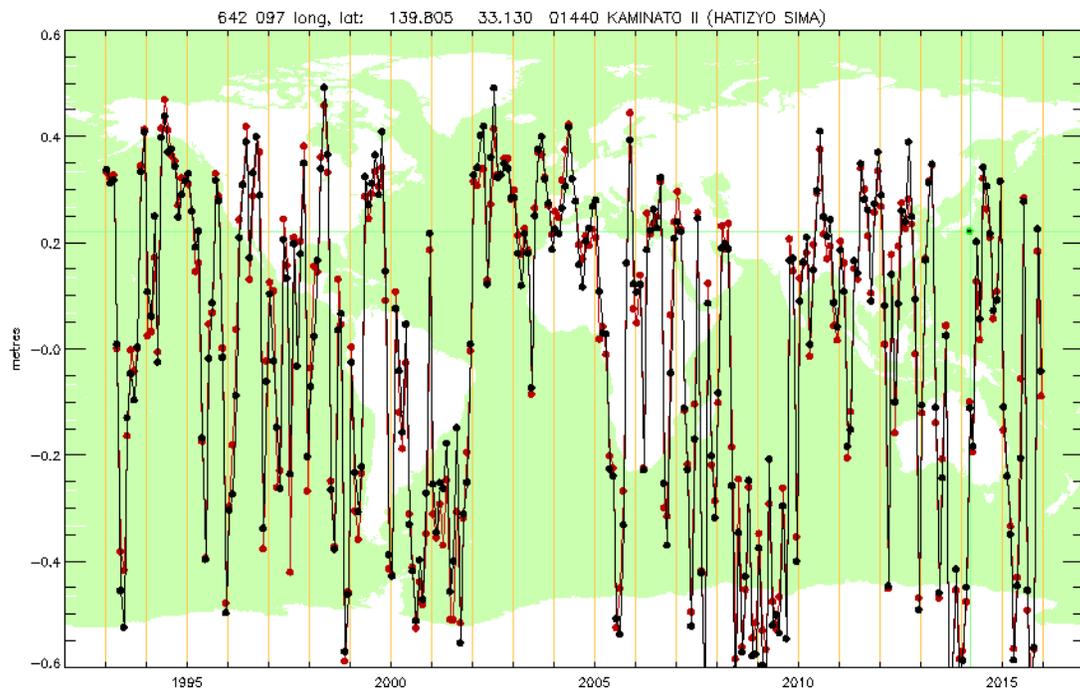
Figure 4: Same as Figure 1, but for Kaminato II tide gauge.
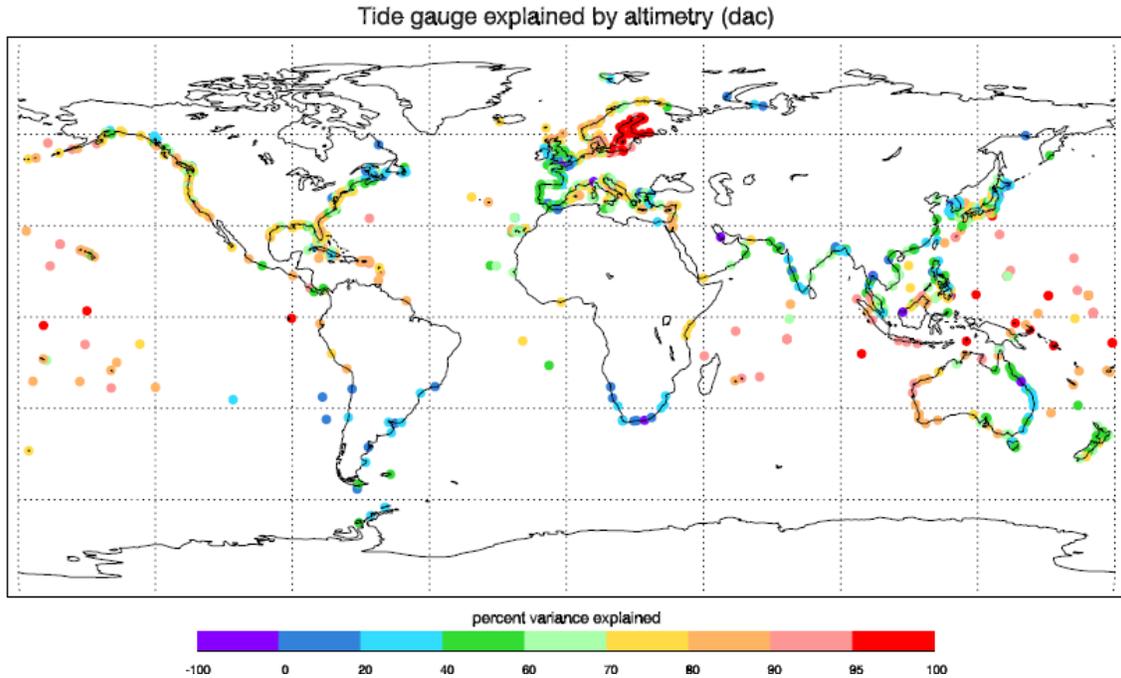
Figure 5: Percent variance of tide gauge data explained by satellite altimetry
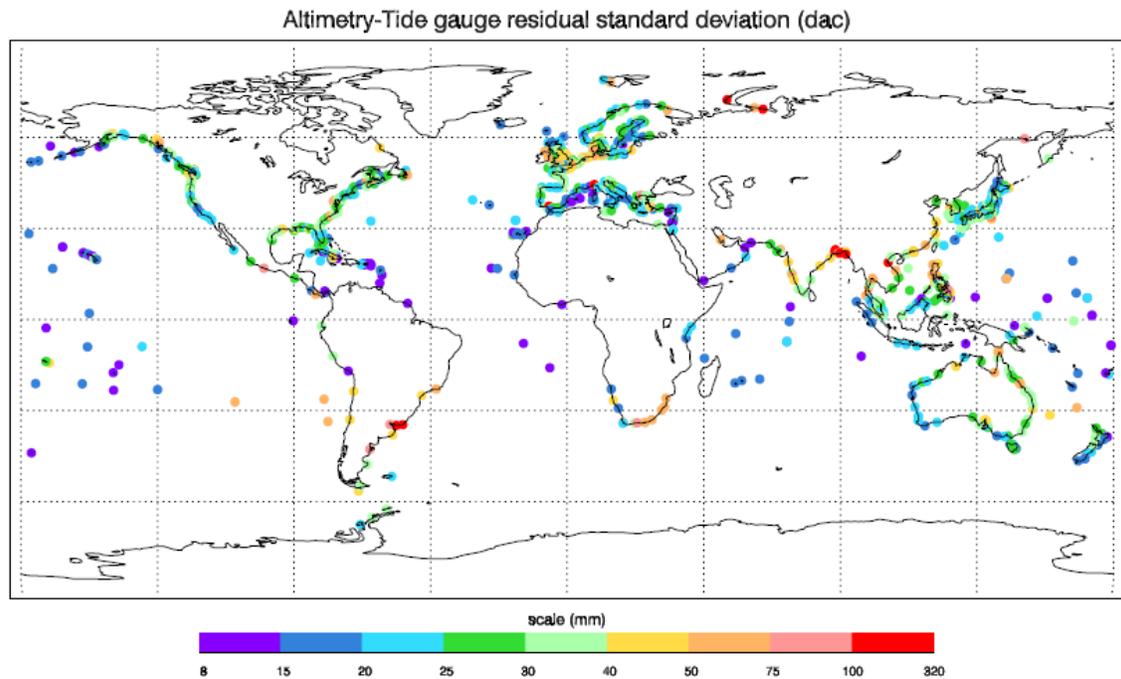
Figure 6: Residual standard deviation at each tide gauge after DAC correction, seasonal cycle, trend and open ocean (altimetry) signal have been accounted for.

Some features are worth highlighting in these figures. The very high variance explained in the Baltic results in a residual standard deviation of less than 40 mm despite the high initial variance in this region. Many tropical islands also have very high variance explained and very low residual standard deviations (often less than 15 mm). Sevilla-Esclusa stands out as having a very high residual variability, and Kaminato II has very high variance explained, but still significant residual variability (> 75 mm).

Some other regions of high residual variability also have clear explanations. Genova II (NW Italy) is a clear error in the tide gauge data (this has been reported to PSMSL and has subsequently been corrected). Two points in Siberia are associated with extremely gappy altimeter records, and the cluster in the northern Bay of Bengal include some tide gauges which are far from the ocean (Calcutta, Tribeni), and others (e.g. Cox's Bazaar) for which there is no obvious explanation (although the PSMSL documentation does show a history of difficulties for that tide gauge). There is no obvious reason for the disagreement in the broad River Plate estuary (Uruguay) or in Hon Ngu (Vietnam).

Low explained variance and fairly high residuals (> 50 mm) are also apparent on the east coast of South Africa, where the strong, narrow Agulhas western boundary current flows very close to the coast. This may be a case of limitations in the ability to map the altimetry data sufficiently close to the coast, though tide gauge problems may also be an issue. Similarly, the variance explained is systematically higher in Western Australia than on the east coast, where the East Australian Current flows close to the coast, and residuals are also higher on the east coast (> 50 mm at Mackay, but generally 25-40 mm).

The reasonable explanations found in most cases show that this comparison can be used to derive a measure of "quality" for each tide gauge. It is important to recognize, however, that we are using the term only in the sense of the tide gauge being representative of the broader ocean, so that it is meaningful to use it as part of an along-coast extrapolation/interpolation. In some cases the tide gauges will not be representative of the ocean because of data quality problems. In other cases, the data are of good quality, but are representing a very local process.

A second method of assessing the tide gauges is to look at the coherence of variability from one tide gauge to another. This accounts for the possibility that there may be signals which are coherent along the coastline, but quite different from those a short distance offshore (as in those western boundary currents which are pressed close to the coast).

Since this study does not require the coexistence of altimetry data, it can use tide gauge data from further into the past. Here we use a start date of 1979 (the limit of the ERA-Interim dataset). This longer time series also allows more focus on long time scales, accordingly we look at running annual averages rather than monthly mean values.

To look at along-coast coherence, we use the PSMSL coastline and station numbers to order the tide gauges. This is not a perfect ordering, though it does generally follow the global coastline in a logical order starting in Siberia, then passing round Europe, Africa, Asia, Indonesia, Australia, Pacific Islands, and the American continent (north to south along the west coast, then north again on the east coast), as shown in Figure 7.

In order to account for the imperfect ordering, we calculate correlations between each tide gauge and the 10 gauges surrounding it in order. Figure 8 shows all of these correlations (dots), and the best for each gauge (black line), together with the separation in that best case (red line, right hand scale).

Tide gauge positions
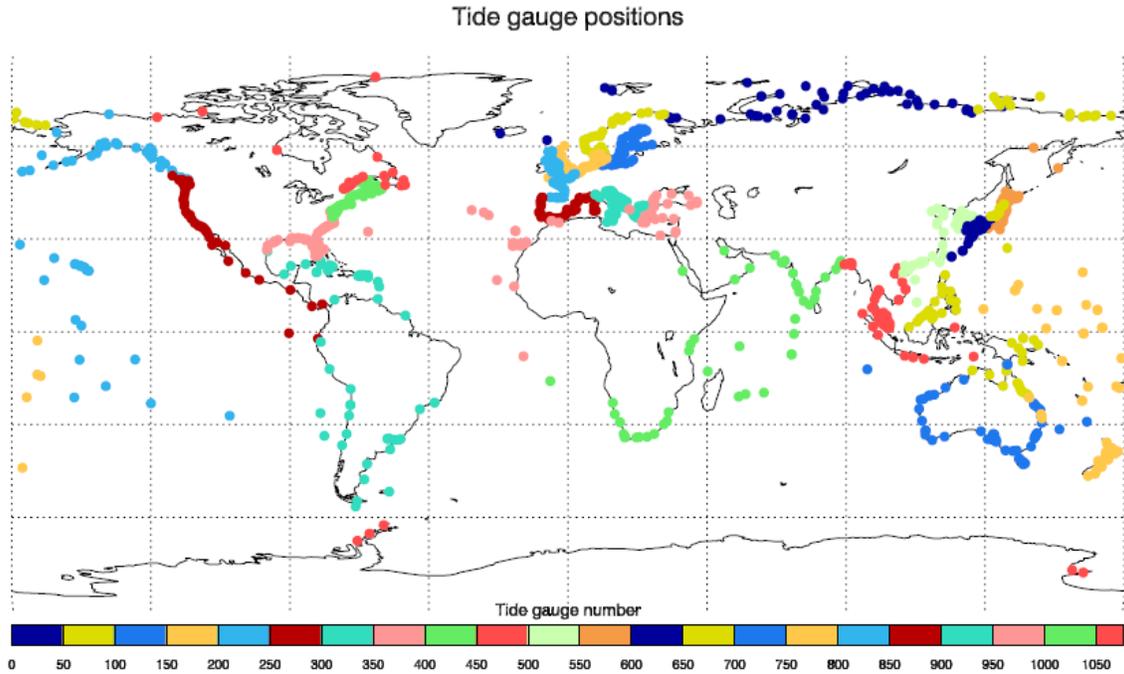
Tide gauge number

Figure 7: Position of tide gauges ordered by PSMSL coastline and station number. The ordering starts with Arctic Russia, then follows the European, Africa, Asian, Indonesian and Australian coasts, then Pacific islands, then Pacific Americas, then Atlantic Americas, ending with Greenland and Antarctica.

PSMSL tide gauge correlation with neighbours
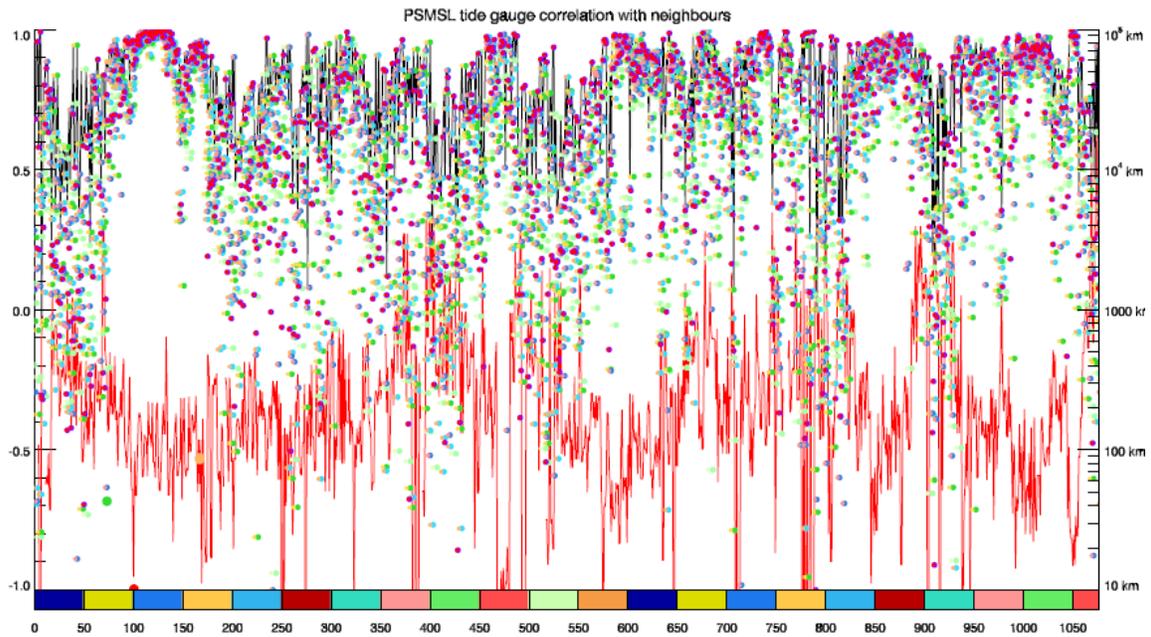
Figure 8: Correlation between running annual means of tide gauge records and their 10 neighbours (dots). Black line shows the best of these at each tide gauge. Red line shows the corresponding separation (right hand scale).

These correlations reveal a highly heterogeneous picture. There are patches of very high correlation, e.g. in the Baltic (around gauge number 100-150), parts of Japan (around 600), and much of the US and Canadian coasts (around 850 and 950-1050), as well as quite high correlations throughout much of Europe (about 60-390), and these generally

correspond to closely spaced tide gauges, but there are also examples of high correlations with very distant spacing, and of low correlations between closely-spaced pairs of gauges. Again, this is indicative of instances of highly local variability interspersed among strongly-correlated regions.

Australia (around 690-750) is an interesting example. Although the strongest correlations are limited to the later end of this range, corresponding to Western Australia, there are still many strong correlations toward the earlier end of the range where the East Australian Current plays a role, suggesting a significant coherence along this eastern coast despite the very short length scales in the offshore direction.

3.1.2 Ocean model mean dynamic topography characterization.

We have gathered together estimates of the MDT from 7 ocean models at resolutions varying from 1 degree to 1/12 degree as described in report WP1300D2 of this project. Annual means have been calculated for the years 1993 up to the last year available in the model run (between 2007 and 2015 depending on the model). In addition, the 5-year mean for our standard reference period (2003-2007 inclusive) has been calculated, and that is the product we will consider here.

Spatial-and-time-mean values in these models are effectively meaningless and, although there may be some interest in the time variation of the spatial means, this is generally unreliable and unhelpful to retain when comparing between models and comparing models with observations. Accordingly, the spatial mean is removed for each field which has global ocean coverage (excluding isolated seas such as the Caspian Sea, which is masked out).

Some fields do not have global coverage, for example lacking an Arctic. In these cases, rather than remove the spatial mean over a different domain (which would introduce a significant bias), the spatial mean of the difference relative to one of the complete models (ECCO2) is subtracted. Removing the "mean" in this way requires the models to be on the same grid, so this step is performed after the regridding step described below.

All models are regridded onto a common grid at 1/8 degree resolution in latitude and longitude (grid cells are centred on the point 1/16 of a degree from the prime meridian and poles, and at 1/8 degree steps from that point). In order to retain as much as possible of the effect of model resolution, this regridding is performed in a manner which ensures that all coastal ocean points on the 1/8 degree grid are derived only from model coastal points, unless there is no model land within a model grid spacing of the true coast (e.g. in the case of islands which are not resolved by the model).

In more detail, the regridding is performed in two steps. All interior (i.e. non-coastal) points on the 1/8 degree grid are filled by bilinear interpolation from the model native grid. For this step, the model data are expanded with a one grid-point fringe of extra ocean data over land points, filled with the average of neighbouring ocean MDT values.

In the second step, coastal values at 1/8 degree are calculated. This is done by eliminating all non-coastal data from the model, then expanding the coastal strip of model data in both directions by averaging neighbouring values, with care taken not to import values from the opposite side of any land bridges. Bilinear interpolation of this expanded coastal strip is then used to fill all coastal values on the 1/8 degree grid. This method guarantees that the information at the regridded coast all comes from the model coast, an important consideration given the strong dynamical constraints on MDT slopes along the coast.

Having calculated these MDTs on a standard grid, we now need to assess how they can be used to help constrain coastal MDT variations derived from observations. Conventionally, this would be done by calculating lagged autocorrelation functions along the coast as input to an interpolation algorithm. Here, though, the heterogeneity of the dynamics precludes the use of a single autocorrelation function for the whole coast – it must be a different function at each position. Such an autocorrelation function could, in principle, be calculated from a sufficiently large ensemble of models, but there is too little variation in patterns in our ensemble even if we were willing to treat the coarse resolution models as equivalent to the finest resolution models.

Instead of calculating a true autocorrelation function, we calculate a proxy for such a function by looking at how far one has to travel from each coastal point in order to find an MDT which differs from the reference point by some threshold value. We choose thresholds of 1, 2, 4 and 8 cm as representative of the expected size of measurement error. This allows us to calculate such distances for each model. We calculate the distances in two ways. In the first case we find the distance to any point beyond the threshold, and in the second case we allow only coastal points. Distances in the second case are therefore constrained to be at least as large as in the first case.

Figure 9 shows the resulting distances plotted as ellipses surrounding each coastal grid point, for the case of the NEMO12b model, and with a threshold of 2 cm. Pink ellipses represent case 1, and are plotted on top of the blue ellipses of case 2 (the elliptical shape approximately accounts for the latitude-dependent distortion of zonal distances on the latitude-longitude projection used).

The result is quite informative concerning the natural length scales of coastal MDT variability. In general, it shows that alongshore variations (blue) have longer characteristic length scales than offshore variations (pink), (they must be at least as long, but are often much longer). This is particularly clear for the western coasts of South America and South Africa. On the east coasts of South Africa and Australia, both scales are short but the offshore scale is reduced to a single grid point, indicating the value of the coherence in the alongshore direction.

The US east coast is particularly interesting, as there are two pinch points in the alongshore length scale. The first, half way up Florida, is the expected position of the Gulf Stream-related step. The second, a little north of Cape Hatteras, is suggestive of a few points with a locally different MDT, rather than a sustained step in MDT.
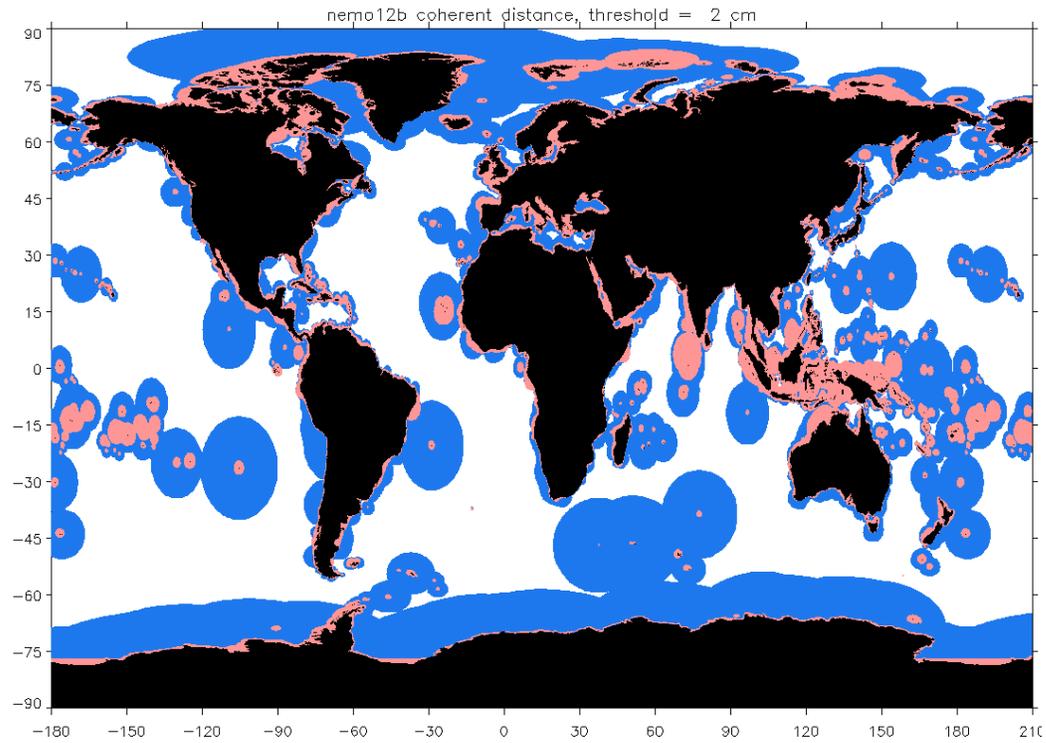
Figure 9: Coherence distances to a threshold of 2 cm MDT change (see text for description) for the NEMO12b model. Distances along the coast are shown in blue, and distances in arbitrary directions (indicative of the offshore scale) in pink.
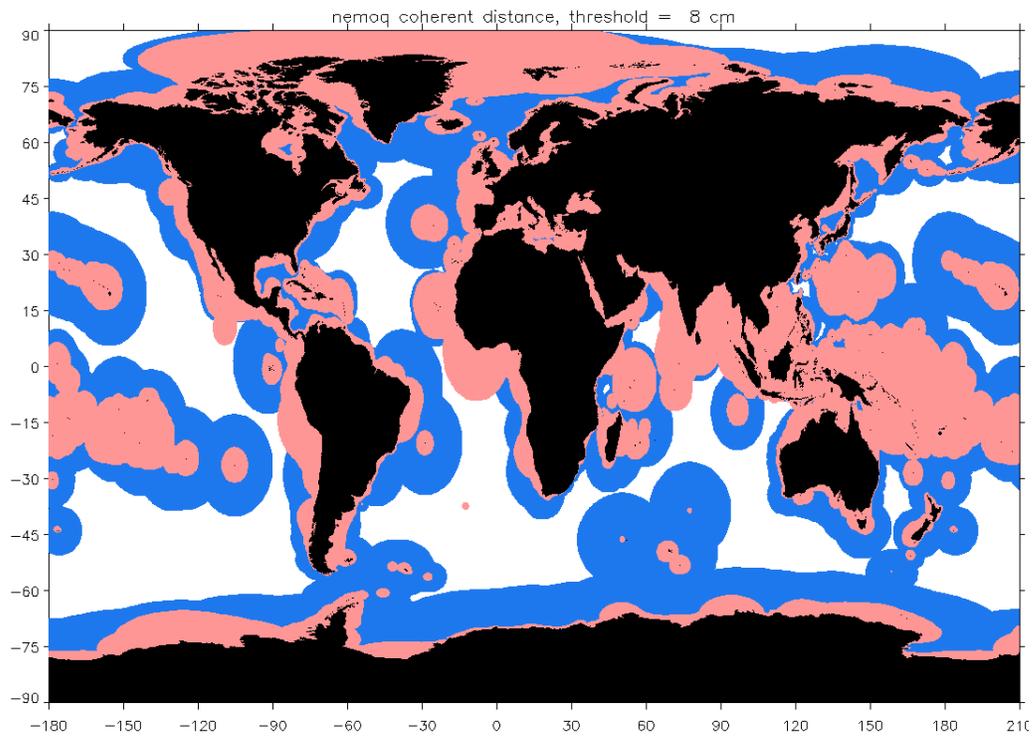
Figure 10: Coherence distances to a threshold of 8 cm MDT change (see text for description) for the NEMO12b model. Distances along the coast are shown in blue, and distances in arbitrary directions (indicative of the offshore scale) in pink.

Figure 10 shows the same as Figure 9, but with a threshold of 8 cm. For the most part this expands all the scales as might be expected, but it is interesting to see how the offshore scale remains at only 1 grid point for eastern Australia and South Africa. This highlights the need to resolve a very narrow coastal strip in these regions, suggesting that tide gauge measurements may be particularly valuable in these regions.
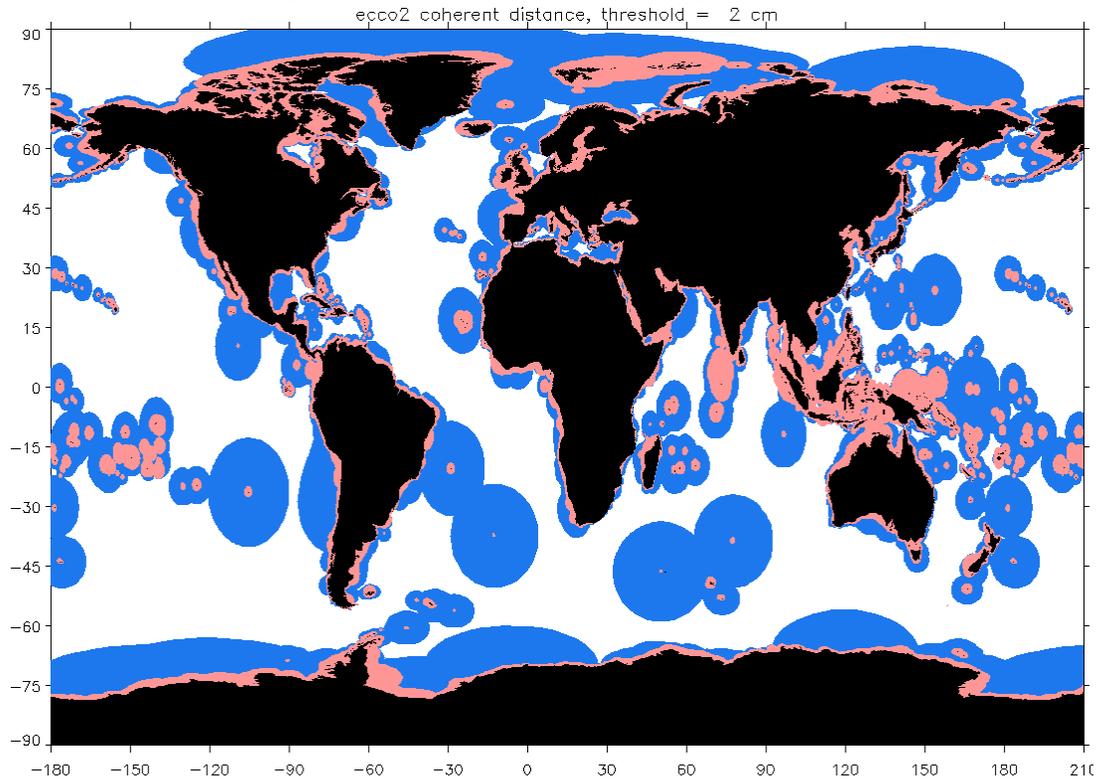
Figure 11: Coherence distances to a threshold of 2 cm MDT change (see text for description) for the ECCO2 model. Distances along the coast are shown in blue, and distances in arbitrary directions (indicative of the offshore scale) in pink.

Finally, Figure 11 reverts to the 2 cm threshold, but now for the ECCO2 model (this has approximately 18 km resolution, in comparison to the 9 km or less of NEMO12b). It is reassuring to see the similarity of many features between these very different models, which suggests that this lower resolution result is also valuable (the value of the 1 degree models is much more questionable, as they often cannot resolve the length scales derived from these finer resolution models).

3.1.3 Case study of MDT derived from tide gauges in Australia

As an initial test of newly-acquired data, we have focused on one of the project's selected regions: Australia. The main results summarized here are documented in more detail in Filmer et al. (2017), a paper submitted to the *Journal of Geophysical Research*.

Vertical coordinates of 32 tide gauges have been identified using collocated GPS measurements. The positions of these tide gauges are shown in Figure 12.
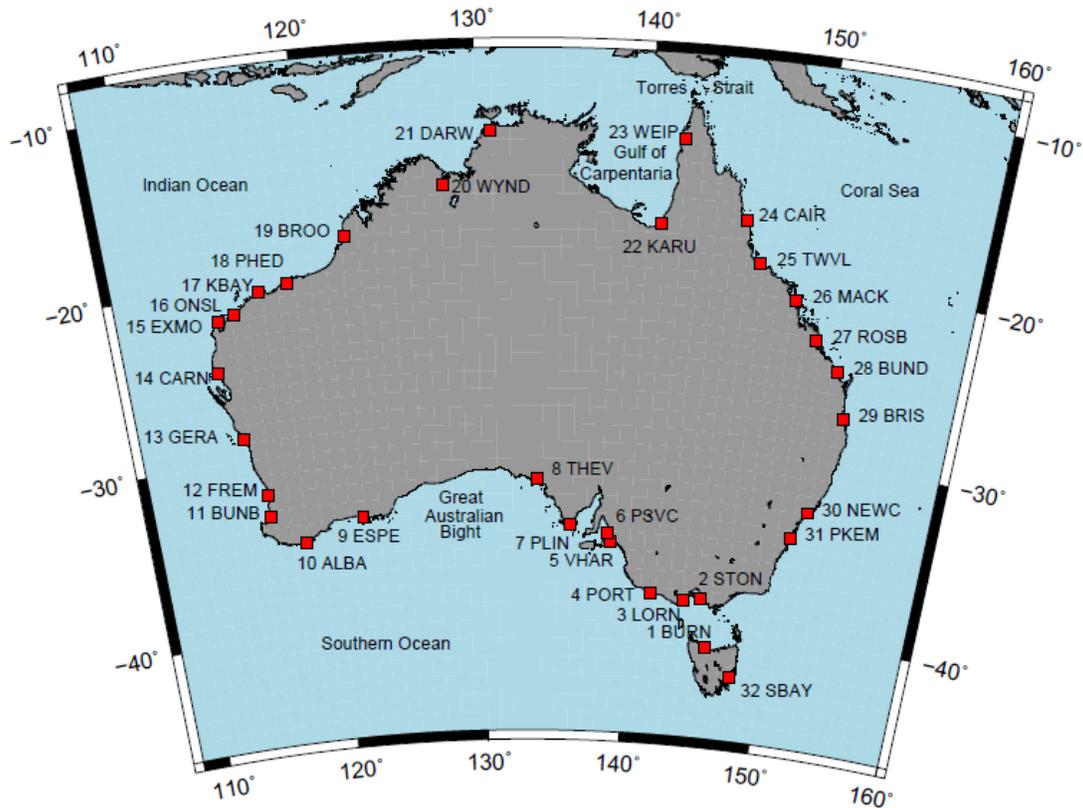
Figure 12: Positions of 32 tide gauges at which a calculation of MDT is possible, together with numbering system and abbreviated names.

The focus here is on variations in MDT around the coast, so in all plots, the mean value has been set to the same constant value. The standard reference period of 2003-2007 inclusive has been used, but tide gauge measurements for other periods have also been investigated and they show that values averaged over our reference period are typically within 20-30 mm of the 19-year mean (1993-2011 inclusive), with a standard deviation of 12 mm (other 5-year periods produce larger differences, with a greatest difference at any one tide gauge of 93 mm).

MDTs from a wide range of ocean models have been collated, together with the latest AVISO absolute dynamic topography and an MDT derived from the CARS climatology (a purely steric sea level computed where the ocean depth is 2000 m or greater, and extrapolated to the coast). These MDTs, all averaged over the standard 5-year reference period, are shown in Figure 13. The typical range among models is about 100 mm at any one tide gauge, and the models also show a similar degree of smoothness between nearby tide gauge positions. The obvious exception is in the Gulf of Carpentaria (gauges 22, Karumba and 23, Weipa), where the model spread is notably larger.
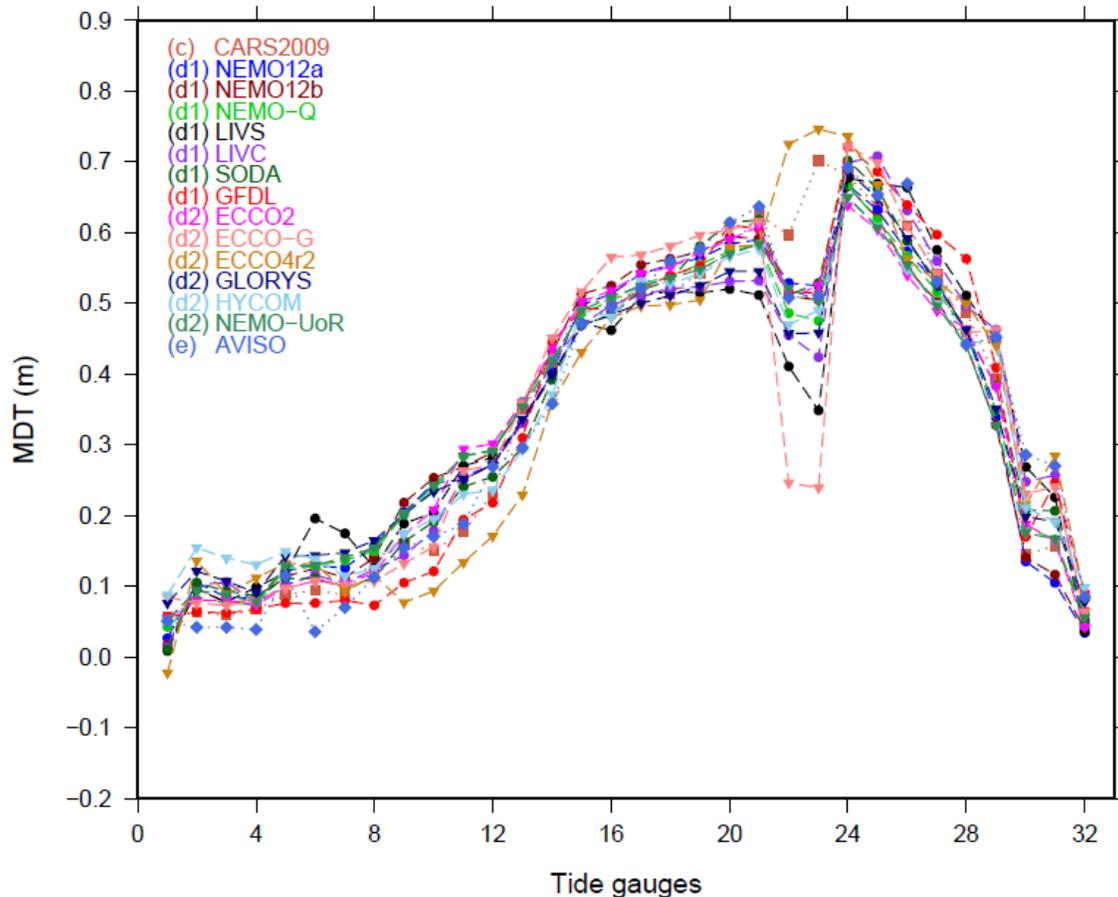
Figure 13: MDTs at Australian tide gauges from the CARS climatology (squares), ocean models independent of geodetic measurements (d1, circles), models incorporating geodetic measurements (d2, inverted triangles), and the AVISO MDT (diamonds).

 The Gulf of Carpentaria is part of a broad, shallow shelf region where large sea level signals result from local wind stresses. It is very distant from the nearest CARS data point, and close to the Torres Strait, which is extremely shallow (a sill depth of 7 m, and shallower than that for much of its width). Two of the ocean models (ECCO-G and LIVC) actually have land bridges across the Strait, and it seems clear that the models are sensitive to the details of friction/barriers in the Strait and probably also to the applied wind stresses in this region.

In order to calculate MDT from the tide gauge data, the geoid at the tide gauge or GPS position is required. Here, we use three different geoids: EGM2008 (Pavlis et al., 2012; 2013), the Australian AUSGeoid09 (AGQG2009, Featherstone et al., 2009), and the TUM13 geoid (Fecher et al., 2015) supplemented with EGM2008 beyond degree 720. The resulting MDT values are shown (stars) in Figure 14. In addition, the figure repeats some curves from Figure 13, and adds an MDT determined from the TUM13 geoid and DTU10 mean sea surface (after correction to the standard reference period).
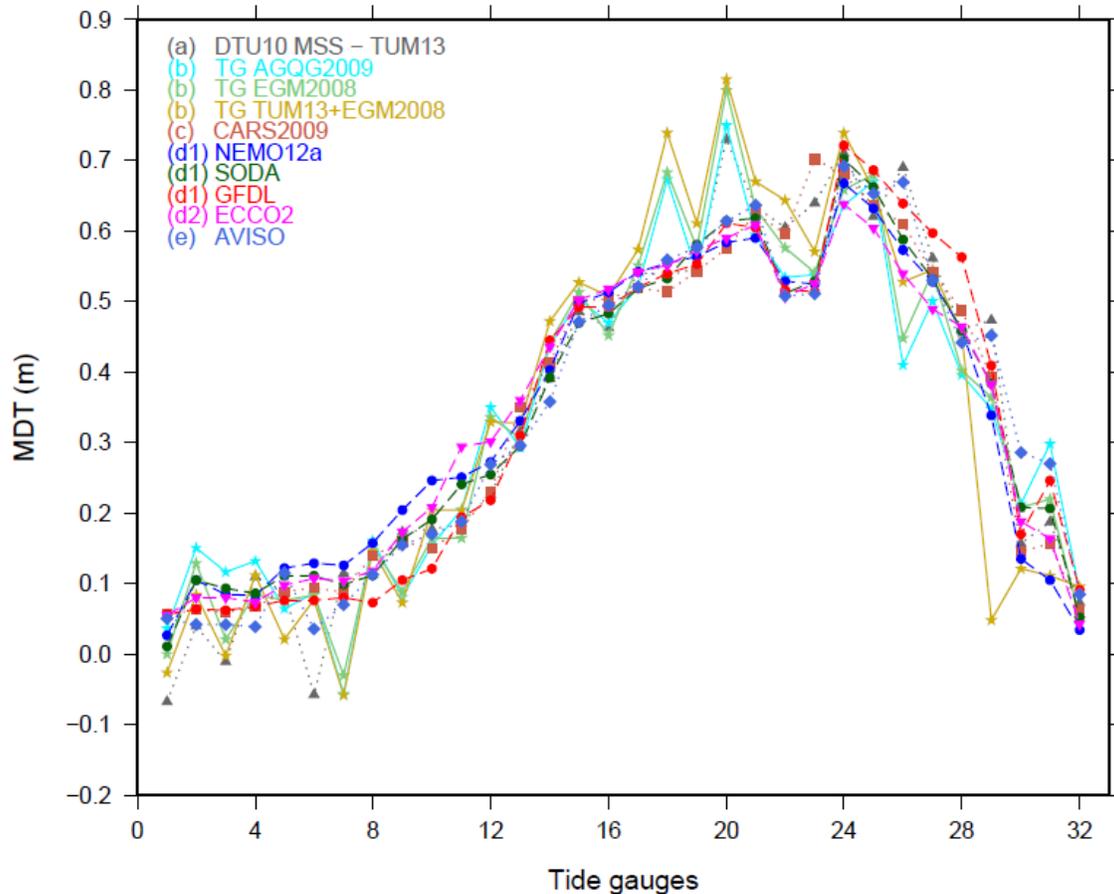
Figure 14: MDTs at Australian tide gauges as measured by tide gauges in combination with GPS and geoid data (stars), and by subtracting a geoid from the mean sea surface determined from altimetry (triangles). Some of the curves from Figure 13 are also repeated for context.

It is clear that the tide gauge results agree in general pattern with the models, but that the curves based on the tide gauges are much more jagged. Differences from the model curves have standard deviations of 70-80 mm (100 mm for TUM13, the difference clearly being mainly due to the discordant value at gauge 29, Brisbane, which should be investigated further).

Generally, the DTU10-TUM13 result is smoother and closer to the model results than the tide gauge results, although there are exceptions such as at gauge 6 (Port Stanvac), and gauge 20 (Wyndham). Wyndham is interesting in that it agrees with the tide gauge result. This may indicate a genuine MDT signal which is unresolved by the ocean models, since Wyndham is in a narrow estuary far from the coast, though that would imply that the DTU10 mean sea surface is also good in this region. The idea that the MDT at this gauge is decoupled from the nearby ocean value is consistent with the increased residual variability seen at this gauge (Figure 6), although that is still only between 40 and 50 mm for monthly mean values. Alternatively, the agreement on the size of the spike may be a result of common geoid errors, though this would imply that those errors are at degrees below 720 rather than at the highest degrees, which is unusual.

In the case of Port Stanvac, investigation of the mean sea surface has shown that it does not have data close to the coast in this region, as a result of limitations in the tidal model used, a deficiency which can be rectified in the latest mean sea surface.

Another gauge showing a spike is number 26 (Mackay) which has also been noted as having higher residual variability than other gauges, though there is no obvious reason for this (it is behind the Great Barrier Reef, but so are Townsville and Cairns, which both have lower residual variability).

Other large spikes are at gauges 7 (Port Lincoln) and 18 (Port Hedland). Although these are in a bay and an inlet respectively, this is not unusual and they do not show particularly high residual variability. Overall, although the oceanographic information suggests that some of the spikes may be at places with increased importance of local dynamics, the most likely explanation for spikes of this size must be errors in the small-scale geoid, though the case of Wyndham remains an interesting exception where the smallest scales of the geoid cannot be the issue, and local ocean dynamics is more likely to be an issue than elsewhere.

A final point worth making concerning this analysis is that the combination of good agreement with models at many positions, and large disagreements at others, is suggestive of an error distribution which is not a normal distribution, but has significantly broader tails. This is a plausible result of either geoid errors, which can have quite different sizes in different regions, or of blunders in deriving the tide gauge coordinates. Although every effort is made to avoid the latter, the complexity of the audit trail required to correctly identify tide gauge coordinates from a wide range of measurement types, levelling campaigns, and multiple tide gauge datums, means that occasional blunders are almost inevitable. In deriving a coastal MDT incorporating tide gauge data, statistically robust method must be used which makes it possible to reject clearly anomalous measurements.

3.1.4 Initial results for a global tide gauge MDT calculation.

Mean ellipsoidal heights of sea level have been calculated at 301 tide gauge positions using a combination of tide gauge measurements, datum information, and GNSS positioning data. The 5-year means are inverse-barometer corrected, and any large gaps have been filled using the nearby best-fitting altimetry data as used in Figures 1-6 (with trends and annual cycles removed and replaced based on valid tide gauge data). The resulting heights, calculated in the Tide-Free system as is usual in GNSS processing, have been converted to the Mean Tide system for comparison with models and altimetric measurements.

As an initial test of MDT calculation, the Eigen6-c4 geoid has been calculated at each tide gauge position using the full degree 2190 spherical harmonic expansion, again translated into the Mean Tide system. The resulting MDT values are plotted in Figure 15 (circles). The background to this figure is the Aviso MDT for the same period, with a mean value shifted so that the median difference at tide gauge positions is zero.
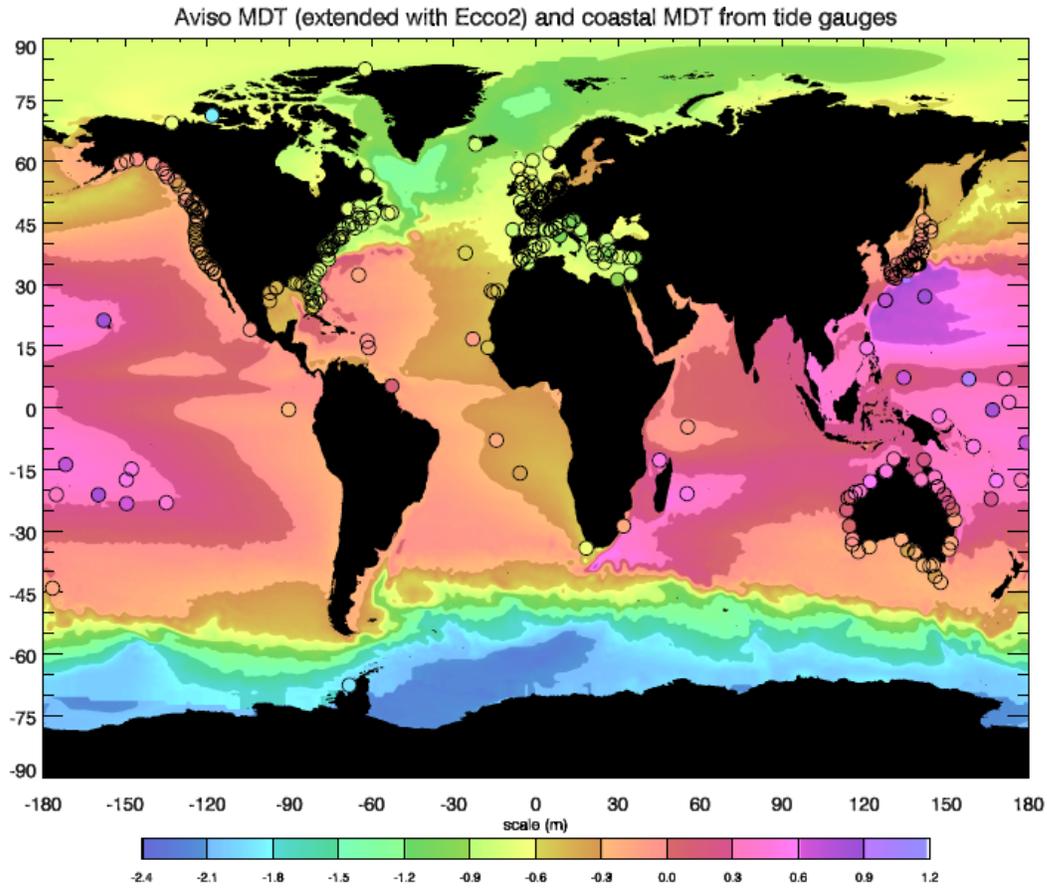
Figure 15: MDT at tide gauges (circles) using the Eigen6-c4 geoid, against a background of the Aviso MDT for the same period (extended with the Ecco2 model MDT over ice-covered regions, the Black Sea and the Baltic). Model and Aviso mean values have been changed so that the median difference at tide gauges is zero.
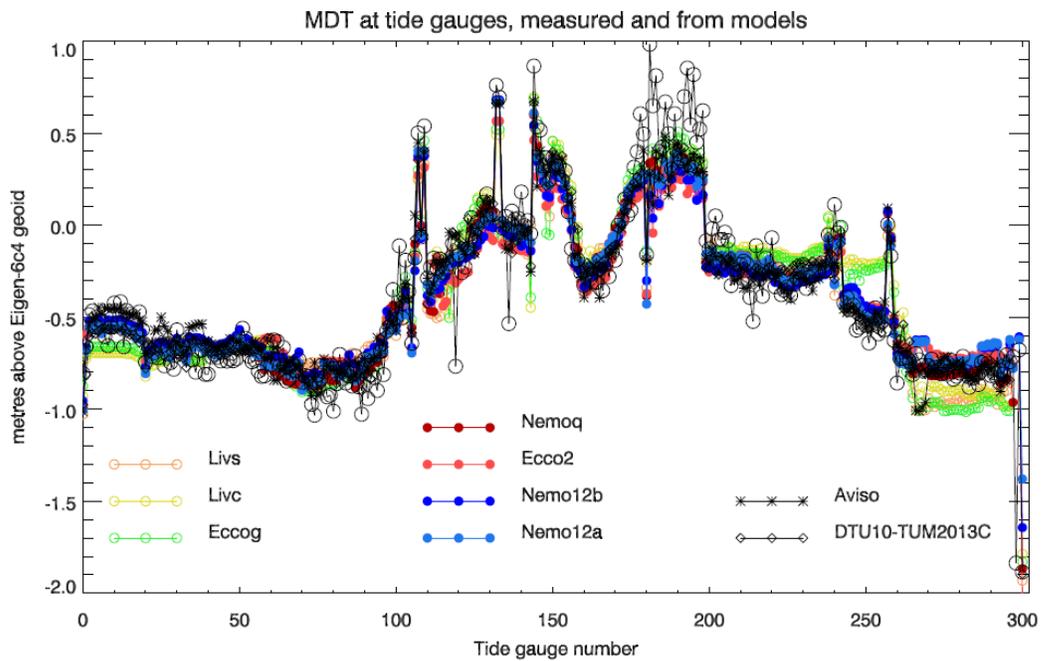
Figure 16: MDT at tide gauges as in Figure 15 (black circles), compared with the nearest coastal point from a variety of models. Tide gauge ordering is as in Figure 7.

At high latitudes, and in the Black Sea and Baltic, the Aviso data are missing. In these regions, the map shows the Ecco2 model MDT with a similar datum shift to match the median tide gauge values.

It is clear that the broad pattern of the MDT is captured well, with particularly good agreement along the continental and Japanese coastlines, including the small number of African points. Many Pacific islands appear to be too high in the tide gauge MDTs, a systematic bias likely to be a result of the similar small scale geoid structures on these large seamounts. Arctic and Antarctic tide gauges also agree well with the Aviso/Ecco2 values, with the exception of Ulukhaktok (formerly Holman) tide gauge on Victoria Island (just north of the Canadian mainland), for which the tide gauge value appears to be too low by about 1 m.

A better sense of the level of agreement is given by Figure 16, which compares the tide gauge MDT with all seven ocean models, and also the Aviso MDT and an MDT derived from the DTU10 mean sea surface and the TUM2013C geoid. Here, the high bias of Pacific island gauges (180-198) is particularly clear. Otherwise, the conclusions are generally similar to the case of Australia: large scale patterns are good, but the tide gauges show more "jitter" in MDT values (spikes which occur in both tide gauge and model MDTs result from sudden changes in position, e.g. to a distant island).

Root-Mean-Square differences are between about 14 cm and 18 cm depending on the field used, with the data-based MTDs and the finer resolution models coming out better, though the comparisons are not fair at this stage as not all tide gauges are represented in all fields (e.g. the data-based fields and coarse resolution models lack Arctic data). The spikiness, and the Pacific island bias, again suggest a non-Gaussian distribution.

The model curves clearly form two groups, with the coarse resolution models (Livs, Livc, Eccog) generally agreeing with each other, and differing from the finer resolution models which tend to follow the data better. A particularly clear example of this is in the Gulf of Mexico (244-254) and along the Atlantic coast of the US and Canada (260-295).

We stress that these are only preliminary results, with a single geoid, and no attempt to check for procedural errors following this initial calculation. The results are encouraging, but need to be investigated in more detail before concrete conclusions can be drawn.

3.1.5 A proposed method to determine a coastal MDT using tide gauge data.

The above analyses present a consistent, but complex picture of how tide gauges represent the MDT. Here we offer a recipe for using this information to produce a coastal MDT while taking errors into account.

A priori errors on the tide gauge MDT are unknown. The patchwork of information which constitutes the extension of geoid models beyond the satellite-resolved range up to degree ~200 makes it very difficult to assess the errors due to this unresolved range (expected to be about 30 cm RMS on a global mean, if no additional data are used, but in

reality very dependent on region, and significantly smaller than 30 cm if good use has been made of auxiliary data). What we do know is that the spatial decorrelation scales of these errors are very short, so the jaggedness of the MDT estimate at tide gauges is likely to be dominated by this error source. The first stage is therefore to estimate this error from the data. In order to do this, we will subtract the best-correlated ocean model MDT from the raw tide gauge MDT, then subtract a large-scale correction from that residual, to account for any global scale biases in the ocean model, and treat the final differences as a measure of error, from which we should be able to produce a quite robust PDF given the 301 tide gauges available. The Australia study is consistent with previous assessments in the North Atlantic in suggesting that this error is likely to be in the range 5-8 cm RMS.

Such an error means that a single tide gauge measurement is unlikely to produce an improved MDT in most coastal locations – the omission error in the MDT is smaller than that in the geoid, so nearby altimetry should produce at least as good an estimate. The potential strength of tide gauges will therefore be in their combination, particularly along coastlines where the MDT changes rapidly offshore (such as eastern Australia). This combination requires that the tide gauges be representative of a broad stretch of coastline, and will rely on being able to supply an autocovariance function for the MDT along that coastline. We will use the above diagnostics to calculate such an autocovariance function (naturally, this will only be possible along extended coastlines; this method cannot be applied to small islands).

We will start by producing a single autocovariance function based on the longest coastlines and the (false) assumption of spatial homogeneity. The distances displayed in Figures 9-11 then represent a means of refining this autocovariance function locally, by forcing the initial curve to fit through the 4 points (1^2, 2^2, 4^2 and 8^2 cm^2 drops from the autocovariance at lag 0, at the respective distances). The most conservative values from all models will be used (alleviating the difficulties with low resolution cases. This will be further refined using the tide gauge cross-correlations shown in Figure 8 (in this case used in combination with variances to ensure that the autocovariance function drops at least as quickly as the tide gauge data imply. This will provide a means of interpolating and smoothing the tide gauge data along the coastlines. All of this will be done against a baseline "first guess" made from a mean of the model data, and a signal size estimated from the variance between model predictions.

The smoothing/interpolation will use a Wiener filter applied at each point along the coast. In addition to the expected signal autocovariance, this also needs an error estimate for each tide gauge. This will be calculated by a sum in quadrature of the estimated geoid error and the "representativeness error" which we will calculate from the difference between tide gauge and altimetry, after temporal smoothing (again, just a running annual mean, to give a conservative estimate). The assumption will be that these errors are not correlated in space.

The result will be a tide-gauge derived MDT along the entire coastline (for the 1/8 degree grid), together with error estimates. In the case of small islands, there will be no benefit from averaging or smoothing, so these will be dominated by the geoid and

representativeness errors. However, there has been no use at this stage of satellite altimetry data. The final stage will be to combine this first estimate with a satellite altimetry-based global field. For this, we will again use the model data to estimate the spatial distributions around each point for which the MDT is within 1, 2, 4 and 8 cm of that at the tide gauge position, to provide weightings for the altimetry in this range. An error estimate for the altimetry will be needed, and this will be a combination of the mean sea surface error and geoid error. The latter will need to be estimated based on the lower of geoid power and satellite commission error, ignoring auxiliary data, since the spatial averaging of the altimetry is the reason for any improvement over the point values at tide gauges.

WP3200 Mean Dynamic Topography and GOCE

While many studies have now demonstrated the contribution GOCE has made to the determination of the open ocean MDT, there has been relatively little work focusing on the MDT where it meets the land. The objective of this work package is to assess our ability to compute a coastal MDT (CMDT) using the latest GOCE gravity models. We begin in section 3.2.1 with an assessment of the signal content of the CMDT as represented by a high resolution ocean model. From this, a model of CMDT omission error is derived. In section 3.2.2 the CMDT omission error is compared with the formal geoid errors from a representative range of gravity models, thereby establishing a likely upper limit (assuming the formal errors to be accurate) on the resolution that can be obtained by the geodetic approach. The impact of mean sea surface (MSS) errors are also considered. CMDTs derived from the range of gravity models are compared with model and GPS based CMDT estimates in section 3.2.3, providing an additional means of validating the formal errors and their relationship with the CMDT omission errors. The MSS is found to be the dominant source of error in the CMDT, which can be attributed to the limitations of altimetry in the coastal zone. This error is much greater than that suggested by the formal MSS errors. As the basis for further refinement, a relatively simple two-stage screening and filtering method is shown to dramatically improve the CMDT while preserving some oceanographically significant differences between the observations and the model.

3.2.1 Coastal MDT omission error

One of the novel features of the GOCE mission was the provision of formal error variance-covariance information. However, the rigorous exploitation of errors must take into account their magnitude in relation to the signal. Thus we begin by considering the magnitude of the coastal MDT (CMDT) signal as a function of degree and order, since the errors are also given in this form. Another, equivalent, way of framing this is as an examination of MDT omission error (MOE). If we take the MDT expressed as a series of spherical harmonic coefficients, then the MDT at a particular point can be calculated to some d/o=L. As L is increased, the MOE is reduced. However, the geoid (and MSS) commission error (GCE) grows as L is increased. If at some d/o=L_{opt} the GCE exceeds the MOE, then there is nothing to be gained by increasing L further, unless a filter can be devised that suppresses the GCE while not attenuating the MDT signal. As we shall see this is particularly challenging given the relative magnitudes of the residual MDT signal and GCE beyond d/o=250.

In this section we examine the first component of this balance, namely the MOE. To do this we take an MDT from a high resolution ocean model (the $1/12^{th}$ of a degree OCCAM12 model). The MDT is extended to fill land areas to produce a smooth global field without discontinuities at land/sea boundaries. From this global field a set of spherical harmonic coefficients up to d/o=2190 was calculated. The complete set of 1600 tide gauge locations were mapped to the nearest ocean points on the model grid and at these points the MDT was calculated from the spherical harmonic coefficients as a

function of d/o up to *L*=2190. These MDT vectors were subtracted from the original MDT values to give a set of residuals which give the MOE. Figure 17a, which shows the RMS MOE calculated over the 1600 TG locations (red), demonstrates that initially the MOE declines rapidly with d/o, reaching 1 cm at just over d/o=250. Subsequent reductions in MOE are harder to obtain, with errors falling to 0.5 cm at d/o=500 and 2 mm at d/o=2000. Figure 17b (red) expresses the MOE in terms of the fraction of signal recovered for a given d/o. At d/o=200 more than 90% of the MDT signal has been recovered, while at d/o=500 over 95% of the signal has been recovered. The RMS MOE was also calculated separately for the TGs within the five study regions. Although the statistics are not as robust, all show roughly the same behaviour. There is, however, quite a wide variation in the d/o at which the error falls below 1 cm, ranging from just under d/o=150 for Australia (blue) to just under d/o=400 for South America (magenta), reflecting the relative mean magnitude of the CMDT for these regions. In terms of skill, for the Northeast Atlantic, Southern Africa and the Pacific islands more 90% of the signal can be recovered with d/o=150, while for South America and Australia more terms are required to recover 90% of the signal.
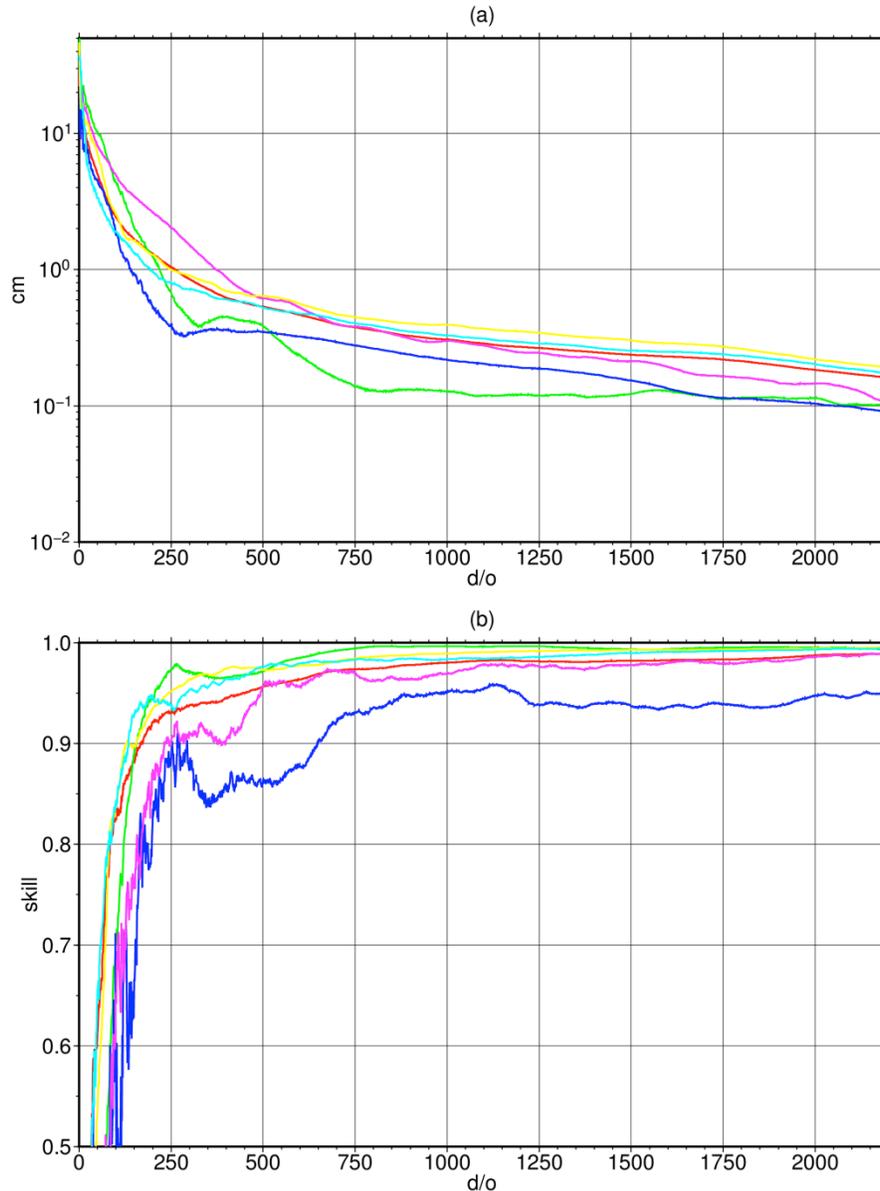
Figure 17. (a) The RMS residual between the original MDT and the truncated MDT as a function of d/o of truncation computed for the global set of tide gauge locations (red) and for sub-sets corresponding to the five study regions: the Northeast Atlantic (cyan), Australia (blue), Agulhas (green), South America (magenta) and the Pacific Islands (yellow). (b) Repeating (a) but expressed as fraction of signal recovered.

Figure 18 shows the d/o required to reduce the MOE at each location by 1 cm, 0.5 cm and 1 mm. In most locations the MOE can be reduced to 1 cm by expansion to d/o<200 and in many places to d/o<100. Similarly in many places the error can be reduced to 5 mm by expansion to d/o<300 and to 1 mm by expansion to d/o<800. However, there are some regions that stand out as requiring higher d/o expansions to reduce the MOE to a given level. Notable among these are the TG locations around Japan and Florida; two places where very strong currents – the Kuroshio and the Gulf Stream – come close to shore. Figure 19 shows the d/o required to reduce the MOE at each location by 10%, 5% and 1%. For most locations the MOE falls to less than 10% of the signal magnitude for

d/o<200 and in many places for d/o<100, less than 5% for d/o<200 and less than 1% for d/o<800.

Figures 20 and 21 consider the absolute and relative errors, respectively, for three specific truncations: d/o=300, corresponding the maximum d/o for the final GOCE models (approximately so for GTIM5 where the maximum d/o=280); d/o=720 corresponding to the maximum d/o for the GOCO05C model, and d/o=2190 corresponding to the maximum d/o of the combined models EGM2008 and EIGEN-6C4, that will be considered further below. Even at d/o=300 the MOE at the majority of TG locations is less than 3 mm, with many locations achieving an accuracy better than 1 mm. There are relatively few locations, including the aforementioned regions around Japan and Florida, where the MOE exceeds 1 cm at d/o=300. At most location this amounts to a error of just a few percent, with the error exceeding 10% of the signal in a handful of locations. At d/o=720 the MOE at the majority of TG locations is less than 1 mm, or 1% of the signal, with many locations achieving an accuracy better than 0.5 mm, and relatively few locations where the MOE exceeds 5 mm. Finally, at d/o=2190, most locations have a MOE of less that 0.3 mm, with relatively few exceeding 1 mm or 1% of the signal.
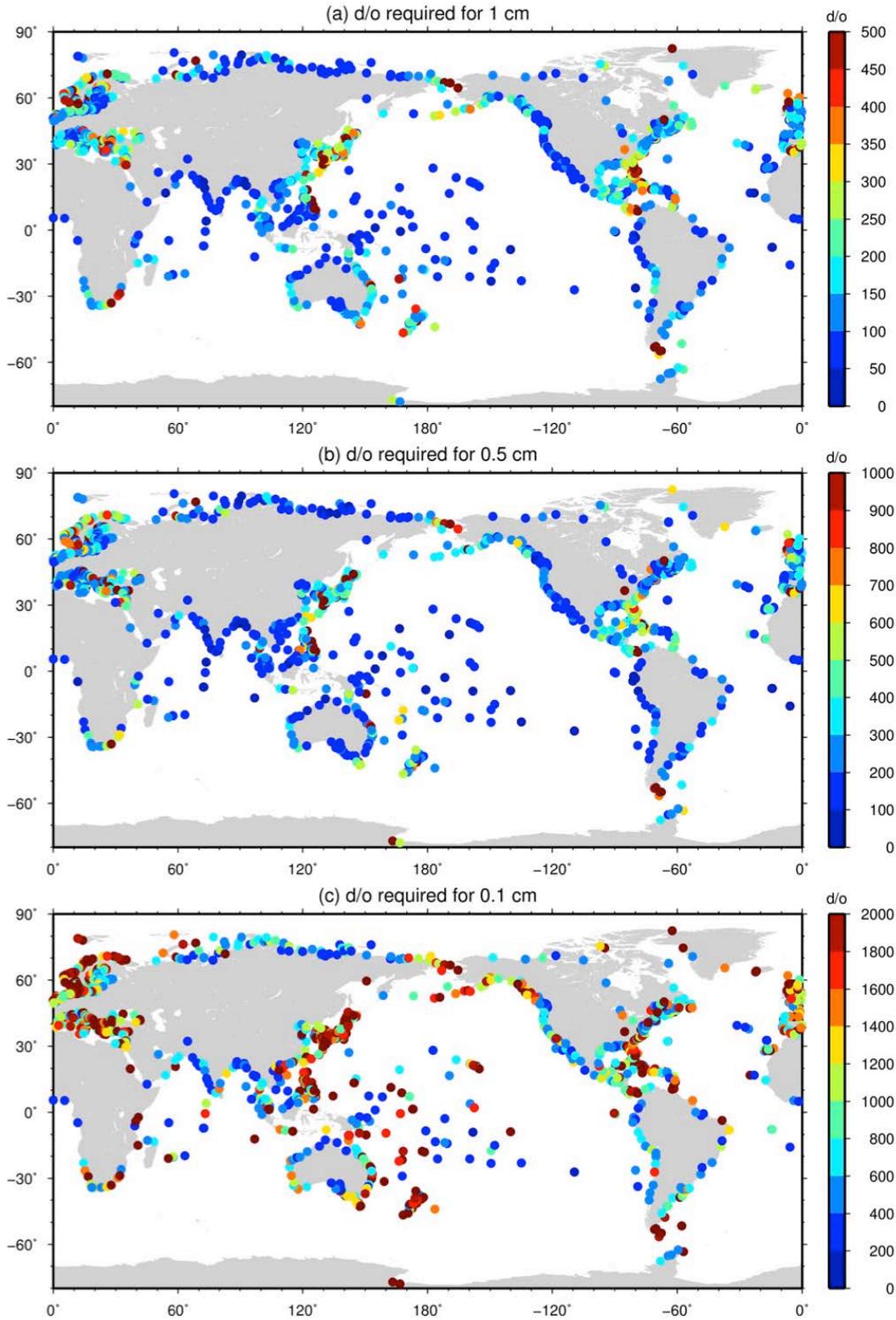
Figure 18. The d/o required to reduce the omission error at each tide gauge location to (a) 1 cm, (b) 0.5 cm and (c) 1 mm.
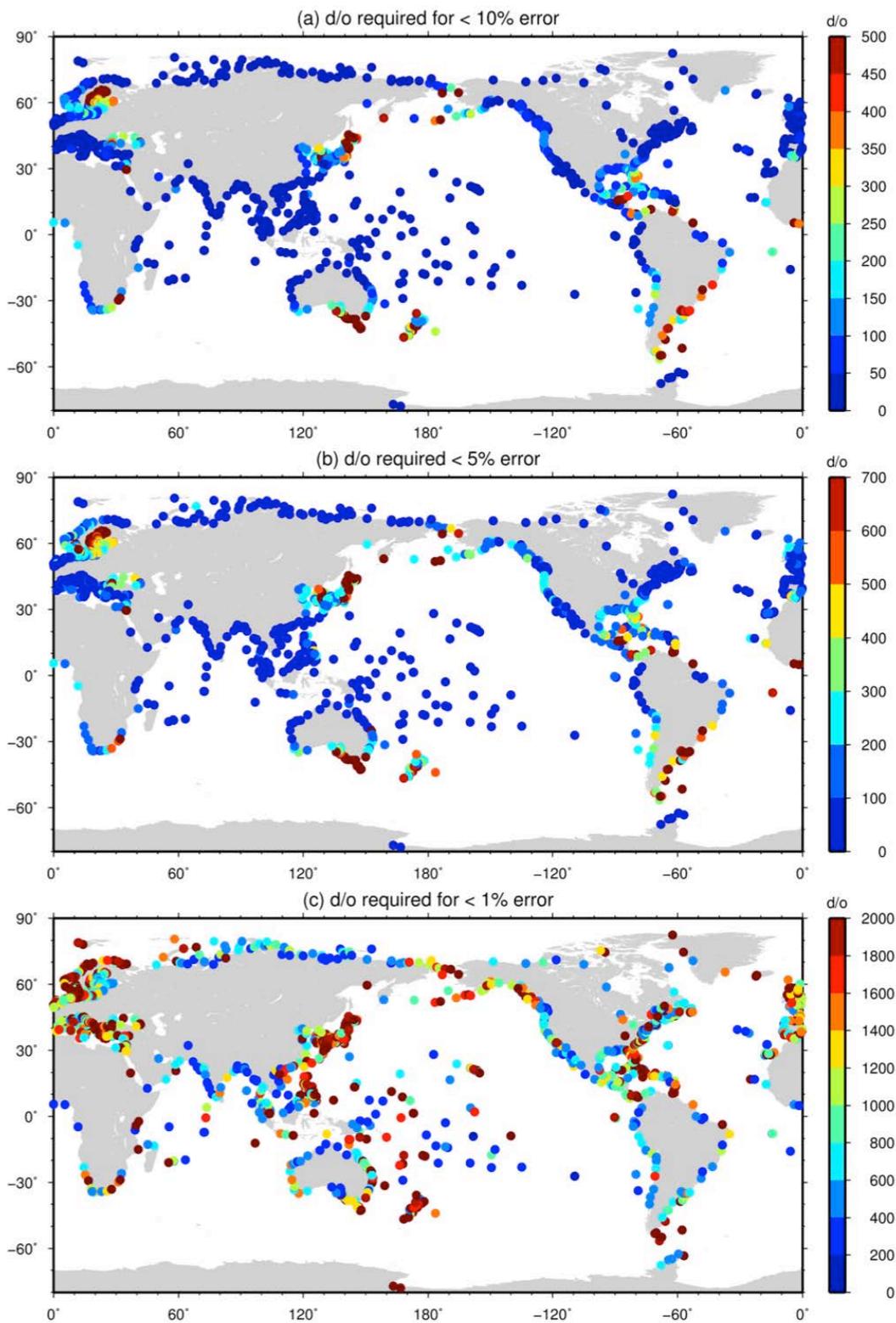
Figure 19. The d/o required to reduce the MDT omission error to (a) 10%, (b) 5% and (c) 1%.
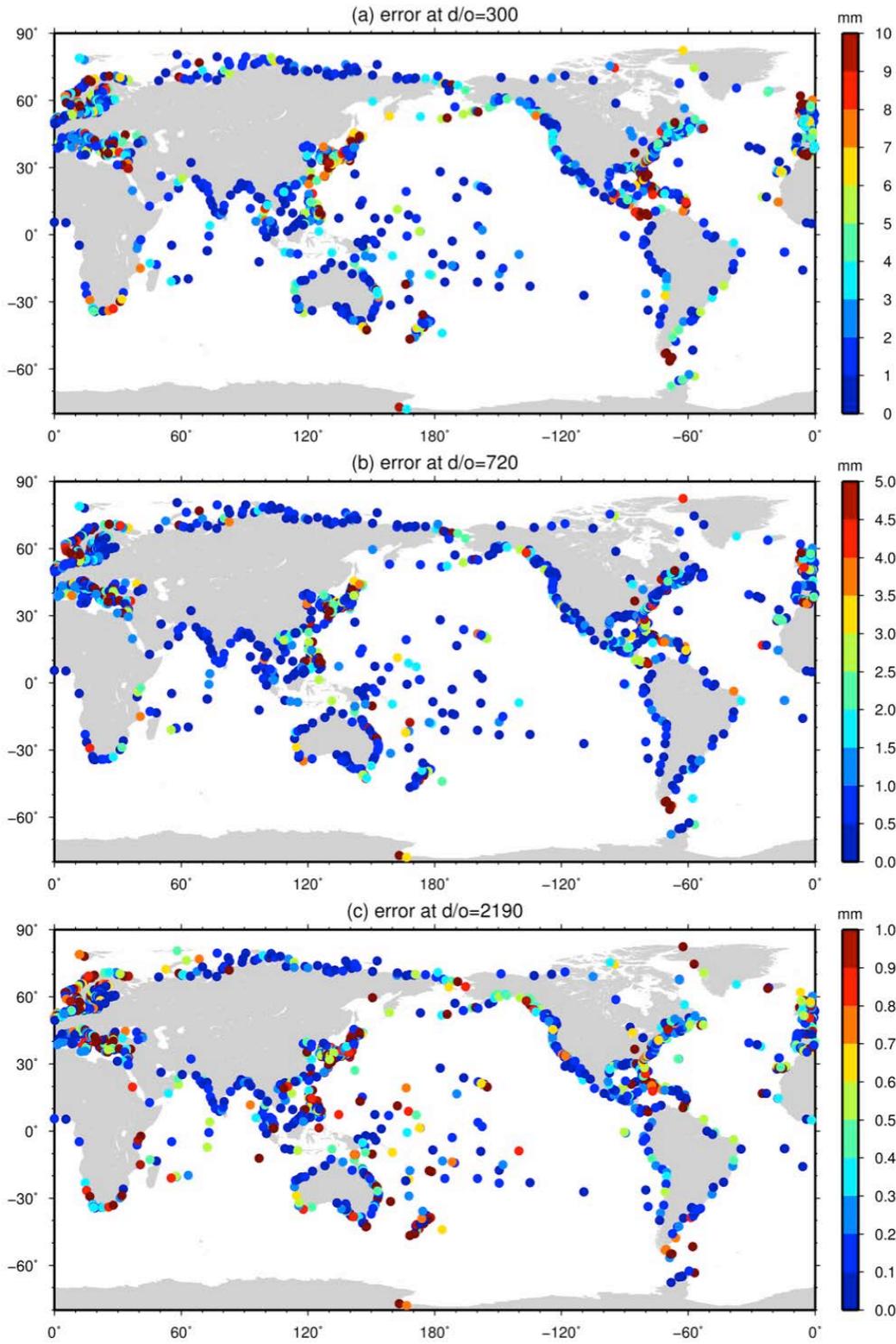
Figure 20. The MDT omission error at tide gauge locations for truncations at d/o (a) 300, (b) 720 and (c) 2190.
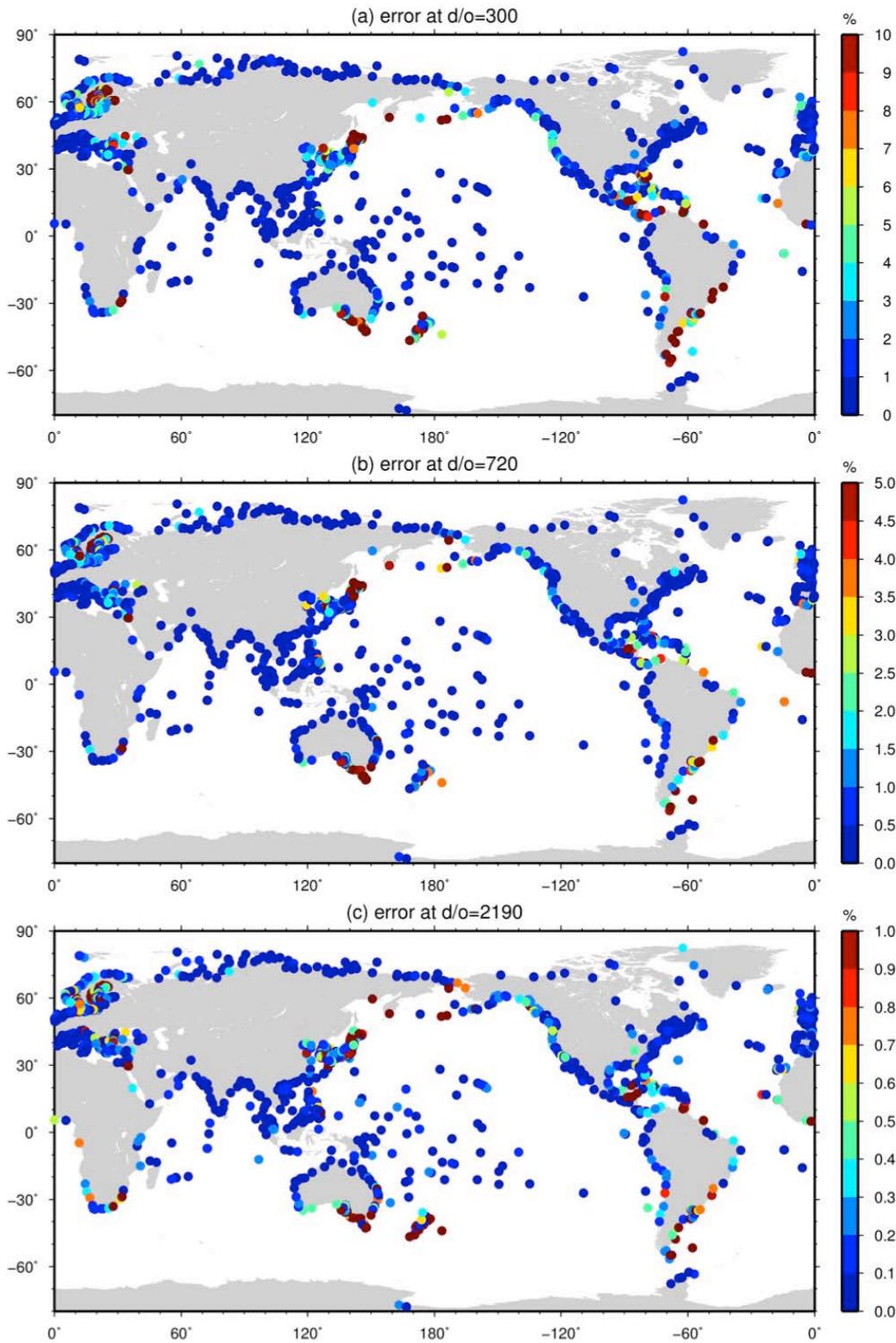
Figure 21. The relative MDT omission error at tide gauge locations for truncations at d/o (a) 300, (b) 720 and (c) 2190.

As identifying individual locations in the global maps is difficult, in Figures 22 to 31 we consider the MOE in each of the 5 study regions. Figure 22 shows that for the majority of the TG locations with the Northeast Atlantic region the MOE falls to less than 1 cm for d/o=200. There are many locations, however, where the MOE is slower to decline and more spherical harmonic terms are required to reduce the error to less than 1 cm. These locations are generally clustered in the eastern North Sea, the North western reaches of the British Isles, along the Spanish Mediterranean coast and the eastern Mediterranean. This may be an artefact of the convoluted nature of the coastline in these regions which may introduce to noise into the spherical harmonic transformations. In the majority of locations the MOE falls to less than 0.5 cm for d/o=400 and in many places for d/o<300. In the majority of locations to achieve a MOE of less than 1 mm requires substantially more spherical harmonic terms. In the majority of locations the MOE falls to less than 1 mm for d/o<1200, but in many locations even expansion to 2190 is insufficient to reduce the error to 1 mm. Figure 23 confirms that at d/o=300 the MOE is generally less than 4 mm and less than 2 mm in many locations. Only in a relatively few locations does the error at d/o=300 exceed 1 cm. At d/o=720 the MOE fall to less than 1.5 mm at most locations, with relatively few locations exceeding 5 mm. Finally, at d/o=2190 the error is less that 1 mm at the majority of locations.

Figure 24 shows that for the majority of the Australian TG locations the MOE falls to less than 1 cm for d/o=200, with several more requiring d/o=250. Only five TG locations, three on the east coast and two Tasmanian locations, require substantially more terms. Given their proximity to locations where less terms are required this most likely reflects some noise in the calculation rather than a true difference in the character in the CMDT at these locations. At the majority of locations the error falls to less the 5 mm for d/o<300, with a handful, excluding the anomalous locations previously mentioned, requiring expansions to d/o>300. Finally for most Australian TGs the MOE falls below 1 mm for d/o<800. Many require more than this. However, 1 mm MOE can be achieved for all within the upper limit of 2190. Figure 25 confirms that at d/o=300 the MOE is less than 5 mm at almost all Australian TG locations, exceeding 1 cm at only two locations. At d/o=720 the error is less than 2 mm at nearly all locations, exceeding 5 mm at only 4 locations. Finally at d/o=2190 the error is less than 1 mm at most TG locations.

Figure 26 shows that for nearly all of the TG locations within the Southern African region an expansion to d/o=200 reduces the error to less than 1 cm. The three anomalous locations along the eastern coast may reflect their close proximity to the Agulhas Current and the MDT gradient associated with it. At the majority of locations the MOE falls below 5 mm for d/o=300, with a handful, including two of the aforementioned locations, requiring expansions up to d/o=700 and one location requiring in excess of d/o=1000 to reduce the error to below 0.5 mm. All locations can achieve a MOE of less than 1 mm for d/o<2190. Figure 27 confirms that at d/o=300 the error is, with the exception of one location, less that 1 cm, with the majority having a MOE of less than 4 mm, while at d/o=720 most have an error of less than 1 mm and all less than 4.5 mm. At d/o=2190 the majority of TG locations have a MOE of less than 1mm.

Figure 28 shows that for almost all of the South America TG locations the MOE falls to less that 1 cm for d/o<200, to less than 0.5 cm for d/o<300 and 1 mm for d/o=800. The Patagonia locations are anomalous, requiring a much higher d/o to reduce the MOE to a given level. This may reflect their proximity to the ACC and/or the convoluted nature of the coastline here. Figure 29 confirms that at d/o=300 almost all TG locations have a MOE of less than 4 mm, the exceptions being the aforementioned Patagonian locations where for four the error exceeds 1 cm. At d/o=720 the error is generally less than 1.5 mm, with the only the Patagonian locations exceeding 5 mm, and less than 0.5 mm at d/o=2190.

Figure 30 shows that the Pacific Island TG locations generally require fewer terms to achieve a given MOE, with the majority achieving an accuracy better than 1 cm for d/o<100 and better than 0.5 cm for d/o<200. This to be expected given that these locations do not lie close to any strong boundary currents. The majority of locations achieve an accuracy better than 1 mm for d/o=800, with many achieving this accuracy with substantially less terms. Figure 31 confirms this picture, with the majority of TG locations have a MOE of less than 3 mm at d/o=300, 2 mm at d/o=720 and 1 mm at d/o=2190.
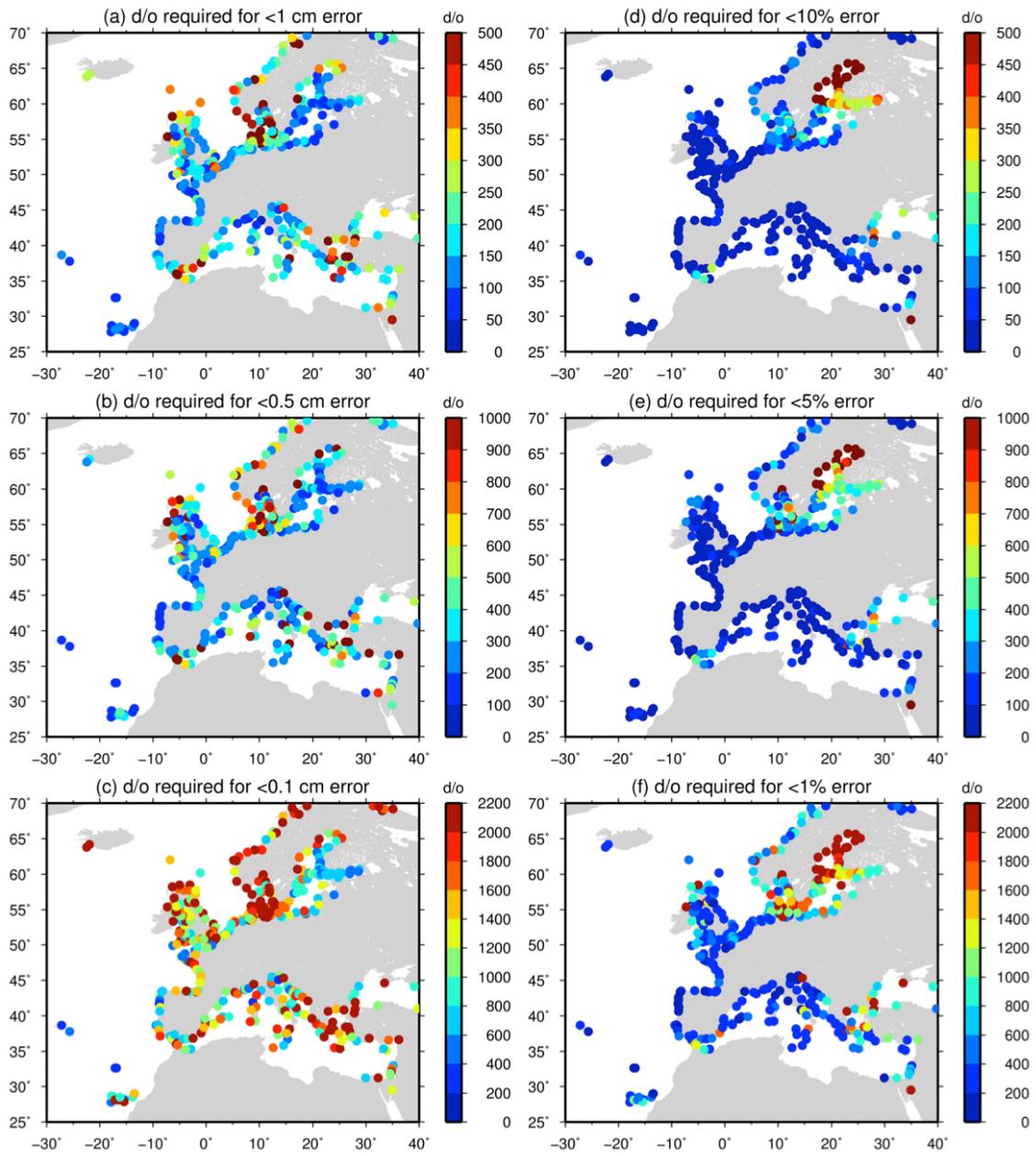
Figure 22. The d/o required at Northeast Atlantic tide gauge locations to reduce the MDT omission error to (a) 1 cm, (b) 0.5 cm, (c) 1 mm, (d) 10%, (e) 5% and (f) 1%.
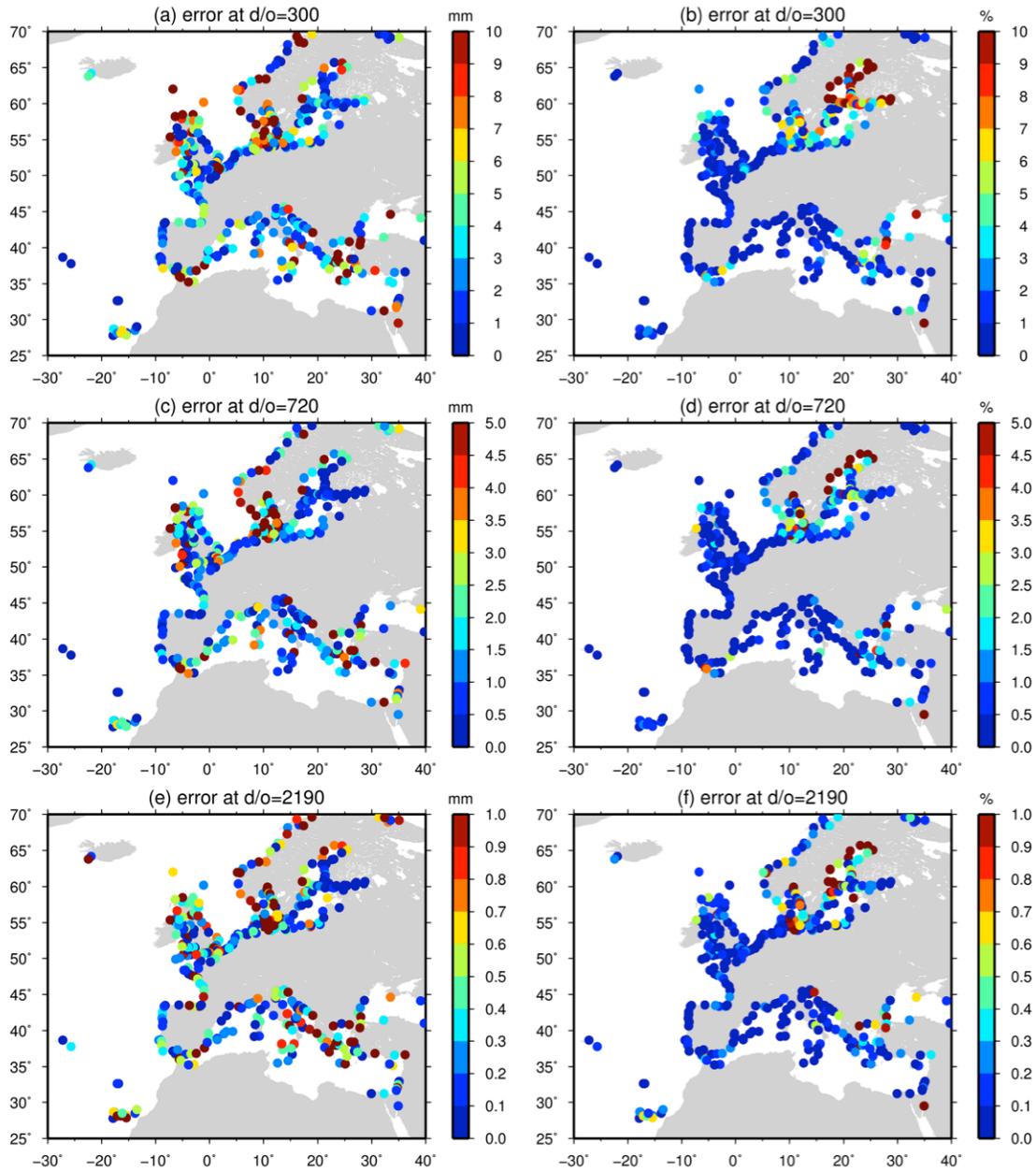
Figure 23 The absolute (left) and relative (right) MDT omission error at Northeast Atlantic tide gauge locations for truncations at d/o (a,b) 300, (c,d) 720 and (e,f) 2190.
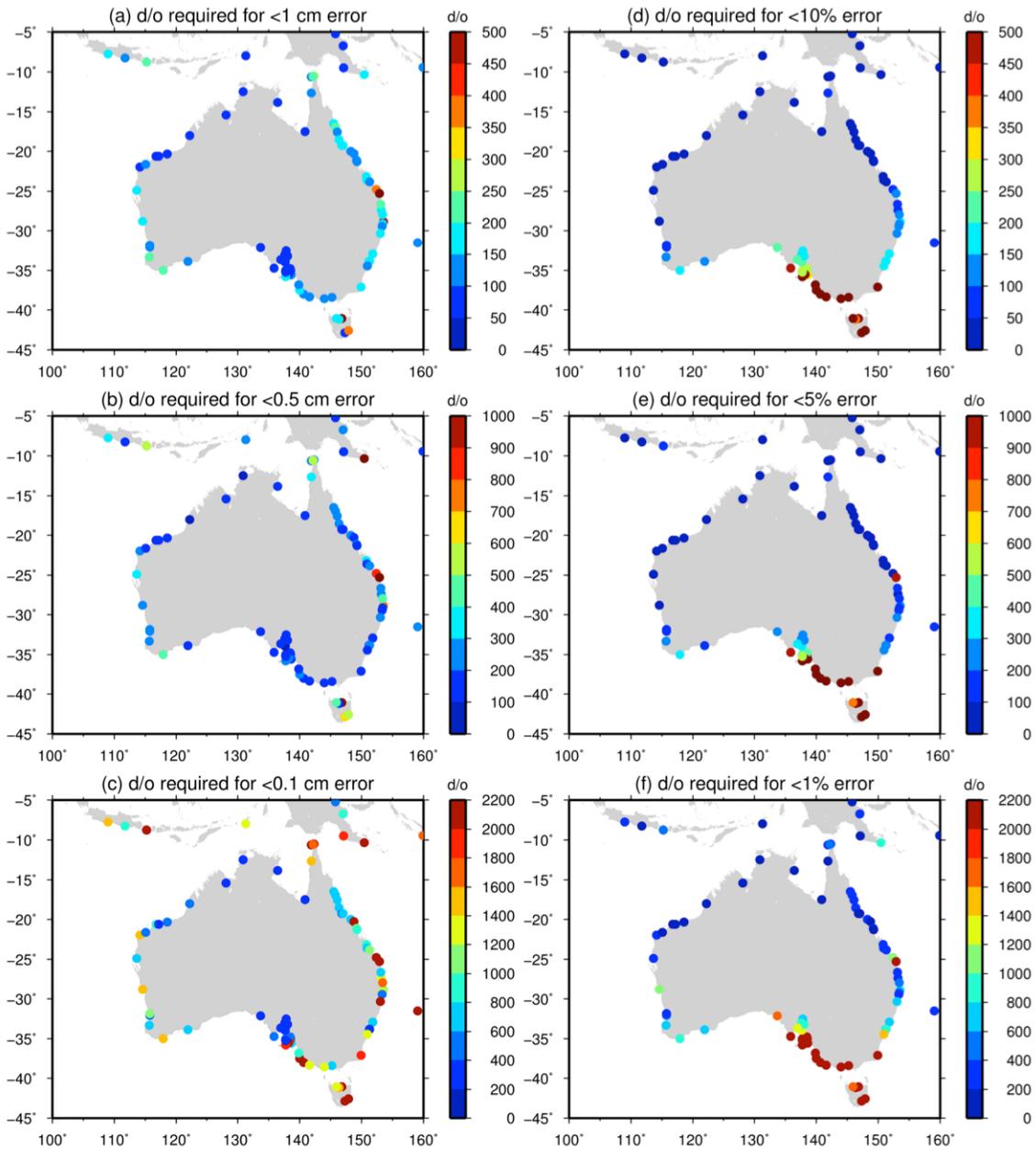
Figure 24. The d/o required at Australian tide gauge locations to reduce the MDT omission error to (a) 1 cm, (b) 0.5 cm, (c) 1 mm, (d) 10%, (e) 5% and (f) 1%.
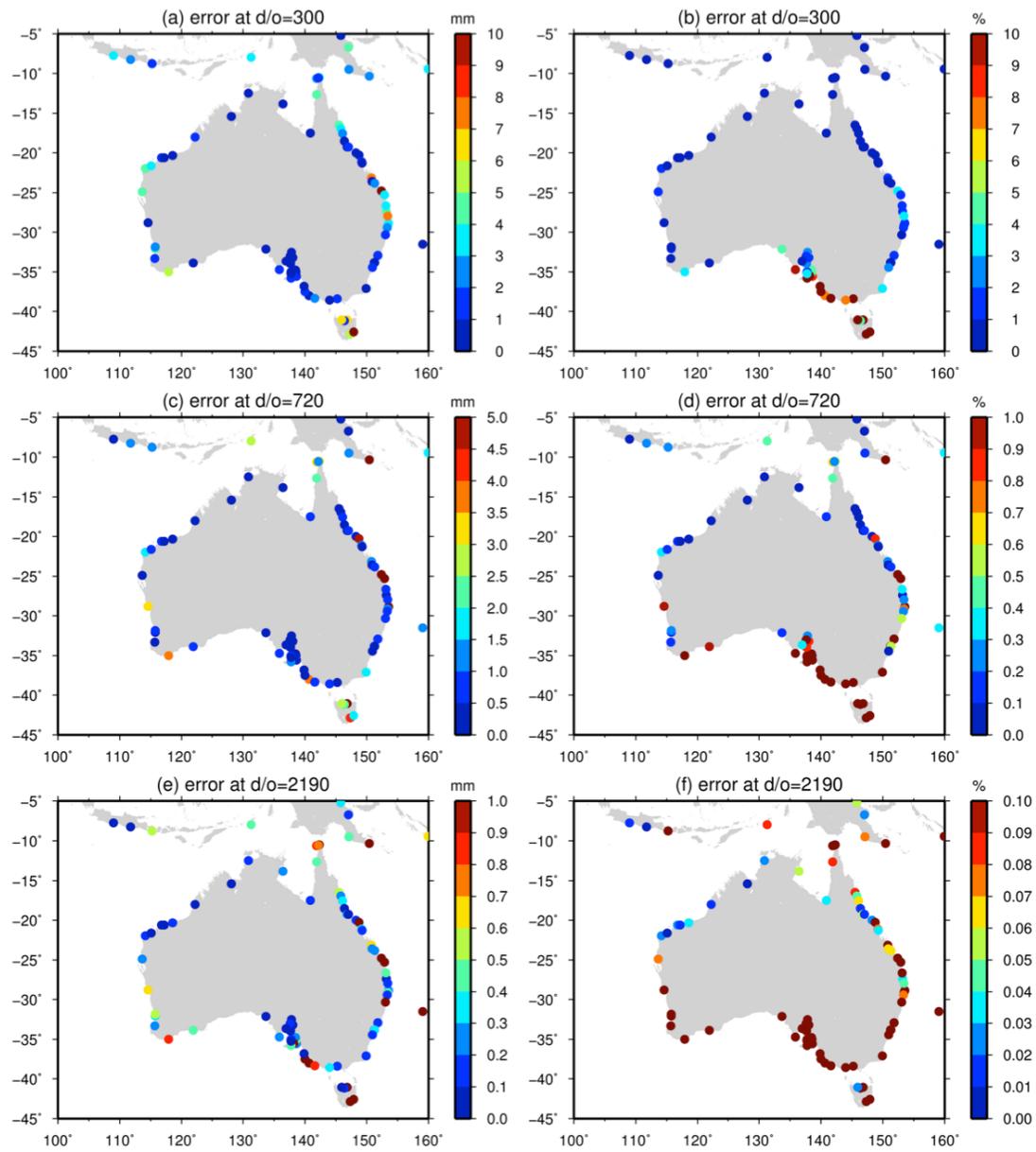
Figure 25. The absolute (left) and relative (right) MDT omission error at Australian tide gauge locations for truncations at d/o (a,b) 300, (c,d) 720 and (e,f) 2190.
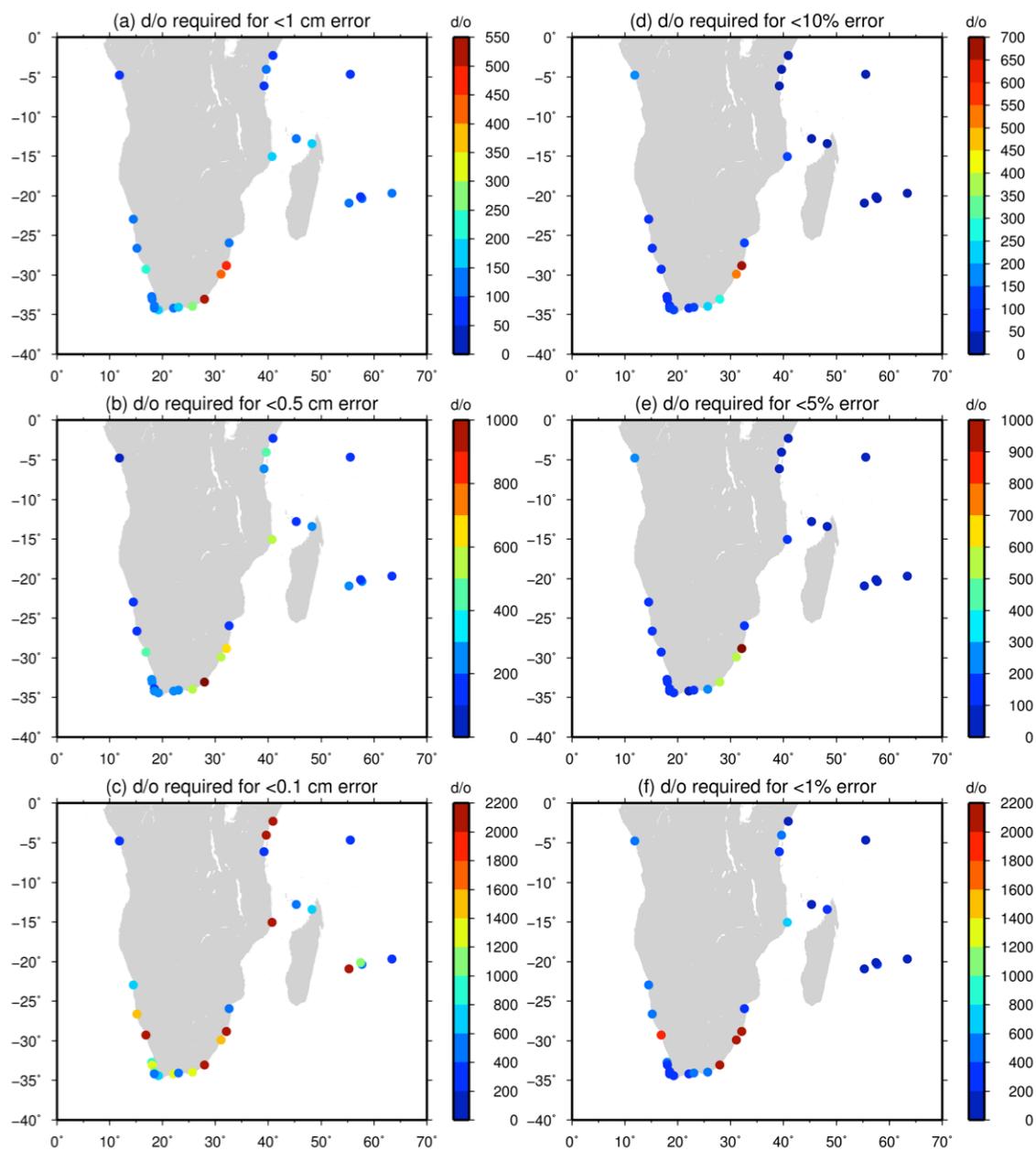
Figure 26. The d/o required at Southern Africa tide gauge locations to reduce the MDT omission error to (a) 1 cm, (b) 0.5 cm, (c) 1 mm, (d) 10%, (e) 5% and (f) 1%.
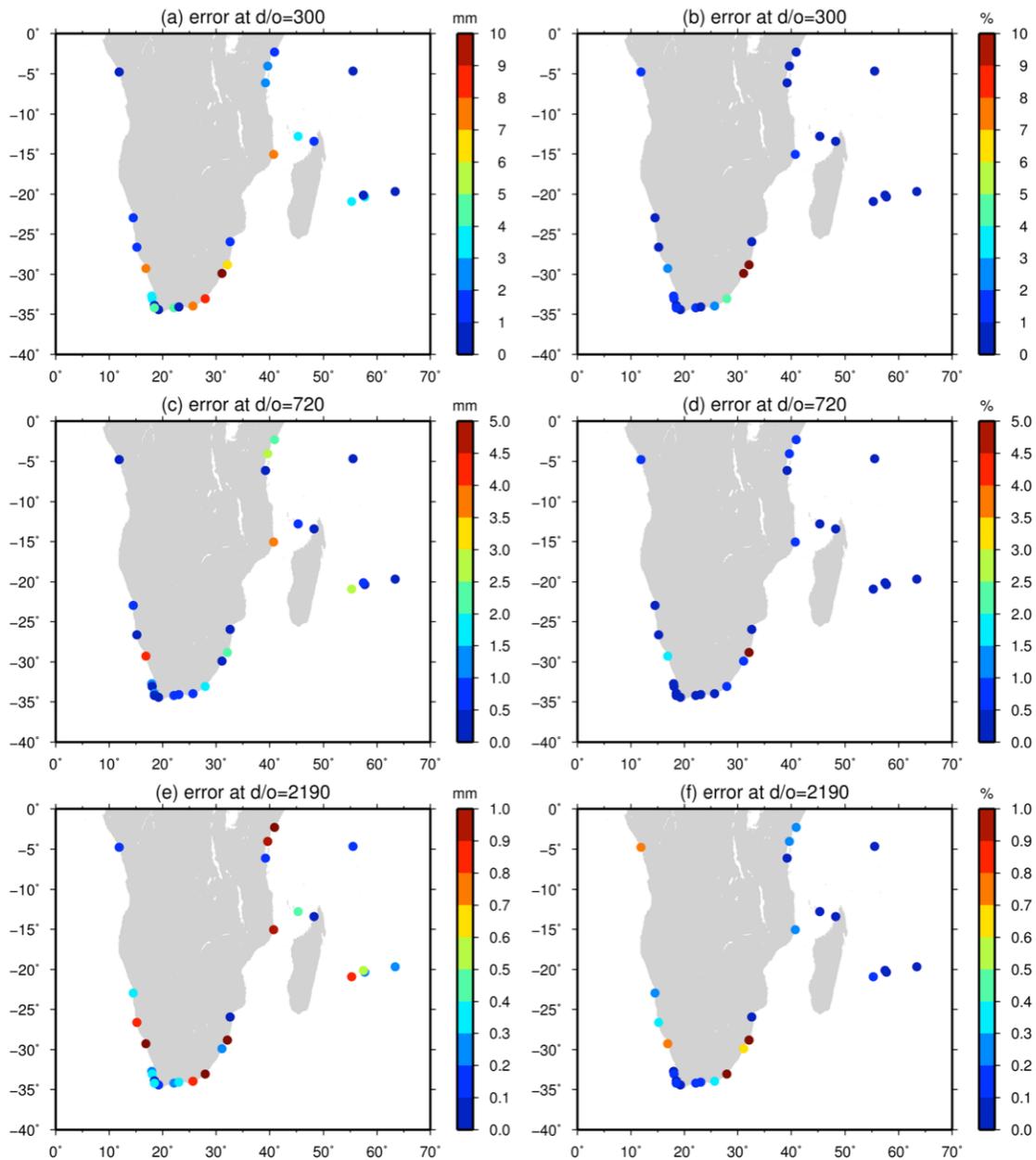
Figure 27. The absolute (left) and relative (right) MDT omission error at Southern African tide gauge locations for truncations at d/o (a,b) 300, (c,d) 720 and (e,f) 2190.
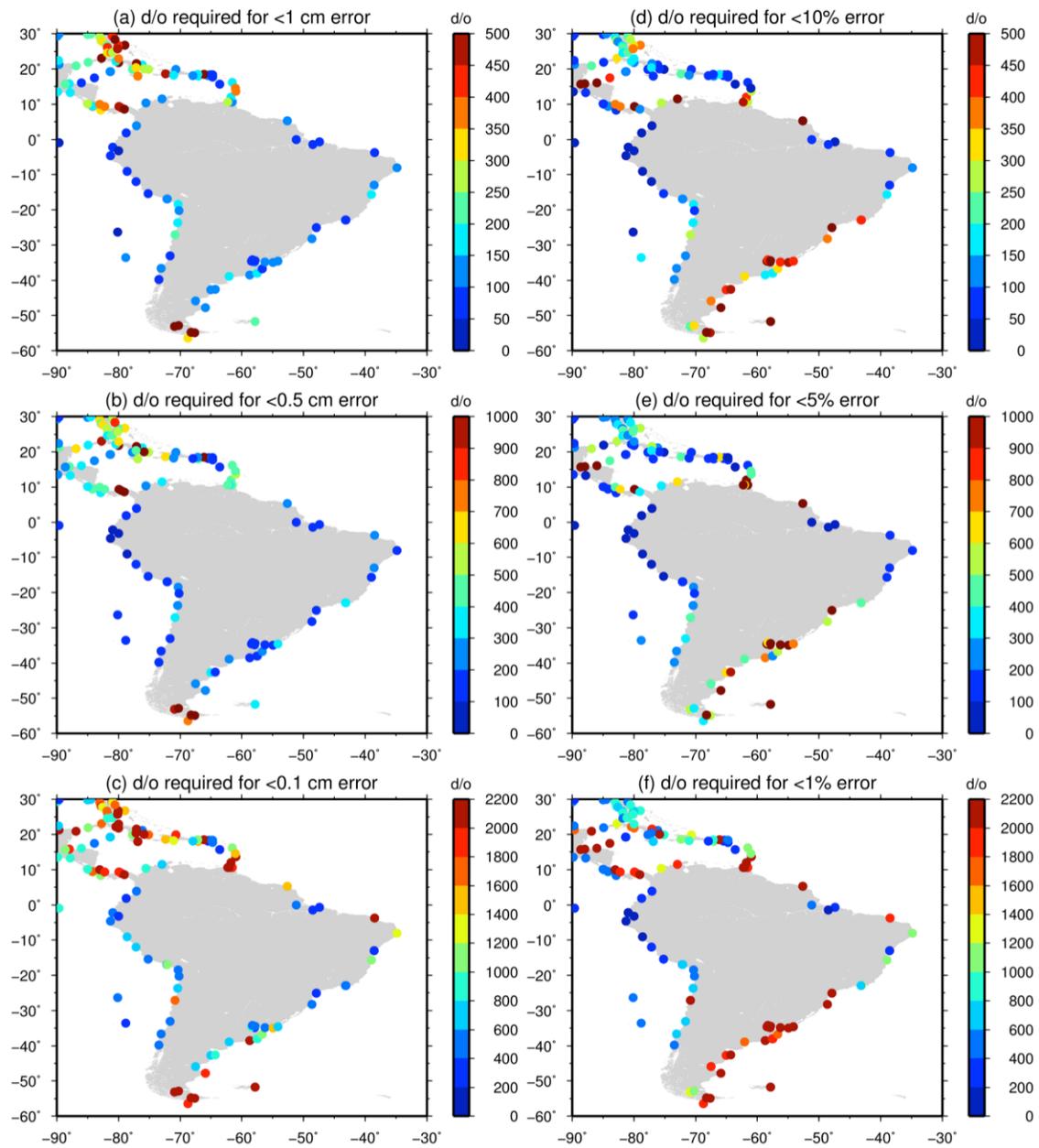
Figure 28. The d/o required at South American tide gauge locations to reduce the MDT omission error to (a) 1 cm, (b) 0.5 cm, (c) 1 mm, (d) 10%, (e) 5% and (f) 1%.
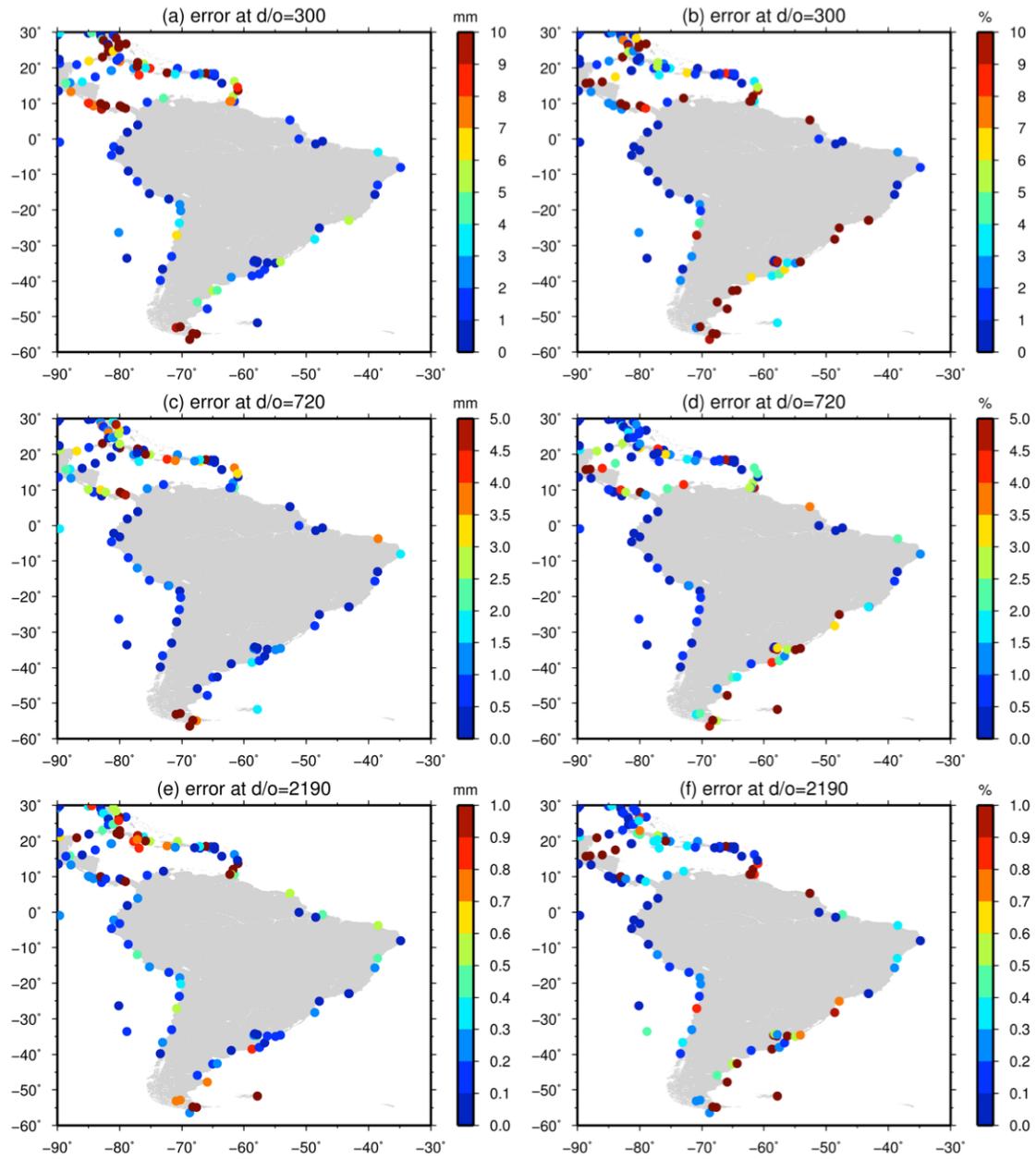
Figure 29. The absolute (left) and relative (right) MDT omission error at South American tide gauge locations for truncations at d/o (a,b) 300, (c,d) 720 and (e,f) 2190.
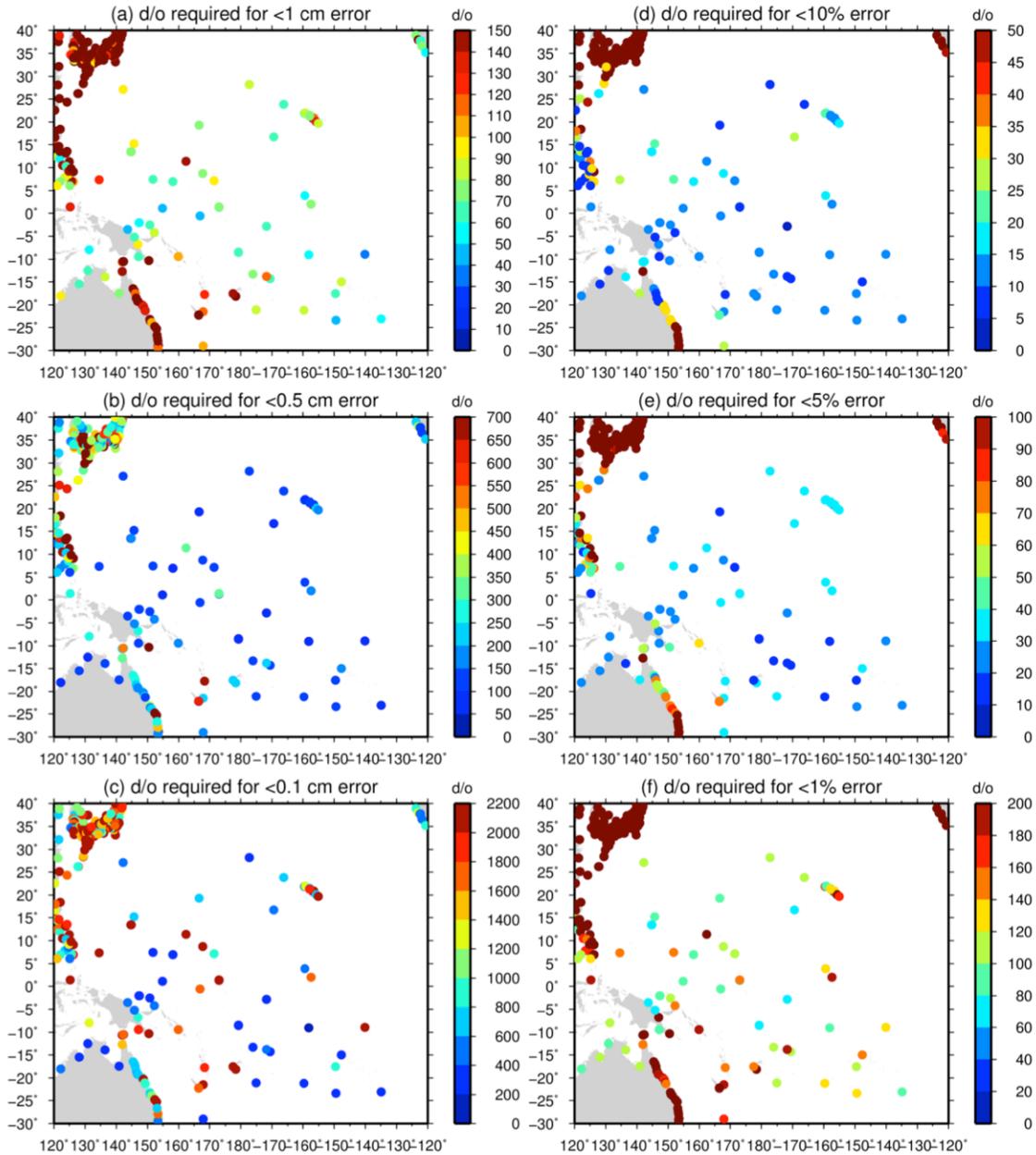
Figure 30. The d/o required at Western Pacific Island tide gauge locations to reduce the MDT omission error to (a) 1 cm, (b) 0.5 cm, (c) 1 mm, (d) 10%, (e) 5% and (f) 1%.
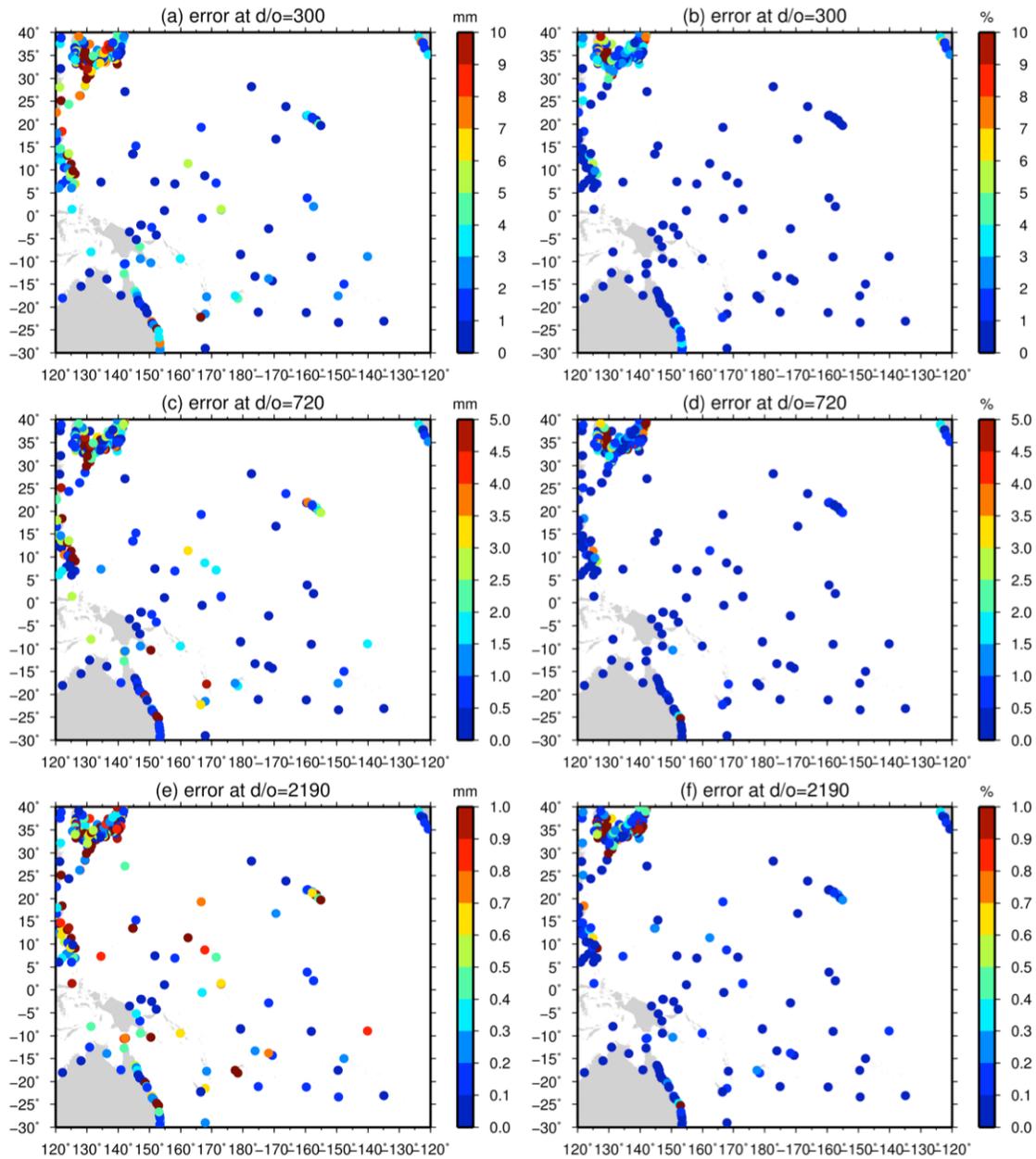
Figure 31. The absolute (left) and relative (right) MDT omission error at Western Pacific Island tide gauge locations for truncations at d/o (a,b) 300, (c,d) 720 and (e,f) 2190.

3.3.2 Geoid and MSS errors

Having examined MDT omission error (MOE) we now consider the geoid commission error (GCE) and the relative magnitude of the two. For this analysis we consider a range of earth gravity models (EGMs): the final pure GOCE model GTIM5 (maximum d/o=280); a recent satellite only solution combining GOCE, GRACE and Lageos data – GOCO05S (maximum d/o=280); and three EGMs combining satellite and in-situ data - GOCO05C (maximum d/o=720); EIGEN-6C4 (maximum d/o=2190) and the pre-GOCE model EGM2008 (maximum d/o=2190). For these five models cumulative formal geoid errors were computed as a function of d/o at each of the 1600 tide gauge locations from the spherical harmonic coefficient standard deviations.

Figure 32 shows the formal GCE for each of the EGMs averaged over the 1600 tide gauge locations. Taken at face value the formal errors show a clear improvement between EGM2008 (cyan) and EIGEN-6C4 (red), for which GOCE data can, in part, be credited. The relative contributions from GRACE and GOCE can partly be discerned by comparing the error curve for the GOCE only model (GTIM5; magenta) with that for the combined satellite only model (GOCO05S; green). EIGEN-6C4 is most accurate model (or at least as accurate) across all spatial scales, while EGM2008 is only more accurate than the satellite only models for d/o>250 and the GOCO05C model for d/o>400. It is worth bearing in mind, however, that as shown by Bingham et al. (2014) these formal errors may not be a true picture of the actual geoid error.
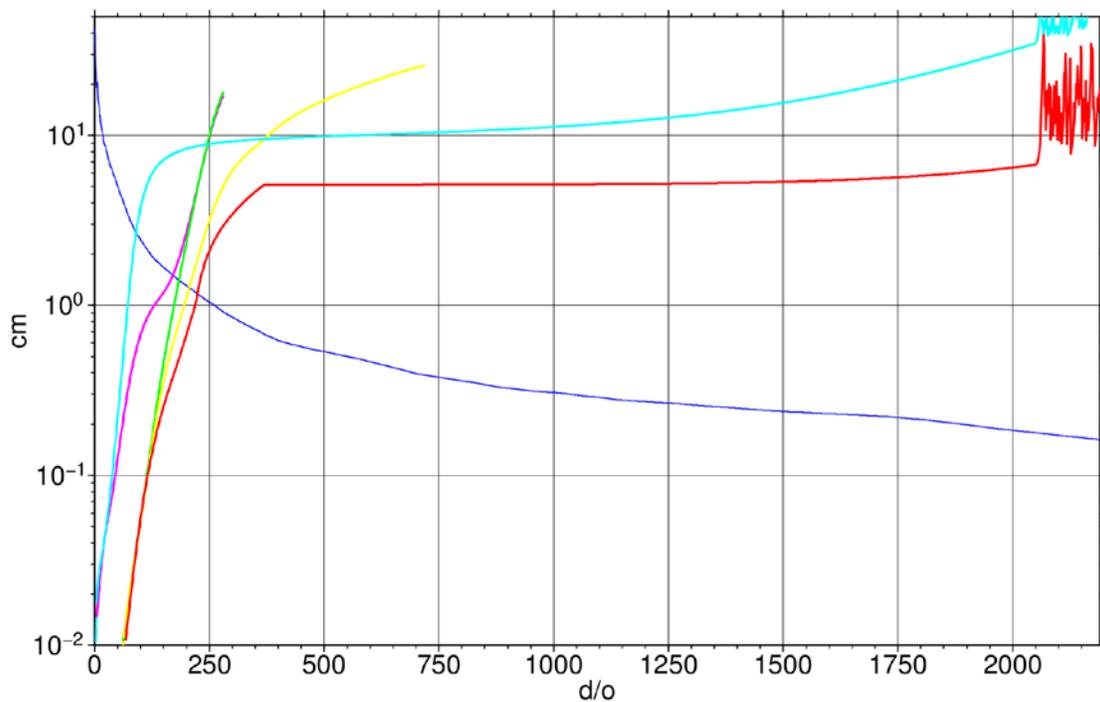
Figure 32. Formal geoid commission error averaged over the 1600 tide gauge locations regions for GTIM5 (magenta), GOCO05S (green), GOCO05C (yellow), EIGEN-6c4 (red) and EGM2008 (cyan) and the TG averaged MDT omission error.

For the purposes of the present investigation, we are interested in the cross-over point between the GCE and MOE, as represented by the blue curve in Figure 32. For all EGMs this occurs for d/o<250 suggesting that although there is signal content in the CMDT for d/o>250 the growth of GCE may mean that little signal can be recovered beyond d/o=250. However, the analysis of the previous section suggests that for most locations most of the CMDT signal can be recovered with d/o=250, with little residual signal (MOE) to be recovered. To enable their clearer identification, Figure 33a repeats Figure 32 but zooming in on the cross-over points. The best case is given by EIGEN-6c4 where the cross-over occurs for just greater than d/o=220, where the DCE and MOE are just over 1 cm. The worst case is given by EGM2008 where the cross-over occurs at d/o=90, where the DCE and MOE are just over 25 cm. Intermediate are GTIM5 (d/o= 170; errors ~16 cm), GOCO05S (d/o=180; errors ~15 cm) and GOCO05C (d/o=210; errors ~12 cm).

The remaining panels of Figure 33 show similar curves but with errors computed separately for the five study regions. The ordering of the cross-over points remains the same for each region but the values and ranges change. The lowest cross-overs occur for Australia – d/o=190, error 6 mm for EIGEN-6C4 – and the highest cross-overs occur for South America – d/o=260, errors = 20 cm for EIGEN-6CE.

The GCE/MOE cross-over points at each of the TG locations for each of the models are shown in Figures 34 and 35, while the corresponding errors at the cross-over points are shown in Figures 36 and 37. Figure 34a shows that for GTIM5 that the majority of locations the cross-over point is less than d/o=180, with many places having a cross-over of d/o<90. As shown in Figure 36a the error at the cross-over point is generally less than 1 cm, with relatively few locations where the error exceeds 2 cm. A marked improvement can be seen for GOCO05S (Figures 34b and 36b) with the cross-over points noticeably higher, although generally not exceeding d/o=180, and with the error at the cross-over point generally less than 0.5 cm and fewer locations exceeding 2 cm. Further, but not as dramatic, improvements are apparent for GOCO05C (Figures 34c and 36c) with the cross-overs at many locations now in the next d/o colour interval and the error exceeding 2 cm in fewer locations. As expected, additional improvements are apparent for EIGEN-6C4 (Figures 35a and 37a) with the cross-overs at many locations now exceeding d/o=210 and the error exceeding 2 cm at only a few locations and generally much less than 1cm. Finally, we see a dramatic difference between EIGEN-6C4 and EGM2008 (Figures 35b and 37b) with the cross-over point at all most all locations now d/o<90 and errors exceeding 2 cm in many locations.
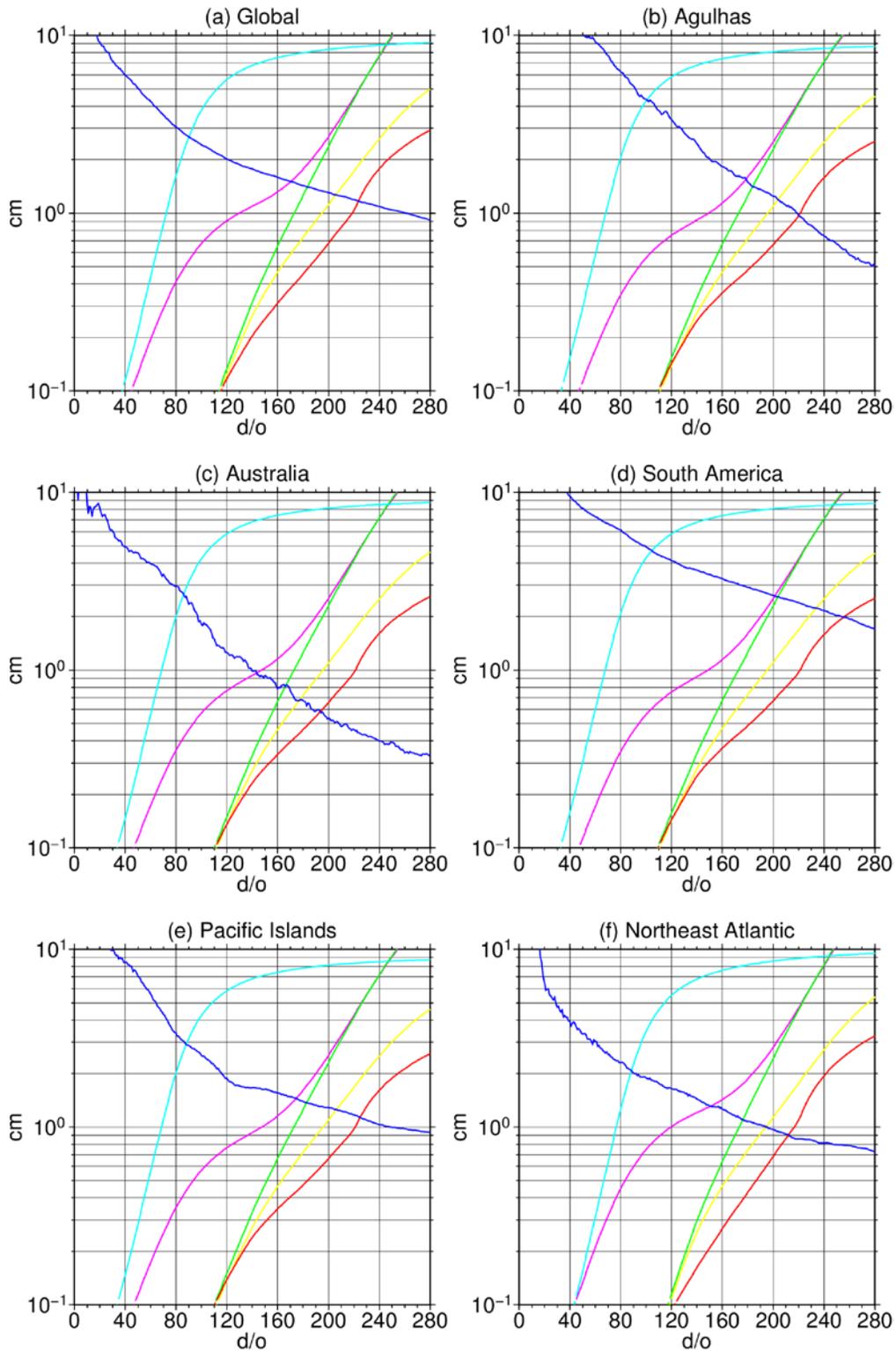
Figure 33. A comparison between MDT omission error (MOE; blue) and formal geoid commission error (GCE) globally and for the five study regions for GTIM5 (magenta), GOCO05S (green), GOCO05C (yellow), EIGEN-6c4 (red) and EGM2008 (cyan).
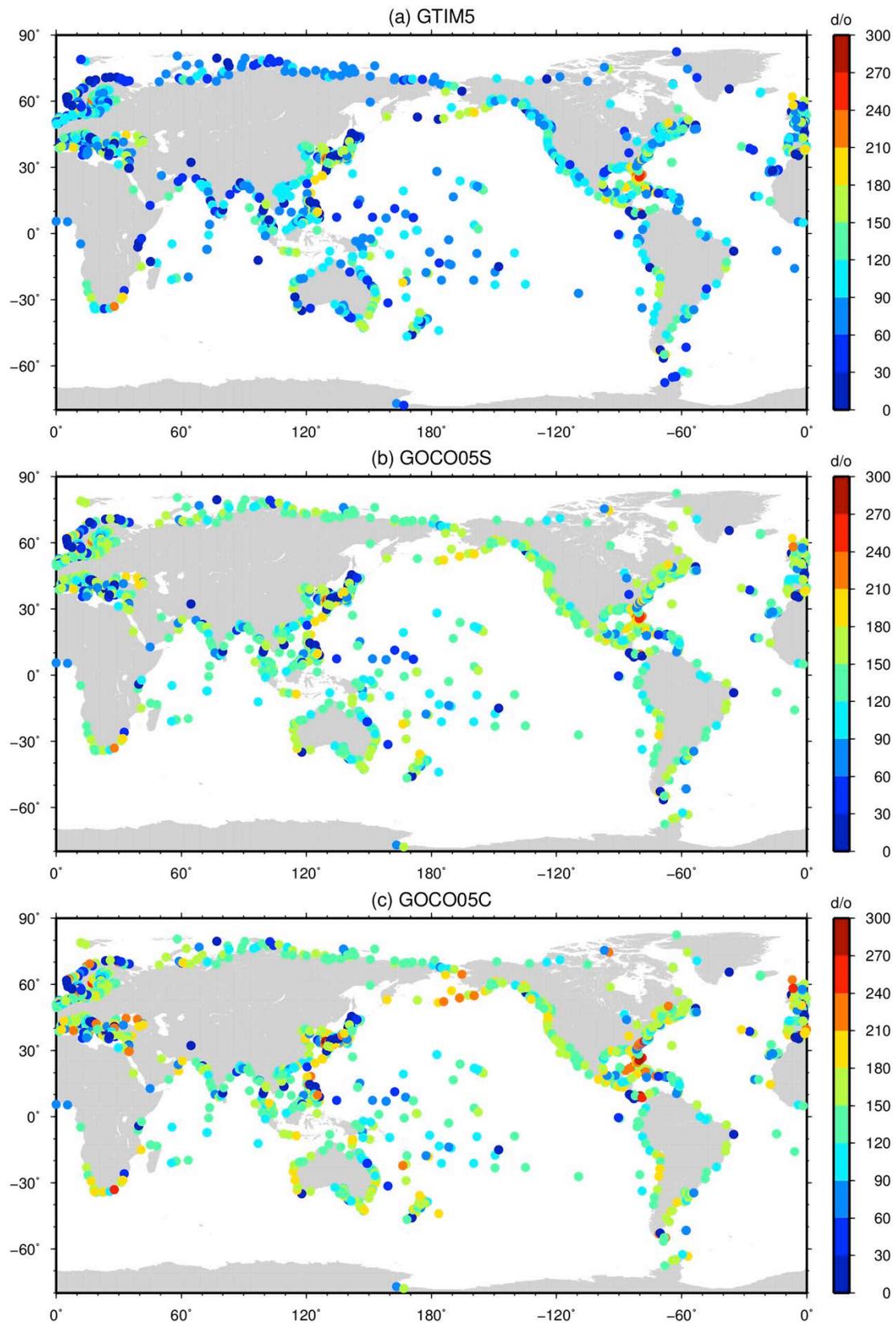
Figure 34. The degree and order at which the formal geoid commission error exceeds the MDT omission error for (a) GTIM5, (b) GOCO05S and (c) GOCO05C.
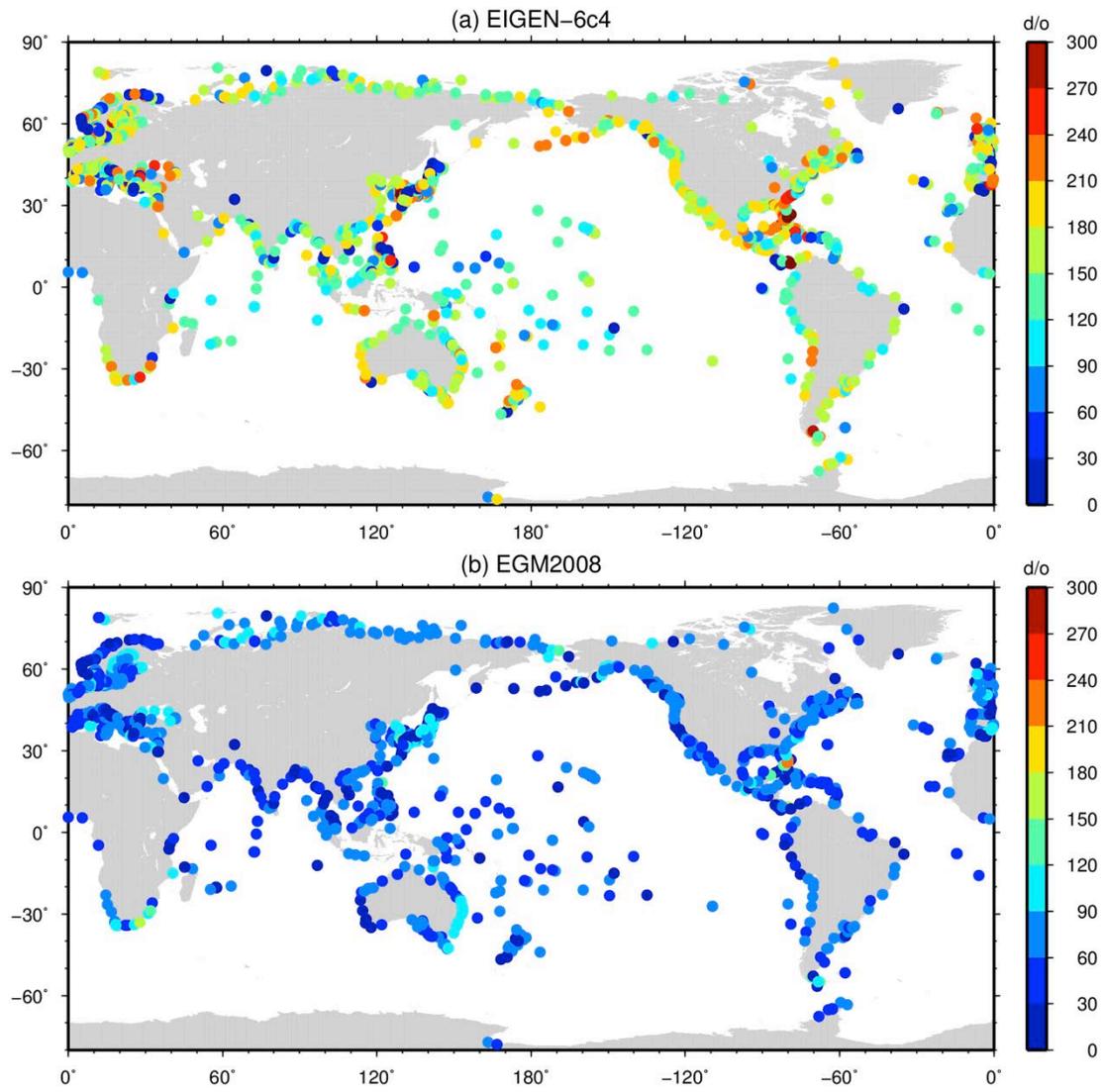
Figure 35. The degree and order at which the formal geoid commission error exceeds the MDT omission error for (a) EIGEN-6c4 and (b) EGM2008.
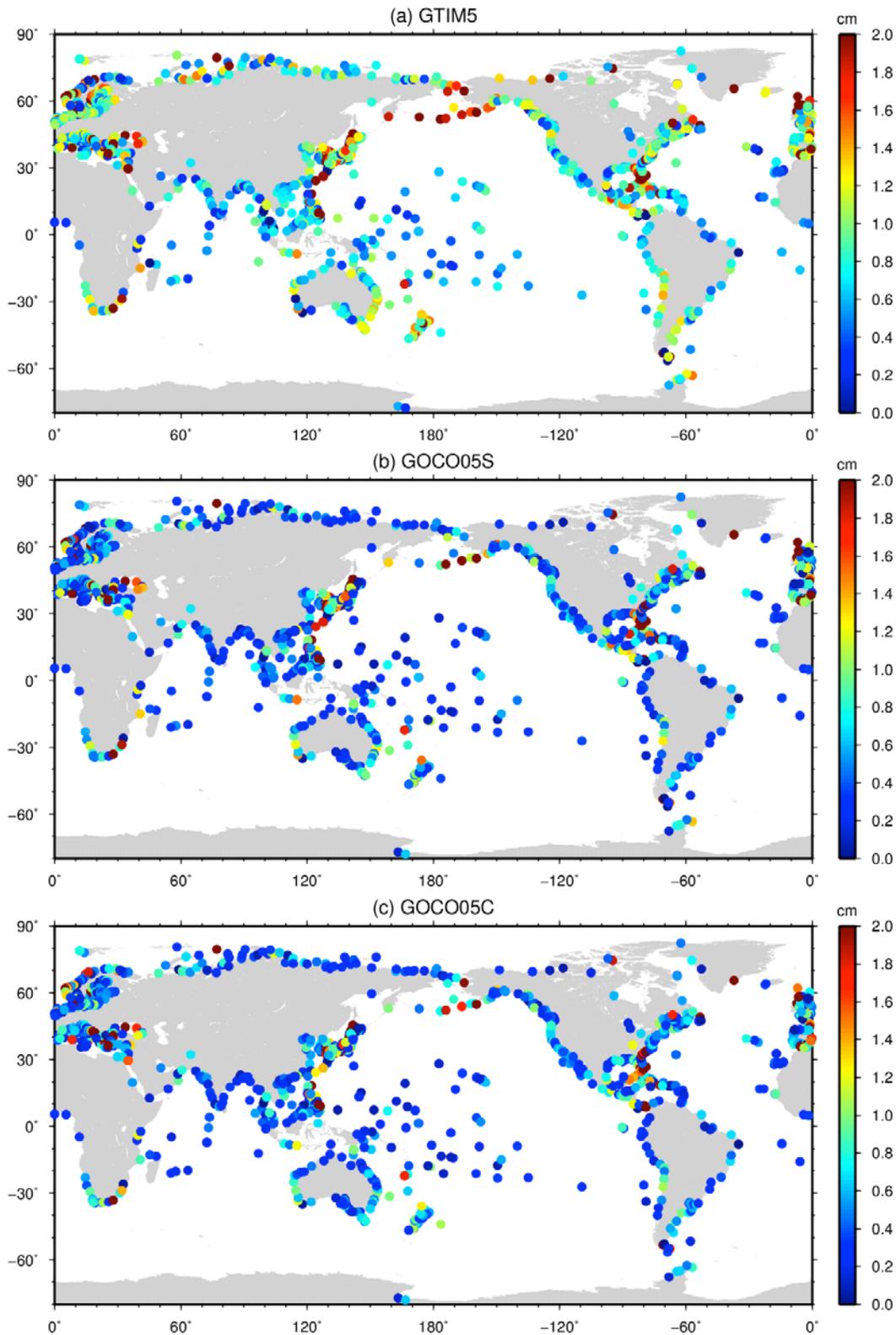
Figure 36. The MDT omission error (or geoid commission error) at the degree and order at which the formal geoid commission error exceeds the MDT omission error for (a) GTIM5, (b) GOCO05S and (c) GOCO05C.
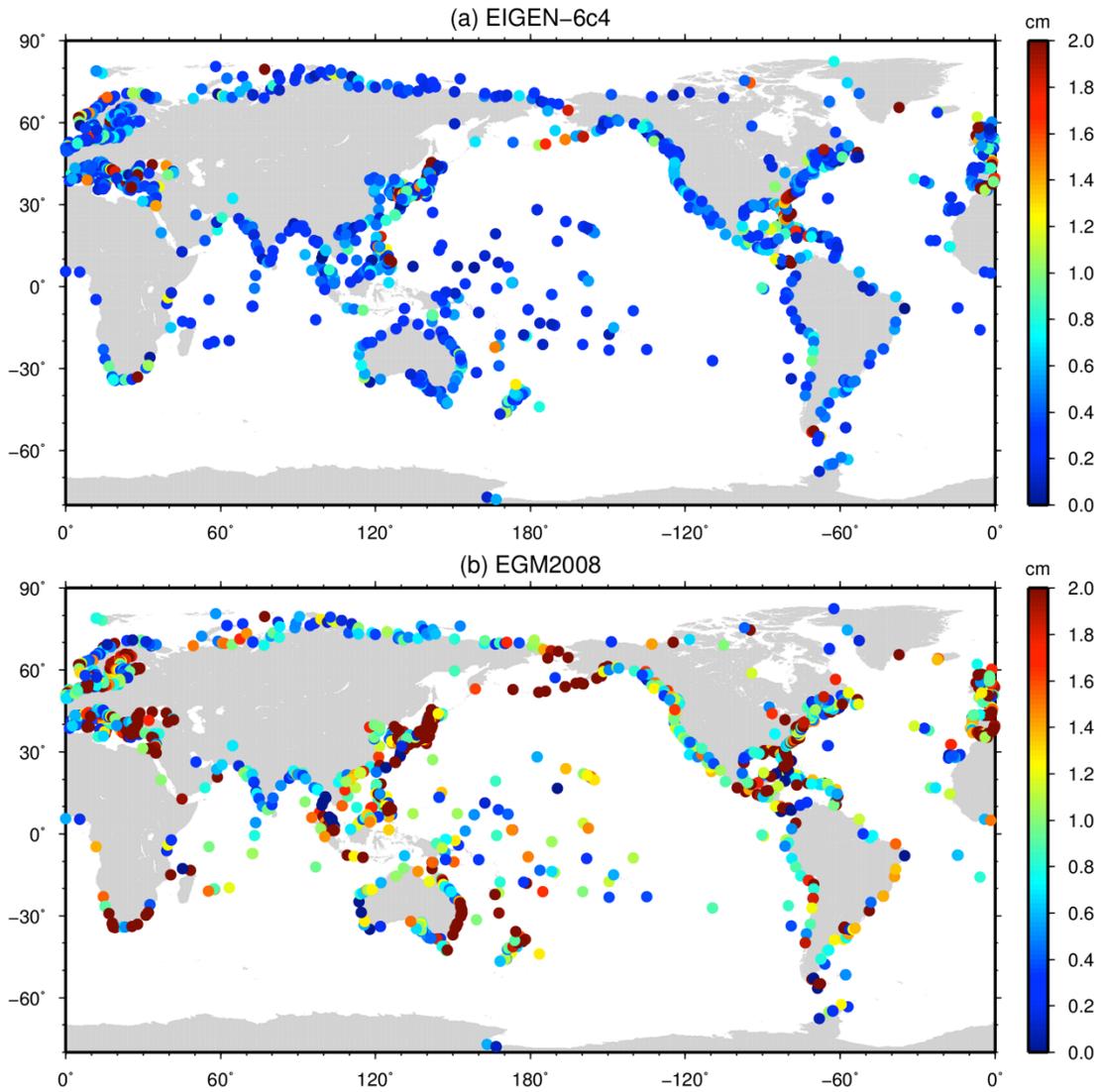
Figure 37. The MDT omission error (or geoid commission error) at the degree and order at which the formal geoid commission error exceeds the MDT omission error for (a) EIGEN-6c4 and (b) EGM2008.

These results apparently demonstrate the true differences between the EGMs as they pertain to the MDT calculation, showing the limit of their resolution and information content and the likely error at that limit. The results suggest that EIGEN-6C4 should provide the best estimate of the CMDT and EGM2008 the worst. However, it worth reiterating that the validity of these conclusions depend on the reliability of the formal error estimates. They also depend on how well the OCCAM model represents the spectral content of the MDT. However, this is likely to of minor importance compared to the correction specification of the formal errors. Nonetheless other models should be investigated.

By "true'' in the above sentence we mean in contradistinction to the false, or apparent, difference, as far as recovery of the MDT signal is concerned, that arises through the power of the higher d/o models to reduce geoid omission error. While reducing this source of error undoubtedly leads to an improvement in the MDT (computed by the point-wise approach, as must be done for the GPS-TG approach), this improvement comes through the reduction in noise rather than increased signal content. It obscures the more fundamental balance between the MOE and GCE that places the true upper limit on the signal that can be recovered by the geodetic (or GPS) approach. To go beyond this limit, as discussed above, would require a filtering method that can be employed to dampen the GCE to a level below the MOE, without attenuating the small residual MDT signal.

Suppose our estimates of the MOE and GCE are accurate, then the above analysis places an upper bound on the CMDT signal content that can be derived from the geodetic approach. However, we must also take into account MSS error. In fact, the combined MSS error and GCE, together with residual numerical error, can be thought of as the MDT commission error (MCE). This error, being greater than the GCE only, must exceed the MOE for lower d/o than the GCE only. Thus, the cross-over points and errors, presented above may, all other things being equal, be optimistic. The extent to which they are optimistic depends on the magnitude of the MSS error at the spatial scales corresponding the relatively large spatial scales at which the MOE/GCE cross-overs tend to occur.

The formal errors for the DTU15 MSS at the TG locations is shown in Figure 38. The errors are generally in the range 2-4 cm. It is difficult to express these as a function of d/o, to assess their impact on a spectral MDT at a particular d/o. But supposing they remain a constant fraction of the signal and considering the rate at which the MSS signal grows with increasing d/o then is reasonable to suppose they would converge asymptotically rather rapidly such that they have relatively constant values close to the plotted values beyond some d/o greater than say d/o=100. In this case, these MSS errors will therefore be the dominant source of CMDT error at the MOE and GCE cross-over points and the true cross-over points may be lower than those presented above. If, on the other hand, the MSS errors only grow rapidly at spatial scales less than those corresponding to d/o=300, which could well be true, then the MOE/GCE cross-over points as presented above will be closer to what can achieved in practice.
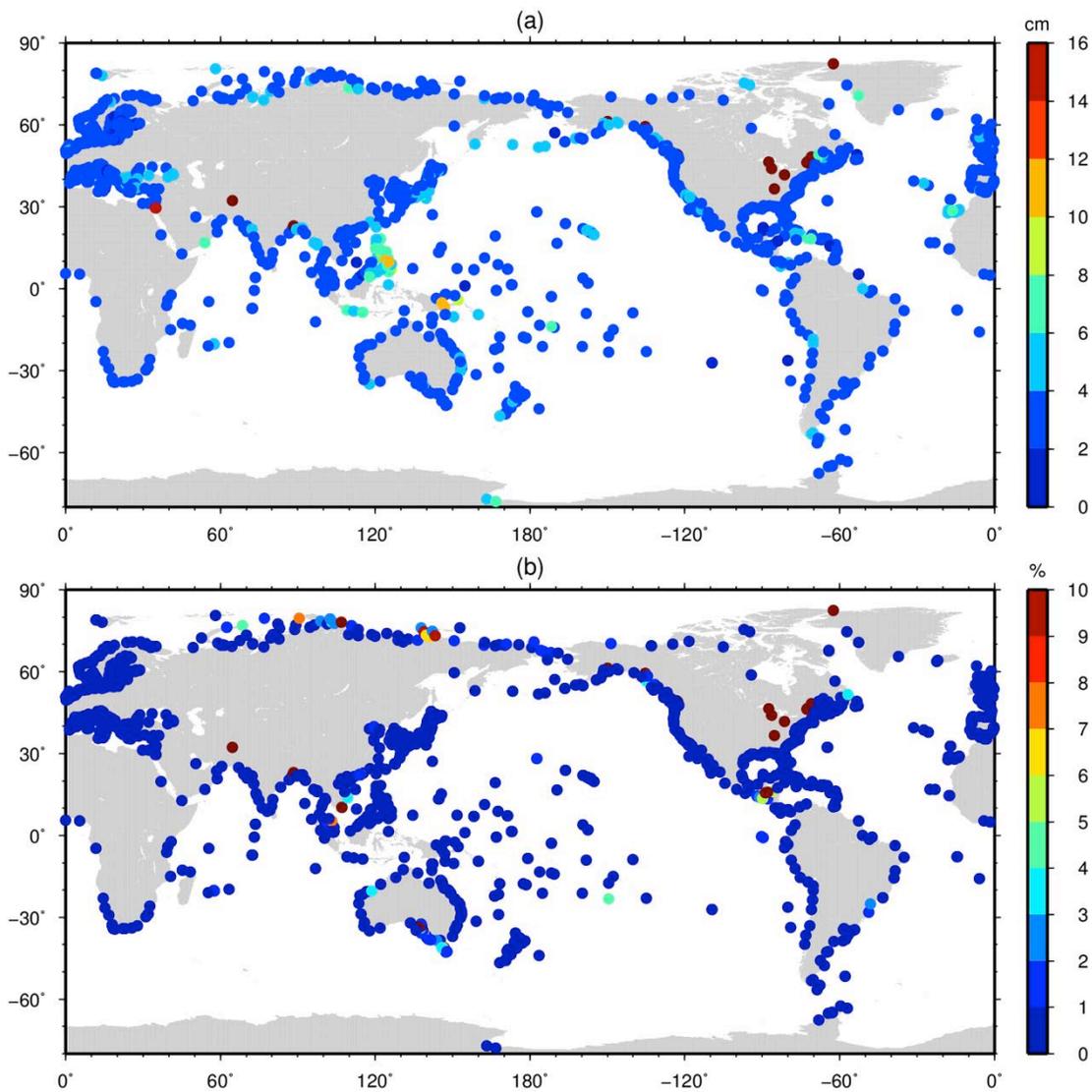
Figure 38. (a) DTU15 MSS errors at tide gauge locations. (b) Errors expressed relative to signal magnitude.

3.2.3. Geodetic coastal MDT

The MDT at the 1600 TG locations where calculated by the spectral approach using the DTU15 MSS and the five EGMs described above. The MSS was first reduced from 1 minute resolution to $1/12^{th}$ of a degree resolution from which a set of spherical harmonics to coefficients to d/o=2190 was calculated. (A subsequent calculation of the spherical harmonic coefficients directly from the 1 min grid was performed but with negligible impact on the results presented below.)

An initial assessment of the CMDT computed in this way is presented in Figure 39 which shows the RMS difference between the geodetic CMDTs and nearest ocean values in OCCAM (panel a) for all 1600 TG locations. Ignoring the minimum that occurs before d/o=50 and the other smaller minimum at d/o=140 (which can be attributed to noise in

the statistics) and focusing on the broad shape of the curves, the RMS difference relative to OCCAM reaches a minimum around d/o=200 for all of the models, with RMS differences growing at different rates beyond this. In line with expectations from the formal errors plotted in Figure 32, the RMS differences for the satellite only solutions grow much more rapidly than is the case for the combined solutions. Also in-line with expectations from the formal errors is that up to a certain d/o the errors for the GOCE-only GTIM5 solution are somewhat greater than the combined satellite solution GOCO05S. For the combined solutions, as expected from the formal errors, the RMS difference for GOCO05C is less than the two satellite only solutions but greater than for EIGEN-6C4. However, the RMS curve for EGM2008 goes against expectations, suggesting true errors that are lower than all the other models including EIGEN-6C4. This suggests that the formal errors from EGM2008 are too pessimistic and the difference in terms of the calculated MDT between the EIGEN-6C4 and EGM2008 is not as great as suggested by the GCE vs. MOE error analysis presented above.

Figure 39b presents a similar analysis but with RMS differences calculated relative to the GPS-CMDT estimate at the 303 GPS-TG locations. With the exception of the of the EIGEN-6C4 and EGM2008 models the ordering of the RMS differences is preserved. GTIM5 and GOCO05S again reach minimum values around d/o=200, with the RMS difference for the former model slightly greater, before growing much faster that the combined models. The combined models reach minima somewhat latter: d/o=308 for GOCO05C and EGM2008 and 374 for EIGEN-6C4. Although the EIGEN-6C4 RMS is less than EGM2008 for d/o>250, EGM2008 still has the lowest RMS difference (albeit marginally so) for d/o<250 and has the second lowest RMS for d/o>250. This again suggests that the EGM2008 formal errors are too pessimistic. This is further supported by the fact that the GPS estimate is based on the EIGEN-6C4 geoid, which may explain why the RMS difference is lower than EGM2008.

The RMS difference minima in Figure 39, particularly those in Figure 39b, are broadly in line with those suggested by the MOE/GCE cross-over analysis. Also, as one would expect the geodetic MDTs are in better agreement with the GPS-MDT than with the model MDT. For this analysis neither the geodetic CMDT values or the OCCAM MDT have been adjusted to the common 2003-2007 time period. However, the RMS difference between OCCAM and the GPS-MDT of 17 cm at d/o>100 suggests that it is noise in the geodetic MDTs that make the largest contribution to the RMS differences in both cases.

Figures 40 and 41 present a further comparison between the geodetic MDT estimates and the OCCAM (left panels) and GPS (right panels) CMDT estimates at the TG locations. For the OCCAM comparisons the geodetic MDTs have been truncated at d/o=200 as suggested by the RMS difference minima shown in Figure 39a, while for the GPS-MDT comparisons they have been truncated at d/=200 for GTIM5 and GOCO05S, d/o=308 for GOCO05C and EGM2008 and d/o=374 for EIGEN-6C4 as suggested by the RMS difference minima of Figure 39b. The comparisons with OCCAM show there is little to separate the EGMs, with the "worst" performing model (GOCO05S) having an r-squared value of 0.53 and a residual standard error (RSE) of 29.0 cm compared with values of 0.6 and 27.7 cm for the "best" performing model (EGM2008). The similarity of the

distribution of points, suggest a common source of error in the geodetic MDTs, namely the DTU15 MSS.
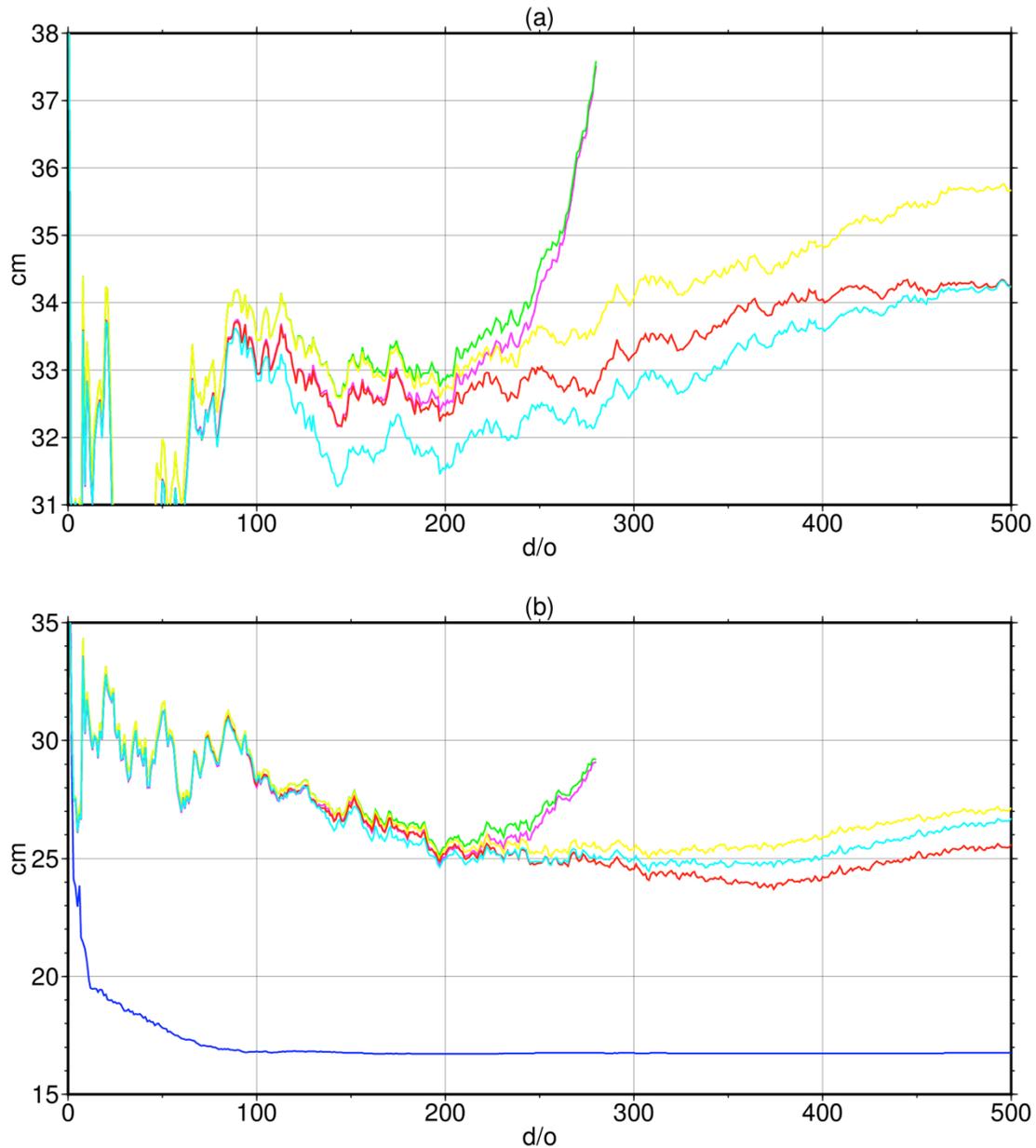
Figure 39. (a) The RMS difference calculated over the 1600 tide gauge location between geodetic MDTs and the OCC12 MDT with the geodetic MDTs calculated using the DTU15 MSS and the GTIM5 (green), GOCO05S (magenta), GOCO05C (yellow), EIGEN-6c4 (red) and EGM2008 (cyan) gravity models. (b) Repeating (a) but with RMS differences relative to the GPS-EIGEN_6c4 MDT and also including the RMS difference with OCC12 (blue).
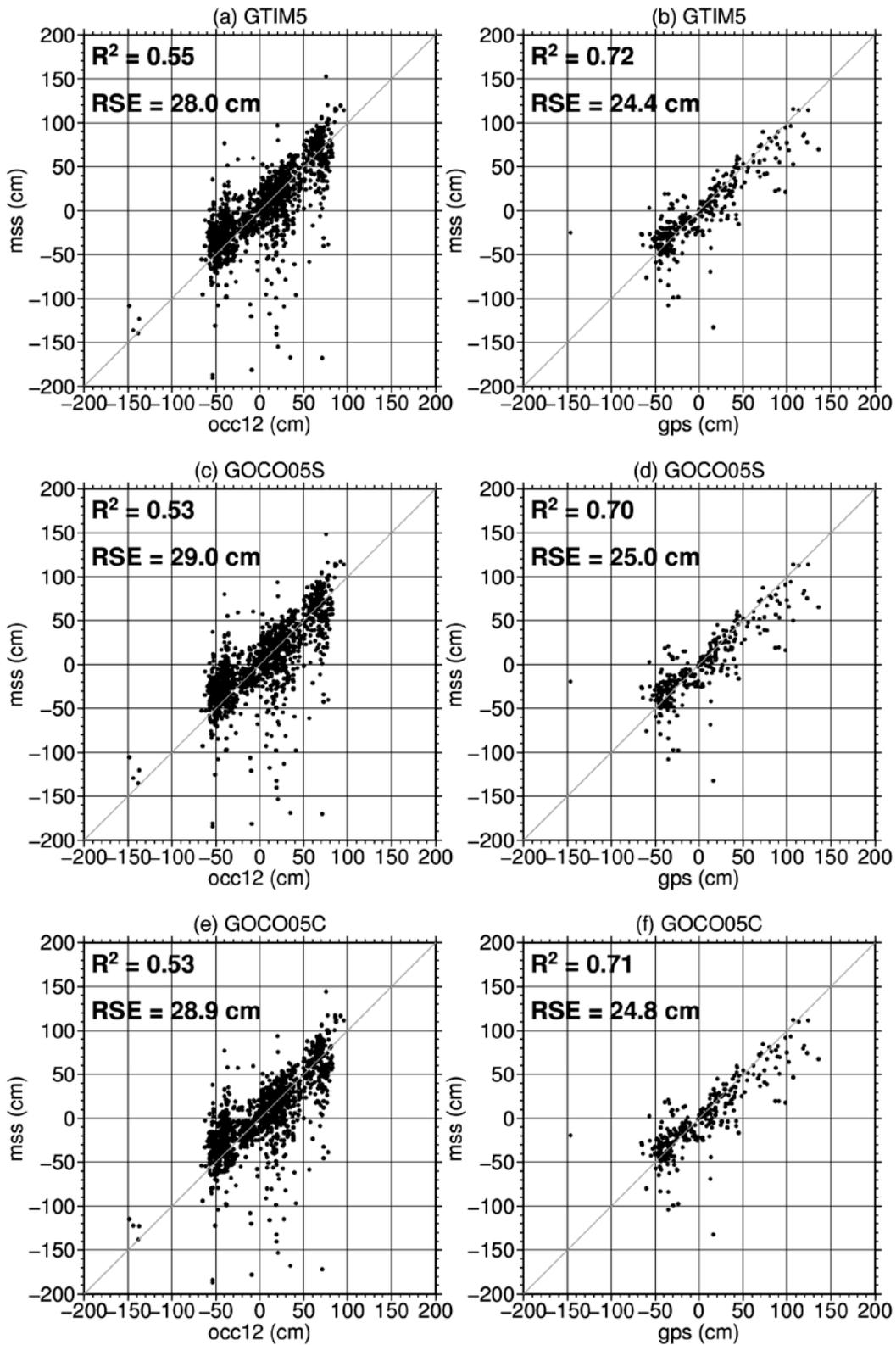
Figure 40. Scatter plots of the geodetic MDT values (y-axes) against (left) OCC12 at the 1600 tide gauge locations and (right) the GPS-MDT ad the 303 GPS tide gauge locations for (a, b) GTIM5 (d/o=200), (c, d) GOCO05S (d/o=200), (e, f) GOCO05C (d/o=200, 308).
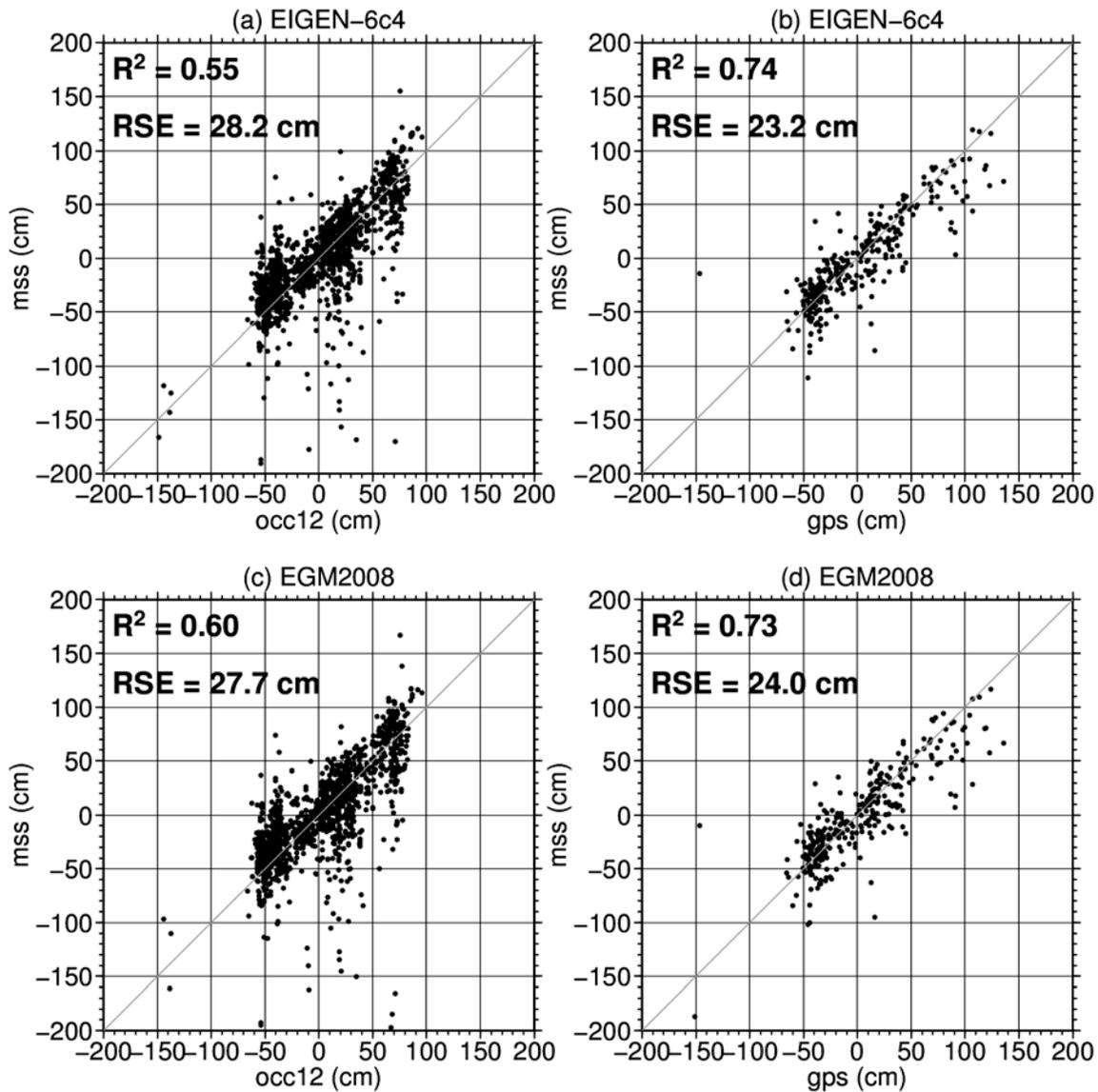
Figure 41. Scatter plots of the geodetic MDT values (y-axes) against (left) OCC12 at the 1600 tide gauge locations and (right) the GPS-MDT ad the 303 GPS tide gauge locations for (a, b) EIGEN-6c4 (d/o=200, 374) and (c, d) EGM2008 (d/o=200, 308).

Confirming Figure 39b there is better agreement with the GPS-MDTs, with r-squared values ranging from 0.70 for GOCO05S to 0.74 for EIGEN-6C4 and RSE's ranging from 25 cm for GOCO05S to 23.2 cm for EIGEN-6C4. Again the distribution of points suggest a common source of noise in the geodetic MDT estimates.

Finally, Figure 42 shows the relatively good agreement between the OCCAM MDT and the GPS-MDT, confirming the geodetic MDTs are the primary contributors to the RMS differences and residual square errors.
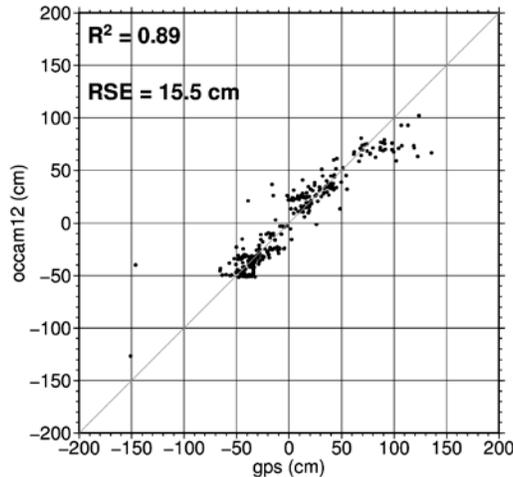
Figure 42. A comparison between the GPS-EIGEN64C and OCCAM12 MDT estimates.

Thus far the analysis has only considered raw, unfiltered geodetic CMDT values. However, the above analysis demonstrates that some form of filtering is required to improve the geodetic CMDT. Filtering presents a number of challenges, especially in the coastal zone. Firstly, one must try to minimise signal attenuation. For the coastal zone this is particularly important for regions where a narrow boundary current is present just off shore. Here filtering can smear the MDT height on the ocean side of the current onto the coast resulting in an over (or under) estimate of the true MDT height. It can also blur step changes and features that may be of particular oceanographic interest. A second problem is that in the MSS the land-sea boundary is blurred and not clearly identified. An error estimate that flags pure geoid values is provided. However, some of that information will be lost if reducing the MSS to a coarser grid. This makes identifying true MDT values and excluding "almost-geoid minus geoid" values ($\approx$0) when filtering difficult. Third, effective filtering in the coastal zone is hampered by the fact that the filter window will not be symmetrical around the coastal point in at least one direction. For these reasons simple filtering is often not effective at removing noise while preserving signal in the coastal zone. Noise can be removed but at the expense of signal resolution.

In attempt to address some of these issues a two-stage filtering method was developed. The first stage involves screening the geodetic MDT for outliers and replacing them with suitable values. This is done globally. The second stage applies a filter to the screened MDT values to obtain an estimate of the MDT at a given coastal location.

For this initial analysis geodetic MDTs where calculated on same 1/12th of a degree grid as the OCCAM MDT. Screening for outliers was performed as follows:

1. For each point of the global grid a mean height is calculated within a window of a suitable radius around that point. Here suitable is defined as the radius required to reduce the difference between the mean height from the geodetic MDT and the mean height from the OCCAM MDT calculated in the same radius window below some threshold value (40 cm).

2. The window mean value is then subtracted from all of the GMDT values within the window.
3. These anomalous values are then screened for outliers by comparing with a range distribution estimated using (for now) the OCCAM model (Figure 43 and Figure 44b). Any values that exceed the expected range for that sized box by one standard deviation are considered to be outliers and are replaced by the mean value within that window. This could be refined by using a wider range of models the estimate the expected range for a given window size.
4. Finally at each coastal (TG) location a filtered MDT estimate is obtained by filtering the screened global MDT in a window of a particular radius around the point. Here the filter radius is determined by modelling the attenuation of the filter using the OCCAM MDT and choosing the filter radius such that the attenuation does not exceed some threshold value (1 cm). This radius is illustrated in Figure 44a.

For this initial analysis no attempt was made to use knowledge of the formal errors and the GMDTs were not computed to an optimum d/o but this could easily be implemented. Also at this state the additional information and constraint provided by the GPS-MDT has not being used. This could also be incorporated into a refined approach.
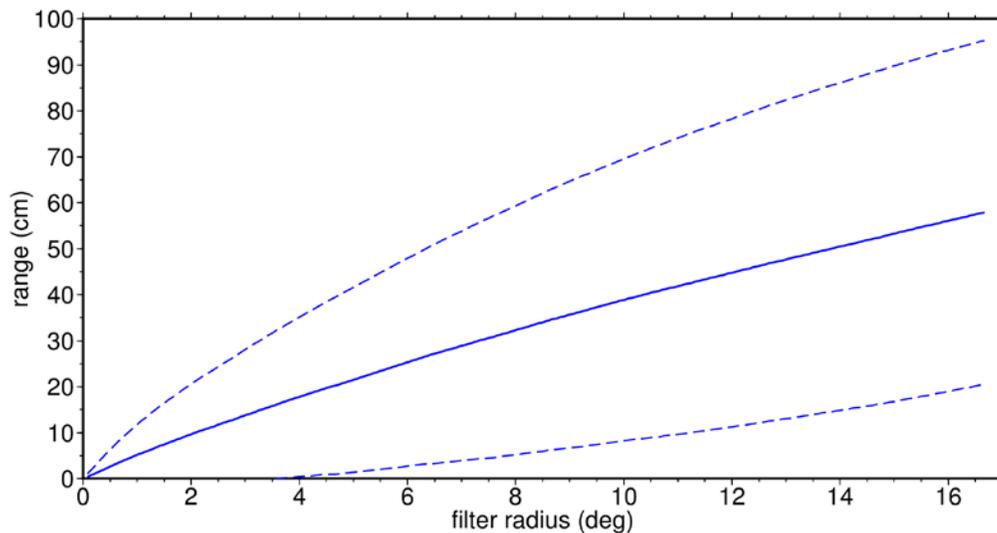
Figure 43. The mean maximum departure from the tide gauge MDT as a function of box radius surrounding the TG point. Dashed lines represent one standard deviation. Values based on the OCC12 MDT.
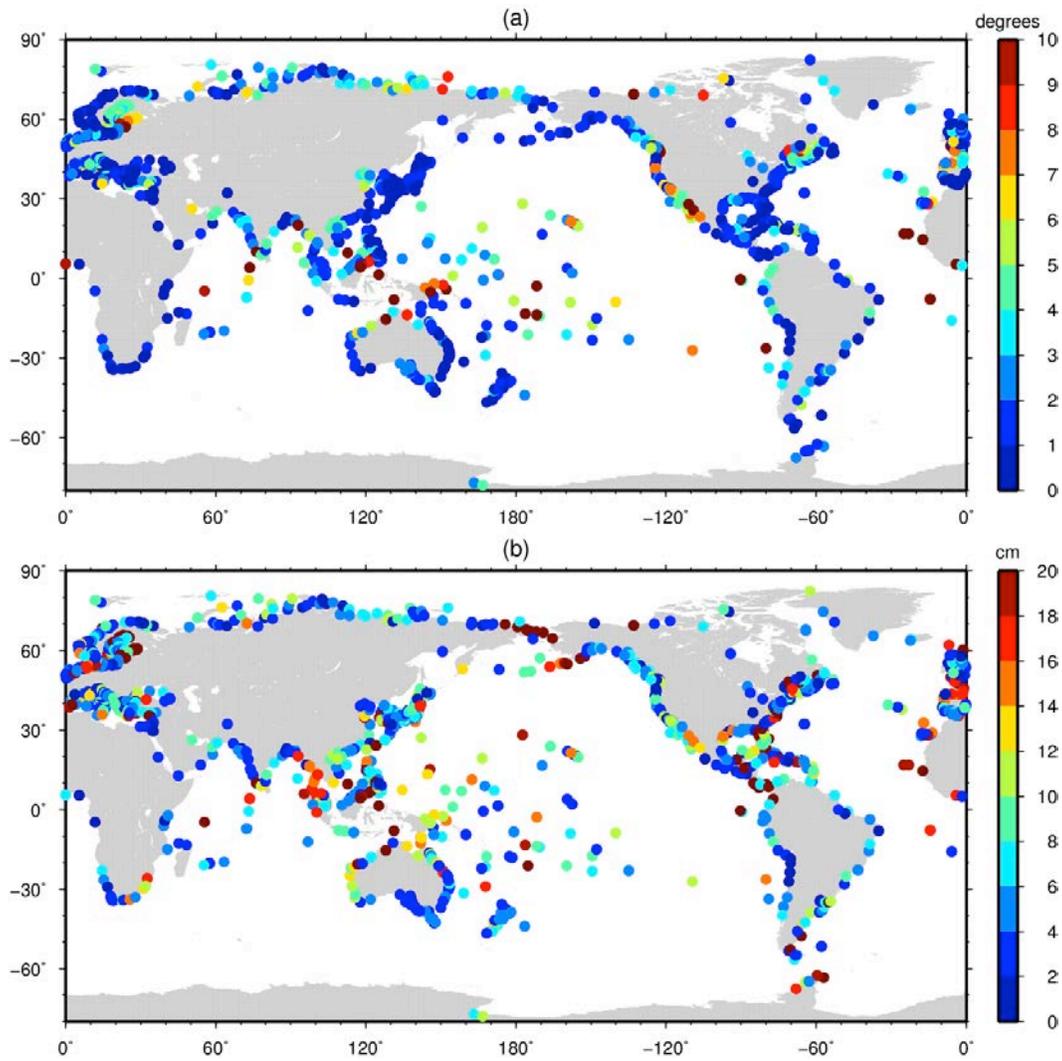
Figure 44. (a) Box-car filter radius that attenuates the MDT by 1 cm. (b) The maximum departure from the tide gauge MDT in a box of radius 5 degrees surrounding the TG point. Values based on the OCC12 MDT.

In spite of the limitations of the filtering method, it is quite successful at reducing the noise in the GMDT estimates and improving the fit with the model and GPS-MDTs. Figures 45 and 46 show scatter plots of the TG MDT estimates from the geodetic MDTs against the GPS-MDT values before (left panels) and after (right panels) screening and filtering. In this case the GMDTs have been computed to the maximum d/o of the EGM (hence the unfiltered values are somewhat different than for the earlier plots). R-squared values have now improved from around 0.7 to around 0.9 and the RSE has reduced from around 26 cm to 16 cm. The best performing model is GOCO05C with an r-squared value of 0.89 and the RSE of 15.4 cm. However, there is very little to separate the models, with the worst performers – the two satellite only EMGs – having r-squared values of 0.87 and RSE's of 16.4 cm. These could potentially be improved by taking account of the MOE/GCE cross-over points to avoid the introduction of additional noise. The similarity of the RSE values with those from the GPS/OCCAM comparison shown in Figure 42, points to noise in the GPS solution now being the limiting factor in this analysis.

Figures 47 and 48, provide a comparison with OCCAM over the 1600 TG locations. Again there is a marked improvement with r-squared values increasing from around 0.55 to 0.77 and the RSE values decreasing from around 28 cm to about 20 cm. There is once again little to separate the models but with the GOCO05C being marginally the best performer with an r-squared value of 0.78 and an RSE of 19.7 cm.
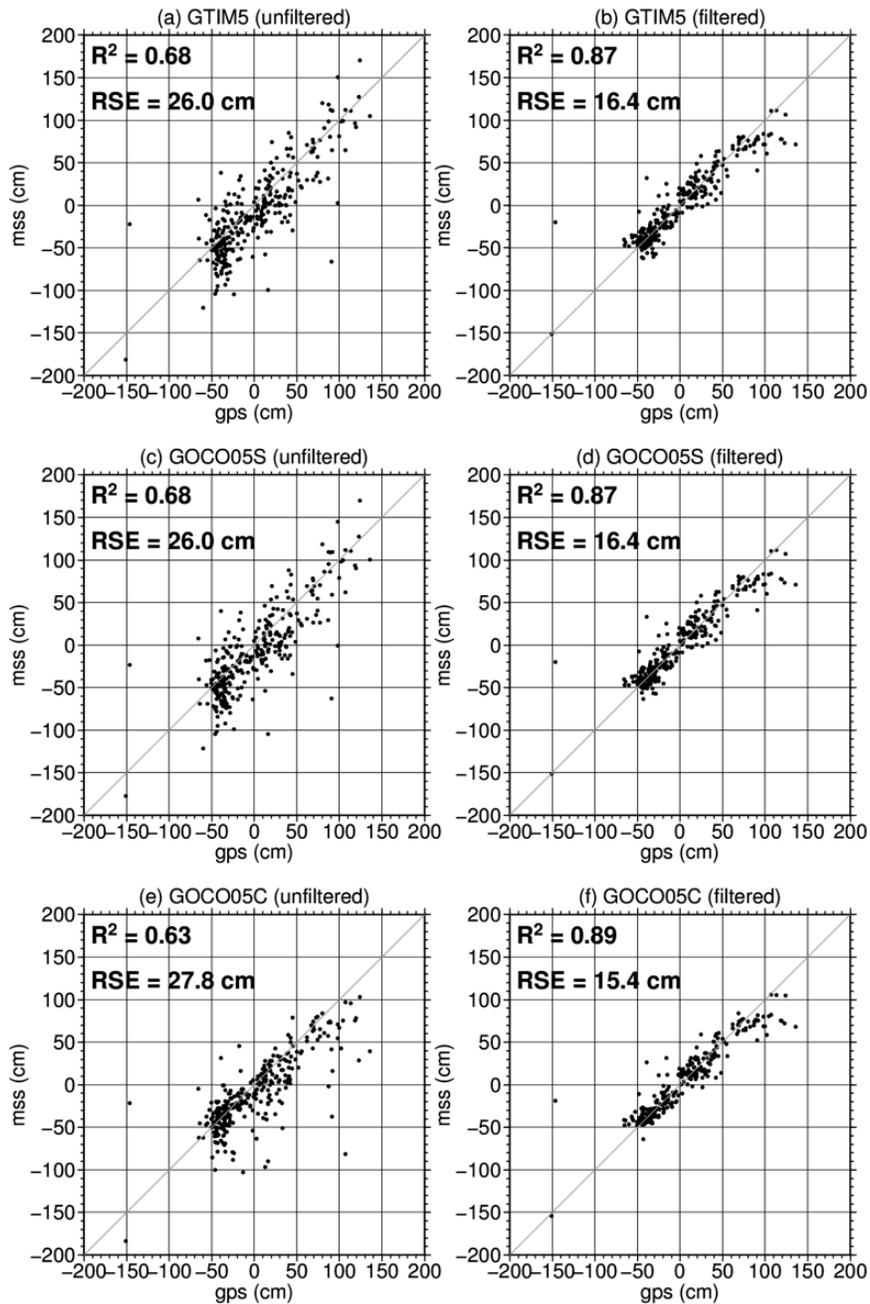
Figure 45. A comparison between the GPS-EIGEN64C and DTU15-geoid MDT estimates. (a) GOCE-TIM5 (d/o=280) with no filtering. (b) As in (a) but with filtering. (c, d) Repeating (a, b) for GOCO05S (d/o=280). (e, f) Repeating (a, b) for GOCO05C (d/o=720).
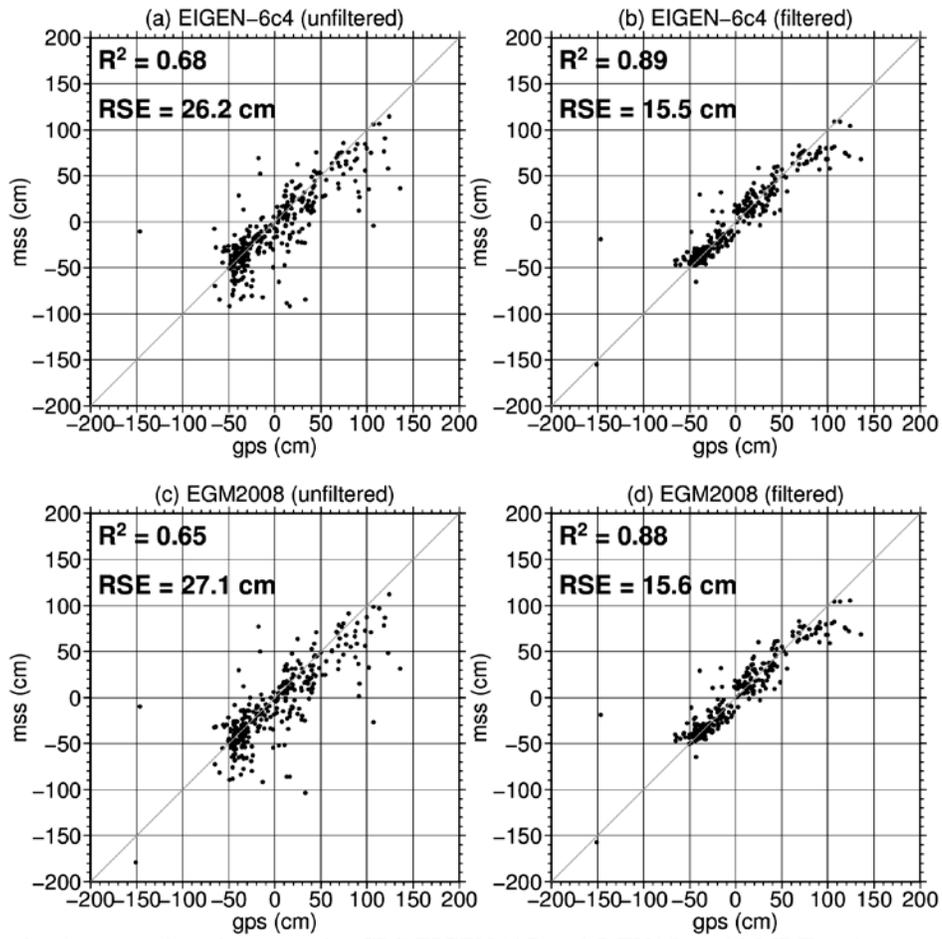
Figure 46. A comparison between the GPS-EIGEN64C and DTU15-geoid MDT estimates. (a) EIGEN-6c4 (d/o=2190) with no filtering. (b) As in (a) but with filtering. (c, d) Repeating (a, b) for EGM2008 (d/o=2190).
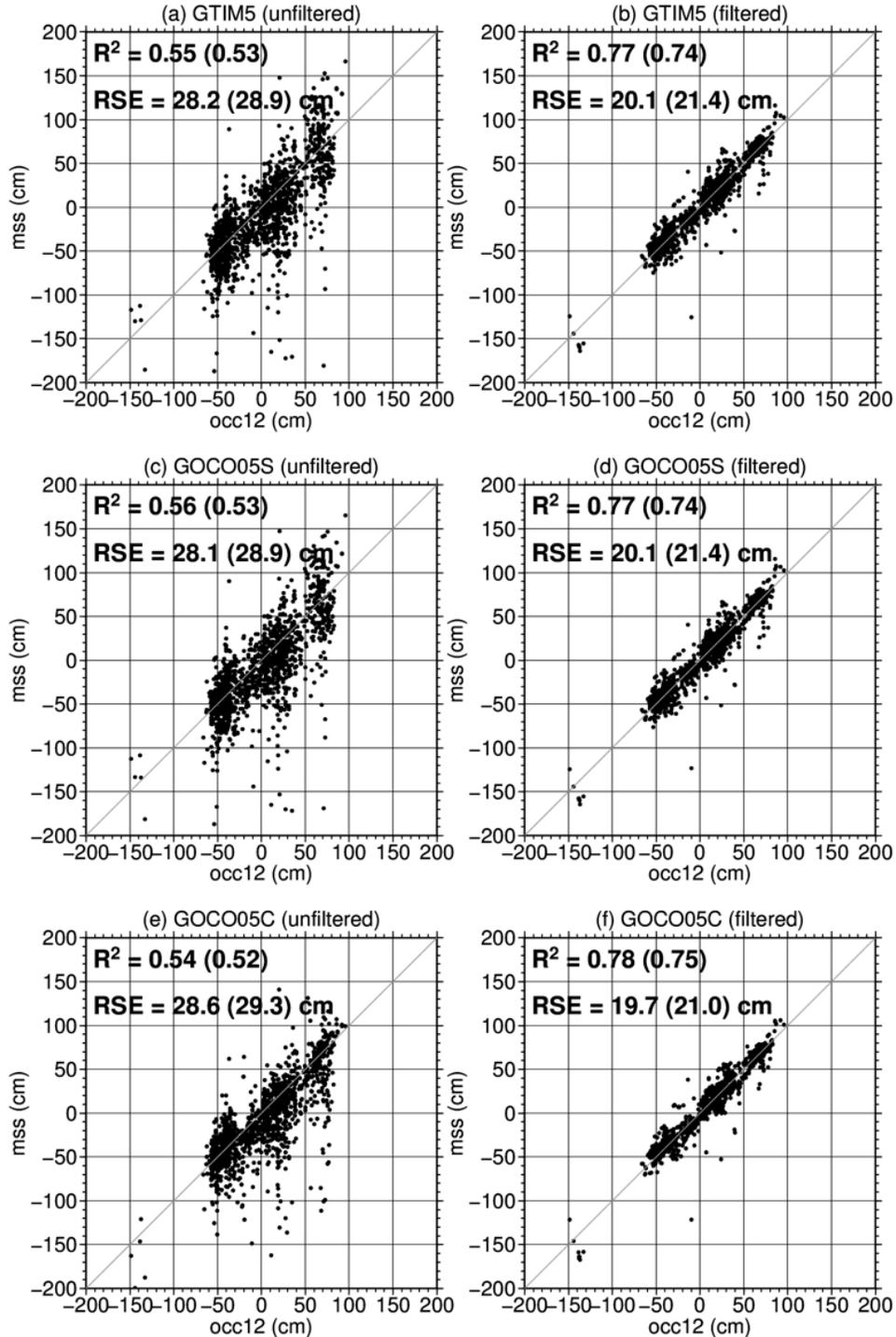
Figure 47. A comparison between OCCAM12 and DTU15-geoid MDT estimates. (a) GOCE-TIM5 (d/o=280) with no filtering. (b) As in (a) but with filtering. (c, d) Repeating (a, b) for GOCO05S (d/o=280). (e, f) Repeating (a, b) for GOCO05C (d/o=720). Values in parenthesis are calculated for GPS locations only.
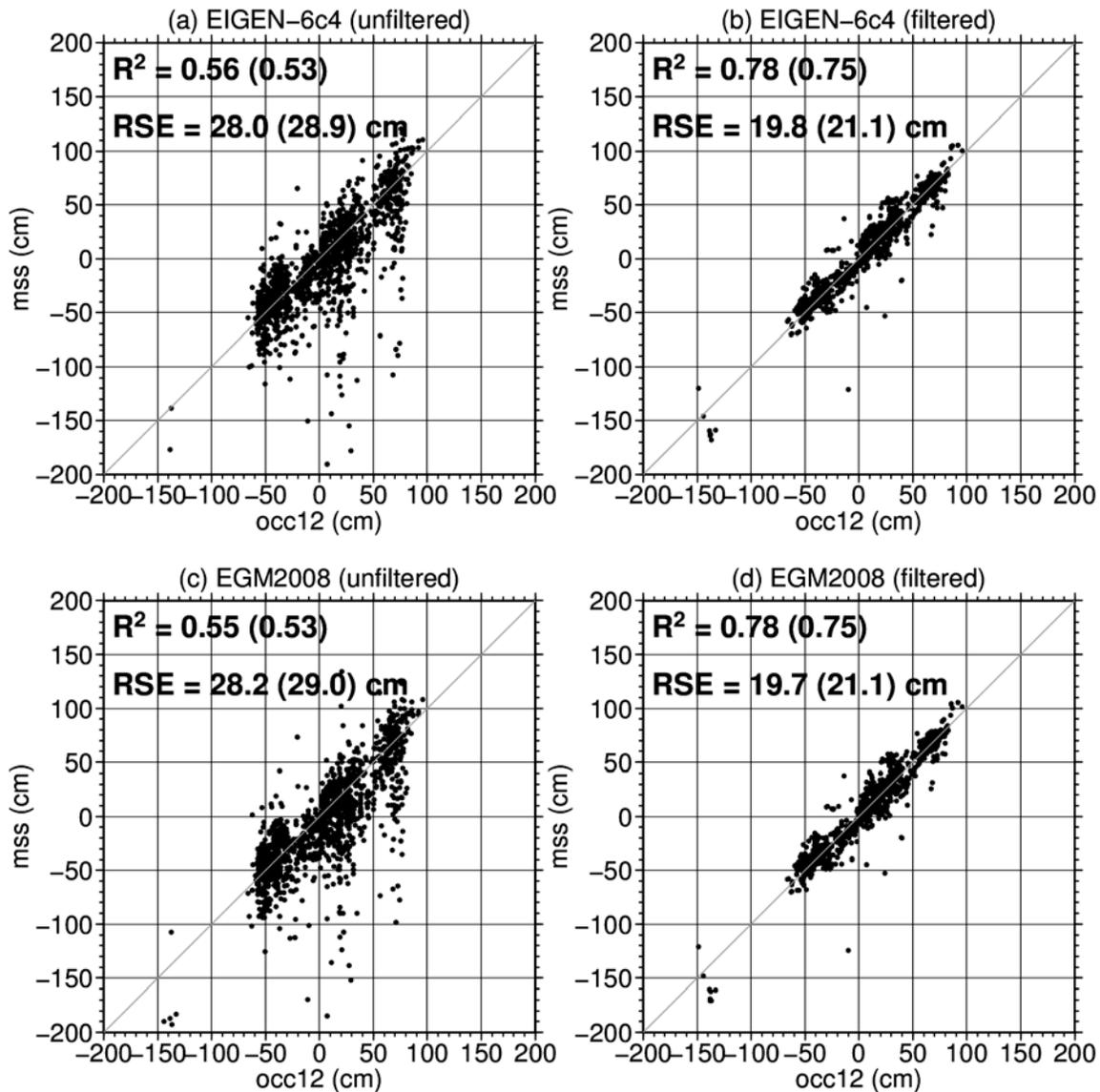
Figure 48. A comparison between OCCAM12 and DTU15-geoid MDT estimates. (a) EIGEN-6c4 (d/o=2190) with no filtering. (b) As in (a) but with filtering. (c, d) Repeating (a, b) for EGM2008 (d/o=2190). Values in parenthesis are calculated for GPS locations only.

Finally, we examine the ability of this approach to estimate a continuous CMDT along several stretches of coastline. The analysis is again conducted on the 1/12th of a degree OCCAM grid, with the coastline being defined by this model. Ultimately, however, the analysis will be conducted on the native 1 min MSS grid with the coastlines defined using e.g. GEBCO. (This work is on-going but it was not possible to complete it with the timeframe of this deliverable.)

Figure 49 shows estimates of the CMDT for Australia, traced clockwise from the north, from the for the five EGMs for a range of truncations. For comparison the OCCAM MDT is also shown. The unfiltered versions illustrate the problem of noise in the

geodetic CMDT estimates, the need for some form of filtering and the challenge of removing this noise while preserving the signal. The noise grows with increasing d/o but remains relatively similar across models, pointing the DTU15 MSS as the common dominant error source. The noise is of comparable magnitude to the signal and is thus difficult to remove while preserving the signal. The right hand panels show that after applying the screening and filtering approach outlined above the noise is much reduced and a CMDT quite similar to that from OCCAM is obtained, including the step across the Torres Strait, which is somewhat more pronounced than it is in OCCAM. An interesting difference is revealed down the eastern Australian coast, where instead of the smoothly declining CMDT seen in the model, the observations suggest a more stepwise decline with a plateau followed by a sharp drop with a subsequent smaller plateau and a further drop. Inspection of the full MDT suggests this to be a reflection of true oceanographic differences between the model and the observations rather than observational error. The solutions for d/o=720 and 2190 after filtering are generally smoother than those at lower truncations, but some residual noise remains. This can be removed by changing the filter parameters. However this is at the expense of resolving the sharp feature in the CMDT. The GPS-MDT values plotted in black are in broad agreement with the geodetic and model CMDTs, although several along the north Australian coast seem too high. More generally the noise in the GPS values appears greater than that in the filtered geodetic MDTs.

Figure 50 shows the CMDT around the coast of Southern Africa. Again, after filtering the, the geodetic and model estimates are in broad agreement. However the observations suggest a sharp drop in sea level not seen to the same extent in the model. Inspection suggest that this is also a true oceanographic difference related to a sharper transition than is seen in the model between the warm water of the Indian Ocean and the cool waters from the south Atlantic that leak around the cape to where the Agulhas Current separates from the coast. The two GPS heights from this regions support this sharp transition.

Figure 51 shows the CMDT for the coast of South America. This coast is traced from the equatorial western Atlantic, down to Drake Passage and up to the equatorial eastern pacific. This coast shows the greatest difference between the model and the geodetic CMDTs. Most notably the model shows a peak around grid point 1500. In the model this peak corresponds to a small region of elevated MDT along the western Patagonian coast that is not seen in the observations. However, this is a region of elevated noise and a very convoluted and broken coast line and the opposing drop in the geodetic CMDTs centred on grid point 1500 is likely error also. More work is required to improve this screening and filtering in this region. Better agreement is found with regard to the increasing CMDT over the remainder of the section travelling northwards along the coast of Chile.

Finally, for interest, in figure 52 the South American CMDT shown in figure 51 is continued around the entire Pacific and Indian Ocean basins and into the Atlantic basin (encompassing the section shown in figure 50). With the exception of the some isolated spikes the agreement between the model and the geodetic CMDTs is good. However, more work (on-going) is required to improve the noise removal while preserve the interesting features of the CMDT.
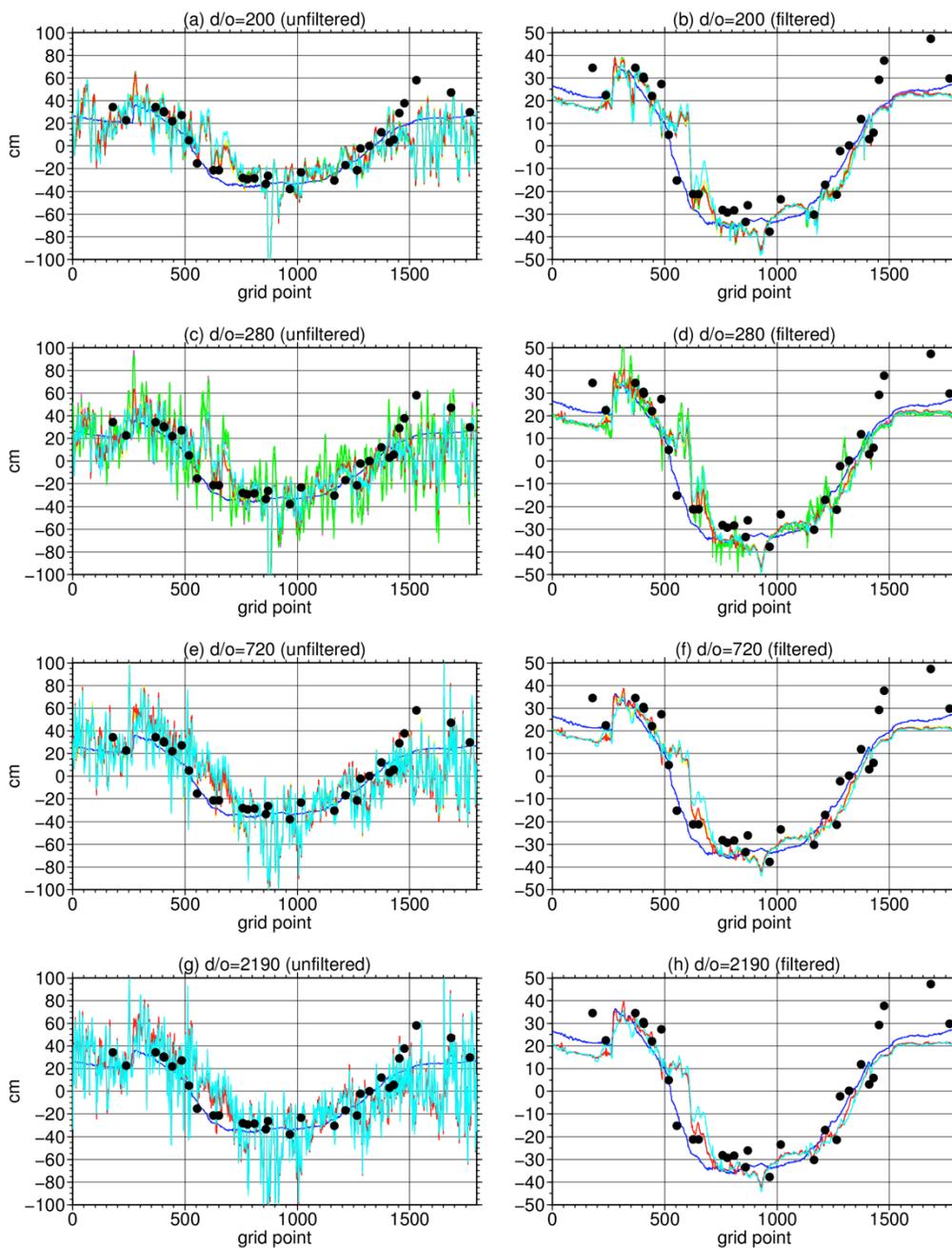
Figure 49. The Australian coastal MDT determined from the DTU15 MSS and a range of gravity models over a range of truncations: GOCE-TIM5 (black), GOCE-DIR5 (green), GOCO05S (blue), GOCO05C (magenta), EIGEN-64C (cyan) and EGM2008 (yellow). The OCCAM coastal MDT is shown in red and the black dots represent the GPS-EIGEN64C MDT. The unfiltered and filtered MSS-geoid MDTs are shown in the left and right panels respectively. Note the different scales in left and right hand panels.
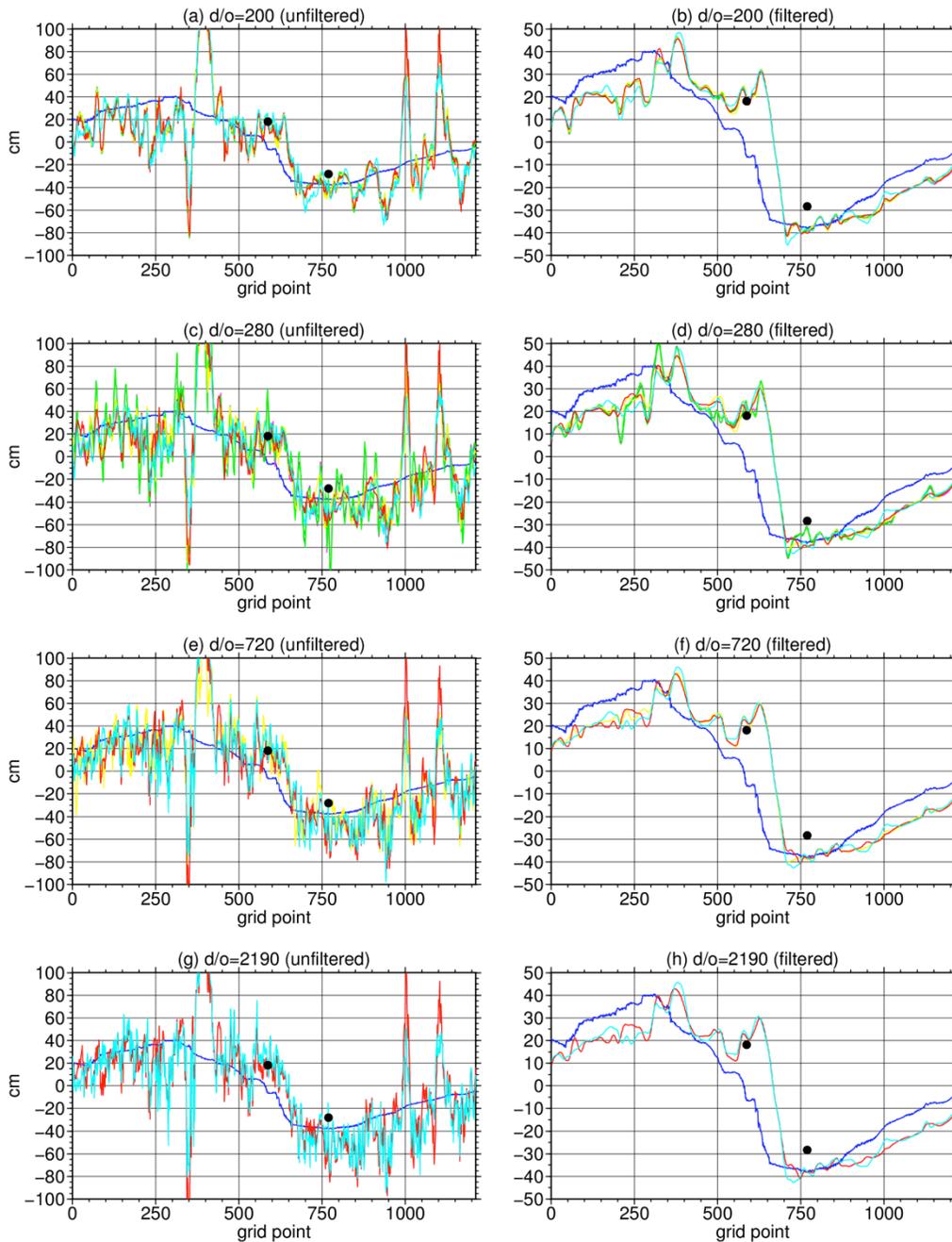
Figure 50. The Southern African coastal MDT determined from the DTU15 MSS and a range of gravity models over a range of truncations: GOCE-TIM5 (black), GOCE-DIR5 (green), GOCO05S (blue), GOCO05C (magenta), EIGEN-64C (cyan) and EGM2008 (yellow). The OCCAM coastal MDT is shown in red and the black dots represent the GPS-EIGEN64C MDT. The unfiltered and filtered MSS-geoid MDTs are shown in the left and right panels respectively. Note the different scales in left and right hand panels.

Figure 51. The South American coastal MDT determined from the DTU15 MSS and a range of gravity models over a range of truncations: GOCE-TIM5 (black), GOCE-DIR5 (green), GOCO05S (blue), GOCO05C (magenta), EIGEN-64C (cyan) and EGM2008 (yellow). The OCCAM coastal MDT is shown in red. The unfiltered and filtered MSS-geoid MDTs are shown in the left and right panels respectively. Note the different scales in left and right hand panels.

Figure 52. The South Atlantic (east coast), Pacific, Indian and South Atlantic (west coast) coastal MDT determined from the DTU15 MSS and a range of gravity models over a range of truncations: GOCE-TIM5 (black), GOCE-DIR5 (green), GOCO05S (blue), GOCO05C (magenta), EIGEN-64C (cyan) and EGM2008 (yellow). The OCCAM coa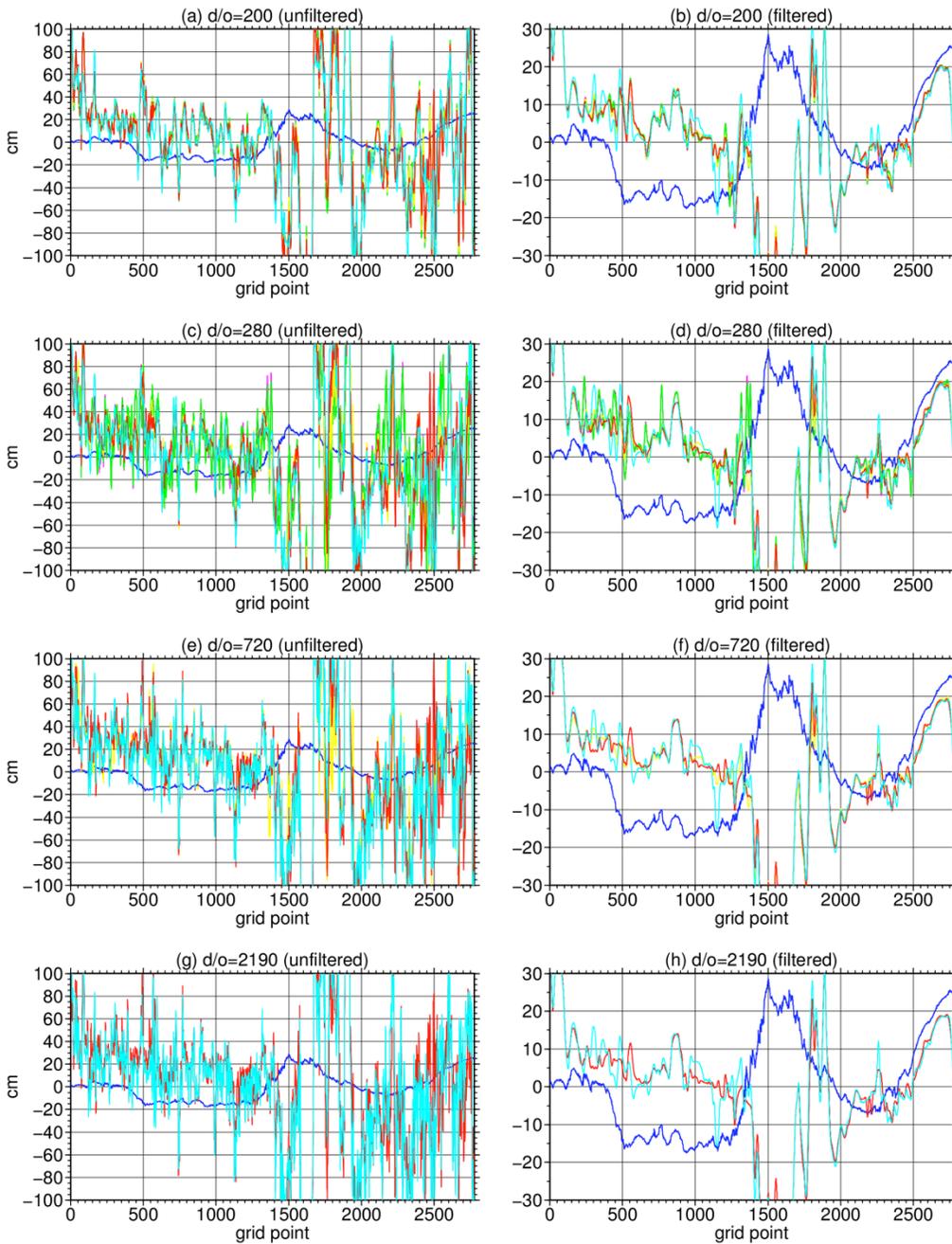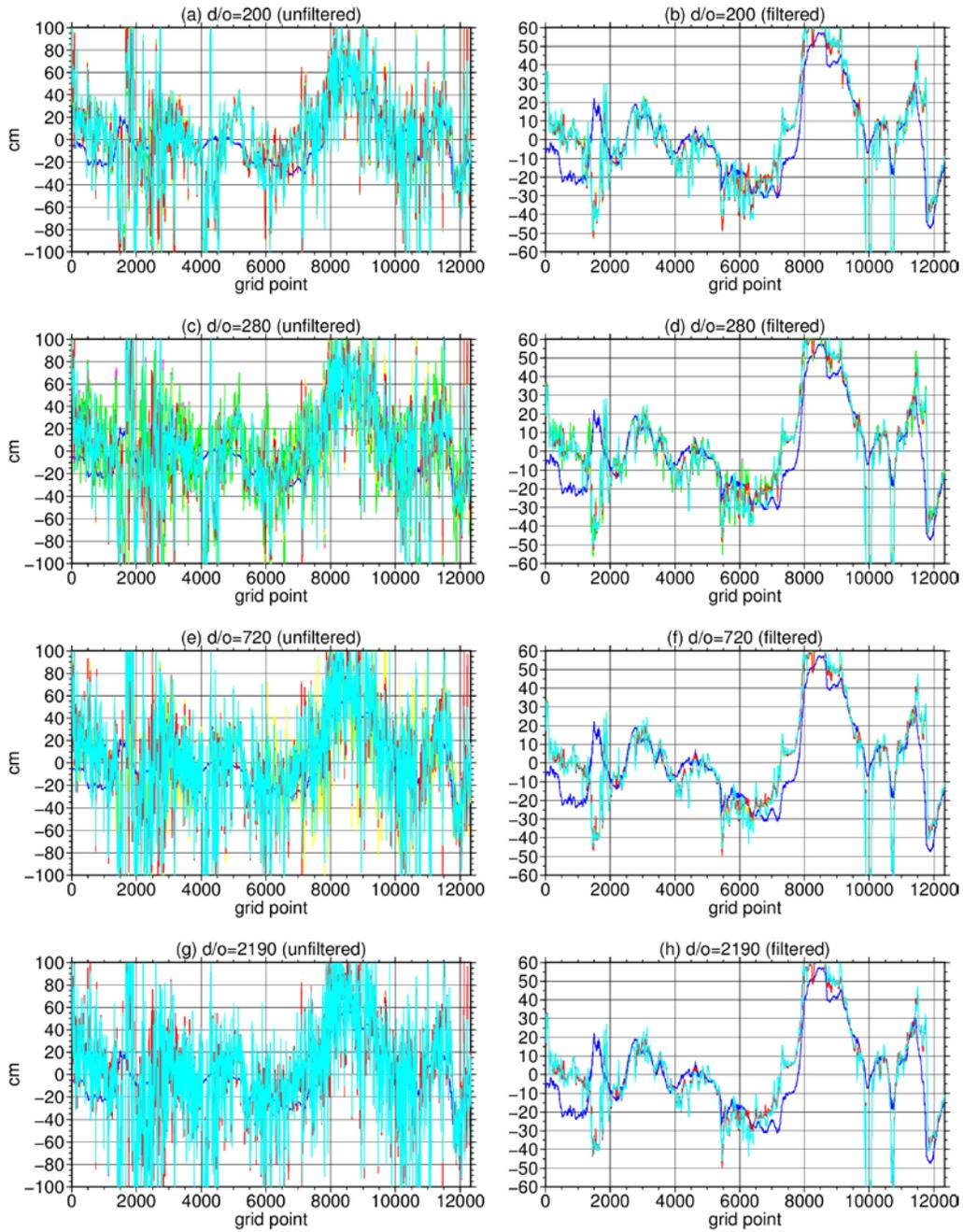stal MDT is shown in red. The unfiltered and filtered MSS-geoid MDTs are shown in the left and right panels respectively. Note the different scales in left and right hand panels.

WP3300 Coastal Altimetry and MSS accuracy

The aim of this section is two fold.
Initially to assess the accuracy of current state of the art MSS models (DTU13MSS) in the 10 km coastal zone. Here a particular effort is put to study the influence of tidal residuals on MSS determination and its effect on degradation of MSS near coast.
(DTU Space Lead)

The Second aim is to investigate the effect of the SAR altimetry selected at distance smaller than 150 Kilometers from the coast.
UBonn and DTU Space.

3.3.1 Comparative assessment of coastal and geodetic MDT along the coast of Norway.

This investigation has been carried as an extension to the work by Vegard Ophaug (NMBU, Norway). K. Breili (Statens Kartwerk, Norway) and C. Gerlach (Bavarian Academy of sciences, TUM, Munich, Germany) in close corporation with Martina Ivanowisz (NMBU, Norway) during a sabattical at DTU Space where the work was extended to include DTU13/DTU15 model and Cryosat-2 altimetry in the coastal zone.

The reason for preferring the Norwegian coastal zone to some of the other test regions in the project is the availability of a high resolution coastal model and high quality tide gauge information at a rate of 10 minutes along with sea level pressure information at all tide gauges during the 2010-2016 period that Cryosat-2 has been operating. This was not readily available in any other region.

In this comparative study various geoids were assessed in a combination with ocean and geodetic MDT models listed and detailed in Table 3.3.1.1. The ocean models were provided for the study by C. Hughes and the MSS model provided by O. Andersen.

	Model	Coverage	Time period	Grid spacing (°) or d/o
Geoid				
	TIM5+NMA2014	$57° \leq \varphi \leq 73.99°$ $-11° \leq \lambda \leq 36°$		0.01×0.02
	DIR5+NMA2014	$57° \leq \varphi \leq 73.99°$ $-11° \leq \lambda \leq 36°$		0.01×0.02
	NMA2014	$53° \leq \varphi \leq 77.99°$ $-15° \leq \lambda \leq 40°$		0.01×0.02
	EGM2008	Global		2190
MSS				
	DTU13MSS	Global	1993-2012	$1/60 \times 1/60$
Ocean				
	Nemo12	Global	1996-2000	$1/12 \times 1/12$
	NemoQ	Global	1996-2000	$1/4 \times 1/4$
	L-MITf	Global	1996-2000	$1/5 \times 1/6$
	L-MITc	Global	1996-2000	1×1
	OCC12	Global	1996-2000	$1/12 \times 1/12$
	POLCOMS	$40.0556° \leq \varphi \leq 64.8889°$ $-19.9167° \leq \lambda \leq 13°$	1996-2000	$1/9 \times 1/6$

Table 3.3.1.1 Details and specification of the geoids, MSS and ocean models assessed in the Norwegial coastal study.
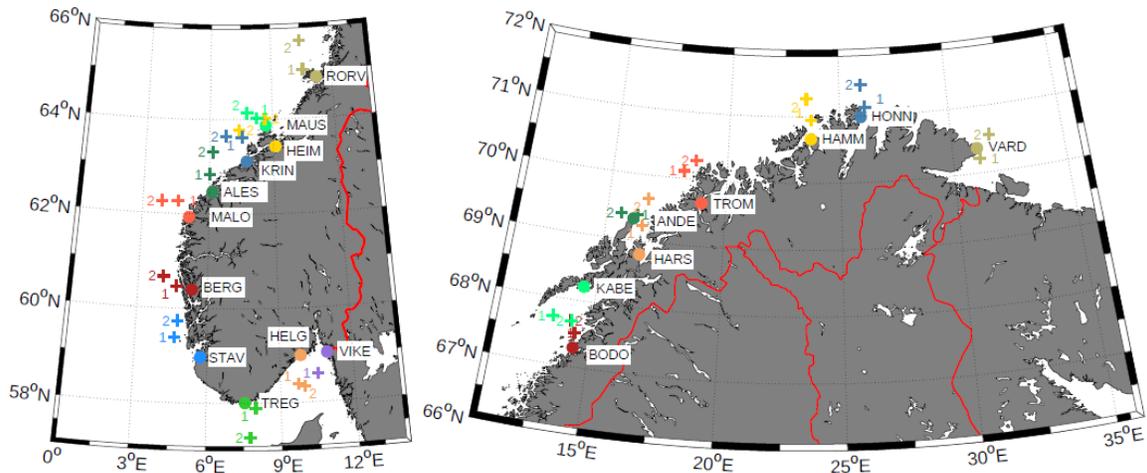
Figure 3.3.1.1. The location of the tide gauges and the closest altimetry points used for the comparison of MDT models. The figure to left shows the tide gauges within the coverage of the TOPEX/POSEIDON-JASON coverage and the figure to the right the tide gauges outside the coverage of T/P-JASON.
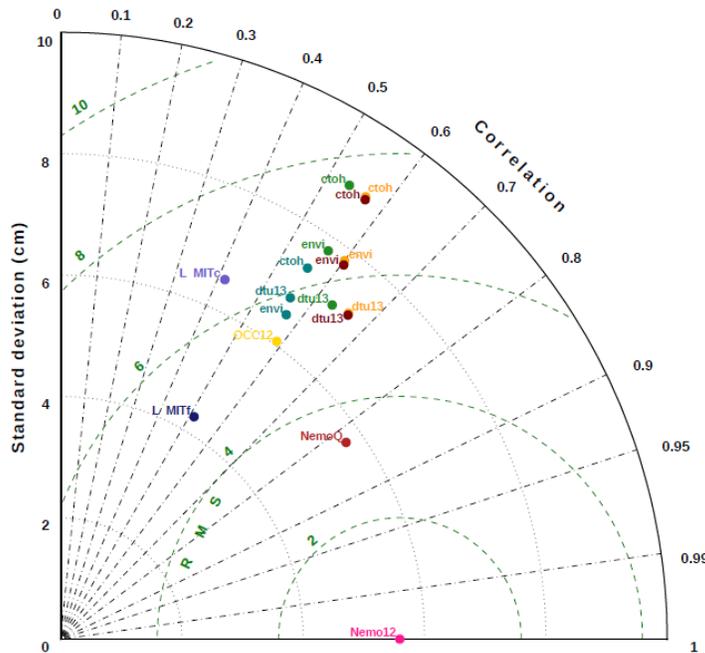
Figure 3.3.1.2 Taylor diagrams showing the standard deviation versus the Nemo12 model for all 23 tide gauges along the Norwegian coast

The Taylor diagrams in Figure 3.3.1.2 uses the MDT from Nemo12 (1/12 degree resolution) as the reference model against which all other MDTs are compared. It was chosen because, on average, it is the best-performing ocean model in comparison with tide gauges.
The model standard deviations are represented as radial distances from the origin, the centered RMS differences are proportional to the distances between reference and test models, and correlations are represented as the azimuthal angle

The comparison for the geodetic MDT based on DTU13MSS perform well in all regions. One of the reasons for the good performance of DTU13MSS could be that the extrapolation towards the tide gauges and points works well when values at equally spaced grid points are estimated from irregularly distributed data through spatiotemporal interpolation. Thus, DTU13MSS may well be more similar to the ocean models, which are also smooth surfaces not only due to their initial model physics and grids but also due to resampling and in general the agreement is within 5 cm. On average the DTU13MSS compares superior to retracked producs like those available through CTOH performance which is interesting but demonstrate the quality of this MSS.

The important conclusion from this study with respect to GOCE ++ is the fact that the agreement between ocean models and geodetic MDT is on average around 5 cm in terms of standard deviation for this very well surveyed region.

3.3.2 Enhanced coastal MDT using Cryosat-2 SARin in Norway

Due to the availability of data as described in the previous section, this study was again carried out in the Norwegian coastal region. This time in close corporation with Martina Ivanowisz and Ophaug Vegard from NMBU to evaluate the potential of Cryosat-2 in improving coastal MDT models.
In the study the Cryosat-2 SARin data were used as Norway is measured under the SARin mast of Cryosat-2. However, the data were treated as SAR data ignoring the possible cross-track SARin correction.
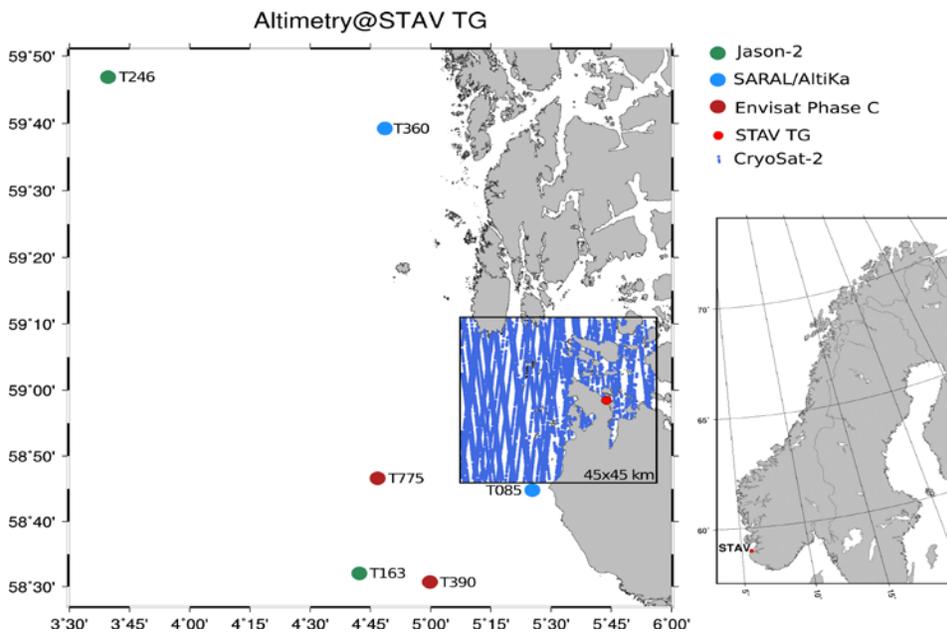
Figure 3.3.2.1 The location of the Cryosat-2 20 Hz altimetry close to the tide gauge at Stavanger in Norway along with the location of the nearby con-temporary altimetric observations by SARAL/AltiKa, Envisat (Phase C) and Jason-2

The importance of the SAR altimetry in the coastal zone is demonstrated in Figure 3.3.2.1 where the location of the Cryosat-2 20 Hz altimetry close to the tide gauge at Stavanger in Norway along with the location of the nearby con-temporary altimetric observations by SARAL/AltiKa, Envisat (Phase C) and Jason-2.
The coast of Norway is complicated with numerous fjords which largely prevents conventional altimetry in the coastal zone and it is seen that Cryosat-2 provides far more data in the near-coastal zone.
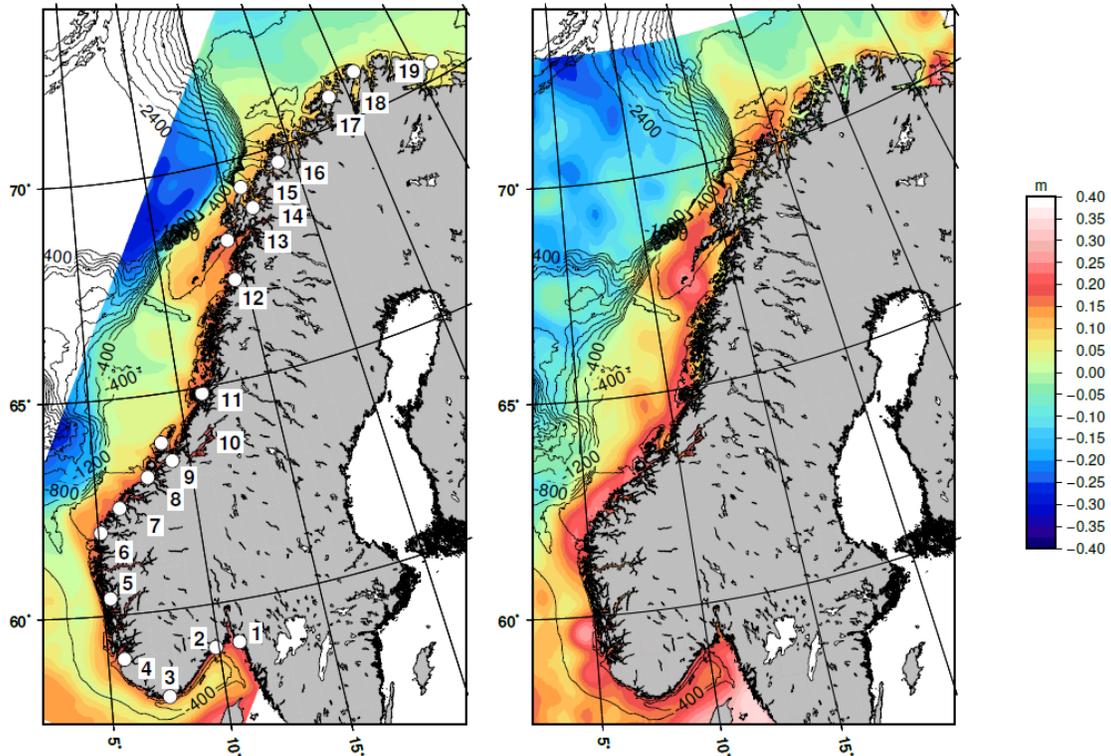
Figure 3.3.2.2 The MDT derived from the Norwegian Nordkyst model (left panel) and from Cryosat-2 altimetry (right panel). Values are given in meters.

We used the Cryosat-2 SARin from 2010-2016 augmented with LRM and SAR data away from the coast to derive an initial MSS. We then converted this into a geodetic MDT for the coastal region of Norway by subtracting the best know local geoid the NKG (Nordic commission of Geodesy) geoid for Scandinatia. This MDT is shown in the right panel of Figure 3.3.2.2. The MDT derived from the Norwegian Nordkyst model (800 meters) is shown in the left panel.

The slope of the Mean dynamic topography were derived using the slopes of the MDT and it illustrate better the quality of the derived MDT from Cryosat-2.
The Norwegian Coast current (NCC) flows northwards along Norway is very narrow and follows the bathymetry as a barotropic slope current (NwASC) the NCC also has a barotropic slope branch. Here we simply aim to compare the Cryosat-2 derived MDTs with NorKyst 800meters resolution coastal hydrodynamic model assuming that the flow follows a pattern to a geostrophically balanced flow for simplicity.

The geostrophic currents were derived from the Norwegian Nordkyst model (left panel) and from Cryosat-2 altimetry are given in Figur 3.3.2.3.
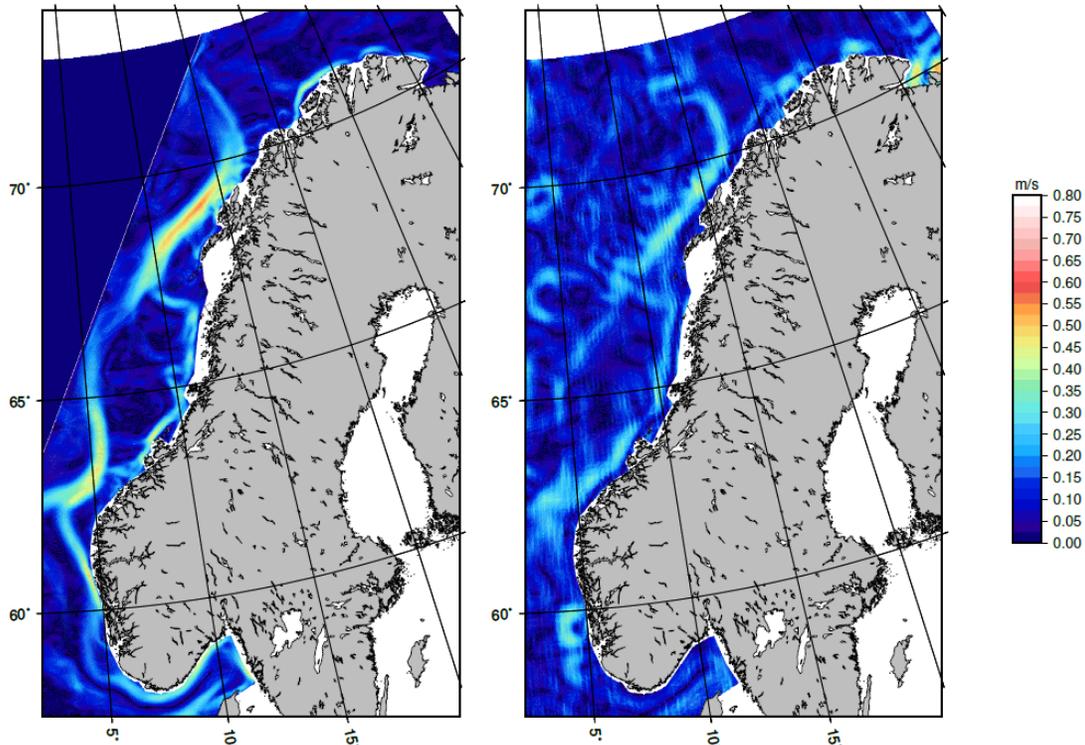
Figure 3.3.2.3 The geostrophic currents derived from the Norwegian Nordkyst model (left panel) and from Cryosat-2 altimetry (right panel). Values are given in meters/second.

3.3.3 Enhanced coastal MDT using Cryosat-2 LRM data in Australia

A detailed evaluation of DTU13MSS in coastal regions as a consequence of the possible degradation of the range and geophysical corrections was carried out in the GOCE++ test region of Australia.

The investigation was a consequence of the results presented internally to the GOCE++ consortium of a detailed comparison between 32 Australian tide gauges are currently submitted and in press by M. Filmer and W Featherstone (Curtain University) and C. Hughes comparing the similar models to the investigation in Norway. The set of Austraian tide gauges is shown in Figure 3.3.3.1

As the investigation in Australia is currently in press we are not allowed to reproduce and present them here. However their overall conclusions were similar to the comparison above by Vegard et al., 2016) where agreement on the sub-decimeter level is found.

The comparison between the DTU13 Mean sea surface and the Australian tide gauges revealed that a few tide gauges stood out beyond the 1 decimeter level as presented in Figure 3.3.3.1 (here only the fraction of the Australian tide gauges along the south coast of Australia from Melbourne to Perth corresponding to (tide gauge index 1 to 12).

The MDT derived using the DTU13MSS is shown with a black triangle in the figure 3.3.3.1 (blue arrow). It is revealed that DTU13MSS yields an MDT which is roughly 10 cm lower than the MDT derived at the Adelaide tide gauge based on tide gauge sea surface height observations combined with a local geoid model.

We subsequently carried out if this misfit can be associated with degradation in any of the range and geophysical corrections applied to the satellite range observations applied in derivation of DTU13MSS.

The data available to derive the DTU13MSS are shown in the left panel of Figure 3.3.3.2. A very regular pattern of missing data close to the coast is seen. This is associated with the ocean tide model used to derive DTU13MSS. For DTU13MSS the state of the art model at the time of deriving it was GOT4.8 from Richar Ray at Goddard Flight Space Center. This model is based on an altimetric correction to the FES95 ocean tide model, This underlying hydrodynamic model FES95 is given on 0.5 degrees spatial resolution. Hence GOT4.8 is also only available at this resolution. It is clear that the land mask in this model can be seen to prevent the interpolation of the ocean tide signal in the coastal zone. Consesquently, the ocean tide correction becomes un-available and the data are rejected in the RADS processing.

It must be noted that the situation is not as severe in all coastal regions of the model. It largely depend on the local information that was available of the time when the FES95 ocean tide model was developed by LEGOS.

The consequence is that there will be no altimetric data available in the coastal zone up to half a cell width in the GOT4.8 model corresponding to 25 km of the coast.

Under such conditions the DTU13MSS was developed to extrapolate follow the long wavelength signal in the DTU13MSS model.
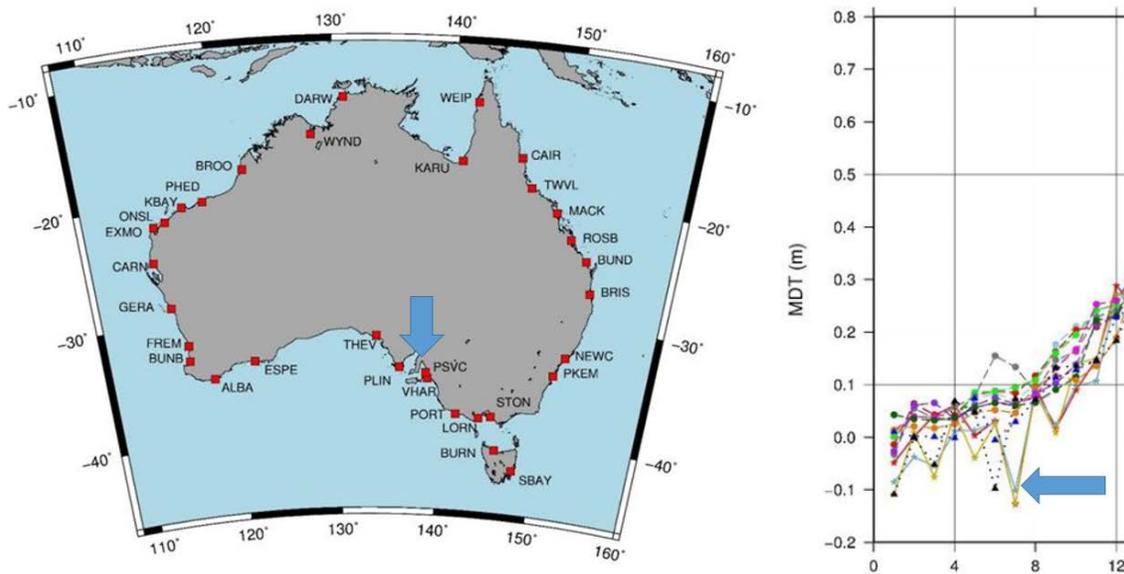
Figure 3.3.3.1 Australian tide gauges. The MDT at the tide gauges along the south coast of Australia is shown in the right figure between Melbourne and Perth corresponding to tide index 1 to 12 (Courtesy to Filmer et al., in press, 2017).

DTU13MSS is specifically developed WITHOUT using and underlying geoid model in order to provide an INDEPENDENT estimate of the mean sea surface not affected by possible errors in the geoid model. This appraoch is different to the CLS sequence of models which are developed by a remove/restore technique with respect to a geoid model)

In order to investigate the effect of the missing ocean tide correction and consequently missing data in the coastal zone we did an investigation of replacing the ocean tide correction with a more recent ocean tide correction. Namely the FES2014 ocean tide model.
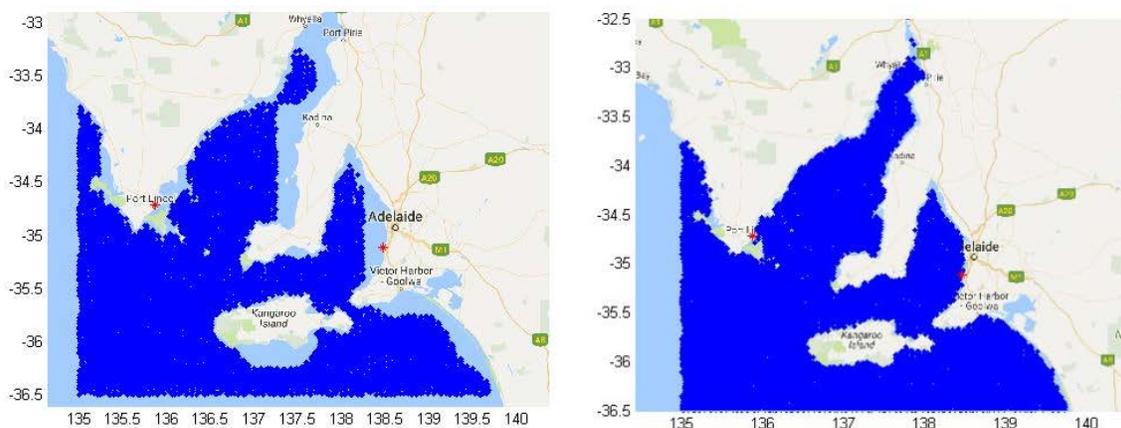
Figure 3.3.3.2 Left panel: The data available (dark blue) in the development of DTU13MSS using the GOT4.8 ocean tide model. Right panel: The data available using the FES2012 ocean tide model.

The number of data available for MSS computation using satellite altimetry processed using the FES2014 model is shown in the right panel of Figure 3.3.3.2. It is obvious that the increased resolution of the FES 2012 model increases the number of data significantly in this particular zone. Particularly the number of Cryosat-2 data increases in the coastal zone very close to the coast.

The DTU13 MSS was consequently updated using 6 years of Cryosat-2 applying the FES2012 by just computing the wavelength shorter than 100 km for each track. The reason for only updating short wavelength is to avoid that longer wavelength of oceanographic or climatic origin in the Cryosat-2 SSH observations would ruin the investigation. The most obvious error would be that Cryosat-2 observed during 2010-2016 whereas the reference period for DTU13 is 1993-2012 with a midpoint of 2003. As sea level trend is an average of 3 mm per year will cause the sea level to increase by 3 cm between 2013 and 2013 which is the mid point of the Cryosat-2 time series.

The result of the computation is shown in Figure 3.3.3.3 which shows the coastal correction to the DTU13MSS in centimeters. It indicate that the corrected MSS should actually be 10-15 cm higher than DTU13MSS and consequently the MDT should be 10-15 cm higher and in much better agreement with the Tide gauge data in Figure 3.3.3.1.
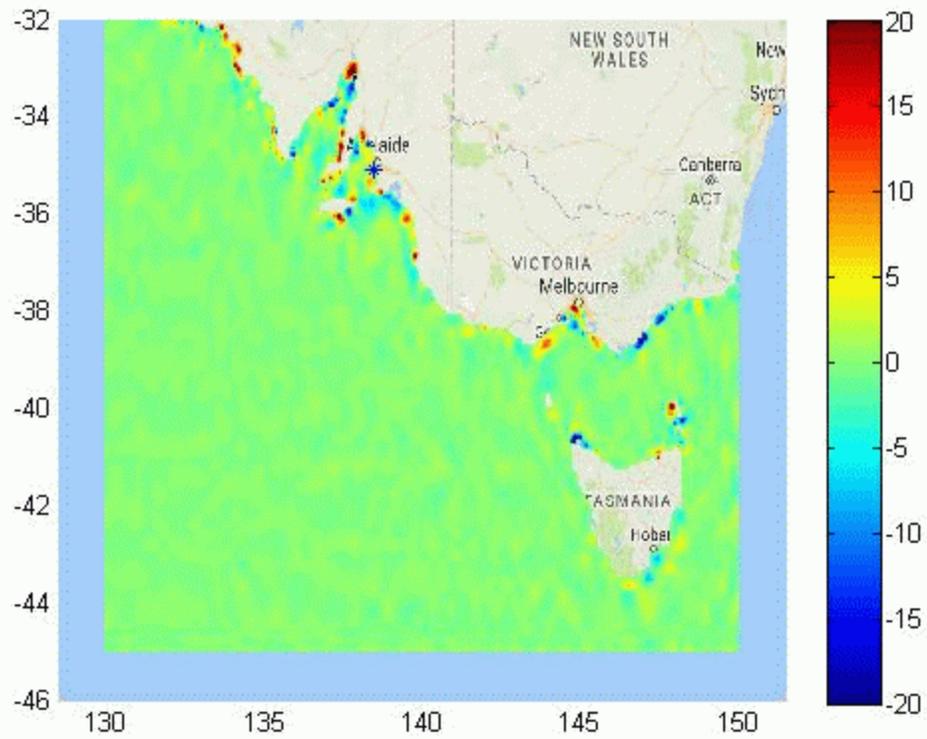
Figure 3.3.3.3 Short wavelength MSS coastal correction computed from 6 years of Cryosat-2 altimetry. The values are given in centimeters.

3.3.4 Comparative assessment of coastal and open ocean SAR and PLRM Altimetry from CryoSat-2.

This investigation is an extension of the work performed for the German Bight region (Fenoglio-Marc et al., 2015, 2015a and Dinardo et al., submitted) within the ESA Project Sea Level Climate Change Initiative (SLCCI). For the GOCE++dycot project we first consider this same region and further on extended it to include the North Eastern Atlantic coast (NEA). Moreover we analyse the Bay of Bengal region.

The regions have been selected based on the relevance for this project and on data availability.
The German Bight region offers a high-resolution coastal model and high quality 1-minute tide gauge during the complete CryoSat-2 mission 2010-2017 (see GEC region in Figure 3.3.4.1). This was not readily available in any other region.
The North-Eastern Atlantic is our first well-surveyed region (Fenoglio-Marc, 2016) and is completely covered by CryoSat-2 in SAR mode as well (Figure 3.3.4.10). Australia, our second well-surveyed region, is in LRM mode. Finally the Golf of Bengal is part of the South Eastern Asia poor-surveyed region and was covered by CryoSat-2 in SAR mode between October 2012 and March 2016. SAR coverage re-started in February 2017 (Figure 3.3.4.7).

The Synthetic Aperture Radar (SAR) mode in CryoSat-2 is expected to provide in coastal zone higher resolution long-track and more accurate altimeter-derived parameters, thanks to the reduced along-track footprint. In the study we regionally quantify the skills of CryoSat-2 SAR altimetry at different time and special scales by comparing SAR altimetry and conventional altimetry in the coastal zone, defined as the locations having distances to coast smaller than 10 km, and in open ocean. The validated geophysical altimeter parameter is sea surface ellipsoidal height (SSH).

All SAR data used have been made available by the GPOD service. They originate from the two different processing chain summarized in Table 3.3.4.1 that can be both selected by the users by choosing between different options available in the ESA-ESRIN GPOD service "SAR Versatile Altimetric Toolkit for Ocean Research & Exploitation" (SARvatore).

We call the first "GPOD Open Ocean Processing (GPODO)" and the second "GPOD Coastal Processing (GPODC)". GPDOC is more suitable for coastal applications. The Delay-doppler processing and the retracking methodology in GPODO and GPODC are partially different. The differences concerning delay-doppler processing are related to (1) the extension of the radar receiving window (128 range bins were used in GPODO, 256 in GPODC) and (2) the estimation of the waveform noise floor using the portions of the stack data (L1b-S) that are not affected by land reflections. The retracker model are SAMOSA2 in GPODO and SAMOSA+ in GPODC. The main differences between the SAMOSA+ and the SAMOSA2 algorithms are in the selection of the first guess epoch and the treatment of the land contaminated waveforms (see Dinardo et al., submitted for details).

The corrections in GPOD data are from the FBR cryosat products. The ocean tide TPXO8-ATLAS (http://volkov.oce.orst.edu/tides/tpxo8_atlas.html, Egbert et al., 2002) is additionally included. The geoid EGM2008 is in the data, use of the more recent geoid model EIGEN-6C4 is suggested. We substitute the standard wet tropo with the regionally improved GNSS-derived Path Delay Plus (GPD+) wet tropospheric correction (Fernandes and Lázaro, 2016)

GPODO/SAM2	Common options in GPOD	GPODC/SAM+
	20 Hz	
	Hamming in coastal only	
	Exact beam forming approximated	
	FFT Zero-Padding	
128 range bins (radar receiving window)		256 range bins (radar receiving window)
	No antenna path correction	
	LUT	
SAMOSA2		SAMOSA+

Table 3.3.4.1: GPOD options used in GPODO and GPODC

Simultaneous operations in SAR and pulse-limited (LRM) mode are not possible, and SAR is generally compared to a proxy of LRM, the Reduced-SAR (RDSAR) or Pseudo-LRM (PLRM) (Scharroo et al., 2016). The PLRM waveforms are here generated by processing the SAR burst data in the pulse-limited sense (Fenoglio-Marc et al., 2015) and retracked by the coastal TALES retracker, an adaptation to CryoSat-2 of the ALES sub-waveform retracker (Passaro et al., 2014). TALES is based on a numerical Brown-based model (SINC2, Buchhaupt et al., submitted).

In this study we first cross-compare altimetric GPODC/SAR and PLRM SSHs and model data, perform an in-situ validation along the coasts and investigate both instantaneous and seasonal behaviour. We finally analyse the GPOCO/SAR to investigate the differences in castal regions with respect to the optimal dataset GPODO.

The cross-validation between PLRM and GPODC/SAR proves the good consistency between PLRM and SAR sea level anomalies in the coastal zone. In the German Bight with bias, standard deviation of the differences and correlation of 2 cm, 52 cm and 0.78 respectively (Figure 3.3.4.2).
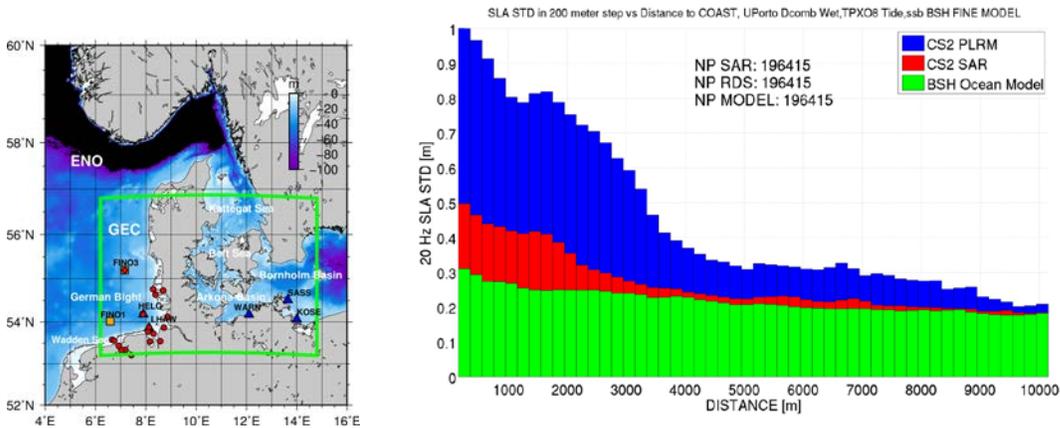
Figure 3.3.4.1: German Eastern Coast (GEC, green box) and GPODC. Corresponding diagram representing standard deviation of SLA in 200 meter bins of distance to coast for SAR, PLRM and BSH Model

The regional ocean model (BSH) shows the highest agreement with the SAR instantaneous dynamic ocean topography (DOTi) above the EIGEN-6C4 geoid. The standard deviation of the differences (stdd) is 24 cm whereas the BSH uncorrected sea level has a stdd of 55 cm with PLRM. The slope with the model is 0.96 for both altimeter products (Figure 3.3.4.2). In Figure 3.3.4.3 we have applied and ocean model correction to both the BSH model and the altimeter data
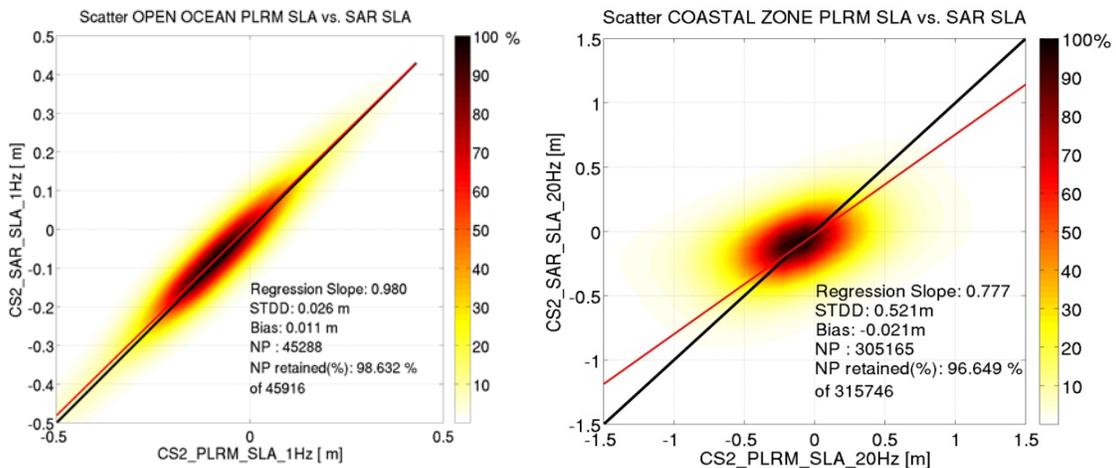
Figure 3.3.4.2. GEC and GPODC: Scatter Plot in open sea at 1 Hz (left) and in coastal zone at 20 Hz between SAR SLA & PLRM SLA (STD3D 2.6 cm, 52 cm)
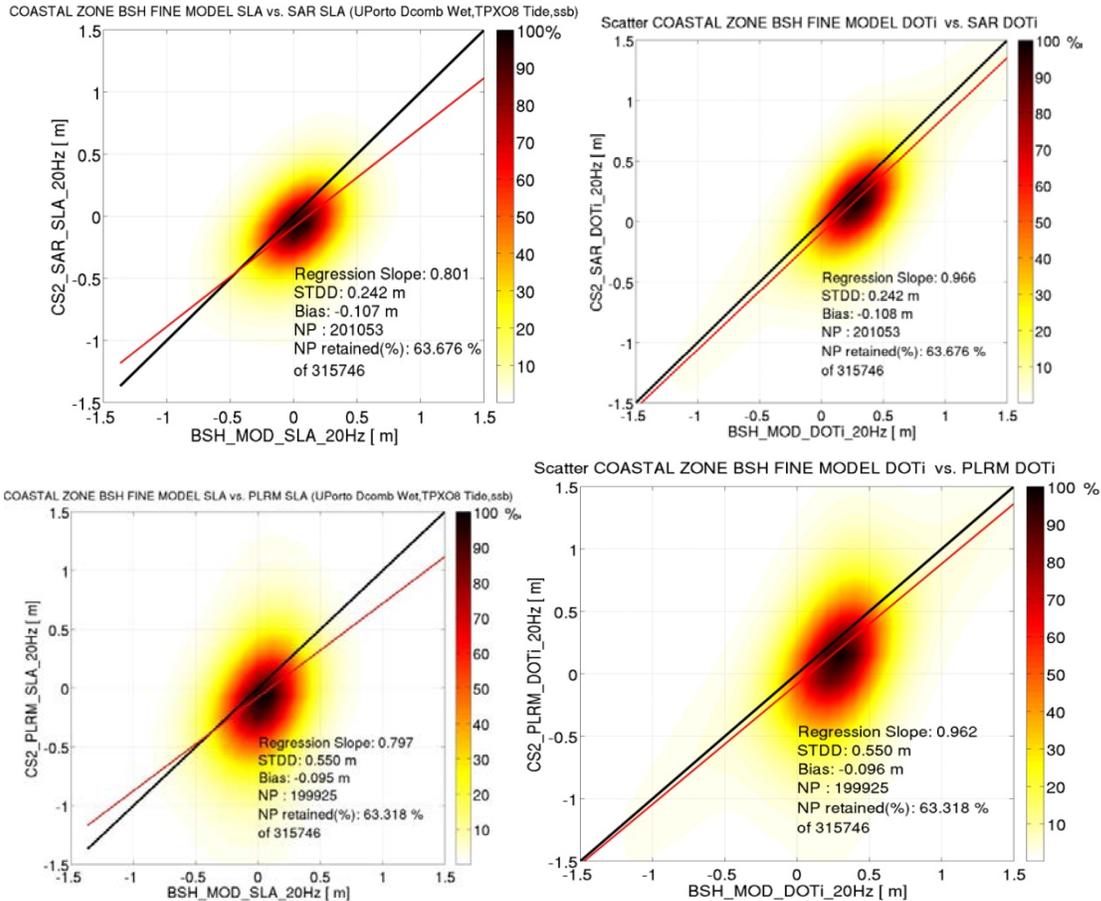
Figure 3.3.4.3. GEC and GPODC: Coastal Cross-val between SAR and BSH Model (left) and
PLRM and BSH Model (right) for DOTi (top) and SLA (bottom). SLA (STD3D 24 cm, 55 cm)

We have computed the standard deviation of the measurements averaged as function of distance to coast in bands of 200 meters. Figure 3.3.4.3 shows that sea level anomalies are affected by land contamination starting at 2 km from coast in SAR and at 3.5 kilometres in PLRM TALES (Fig. 3.3.4.3).

The analysis of monthly mean time-series shows the capacity of SAR Altimetry to measure the sea level annual cycle in the coastal zone during the mission time more accurately than PLRM (Figure 3.3.4.4). Also the in situ cross-comparison exercise proves the higher accuracy of SAR SAMOSA+ compared to PLRM TALES in the coastal zone with average SLA stdd of 5.7 cm and 7.5 cm respectively. A similar conclusion holds for the in situ cross-comparison with open ocean altimeter data, with average stdd of 3.9 cm and 4.6 cm respectively in SLA retrieved from SAR and PLRM TALES.
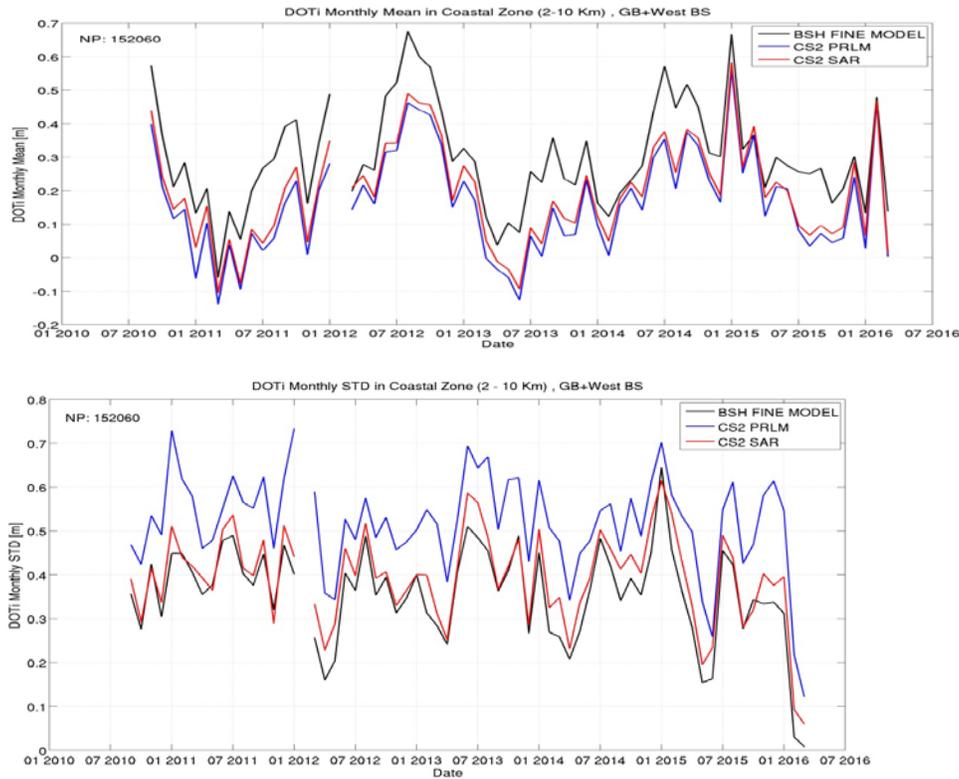
Figure 3.3.4.4. GEC and GPODC. Monthly mean (top) and standard deviation (bottom) of 20 Hz DOTi in coastal zone (2-10 km) for SAR, PLRM and BSH Model

Similar results are obtained for the cross-validations of GPODC/SAR and PLRM in the Bay of Bengal, where the mean, standard deviation of the differences and correlation between SAR and PLRM in coastal zone are 3 cm, 61 cm and 0.98 respectively (Figure 3.3.4.5). The higher standard deviation of the differences and correlation of the SLAs could indicate deficiencies in the tide ocean correction used, TPX0 in this case. The cross-validation with the year 2014 of the Numerical Ocean Circulation Model from the Institute of Water Modelling (IWM) of Bangladesh show better agreement of the model with SAR than with PLRM. Also in this region land contamination begins to affect sea level and wave measurements at 3 km from the coast in SAR and at 4 kilometres in PLRM TALES (Fig. 3.3.4.7). The noise due to contamination after 3 km is at the same level in SAR and PLRM, which was not the case in the German Bight. We also observe a higher level of variability in the ocean model in this region.
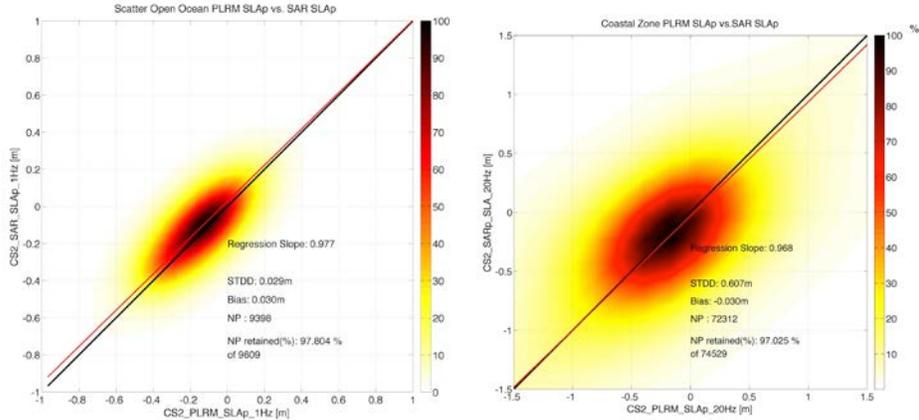
Figure 3.3.4.5. BoB and GPODC : Cross-val in open ocean (1Hz) and coastal zone (20Hz) between SAR SLA & PLRM SLA; correspond to Fig. 1 for GEC (STD3D 3 cm, 60 cm)
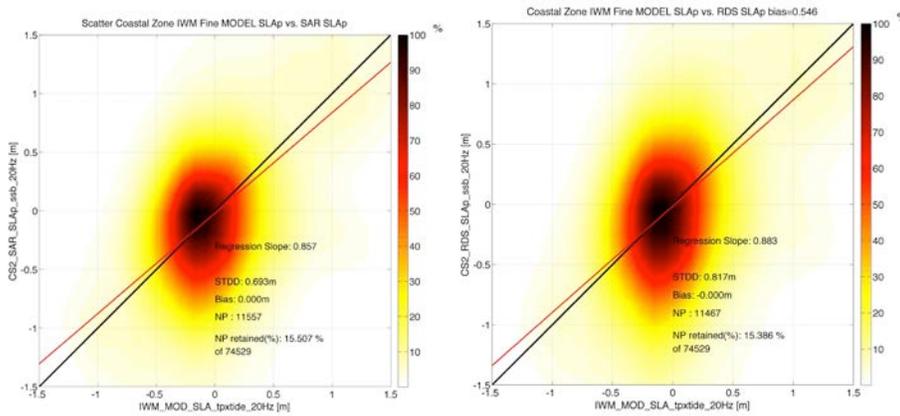
Figure 3.3.4.6: Bay of Bengal and GPODC : Cross-val in coastal zone between SAR and BSH Model (left) and PLRM and IWM Model (right) for SLA (STDD 69 cm , 82 cm).
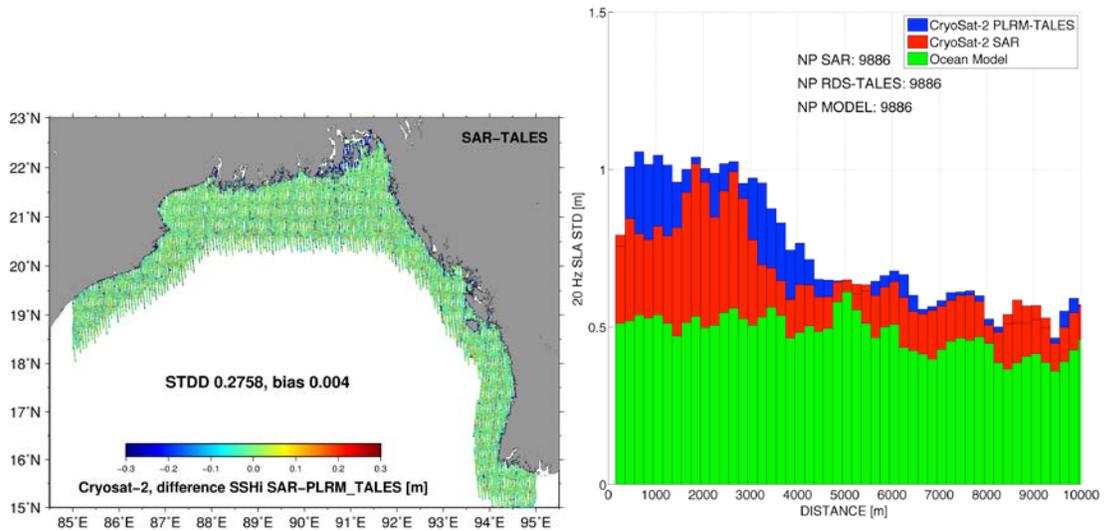
Figure 3.3.4.7. BOB and GPODC : with SAR minus TALES instantaneous heights (left) and corresponding diagram representing standard deviation of SLA in 200 meter bins of distance to coast for SAR, PLRM and IWM Model (right)

In third part of our analysis we have evaluated the differences between the data processed using GPODO and GPODC receipts in the GEC region and we have comparaed PLRM and GPODO in the NEA region. Figure 3.3.4.8 shows that in the GEC region the results of the GPDO processor are more affected than GPODC by land contamination, which starts already at 3 km from coast. The difference between GPODC and GPODO data is smaller in open sea than in coastal zone as expected (stdd of the difference is 5 cm and 22 cm respectively, see Figure 3.3.4.9). The analysis, repeated for the set of regions in Figure 3.3.4.10, gives similar results for the comparison of PLRM and GPODO in each of the four regions. We expect that GPODC is less contaminated that GPODO in the complete NEA region.
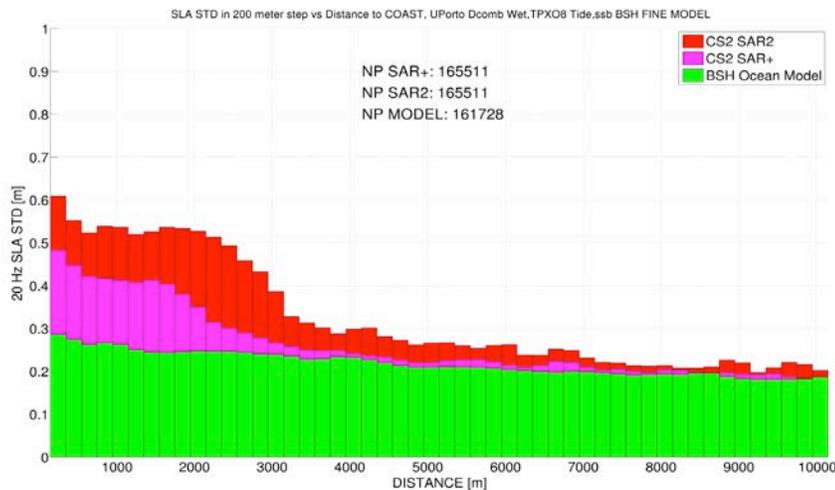
Figure 3.3.4.8. GEC with GPODC and GPODO: diagram representing the standard deviation of SLA in 200 meter bins of distance to coast for SAR, PLRM and BSH Model, 2011-2015.

The values of validation skills (mean, correlation, standard deviation of residuals) are summarized in Table 3.3.4.2. They show that in coastal zone SAR altimetry is twice more accurate that PLRM. The STDD of difference with model is 22 and 55 cm for GPODC/SAR and PLRM respectively. A significant reduction of errors in sea level anomalies is therefore possible with SAR.

The Table also indicate that SAR processing options need to be selected with care, as the STDD differences in coastal zone between different SAR processing chains can amount to 24 cm and cannot be neglected. It is therefore very important to select the more accurate SAR altimetry coastal processing for further analysis. The new limit for use of SAR altimetry data is 2-3 kilometres from coast.
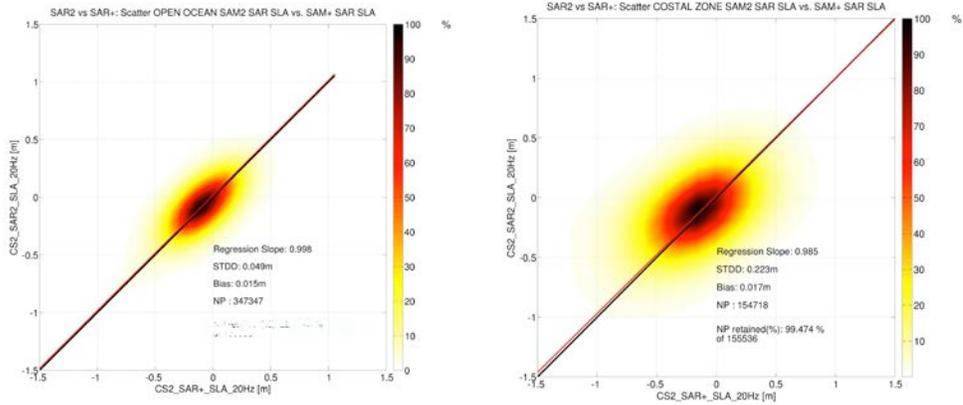
Figure 3.3.4.9: GEC, GPODC and GPODO: scatterplots of sea level anomalies SLA corresponding to the GPODO and GPODC processing for open sea (left) and coastal zone (right). 2011-2015, (STDD 5 cm , 22.3 cm).
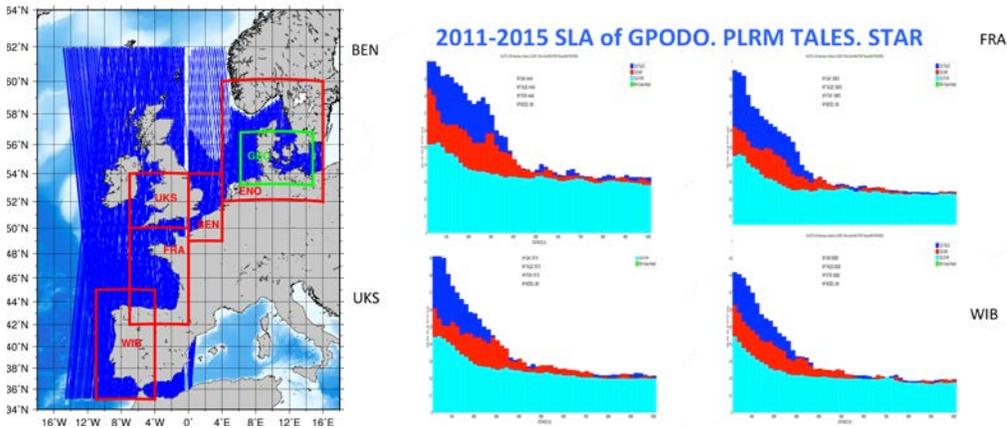
Figure 3.3.4.10. GPODO in the Eastern North Atlantic: Region (left) and corresponding diagram of SLA standard deviation in 200 meter bins of distance to coast for SAR, PLRM, Interval 2011-2015 in the 4 selected regions (right).

	Open sea (1Hz) PLRM/GPODC SLA	Coastal (20Hz) PLRM/GPODC SLA	Coastal (20Hz) GPODC/BSH SLA	Coastal (20Hz) PLRM/BSH SLA	Open sea (1Hz) GPODC/GPODO SLA	Coastal (1Hz) GPODC/GPODO SLA
GEC SLA 2010-2015	0.98, 0.026, 0.01	0.78, 0.52, -0.02	0.80, 0.24, 0.11	0.80, 0.55, -0.1	1, 0.049, 0.015	0.98, 0.223, 0.017
GEC DOTi 2010-2015			0.97, 0.24, 0.11	0.96, 0.55, -0.1		
BoB SLA 2012-2015	0.98, 0.029, 0.03	0.97, 0.61, -0.03	0.86, 0.69, 0.0	0.88, 0.817, 0.0		

Table 3.3.4.2: Summary of statistics. Parameters are correlation, standard deviation of the difference and bias. Units are meters. See corresponding Figures 3.3.4.2, 3.3.4.3, 3.3.4.6, 3.3.4.9.

References

Buchhaupt C., Fenoglio-Marc L., Dinardo S. Retracking CryoSat-2 data with pulse limited processing, AdSR special session CryoSat-2, submitted January 2017

Dinardo S., Fenoglio-Marc L. Buchhaupt C., Becker M., Scharroo R., Fernandez J., Benveniste J. CryoSat-2 performance along the german coasts, AdSR special session CryoSat-2, submitted January 2017

Featherstone, W. E., J. F. Kirby, C. Hirt, M. S. Filmer, S. J. Claessens, N. J. Brown, G. Hu, and G. M. Johnston (2011), The AUSGeoid09 model of the Australian Height Datum, J. Geod., 85(3), 133-150, doi: 870 10.1007/s00190-010-0422-2.

Fecher. T., R. Pail, and T. Gruber (2015), Global gravity field modeling based on GOCE and complementary gravity data, Int. J. Appl. Earth. Obs. Geoinf., 35, 120–127. doi:10.1016/j.jag.2013.10.005

Fenoglio-Marc, L., S. Dinardo, R. Scharroo, A. Roland, M. Dutour Sikiric, B. Lucas, M. Becker, J. Benveniste, R. Weiss (2015). The German Bight: A validation of CryoSat-2 altimeter data in SAR mode, Advances in Space Research, 55, 11, 2641-2656, 2015. http://dx.doi.org/10.1016/j.asr.2015.02.014

Egbert G. and Erofeeva S. (2002). Efficient Inverse Modeling of Barotropic Ocean Tides. J. Atmos. Oceanic Technol., 19, 183204,

Fenoglio-Marc L., R. Scharroo, A. Annunziato, L. Mendoza, M. Becker, and J. Lillibridge (2015a). Cyclone Xaver seen by geodetic observations, Geophys. Res. Lett., 42, 9925–9932, http://dx.doi.org/10.1002/2015GL065989.

Fenoglio-Marc L. (2016). WP1300 Technical Report: report on selection and justification of test area GOCE++ Dynamic Topography at the coast and tide gauge unification GOCE ++ DYCOT, ESTEC

Fernandes M. J., Lázaro C. GPD+ Wet Tropospheric Corrections for CryoSat-2 and GFO Altimetry Missions, Remote Sensing 2016, 8(10), 851, 2016. http://dx.doi.org/10.3390/rs8100851

Filmer, M. E., C. W. Hughes, P. L. Woodworth, W. E. Featherstone and R. J. Bingham, 2017: Comparison of oceanographically and geodetically derived ocean mean dynamic topography at Australian tide gauges. *J. Geophys. Res. (Oceans), submitted.*

Passaro, M. et al., ALES: A multi-mission adaptive subwaveform retracker for coastal and Remote Sensing of Environment, 4 April, pp. 173-189, 2014.

Pavlis, N. K., S. A. Holmes, S. C. Kenyon, and J. F. Factor (2012), The development and evaluation of Earth Gravitational Model (EGM2008), J. Geophys. Res., 117, B04406, doi: 10.1029/2011JB008916.

Pavlis NK, Holmes SA, Kenyon SC, Factor JK (2013) Correction to "The development and evaluation of the Earth Gravitational Model 2008 (EGM2008)", J. Geophys. Res. - Solid Earth 118(5): 2633, doi: 948 10.1029/jgrb.50167.

SARvatore Software Prototype Wiki User Manual Page, 2016, http://wiki.services.eoportal.org/tiki-index.php?page=GPOD+CryoSat-2+SARvatore+Software+Prototype+User+Manual

Scharroo, R., RADS RDSAR Algorithm Theoretical Basis Document, Version0.3, CP4O Project Report, 2014 - updated May 2016. URL: http://www.satoc.eu/projects/CP4O/docs/tud_rdsar_atbd.pdf

9 Appendix H, D7: Technical Note: Connected global tide gauges including trend analysis for selected epoch
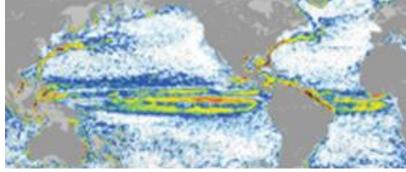
GOCE++ Dynamic Topography at the coast and tide gauge unification
GOCE ++ DYCOT

TITLE. WP 3300-D7 Technical Note: Connected global tide gauges including trend analysis for selected epoch

Authors: Médéric Gravelle, Luciana Fenoglio-Marc, Christopher Hughes, Sara Padilla Polo, Guy Wöppelmann.

ESTEC Ref: ITT AO/1-8194/15/NL/FF/gp "GOCE++ Dynamic Topography at the coast and tide gauge unification"- Coordinator: Ole B. Andersen (DTU)

DOCUMENT CHANGE LOG				
Rev.	Date	Sections modified	Comments	Changed by
1	11-01-2017	All	Draft	Médéric Gravelle
2	30-03-2017	All	Draft	Guy Wöppelmann
3	21-04-2017	2.2.1.2	Draft	Chris Hughes
4	28-06-2017	2.4, 3.4, 3.5	Draft	Luciana Fenoglio-Marc
5	11-07-2017	All	Draft	Médéric Gravelle

Table of Contents

1   Introduction

Connecting global tide gauges implies expressing their observations in the same global geocentric reference, which space geodesy (and particularly the Global Navigation Satellite System (GNSS) technology) has made possible. Thus, the link to this global reference (in our case the ITRF08 (Altamimi et. al, 2011) with the GRS80 ellipsoid attached to it) can be made using GNSS measurements (either episodic or permanent) whenever they are available at the tide gauge sites.

To be able to compare in-situ (i.e from tide gauges) mean dynamic topography (MDT) values over the selected periods of the project ([2003-2007] and [2008-2012], see WP1300 Technical Report) with models, the objective of this task is to build a global network of tide gauges where all the links allowing to express the sea level observations with respect to the ellipsoid in the ITRF08 are available.

A trends analysis will be also presented here, especially the method to account for the vertical land movements at a maximum of tide gauge sites to express rates of sea level change in a global (i.e geocentric) reference frame.

2   Ellipsoidal mean sea level

The aim of this part is to build the most complete dataset of ellipsoidal mean sea level measurements from tide gauges to obtain in-situ mean dynamic topography values over the two selected epochs ([2003-2007] and [2008-2012]) following:

$$MDT_{TG} = EMSL_{TG} - GEOID_{TG} \tag{1}$$

where MDT_{TG} is the mean dynamic topography value at the tide gauge, $EMSL_{TG}$ is the ellipsoidal mean sea level value at the tide gauge and $GEOID_{TG}$ is the geoid value at the tide gauge.

To obtain the ellipsoidal mean sea level, the ellipsoidal height of the tide gauge reference datum needs to be added to the mean sea level from tide gauge observations (Figure 1).

2.1   Calculating the ellipsoidal heights of RLR datums

Starting from the RLR PSMSL databank (http://www.psmsl.org/data/obtaining/rlr.php), a significant part of the work was to investigate the availability of the information required to express the RLR datum (reference of the PSMSL mean sea levels) as ellipsoidal heights in the global reference. This information primarily relies on the availability of GNSS measurements performed at the tide gauge site. It usually involves two quantities: the GPS-derived ellipsoidal height of a tide gauge benchmark in the global reference, obtained from the processing of permanent or episodic GNSS measurements (A in Figure 1) and the height of this benchmark with respect to the RLR datum (B in Figure 1). If the height of the benchmark with respect to the RLR datum is not known, then a supplemental quantity is needed to connect this benchmark to one for which it is known (mostly using spirit

leveling). This is commonly called a geodetic tie, and ultimately yields B inFigure 1. As a matter of fact, the benchmarks nearby the tide gauge for which GPS data were available were not expressed in the RLR datum, and hence it was crucial to find a geodetic tie between the GPS-observed benchmark and a tide gauge benchmark.
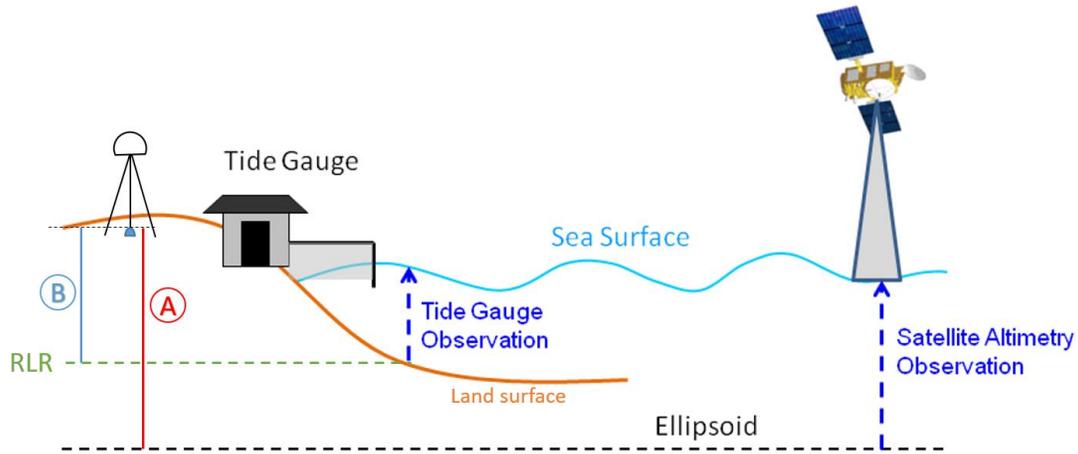
Figure 1: Basic references and quantities at a TG-GNSS colocation site

2.1.1 From permanent GNSS station

2.1.1.1 Geodetic ties

The geodetic ties of 113 RLR tide gauges with nearby permanent GNSS stations were collected from the SONEL data assembly centre (http://www.sonel.org/-Stability-of-the-datums-.html?lang=en). 14 ties were provided by Luciana Fenoglio for German tide gauges, which are not in the RLR dataset yet.
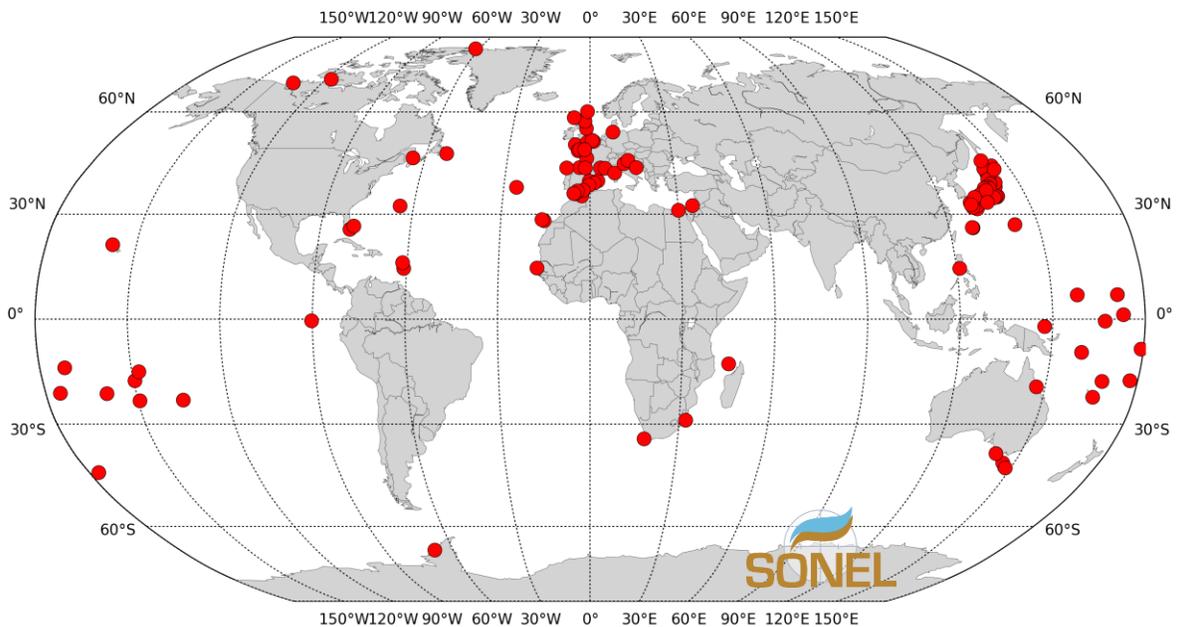
Figure 2: Tide gauges for which a geodetic tie with a nearby GNSS station is available

2.1.1.2 Ellipsoidal heights

The ellipsoidal heights of these permanent GNSS stations were extracted from the last GPS solution (ULR6a) of the ULR analysis centre in SONEL (http://www.sonel.org/-Vertical-land-movement-estimate-.html?lang=en). All the ellipsoidal heights are expressed in the ITRF08 reference frame. For stations that were not included in this solution, the ellipsoidal heights were obtained from the average of three daily positions processed using the Canadian CSRS-PPP tool (https://webapp.geod.nrcan.gc.ca/geod/tools-outils/ppp.php), also expressed in the ITRF08 reference frame.

The ellipsoidal heights coming from permanent GNSS stations are associated to an epoch and an uncertainty. As the adjustment model used in the ULR6a computation includes a vertical velocity and the ULR6a heights refers to the epoch 2004.5, the ULR6a heights were retrieved and propagated to the mean epochs of the two selected periods in the GOCE++ project: 2005.5 for [2003-2007] and 2010.5 for [2008-2012].

2.1.2 From episodic GNSS

Ellipsoidal heights from GNSS campaigns at tide gauge sites were searched and retrieved from different sources, mostly via P. L. Woodworth (Woodworth et. al, 2013; Woodworth et. al, 2015) and M. Filmer for Australian tide gauges (Featherstone & Filmer, 2012), but also from Lin et al (2015) for USA and Japan tide gauges, SHOM (http://www.shom.fr/) for French tide gauges and SONEL.
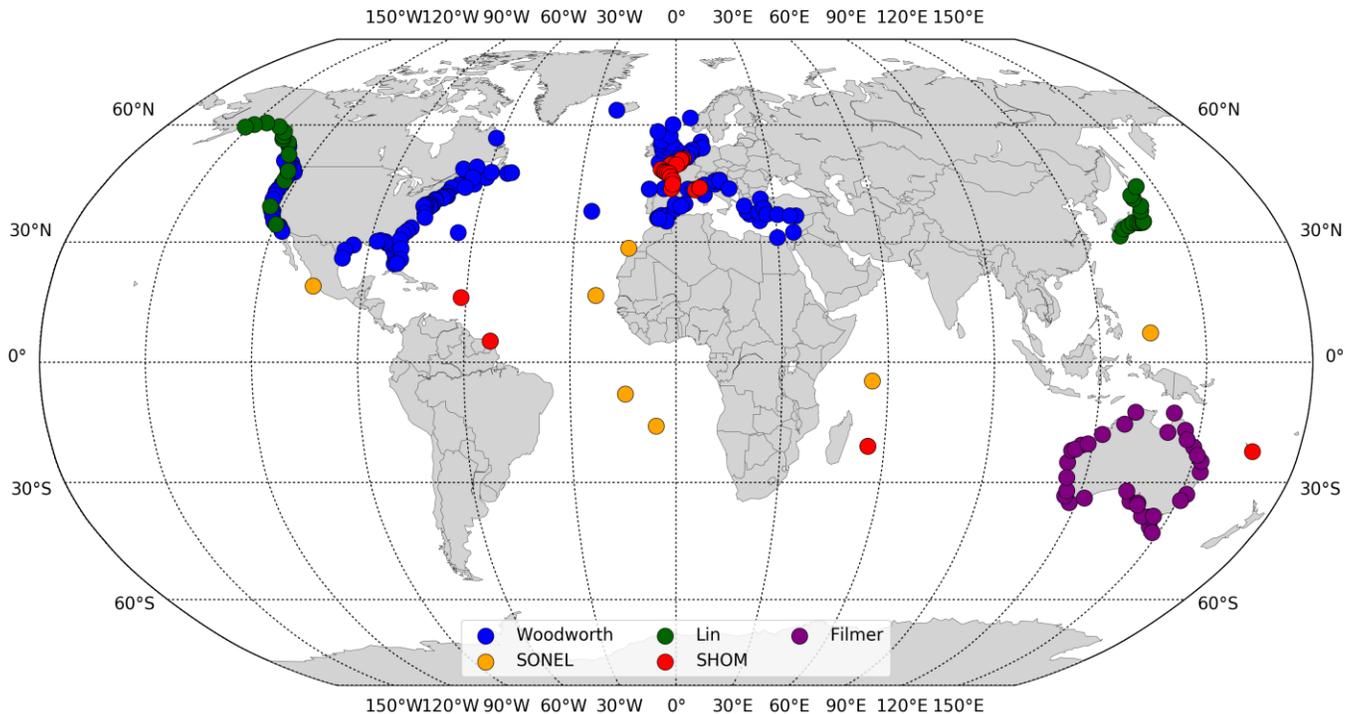
Figure 3: Tide gauges for which a geodetic tie with an episodic GNSS station is available

For most of the ellipsoidal heights coming from episodic GNSS measurements, the epoch and the uncertainty is often unknown. In that cases, there is no means to propagate the heights to the mean epochs of the selected periods (they are adopted as is), and a 3 cm uncertainty was associated by default (arbitrary based on our personal experience).

2.2 Computing the mean sea level

For the German stations that are not in the PSML databank yet, monthly time series were computed from high frequency tide gauge data following the PSMSL guidelines (http://www.psmsl.org/data/supplying/)

For the RLR stations, the monthly mean sea levels from PSMSL were used to compute the mean sea level over [2003-2007] and [2008-2012] periods. For records with more than 70% of data over each period, a classic average was computed. For tide gauge records with less than 70%, two reconstruction methods were investigated to fill gaps in the tide gauge time series.

2.2.1 Filling gaps in the RLR monthly time series

Over the 302 selected tide gauges considered in this study, 56 had less than 70% of valid data over at least one of the two [2003-2007] and [2008-2012] periods. Here we present the two methods that were investigated to fill the gaps in these records and hence to obtain more robust mean sea level values over these two periods.

2.2.1.1 Using neighbor tide gauges

This method aims at filling gaps using neighbor well correlated tide gauges that are closer than 500 km (Figure 4).
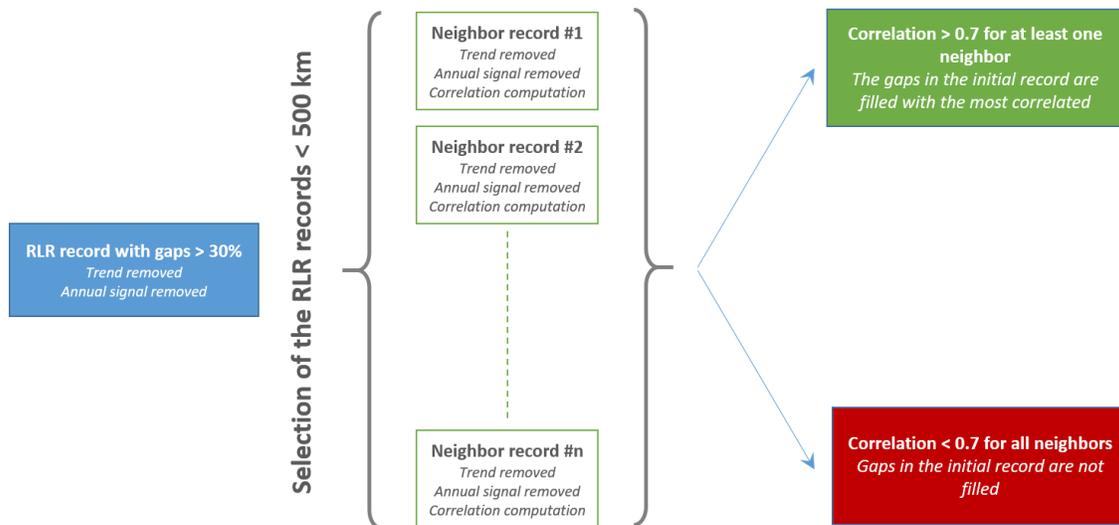
Figure 4: Schematic description of the reconstruction method using neighbor tide gauges

Among the 56 RLR records with large gaps (> 30%), only 33 could be reconstructed using this method; no neighbor record closer than 500km with a correlation coefficient larger than 0.7 could be found for the 23 remaining records.

2.2.1.2 Using altimetry data

A second method was investigated to fill gaps in the PSMSL records using observations from satellite altimetry. There are three stages to the method. First, a least squares fit of IB-corrected tide gauge data on an annual cycle, semiannual cycle, linear trend, and altimeter time series was computed for every altimeter point (using the AVISO gridded dynamic topography) within 150 km of the tide gauge. Second, the altimeter point for which the resulting fit explained the largest percentage variance of the tide gauge data was selected, and tide gauge data predicted from that least squares fit for every month. Third, that predicted tide gauge time series was used to fill gaps in the tide gauge data.

Of the 56 tide gauges considered, two did not have any overlap with altimeter data. For the remainder, correlations were commonly above 0.9 (there were 12 cases between 0.8 and 0.9, and three between 0.746 and 0.8). This represents the correlation of the full reconstructed time series, including trend and seasonal cycle, with the tide gauge data. Residuals had lower correlations, between 0.41 and 0.81

In filling gaps by interpolation, the end points to either side of the gap were made to match the tide gauge data exactly by adding a trend and bias term to the predicted time series within the gap. This means that the trend term in the least squares fit became irrelevant for such gaps. However, in the case of extrapolation, in which there is tide gauge data only before or after a "gap", this method could not be used. Instead, only a bias was introduced to match the single end point, and two options were considered: using the trend derived from the least squares fit, or using instead a least squares fit in which no trend had been estimated (thus importing the altimeter trend directly).

In some cases there could be large differences between these methods. For example, at Iskenderun II (Turkey), a large trend in relative sea level from the tide gauge (~4 cm/yr), attributed to vertical land movement, meant that the extrapolated time series depended strongly on whether this trend was included. It clearly should be included if the vertical land movement is linear over the period, but not otherwise. In other cases the quality of the trend estimate becomes an issue. For example, at Alicante I (Spain), the overlap between tide gauge and altimeter data consisted of only about 3 years near the start of the altimetry period. With such a short period, the fitted trend is unlikely to be statistically significant, but is sufficient to cause a difference of more than 10 cm between different extrapolations to the 2003-2007 reference period, and more for the later period.

As there is no objective way to decide which is the best reconstruction method, the difference between these two methods was considered to be an estimate of the size of the reconstruction error.

The clear benefit of the satellite altimetry method is that any tide gauge record that has data overlapping the altimetry period can be reconstructed.

2.2.1.3   Comparison between both methods

Erreur ! Source du renvoi introuvable. displays the mean sea levels computed over the periods of interest, using the satellite altimetry method against the tide gauge neighbor method. From the 33 tides gauges that were reconstructed using the neighbor tide gauge method, 39 mean sea levels over one or the two periods of interest were compared with the ones obtained using the satellite altimetry data method (21 mean sea level values over the period [2003-2007] and 18 over [2008-2012]). Both methods are consistent within 3 cm RMS, which is suitable for our application.
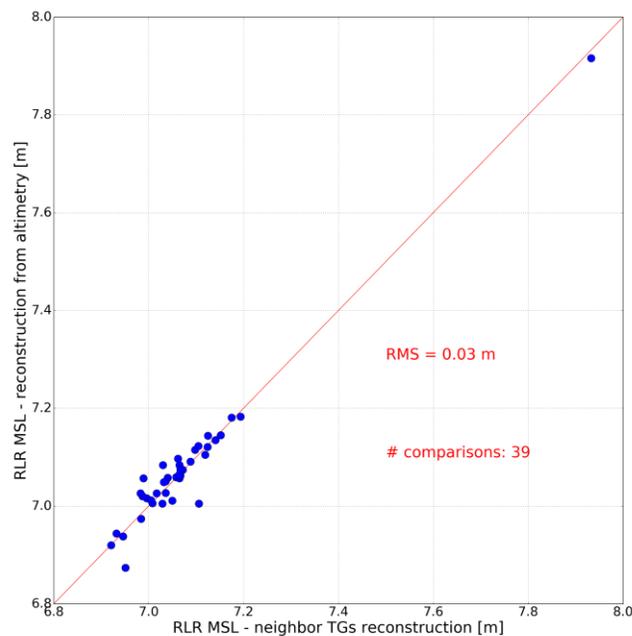
Figure 5: Comparison of both reconstruction methods

Since the reconstruction method using altimetry data could reconstruct 100% of the tide gauge records, it was decided to reconstruct the RLR time series using this method only.

Finally, a total of 302 ellipsoidal mean sea levels over [2003-2007] and [2008-2012] form the outcome data set of our study. Figure 6 shows their geographical distribution for the period [2003-2007]; the ellipsoidal mean sea level values for [2008-2012] do not show significant visible differences.
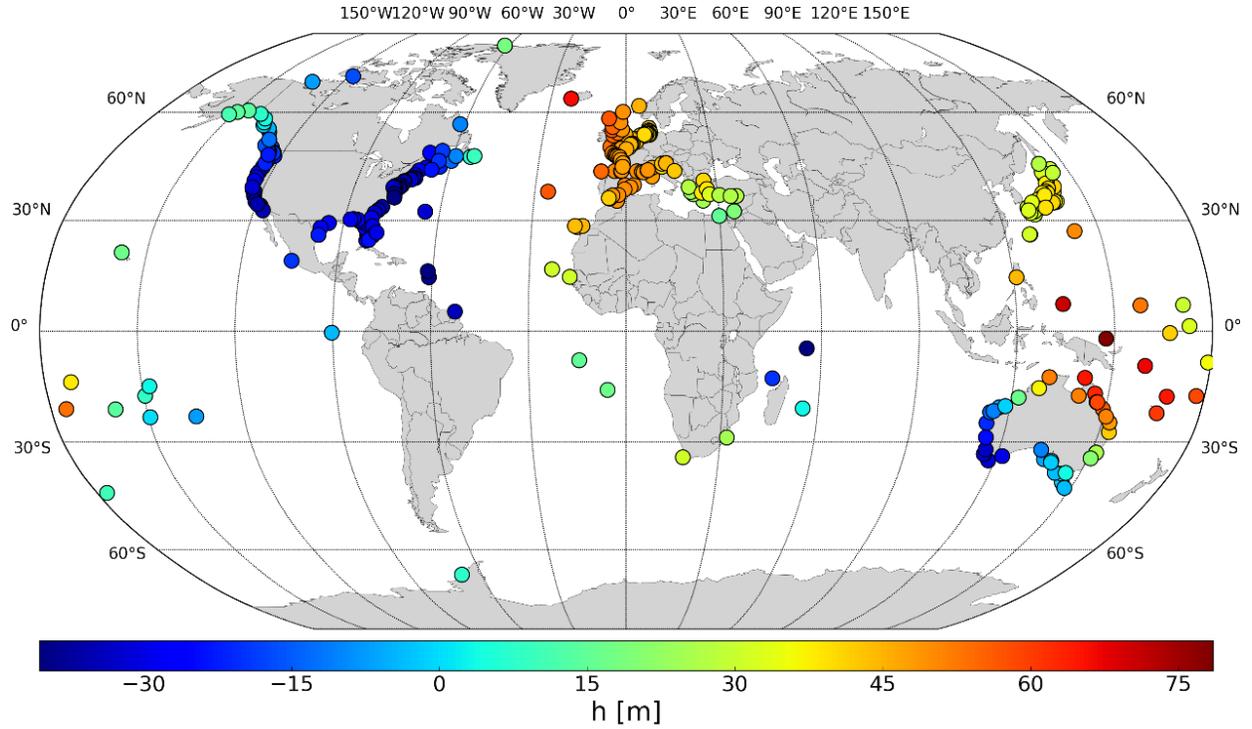
Figure 6: Mean sea level ellipsoidal heights at tide gauges over [2003-2007]

2.3 Computing the MDT values

If the geodetic tie comes from conventional leveling between the tide gauge and a distant GNSS station, the geoid slope between the tide gauge and the GNSS is not included in the tie, and is important to evaluate. In this case, the ellipsoidal mean sea level at the tide gauge is:

$$EMSL_{TG} = H_{GNSS} - tie_{leveling} - (GEOID_{GNSS} - GEOID_{TG}) \qquad (E2)$$

where H_{GNSS} is the ellipsoidal height of the GNSS station, $tie_{leveling}$ is the geodetic tie (height difference) between the GNSS station and the tide gauge coming from conventional leveling, and $GEOID_{GNSS}$ and $GEOID_{TG}$ are the geoid values at the GNSS and TG points, respectively. Hence, the MDT can be derived from equation (E1) as:

$$MDT_{TG} = EMSL_{TG} - GEOID_{TG} = H_{GNSS} - tie_{leveling} - GEOID_{GNSS} \qquad (E3)$$

If the geodetic tie comes from differential GNSS measurements, the geoid slope is not relevant, and (E1) reduces to:

$$EMSL_{TG} = H_{GNSS} - tie_{DGNSS} \qquad (E4)$$

where tie_{DGNSS} is the geodetic tie between the tide gauge and the GNSS station coming from differential GNSS measurements.

10

Hence, from equation (E4) we can derive:

$$MDT_{TG} = H_{GNSS} - tie_{DGNSS} - GEOID_{TG} \qquad \text{(E5)}$$

Consequently, to compute the MDT values, the type of geodetic tie (either conventional leveling or differential GNSS) needs to be identified to determine what geoid values need to be extracted (either at the GNSS point or at the TG point). Since it can be assumed that for the ties coming from episodic GNSS measurements the GNSS point is at the tide gauge site (and so the geoid slope between the GNSS and the tide gauge is negligible), only the ties coming from a permanent GNSS station were considered. Figure 7 shows the results in terms of MDT for the period [2008-2012]. No visible change is observed on the MDT over the period [2003-2007].
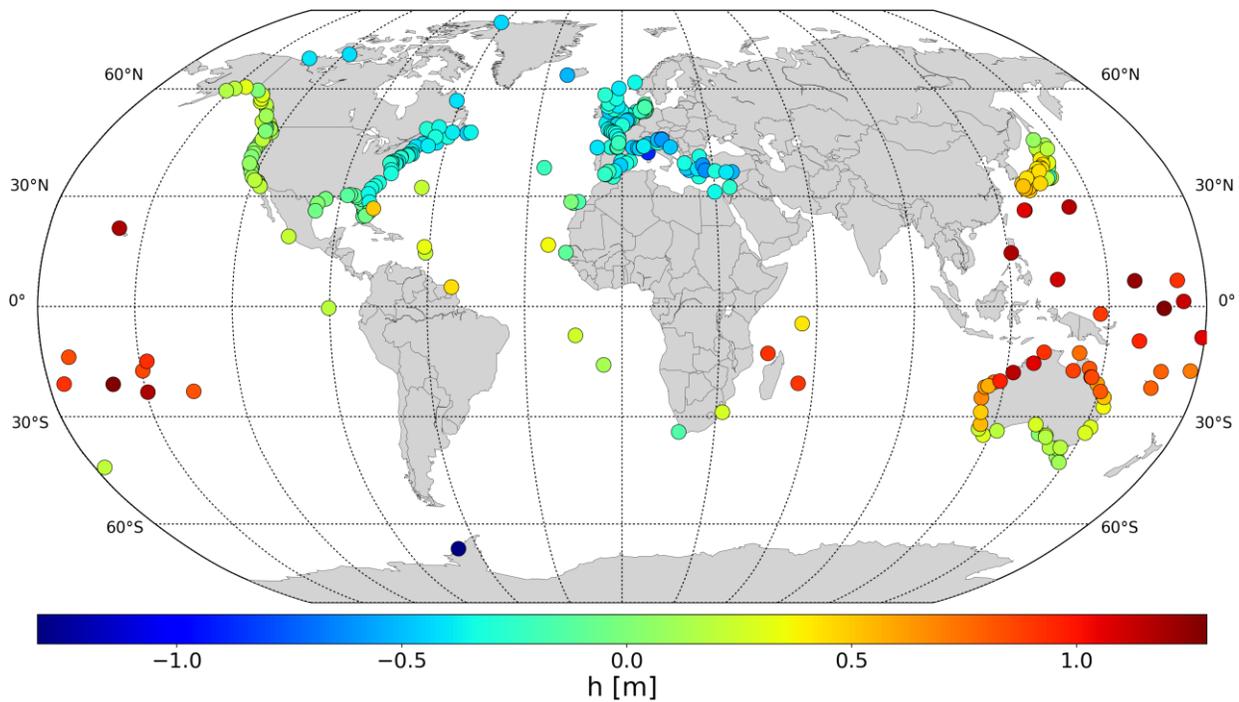
Figure 7: MDT values at tide aguges over [2008-2012] using EGM2008 geoid model

2.4   Comparison of MDTs at tide gauge locations in the German Bight

For fifteen tide gauge stations in the German Bight, the ellipsoidal heights of the tide gauge reference level (tide gauge zero (TG0)) has been obtained from the ellipsoidal height of a nearby GPS station and the computation of the height difference between the reference points of GPS and tide gauge (Weiss and Sudau [2011] and Weiss [2013]) , see Technical Report for WP1300. The horizontal distance between the GPS and the tide gauge locations is smaller than 1 Km, except for Wilhelmshaven station (Table 1).

To compare the mean dynamic topography measured from tide gauge records to the analogous measured from satellite altimetry, the following considerations are needed.

Since the oceanographers correct for tides the sea level observations from satellite altimetry, the altimetric ellipsoidal sea level heights above the reference ellipsoid are given in the mean tide system. Meanwhile, gauge data connected with GPS are given in the tide-free system because of the GPS processing required for the determination of tide gauge ellipsoidal heights. The reference ellipsoid for the different altimetric missions is the Topex ellipsoid for the CNES/NASA missions and the WGS84 ellipsoid for the ESA missions.

The conversion of heights in mean tide system to heights in tide-free system (from h_m to h_f) is performed using:

$$h_m - h_f = h_2 \cdot (0.099 - 0.296 \cdot sin^2\varphi)\ [in\ m] = h_2 \cdot D \cdot (1/3 - sin^2\varphi) \tag{E6}$$

where h_2 is the Love number describing the vertical displacement of the crust relative to the ellipsoid (h$_2$=0.62). The factor h_2 D is equal to 0.18352 in Ekman [1989] and Fenoglio [1996] and is 0.1809238 for GOCE+HSU. The small difference (0.0025962) corresponds to a maximum difference of 0,87 mm for latitude = 0. Note that neglecting the 0.01 factor in McCarthy and PetThit section 7.1.1, the parameter D is 0.296.

2.4.1   Mean dynamic topography from tide gauge records

At each tide gauge station, the ellipsoidal height of the TG0 has been referenced to the epoch 2010.5. It has been then propagated to 2005.5 epoch using the vertical velocity, as for the ULR6 ellipsoidal heights (section 2.1.1.2). The ellipsoidal height are above the WGS84 ellipsoid and in the tide free system. Both height and its uncertainty input to the costalMDT Toolbox.

At each tide gauge station, the mean sea surface over the interval 2003-2007 has been computed by adding the mean over 2003-2007 of the tide gauge records to the ellipsoidal height of the TG0. Then, the height is transformed from the tide free to the mean tide system and from above the WGS84 ellipsoid to the Topex ellipsoid. The final MSS is then given by the following equation:

$$MSS_{TG} = TG0_{ell(2005.5)} + MSL_{[2003,2007]} + corr_{TF2MT} + corr_{WGS2TOP} \tag{E7}$$

where $TG0_{ell(2005.5)}$ is the ellipsoidal height of the tide gauge reference at the epoch 2005.5, $MSL_{[2003,2007]}$ is the mean over the [2003,2007] period, $corr_{TF2MT}$ is the transformation of heights from tide free to mean tide systems and $corr_{WGS2TOP}$ is the transformation from the WGS80 to the Topex reference ellipsoid. The MDT is then evaluated by subtracting the geoid surface. Here we consider the geoid Eigen6c4.

2.4.2   Mean dynamic topography from satellite altimetry

The altimeter-derived MSS surface DTU2015, which is given for a long time interval, is selected. The average difference between the MSS measured in the interval 2003-2007 and the long-term MSS solution is added. The

long-term change of the MSS in 2003-2007 due to atmospheric pressure (inverse barometer (ib) effect) is also added to be consistent with the MDT from tide gauge stations, which have not been corrected for the atmospheric pressure effect (see equation E8). MSS and geoids have been both reduced to grids of 1/8 x 1/8 degrees before subtraction to evaluate the MDT.

$$MSS_{alti} = MSS_{DTU15} + diff_{DTU15\_[2003,2007]} + IB_{[2003,2007]} \qquad \text{(E8)}$$

where MSS_{DTU15} is the mean sea surface value from DTU15 product, $diff_{DTU15\_[2003,2007]}$ is the difference between the mean sea level measured over [2003,2007] and MSS_{DTU15}, and $IB_{[2003,2007]}$ is the iverse barometer correction over [2003,2007].

The MDT is than obtained by substracting the Eigen6c4 geoid (Figure 8).

The root-mean-square deviation (RMSD), or root-mean-square error (RMSE), is a measure of the differences between the MDTs computed from tide gauges and from satellite altimetry respectively. Over 13 of the 15 stations, the standard deviation of the difference is 9 cm, the bias is 2 cm.
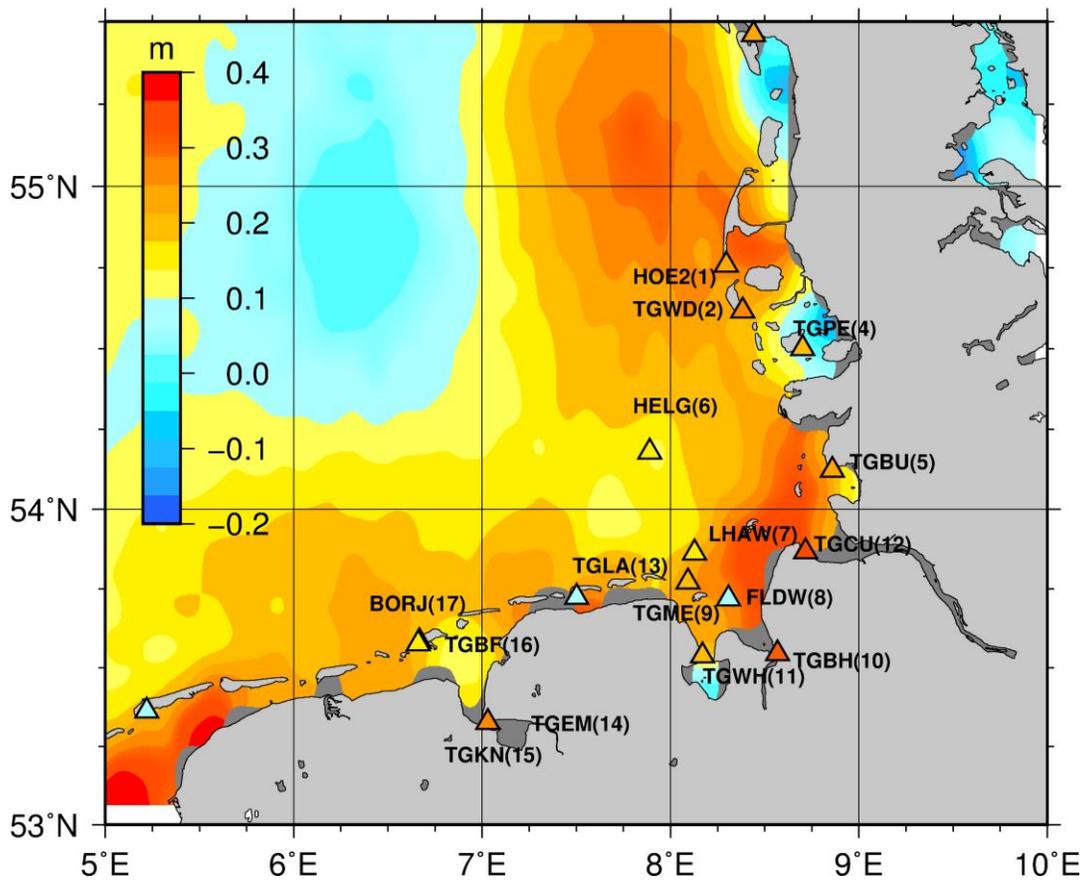
Figure 8: Geodetic MDT at tide gauge and on sea

13

3   Trends analysis

Since the tide gauges are grounded on the coast, the vertical land movements (VLM) of the coast can be recorded as well by tide gauges. In order to express the rates of sea level change from tide gauges in a geocentric reference frame (as satellite altimetry, Figure 1), it is necessary to estimate these vertical land movements.

There is currently only one geophysical process that causes vertical land movements for which accurate global geophysical models exist: the Glacial Isostatic Adjustment (GIA). Thus, it is preferable to use observations from space geodesy to account for every type of VLM that can impact the tide gauge site.

3.1   Selection of RLR tide gauge records

This trend analysis was performed over three different periods: a long-term period ([1960-2015]) and the two short periods of the MDT analysis ([2003-2007] and [2008-2012]).

Over each of these periods, the records with more than 70% of data were selected yielding a number of 352, 748 and 777 RLR records for the respective periods [1960-2015], [2003-2007] and [2008-2012].

3.2   VLM datasets

In order to be able to correct VLM for a maximum number of tide gauges, different VLM datasets were used. We present them here by order of "priority".

3.2.1   ULR6a GPS solution

The ULR6a GPS solution from the University of La Rochelle, is the result of a reprocessing of a global network of permanent GPS stations. It provides 349 "robust" vertical velocities at tide gauge sites, expressed in the ITRF08 reference frame.

The uncertainties of the velocities are on average of 0.3 mm/yr, which is suitable for long-term sea level studies.

The ULR6 GPS solution is available on the SONEL portal: http://www.sonel.org/-Vertical-land-movement-estimate-.html?lang=en.
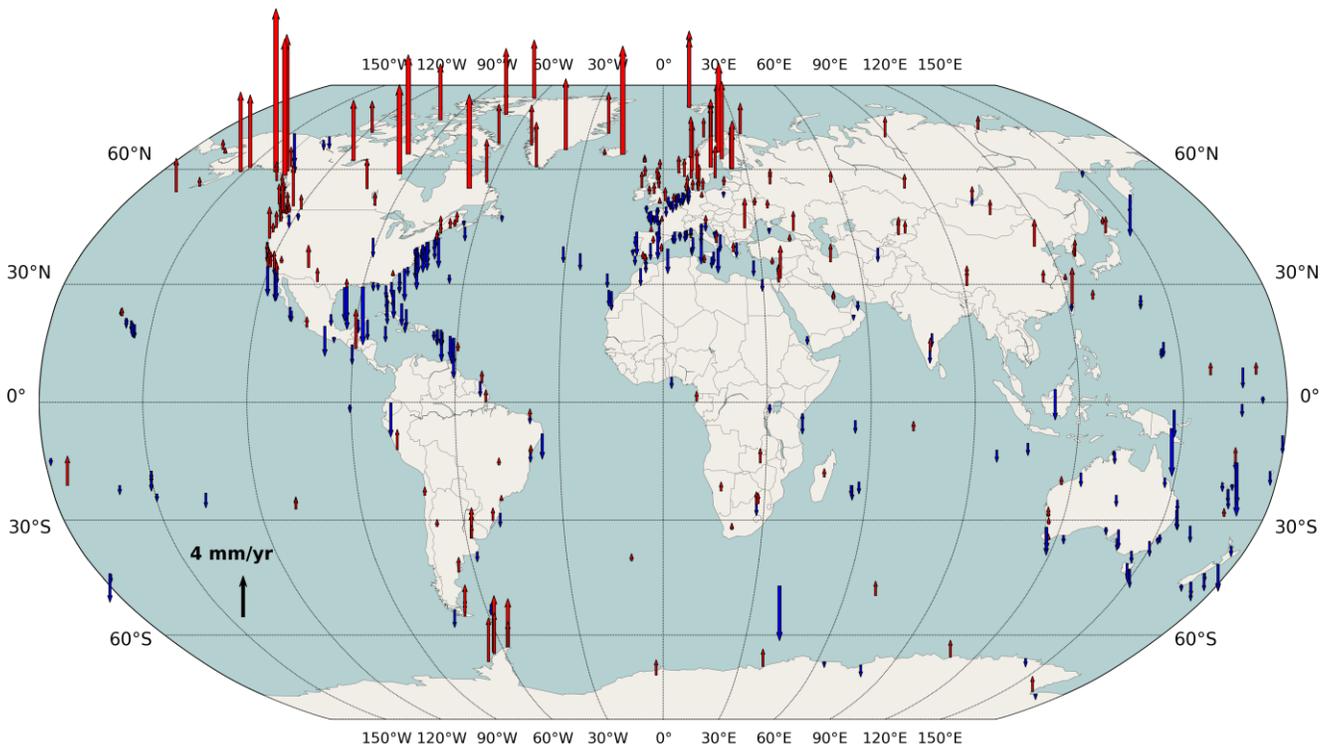
Figure 9: ULR6a GPS vertical velocity field

3.2.2 Using altimetry minus tide gauges: the ALTG solution

Combining tide gauge and satellite altimetry data can be useful to estimate vertical land motion at the tide gauge, which is of particular interest since many tide gauges are not co-located with GNSS stations yet. Even though the tide gauges were equipped with continuous GNSS stations, the GNSS results can be subject to many systematic errors that an independent approach can reveal.

The approach consists in subtracting the sea level time series from a tide gauge with an equivalent time series from satellite altimetry. To the extent that both instruments measure identical ocean signals, their difference is a proxy for the vertical position of the tide gauge (Figure 1). Assuming that the instrumental drifts are negligible, the time series of the sea level differences will then be dominated by vertical land motion at the tide gauge.

The results, published in Wöppelmann and Marcos [2016], consist in VLM estimates at 478 PSMSL RLR sites using AVISO altimetry product (Figure 10). These estimates are available through a demonstration product on the SONEL website (http://www.sonel.org/-Vertical-land-movement-estimate-.html?lang=en).
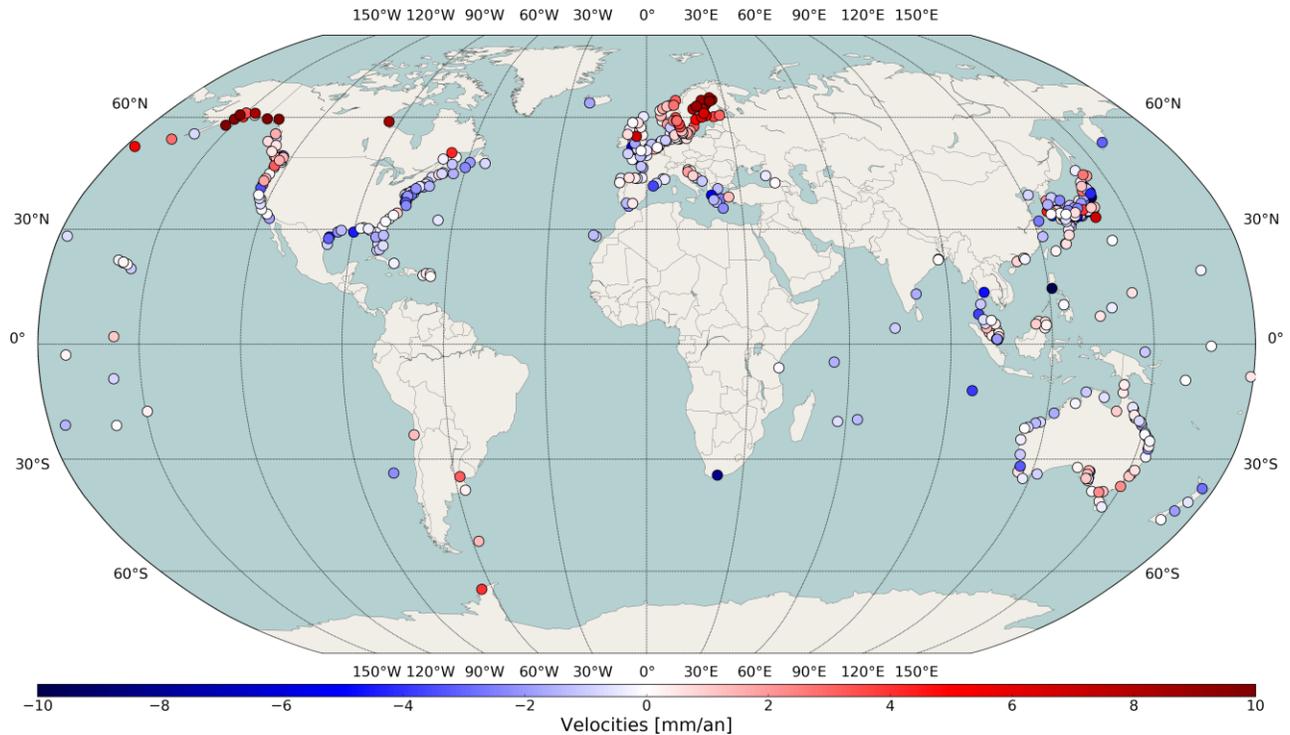
The comparison with the ULR6a vertical GPS velocities at the 190 common sites gives a 1.35 mm/yr RMS value.

3.2.3   Using relative VLM between pairs of tide gauges: the ASG14 solution

This dataset has been published in [Santamaria-Gomez et.al, 2014]. It estimates vertical land motions at 86 sites by double-differencing long tide gauge records and satellite altimetry data.

The comparison with the 26 common ULR6a sites exhibits an RMS of 0.89 mm/yr.

3.2.4   The GPS velocity field from NGL (MIDAS estimator)

Blewitt et al., [2016] propose an original approach to estimate vertical velocities from GPS time series. According to the authors, this approach is robust with respect to the offsets in the position time series that usually affect the linear trend estimate, if not detected and taken into account.

The MIDAS velocities are in agreement with the ULR6a velocities at the level of 1.9 mm/year (RMS of differences using 487 common GNSS stations).

The scatterplots in Figure 11 summarize the comparison of the VLM datasets presented above.
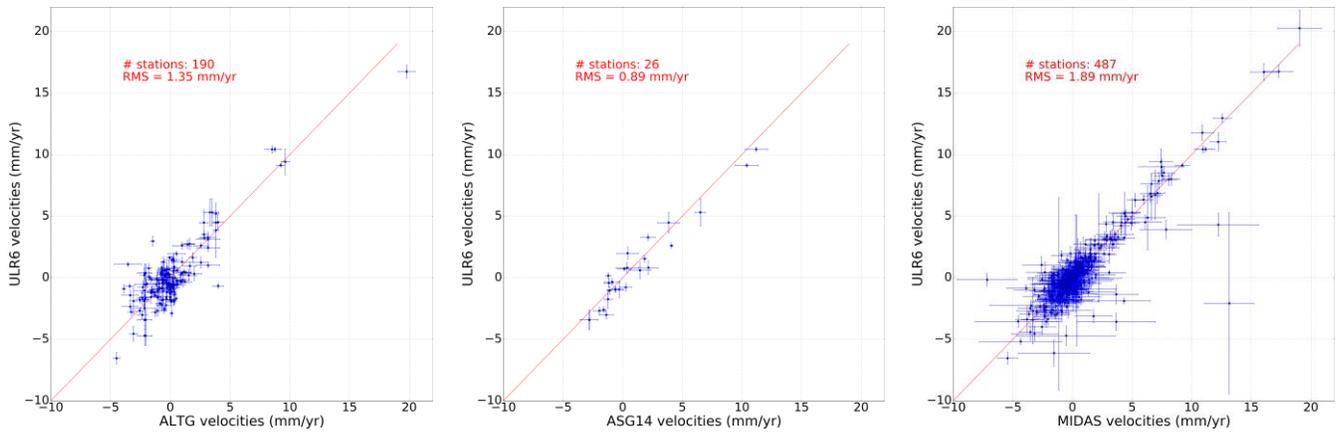
Figure 11: Comparison of the vertical velocities estimated by [Wöppelamn & Marcos, 2016], [Santamaria-Gomez et. al, 2014] and [Blewitt et. al, 2016] with the ULR6a velocities

3.3 Geocentric sea level trends

The four VLM datasets enabled to correct the 87%, 79% and 74% of the selected RLR tide gauge records over the periods [1960-2015], [2003-2007] and [2008-2012], respectively.

According to [Spada & Galassi, 2012], the published estimates of the global mean sea level rise from tide gauges range between 1.0 mm/yr and 2.0 mm/yr over the XXth century. Wöppelmann et.al, [2009] have shown that a substantial part of the spread of the individual TG trends comes from local vertical land motions. This study confirms that the spread of the sea level trends reduces from 3.05 mm/yr (relative) to 1.83 mm/yr (absolute) which can be interpreted as a positive outcome (reducing the spatial noise due to non-climatic signals).
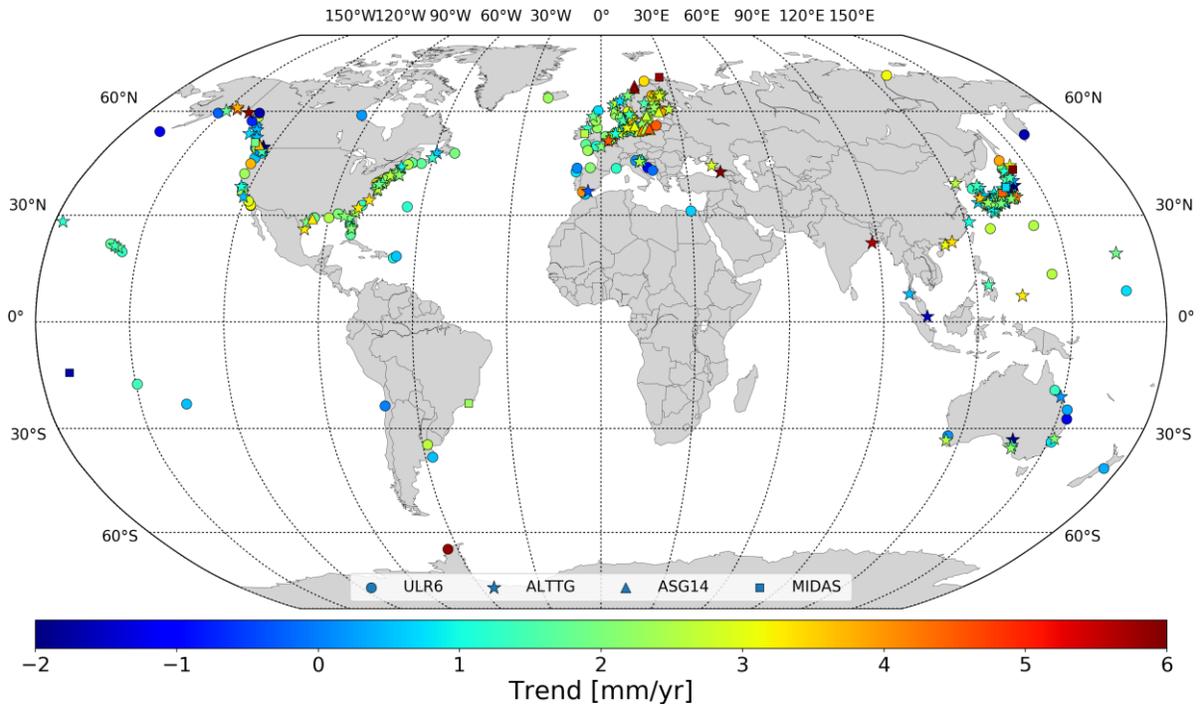
Figure 12: Absolute (geocentric) sea level trends at tide gauges over [1960-2015]

The range of the sea-level trends over the short periods [2003-2007] and [2008-2012] is much larger due to multiannual oceanographic oscillations and processes. In these cases, the VLM have a negligible impact in the global estimate of sea-level change from tide gauges, and no significant reduction of the dispersion of the trends is observed.
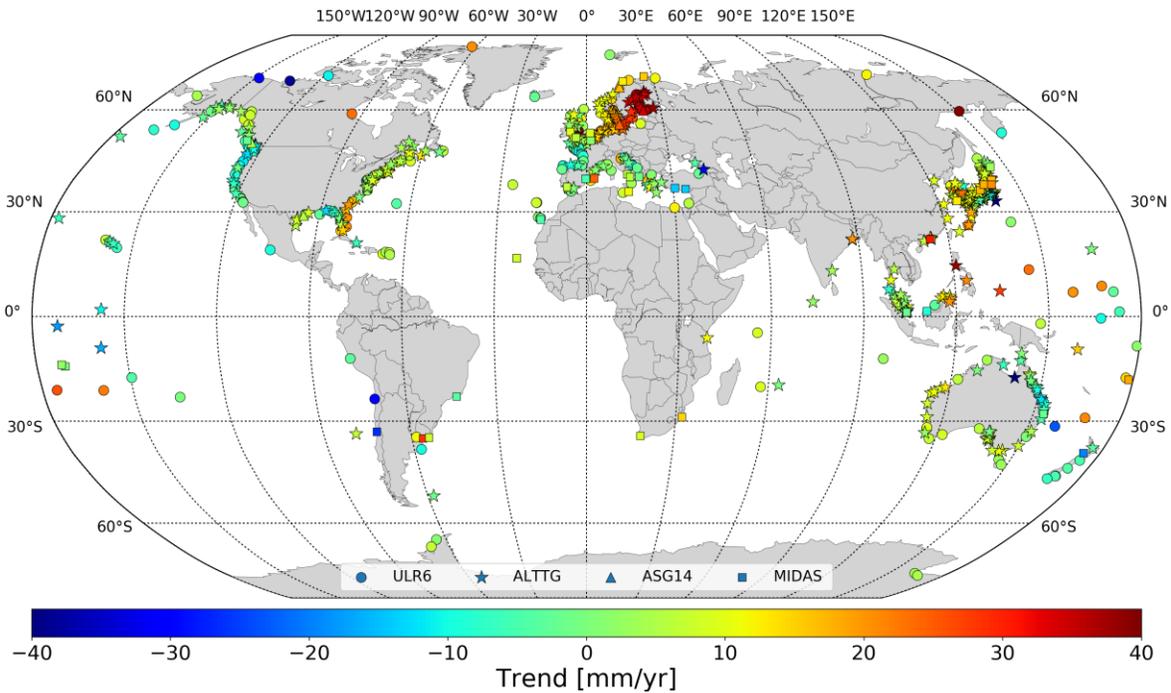
Figure 13: Absolute (geocentric) sea level trends at tide gauges over [2003-2007]

18
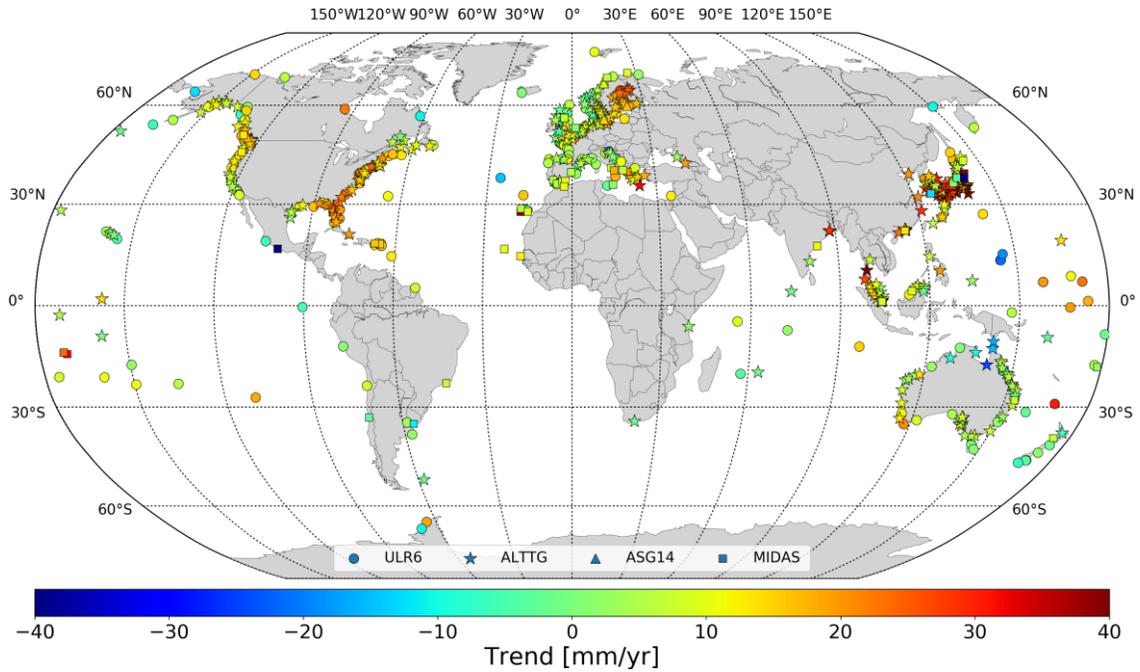
Figure 14: Absolute (geocentric) sea level trends at tide gauges over [2008-2012]

3.4 Vertical Land Motion from altimetry and tide gauge in the German Bight

3.4.1   Methodology

We use the fifteen tide gauge stations listed in Table 1. Three of the 15 stations are included in the PSMSL databank and in SONEL. Additionally, we include a second gauge station in Helgoland (HELGS) and three PSMSL tide gauge stations (TGBF, TGCU, TGWD); only the PSMSL data from 1993 were considered.
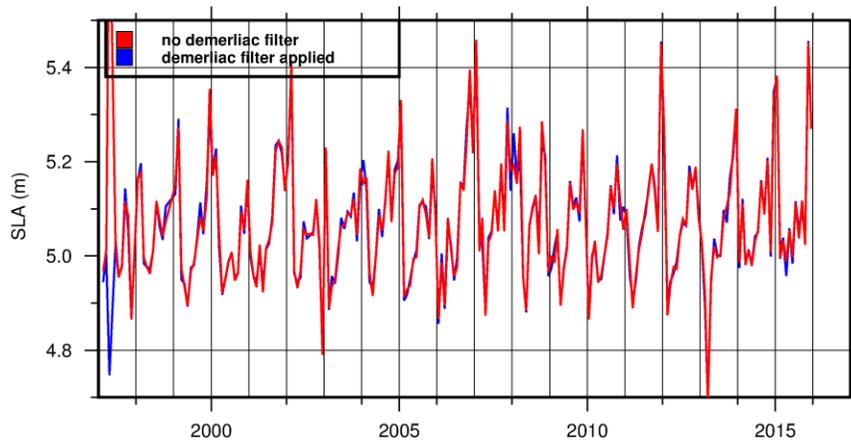
Figure 15: Monthly time-series corrected for DAC with Demerliac filter applied (blue) and without (red)

For the tide gauges that are not included in the PSMSL portal, the processing of monthly values from high-frequency measurements (1-minute) was required. For this aim, the PSMSL guidelines were followed (http://www.psmsl.org/data/supplying/). The tide has been filtered in the hourly values to obtain daily values using the Demerliac filter (see the impact of the filtering on Figure 15).

Nstat	TG Acronym	Code	Lat	Lon	Dist Alt-tg (km)	Dist TG-GPS (km)	TG Name
1	TGBF	1037	53.5574520 53.5574270	6.74790200 6.74791910	11.050	0.00182	Borkum Fischerbalje
2	TGCU	7	53.867699 53.8677299	8.717343 8.71746730	10.367	0.00563	Cuxhaven Steubenhöft
3	HOE2	3001	54.758108 54.75875310	8.295935 8.2933901	13.947	0.18487	Hörnum
4	TGPE	3003	54.500936 NaN	8.701924 NaN	14.657	0.00532	Pellworm
5	TGBU	3004	54.121776 54.1217361	8.859017 8.85917200	1.102	0.00532	Büsum
6	HELGB	3006	54.176151 54.1744824	7.901487 7.89309370	6.071	0.53265	Helgoland Binnenhaven
7	LHAW	3007	53.86322333 53.86322380	8.12766222 8.12766310	1.321	0.00785	LighthouseAlte Weser
8	FLDW	3008	53.71862700 53.71862750	8.30762600 8.30762680	11.319	0.00123	Frontlight Dwarsgat
9	TGME	3009	53.77170987 53.77171040	8.09263657 8.09263750	11.680	0.00855	Mellumplate
10	TGBH	3010	53.54497496 53.54497530	8.56818330 8.56818380	15.540	0.00222	Bremenhaven
11	TGWH	3011	53.53830685 53.53830720	8.17017144 8.17017210	10.090	3.12268	Wilhelmshaven
12	TGLA	3012	53.723239 NaN	7.501568 NaN	18.715		Langeoog
13	TGKN	3013	53.32717156 53.3271721	7.03068299 7.03068380	33.696	0.00068	Knock
14	BORJ	3014	53.5768710 53.5789087	6.66142300 6.66643190		0.40234	Borkum Südstrand
15	TGWD	3016	54.631776 54.6317708	8.3838460 8.3839406		0.00116	Wittdün
16	HELGS	3005	54.176151 54.1744824	7.901487 7.89309370	6.071	0.09623	Helgoland Südstrand
1	TGBF	1037	53.5574520 53.5574270	6.74790200 6.74791910	11.050	0.00182	Borkum Fischerbalje
2	TGCU	7	53.867699 53.8677299	8.717343 8.71746730	10.367	0.00563	Cuxhaven Steubenhöft
15	TGWD	1036	54.631776 54.6317708	8.3838460 8.3839406		0.00116	Wittdün

Table 1: In-situ stations (15) of the German network used for the in-situ validation. The columns corresponds to: (1) station acronym, (2) longitude of TG (above) and GPS station (below), (3) latitude of TG (above) and GPS station (below), (4) distance between altimetry and tide gauge, (5) distance between tide gauge and GPS station, (6) station name. For the three stations TGBF, TGCU and TGWD the PSMSL data are considered for the second interval (last three lines). HELGS could not be considered as 16th station because the tide gauge records are not yet available

The altimetry data are from the Essential Climate Variable (ECV) of the Sea Level CCI initiative. Monthly sea level anomalies over 1993-2015 are available in a 0.125 degree grid and include all corrections, in particular ocean, earth, tidal loading and atmospheric dynamic (DAC) correction.

For each tide gauge, we consider the nearest ECV grid node and analyze the altimetric and tide gauge monthly time-series. The seasonal component is evaluated as the mean variability for each month in the interval of analysis and is then removed to obtain de-seasoned monthly values. The de-seasoned time-series are subtracted over the common interval and their trend and associated standard error are estimated by a linear regression. We then assess the trend significance by applying the t-test to the ratio between the estimated trend and its standard error. The consistency between the GPS rate and the difference of the trends between co-located altimeter and TG sea level (altimetry minus TG = GPS) is a measure of accuracy of the derived VLM (Fenoglio et al., [2004], [2012a], [2012b]; Trisirisatayawong et al. [2011], Braun et al., [2008]). The error reported for the GPS method is generally lower than 0.5 mm/yr, the accuracy of the altimeter/tide gauge method is often larger than 1 mm/yr.

The following skill metrics is adopted to validate the ECV against in-situ data at the nearest point:

- standard deviation of differences between in-situ and altimetric SSH
- correlation between in-situ and altimetric SSH
- difference of the VLM rates derived from GPS and from difference of altimetric and tide gauge time-series (altimetry minus tide gauge)

Cooperation with SONEL within this project (G. Wöppelmann, M. Gravelle) helped both SONEL and PSMSL to improve the location information. The coordinates of the stations made available as Gauss-Krüger coordinates by BfG, have been transformed in longitude and latitude of the WGS84 ellipsoid (Table 1). The distance between tide gauge and GPS is mainly smaller than one meter, with maximum in Wilhemshaven (3 Km) and Helgoland Binnenstrand (0.5 km).

As the gridded ECV are corrected for atmospheric effect, we subtract the monthly DAC correction from the monthly tide gauge time-series, as in equation (E16).

$$h_{tgDacmonthly} = h_{tgmonthly} - \Delta h_{dacmontly} \qquad (E16)$$

To evaluate the effect of a selected correction, we consider three corrections: ERA IB, DAC AVISO and DAC CCI. Differences between DAC AVISO and IB are smaller than 3 cm (Figure 16), while difference between the two DACs is also very small (not shown).
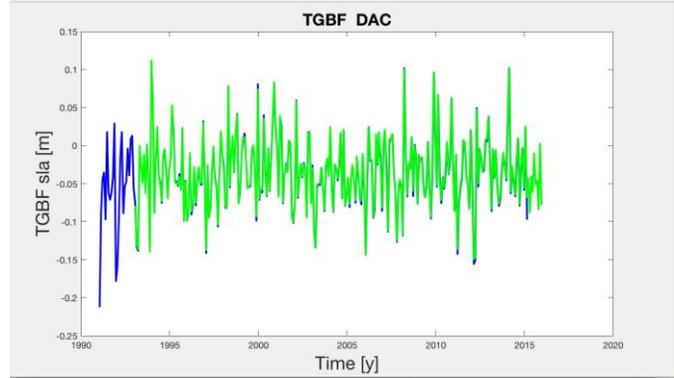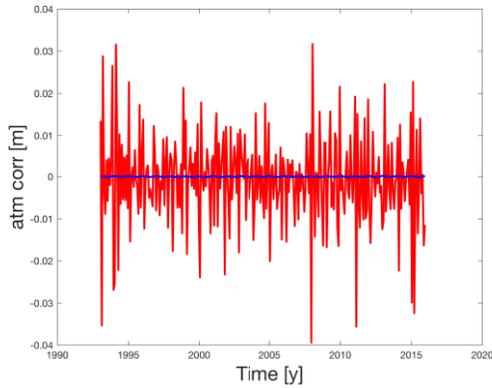
Figure 16: TGBF: Difference (m) between DAC and IB (red) (left), DAC from AVISO (blue) and DAC (right)

3.4.2 Results

The Vertical Land Motion (VLM) rates derived from GPS are negative along the coast and positive at Helgoland and LHAW (Figure 17 left). The error is smaller than 0.5 mm/yr at all stations except in FINO3 (TGF3) (Figure 17 right).

The trends of altimeter and tide gauge time-series are computed over the longest common period (Table 2, columns 9, 10, 11). The difference of the trends for each pair is compared to the GPS vertical rate. We observe more similarity in the VLM from the two methods for time intervals longer than 25 years. Figure 18 shows the values for the longest interval.
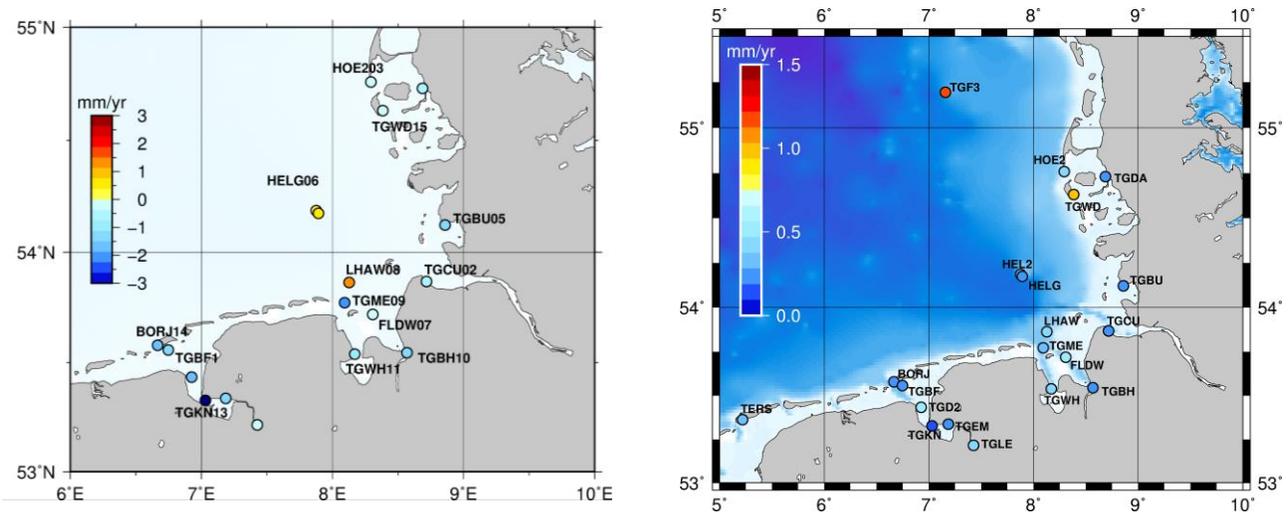
Figure 17: VLM from GPS (left) and its error (right). (Reichel et al., 2017).

The error of the estimated trends of sea level is larger than 1 mm/yr in all cases. As an example, for the station TGBF trends are 0.84 +/- 1.6, 2.73 +/- 1.6 for altimetry and tide gauge respectively. The error of the difference of the trends is lower than 1 mm/yr for long time series, but larger than the GPS rate.

22

Table 2 (last column) gives the difference between the VLM estimated from the two methods, the values smaller than 1 mm/yr are marked in bold. The absolute values of the differences are represented in Figure 18 (top-left), the scatteplot of the values in Figure 18 (bottom). At the five stations TGBF, HELG, TGWD, TGCU, FLDW, where the length of the time-series is longer than 25 years, the agreement between tide gauges and altimetry is higher. As an example, in TGBF over the interval 1993-2010, the de-seasoned time-series have correlation 0.8, standard deviation of differences 70 mm and trend of the differences -0.19 +/- 0.9 mm/yr. The elimination of outliers and any effect of extreme events in the tide gauge measurements could also have an impact on the residuals. Indeed, for the intrinsic characteristics of satellite altimetry, the probability of altimetry to see an extreme event lasting a few hours or days in a particular location, is small. Therefore, also the tide gauge time-series need to exclude these effects, as the DAC correction cannot fully correct the atmospheric effect that contaminate the tide gauge monthly time-series. The selection of the point of comparison plays also a significant role. As in Figure 18 (top-left) for a "nearest point" in coastal zone, the signal could be contaminated by land. Restriction for the altimeter data location needs to be investigated, as for example with a distance to coast parameter. Other selections based on maximum correlation, more similar trend and minimal distance to coast could be considered. Impacts of chosen altimeter corrections and specialized waveform re-trackers need to be further investigated (Fenoglio-Marc et al., 2015).
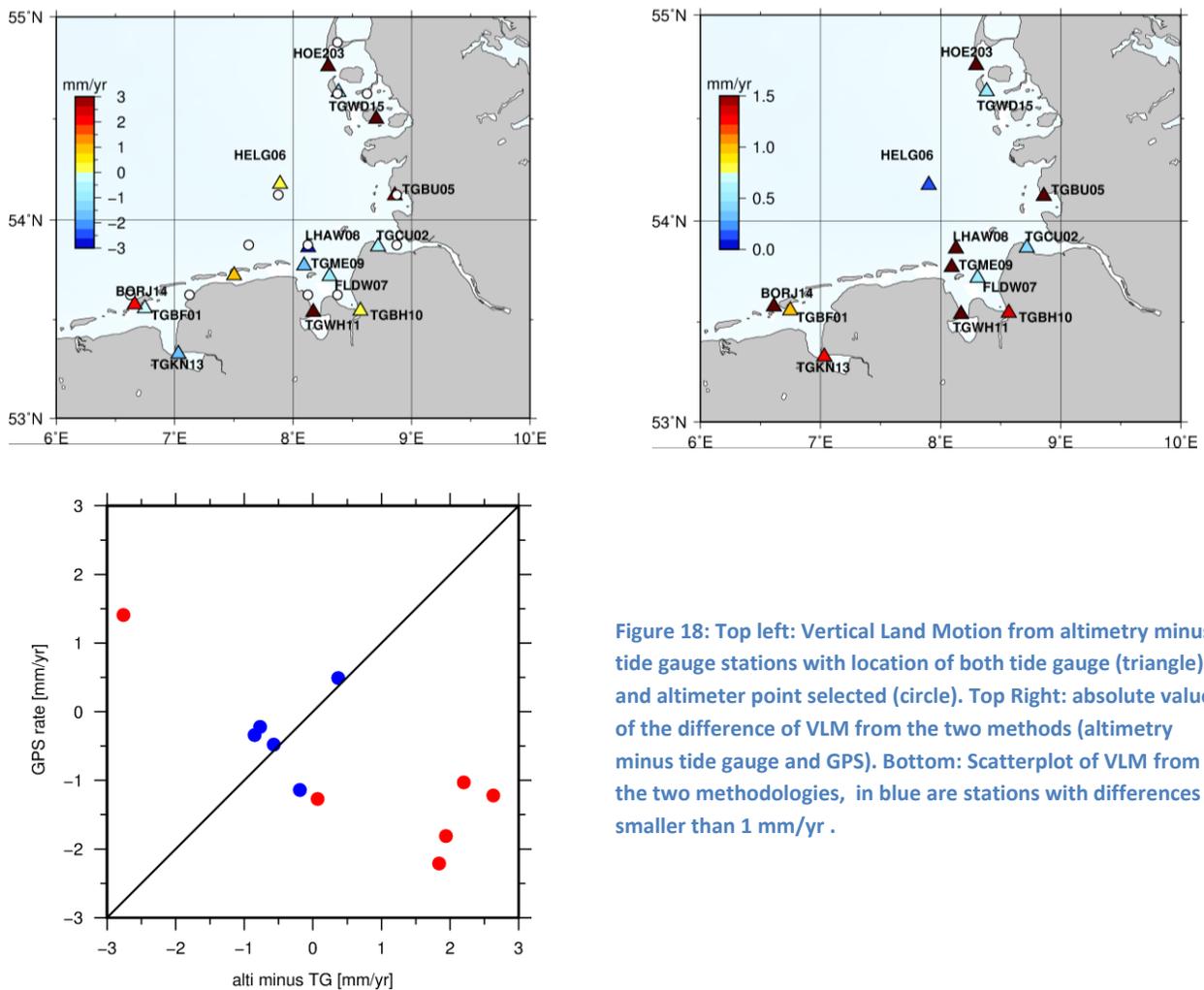
Figure 18: Top left: Vertical Land Motion from altimetry minus tide gauge stations with location of both tide gauge (triangle) and altimeter point selected (circle). Top Right: absolute value of the difference of VLM from the two methods (altimetry minus tide gauge and GPS). Bottom: Scatterplot of VLM from the two methodologies, in blue are stations with differences smaller than 1 mm/yr .

TG N.	TG Acronym	Corr ia/ mv	STDD (mm) ia/ mv	Trends al (mm/yr) ia / mv	Trend TG (mm/yr) ia / mv	Trend al-tg Ia/mv	GPS rate	Interval of al-tg	Diff Al-tg-GPS
1	TGBF	0.715 0.792	78 25	0.84 +/- 1.6 0.21	2.73 +/- 1.6 1.3	-1.9 +/- 0.8 -1.1	-1.14+/-0.22	1997-2016	-0.8
2	TGCU	0.560 0.864	104 24	2.27 2.3	0.10 -0.44	2.17 2.74	-0.48 +/-0.25	1998-2016	2.57
3	HOE2	0.803 0.792	71 30	4.31 4.85	0.89 0.84	3.42 4.01	-0.36+/-0.38	2000-2016	3.06
4	TGPE	Not used						1998-2001.4	
5	TGBU	0.563 0.845	113 2	3.35 3.44	0.72 0.59	2.63 2.85	-1.22+/ 0.22	2000-2016	3.85
6	HELGB	0.67 0.70	112 44	3.82 3.40	3.44 0.90	0.37 2.50	0.49 +/- 0.26	2000-2016	-0.12
7	LHAW	0.665 0.80	109 36	3.40 3.45	6.16 5.53	-2.76 -2.08	1.41+/-0.22	1995-2016	4.17
8	FLDW	0.64 0.823	96 31	3.06 3.23	3.91 4.08	-0.85 -0.84	-0.34+/-0.5	1995-2016	-0.51
9	TGME	0.67 0.84	106 28	3.44 3.17	1.60 1.58	1.84 1.59	-2.21+/-0.4	2000-2016	4.05
10	TGBH	0.61 0.78	109 38	3.28 2.91	3.21 2.99	0.07 -0.08	-1.27+/-0.3	1994-2016	1.34
11	TGWH	0.63 0.734	94 31	2.72 2.46	0.52 -0.47	2.2 2.94	-1.03 +/-0.4	2000-2016	3.03
12	TGLA	0.691 0.829	100 27	2.71 2.26	1.67 1.82	1.05 0.44		2000-2016	NaN
13	TGKN	0.773 0.852	71 24	1.8 1.4	3.7 3.05	-1.9 -1.7	-3.12+/-0.2	2000-2016	1.22
14	BORJ	0.727 0.776	77 27	0.95 0.21	-0.98 -1.11	1.94 1.32	-1.81+/-0.22	2000-2016	3.75
15	TGWD	0.801 0.649	70 42	3.4 3.8	-3.2 -4.0	6.64 7.83	-0.22+/- 1.0	2000-2016	6.86
16	HELGS	Not used							NaN
1	TGBF	0.793 0.884	70 23	4.82 +/- 1.7 5.29	5.01 +/- 2.0 5.68	-0.19+/- 0.9 -0.39	-1.14+/-0.2	1993-2010	0.95
2	TGCU	0.603 0.910	112 30	2.71 3.58	3.58 3.78	-0.87 - 0.20	-0.48+/-0.3	1993-2011	-0.39
15	TGWD	0.851 0.889	70 30	2.43 3.17	3.20 4.52	-0.77 -1.35	-0.22+/- 1.0	1993-2011	-0.55

Table 2: In-situ stations (15) of the German network used for the in-situ validation. The columns corresponds to: (1) TG number, (2) station acronym, (3) correlation of interannual (ia) and interannual filtered (mv) time-series, (4) standard deviation of differences (STDD) between altimetric and tide gauge ia and mv, (5) trends of Altimetric de-seasoned and de-seasoned and filtered time-series, (6) the same for TGs, (7) difference of trends, (8) GPS rates, (9) time interval for al-tg
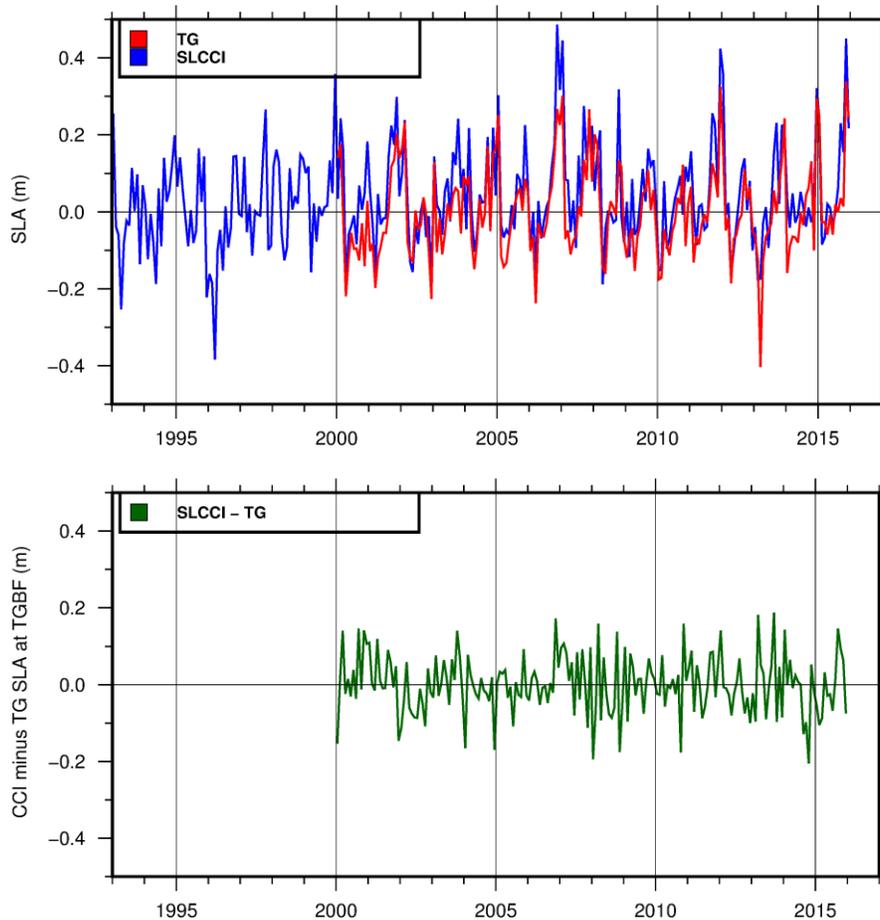
Figure 19: Deseasoned Time-series (top) and their differences (bottom) at TGBF

3.4.3 Conclusions

First, we observe that SLCCI gridded products and tide gauges agree well in terms of de-seasoned time-series, with statistically significant correlations at all stations.

Secondly, we note that in the analyzed region the VLM rates from GPS are relatively small, less than 3 mm/yr, with an error generally lower than 0.5 mm/yr, while the error of the altimetric minus tide gauge time-series is often larger than 1 mm/yr. We further observe that altimetry-derived and tide gauge-derived trends are not statistically different at any station, given the uncertainty in the estimates. The uncertainty is still too large for an accurate computation of vertical land motion rates from tide gauge and altimetry data. However, we observe that trends evaluated over more than 25 years are closer to the GPS trends that trends evaluated over shorter intervals. Therefore, we expect a better agreement of the rates with increasing length of the altimetry and tide gauge time-series.

3.5   Vertical Land Motion from altimetry and tide gauge at global scale

We evaluate in this section the vertical land motion (VLM) from altimetric and tide gauge monthly time-series for the interval between January 1993 and end of December 2015 at global scale.

3.5.1   Methodology

The methodology is the same as in the regional analysis (section 3.4). Implicit assumption of the method is that the differences between de-seasonalised time-series arise from the vertical motion. However, sea level variation in coastal zone results from a large variety of oceanic and land processes of natural and anthropogenic source. At global scale, hundreds of stations are used and the relative location of altimetry and tide gauge time-series is generally unknown. Tide gauge PSMSL sea level monthly time-series available for more than 70% of the analyzed interval are considered. To assess the resulting VLM we compare our results with the vertical velocity fields produced at the University of La Rochelle (ULR) for 493 stations (see Santamaria et. al, [2017]). We consider tide gauges co-located within 10 Kilometres from one of the 493 ULR6 GPS stations. Thus, this comparison can be performormed for a limited number of stations. Then, among the stations used by Wöppelmann and Marcos [2016] (see section 3.2.2), we select those that have data available for more than 70% of the interval and perform the same analysis.

The altimeter input data are sea level anomalies above the DTU2015 mean sea surface, which are extracted from the 0.125 degrees gridded altimeter data of the sea level Essential Climate Variable of the Sea Level CCI initiative. Usual corrections are applied, which include the Dynamic Atmosphere Correction (DAC). The land/sea mask derived from the Land Cover CCI project has been applied on each sea level map. The monthly DAC correction is applied to the tide gauge time-series for consistency with the SLCCI sea level data.

3.5.2   Results

We define a criteria to select pairs of altimeter and tide gauge sea level time-series used to evaluate vertical land motion at the tide gauge location. Suitable elements of the criteria are correlation, standard deviation of the difference (stdd), distance between altimeter point and tide gauge, vertical land motion and its error computed both accounting and not-accounting for serial correlation. Figure 20 shows the distribution of some statistical parameters for the 170 pairs of altimeter and tide gauge de-seasoned time-series. Altimeter and tide gauge de-seasoned time-series have correlations with median 0.72 and standard deviation with median 4 cm. The distance between the altimeter and tide gauge points is smaller than 30 km for most of the stations.

We consider the deseasoned time-series. Figure 21 (left) shows the histogram of the difference between the altimeter minus tide gauge vertical motion and the GPS-derived vertical motion from ULR6 solution. Figure 22 (left) indicates a reasonable agreement between the rates (correlation 0.45, standard deviation of the difference 3.2 mm/yr with the 170 stations). The median of the correlation between altimetry and tide gauges is 0.72. The agreement with the Wöppelmann and Marcos [2016] rates is higher (correlation 0.8, standard deviation of the difference 2.3 mm/yr with the 462 stations in Figure 23.
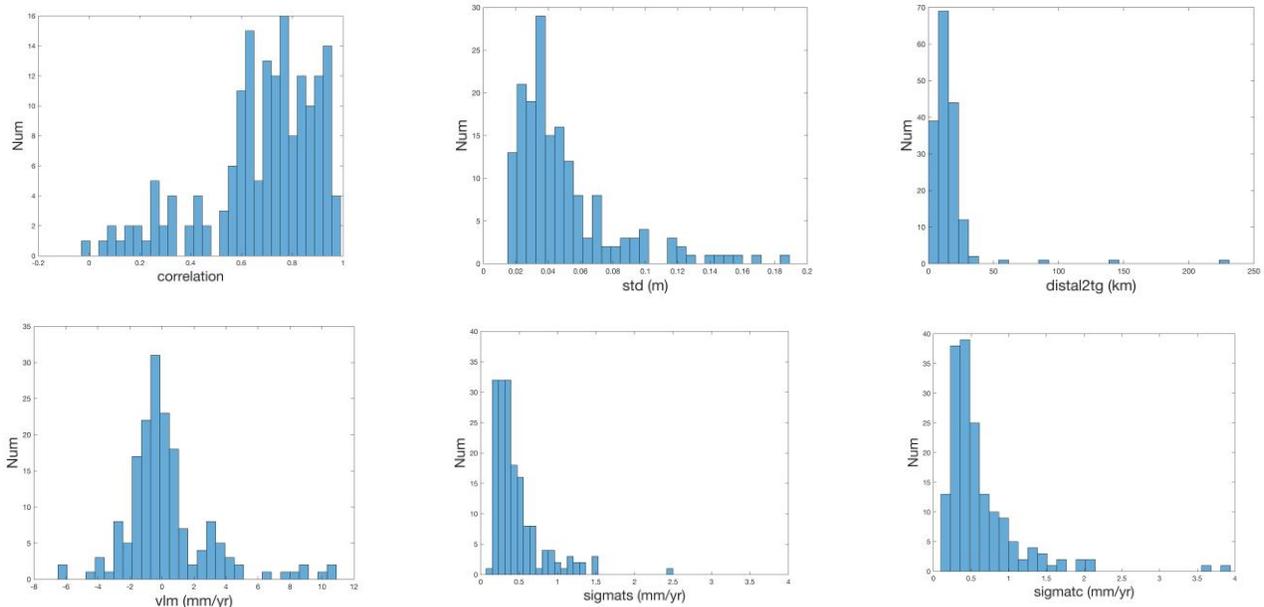
Figure 20: Histograms of parameters in Table 1 for distance from GPS station smaller than 10 Km (170 selected stations in Table 2). Correlation (a), standard deviation of the de-seasoned differences (b), distance between tide gauge and altimetry (c), Trend of the differences (d), standard error of the vlm without (e) and accounting for auto-correlation (f), Difference wrt GPS trends (g)
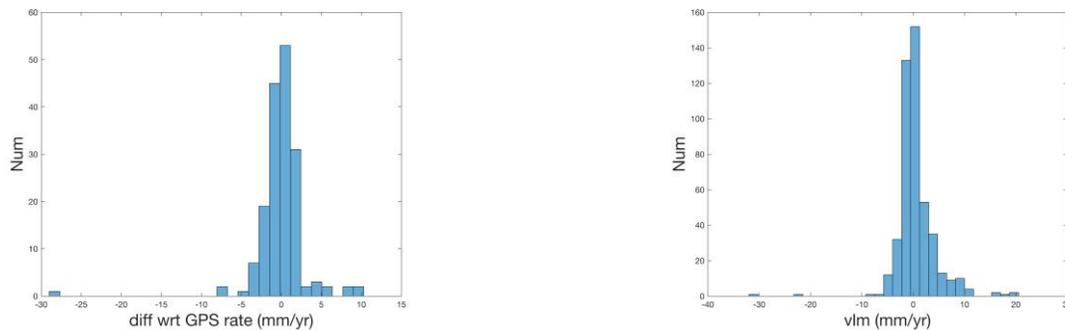
Figure 21: Left: Histogram of difference between vlm derived from altimetry and tide gauges and from GPS. Right: the same for two altimeter-derived verical motion (this study and Woppelmann 2016).

Several criteria have been used in previous studies to select collocated tide gauge and altimetric sea level time-series. Fenoglio-Marc et al. (2004) applied five criteria based on: (1) relative distance (< 110 km), (2) correlation (> 0.6), (3) standard deviation of differences (< 8 cm), (4) formal error of the vlm (< 5 mm/yr), (5) minimum number of months N (> 50). In Fenoglio-Marc and Tel [2010] we used instead the four criteria based on : (1) distance (150 Km), (2) correlation (> 0.5), (3) standard deviation of the differences (< 8 cm), (4) VLM and its standard error (< 5 mm/yr). Fenoglio-Marc et al. [2011]. Finally the two criteria used in Fenoglio-Marc and al. [2011] were based on: (1) correlation (0.7) and (2) length of the time-series (90%).

Using four additional criteria based on (1) correlation (> 0.6) and (2) standard deviation of differences (< 8 cm), (3) distance (< 30 km) and error of VLM (1 mm/yr) the number of stations reduces to 121 and the agreement

increases with a standard deviation of 1.5 mm/yr in agreement with published results (Wöppelmann and Marcos [2016] and Pfeffer [2017]). The spatial distribution is good in Europe, North America and Tropical Pacific from Figure 24 (right). Trends are in general agreement with Wöppelmann and Marcos [2016] with, for example, positive values in the Baltic Sea and mainly negative values along the Northern Eastern Atlantic coasts.
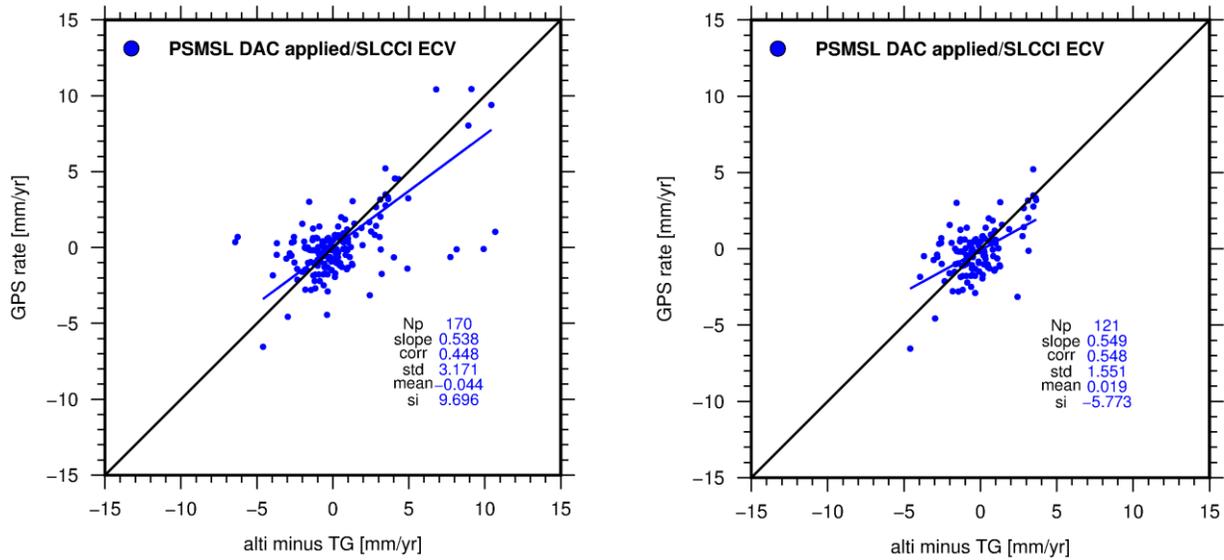
Figure 22: Difference between vlm derived in this study from altimetry and tide gauges and the rate of the URL6 GPS solution. No selection criteria is applied in left panel. Selection criteria are applied in the right panel.
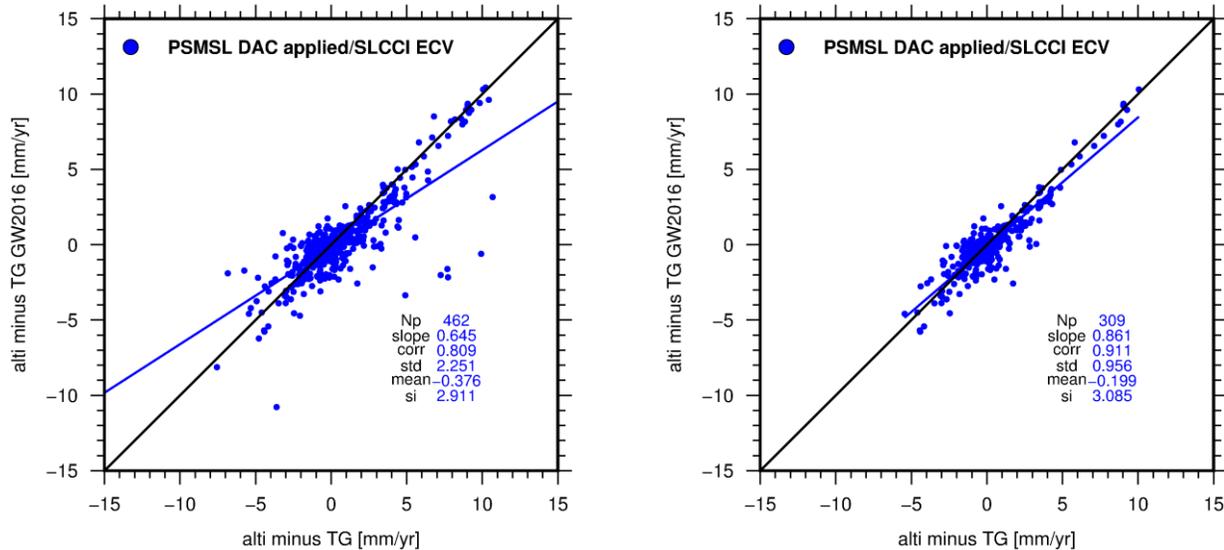
Figure 23: Difference between vlm derived in this study (left) and by Woppelmann 2017, both from altimetry and tide gauges. Selection criteria are applied (right) and not applied (left).
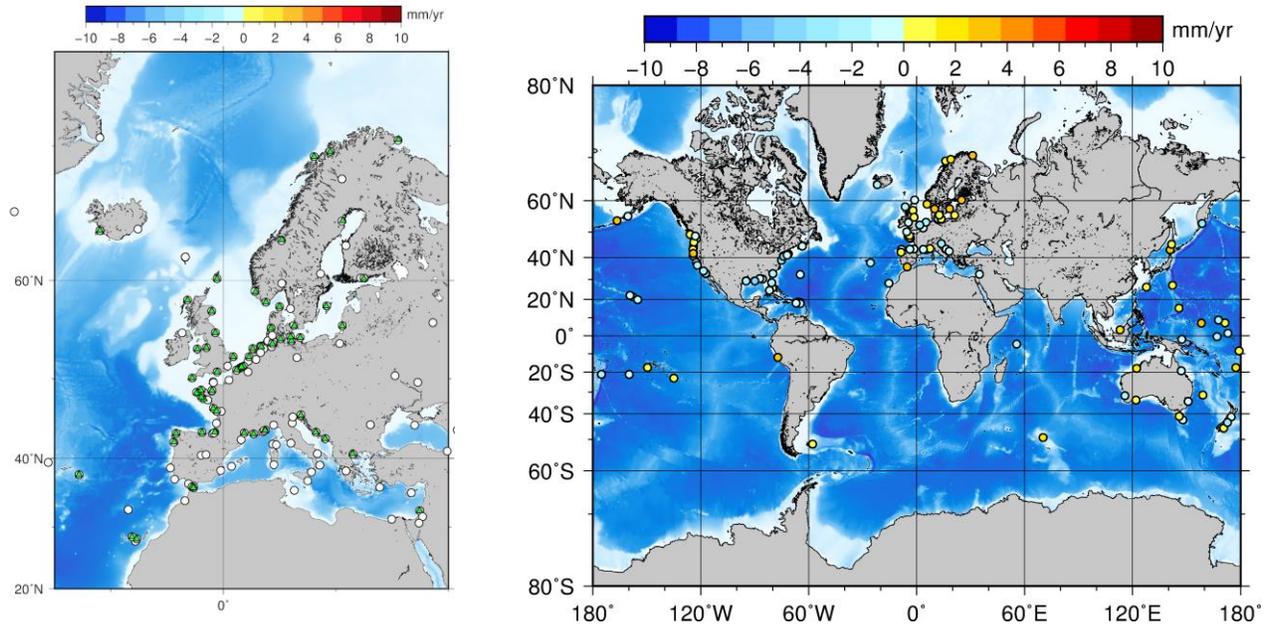
Figure 24: Left: Location of the European ULR6 GPS stations (white circles) and of the tide gauge stations with at least 70% of the data and within 10 km from one of those GPS stations. Right: VLM from altimetry minus tide gauges corresponding to Figure 22 (right), i.e. tide gauge within 10 Km from ULR6a GPS station with the additional selection criteria in Table 3 right column).

criteria	Fenoglio et al. 2004	Fenoglio et al. 2010	Fenoglio et al. 2011	This study
Dist_al-tg (km)	110	150	-	30
Corr	0.6	0.5	0.7	0.6
Stdd_al-tg (m)	0.08	0.08	-	0.08
Vlm (mm/yr)		5	-	-
Error vlm (mm/yr)	5	5	-	1
Length ts (mo, %)	50 month	-	90%	70%

Table 3: Selected criteria used for comparison between altimetric and tide-gauge time-series

Distance from GPS	Selected tide gauge stations
1	76
10	170
30	217
100	327
1000	620
10000	666

Table 4: Number of tide gauge stations considered depending on allowed distance to GPS stations

3.5.3 Conclusions on global analysis

Firstly, like in the regional analysis in section 3.4, we observe globally a good agreement between de-seasoned sea level variability from tide gauges and from the nearest grid point of the SLCCI gridded products. Correlation and standard deviation of difference of de-seasoned time-series are 0.70 and 4.6 cm respectively.

Second, we note that the agreement with the VLM derived from GPS at ULR at 170 stations has a STD of 3.2 mm/yr which is reduced to 1.5 mm/yr when a sub-set of 120 stations is selected. The screening of the stations uses four criteria to check the agreement between altimeter tide gauge time-series based on (1) correlation, (2) standard deviation of difference, (3) estimated error of the VLM trend and (4) distance between altimeter and tide gauge station.

The same test was applied to check the agreement with another estimate of altimeter-derived VLM by Wöppelmann and Marcos [2016]. We find at 462 stations a STD of 2.2 mm/yr which is reduced to 0.9 mm/yr when a sub-set of 309 stations is selected. Those differences between the VLM rates are due to the altimeter data used and to the methodology used to select the altimeter time-series corresponding to the tide gauge time-series. Further analysis could be done to investigate the spread of the solutions depending on different choices.

4   References

Ablain M., J.F.Legeais, P. Prandi, M. Marcos, L. Fenoglio-Marc, J. Benveniste, H.B. Dieng and A. Cazenave. (2016). Altimetry-Based Sea Level at Global and Regional Scales, Surveys in Geophysics, Special Issue on Sea Level, Integrative Study of the Mean Sea Level and its Components,   DOI: 10.1007/s10712-016-9389-8

Altamimi, Z., Collilieux, X., Métivier, L., (2011). ITRF2008: an improved solution of the international terrestrial reference frame. Journal of Geodesy 85 (8), 457–473. http:// dx.doi.org/10.1007/s00190-011-0444-4.

Blewitt, G., C. Kreemer, W.C. Hammond, J. Gazeaux (2016), MIDAS robust trend estimator for accurate GPS station velocities without step detection, accepted for publication in the Journal of Geophysical Research, doi: 10.1002/2015JB012552.

Ekman, M. (1989). Impacts of geodynamic phenomena on systems for height and gravity .Bull. Geodesique, 63: 281. doi:10.1007/BF02520477

Featherstone, W. E., and M. S. Filmer (2012), The north-south tilt in the Australian Height Datum is explained by the ocean's mean dynamic topography, J. Geophys. Res., 117, C08035, doi:10.1029/2012JC007974.

Fenoglio-Marc L. C. Braitenberg and L. Tunini (2011). Sea level variability and trends in the Adriatic Sea in 1993-2008 from tide gauges and satellite altimetry, Physics and Chemistry of the Earth, doi:10.1016/j.pce.2011.05.014

Fenoglio-Marc, L., R. Scharroo, A. Annunziato, L. Mendoza, M. Becker, and J. Lillibridge (2015), Cyclone Xaver seen by geodetic observations, Geophys. Res. Lett., 42, doi:10.1002/2015GL065989.

Fenoglio-Marc, L., Dinardo, S., Scharroo, R., Roland, A., Dutour, M., Lucas, B., Becker, M., Benveniste, J., Weiss, R. (2015). The German Bight: a validation of CryoSat-2 altimeter data in SAR mode, *Advances in Space Research*, doi: http://dx.doi.org/10.1016/j.asr.2015.02.014

Lin, H., K. R. Thompson, J. Huang, and M. Véronneau (2015), Tilt of mean sea level along the Pacific coasts of North America and Japan, J. Geophys. Res. Oceans, 120, 6815–6828, doi:10.1002/2015JC010920.

McCarthy and Petit IERS Conventions (2003), International Earth Rotation and Reference Systems Service ,IERS Technical Note ; 32) Frankfurt am Main: Verlag des Bundesamts für Kartographie und Geodäsie, 2004. 127 pp., paperback, ISBN 3-89888-884-3

Santamaria-Gomez A., Gravelle M., Wöppelmann G. (2014). Long-term vertical land motion from double-differenced tide gauge and satellite altimetry data. Journal of Geodesy, 88, 207-222

Santamaría-Gómez A., M. Gravelle, S. Dangendorf, M. Marcos, G. Spada, G. Wöppelmann (2017). Uncertainty of the 20th century sea-level rise due to vertical land motion errors. Earth and Planetary Science Letters, 473, 24-32.

Spada, G. and Galassi, G. (2012), New estimates of secular sea level rise from tide gauge data and GIA modelling. Geophysical Journal International, 191: 1067–1094. doi:10.1111/j.1365-246X.2012.05663.x

Wöppelmann G., and Marcos M. (2016), Vertical land motion as a key to understanding sea level change and variability, Rev. Geophys., 54, 64–92.

Wöppelmann, G., C. Letetrel, A. Santamaria, M.-N. Bouin, X. Collilieux, Z. Altamimi, S. D. P. Williams, and B. Martin Miguez (2009), Rates of sea-level change over the past century in a geocentric reference frame, Geophys. Res. Lett., 36, L12607, doi:10.1029/2009GL038720.

Woodworth P. L., M. Gravelle, M. Marcos, G. Wöppelmann, C. W. Hughes. (2015). The status of measurement of the Mediterranean mean dynamic topography by geodetic techniques. Journal of Geodesy, Journal of Geodesy, 89, 811-827.

Woodworth P.L., C.W. Hughes, R.J. Bingham, T. Gruber (2013). Towards worldwide height system unification using ocean information. Journal of Geodetic Science, 2(4), 302-318.

10 Appendix I, D8: Technical Note describing the work performed in Work Package 4000
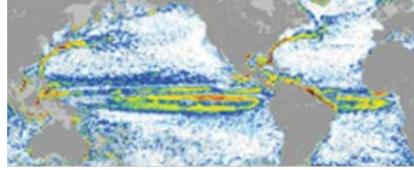
GOCE++ Dynamic Topography at the coast and tide gauge unification
GOCE ++ DYCOT

TITLE. Deliverable 8

Author Chris W. Hughes and Rory Bingham

ESTEC Ref: ITT AO/1-8194/15/NL/FF/gp "GOCE++ Dynamic Topography at the coast and tide gauge unification"- Coordinator: Ole B. Andersen (DTU)

DOCUMENT CHANGE LOG				
Rev.	Date	Sections modified	Comments	Changed by
1	10-11-2017	All	Draft	Chris W. Hughes
2	26-11-2017	Sec 1	Merged two sections	Rory Bingham

WP4100: Impact Assessment

We begin with an assessment of the DYCOT approach to computing the coastal MDT (CMDT), taking the data supplied with the coastMDT software (henceforth the software) and the default parameters for filtering as constituting *the* DYCOT CMDT. We shall refer to this CMDT as DYCMDT. The DYCMDT can be thought of as coming in three versions: A version obtained by using just the initial altimetric MDT itself to extrapolate the MDT over land (DYCMDTal); a version obtained by using just the tide gauge (TG) MDT to extrapolate the MDT over land (DYCMDTtg); and finally a version that uses both the altimetry and TG MDTs to extrapolate the MDT over land (DYCMDTbt).

Global analysis

Considering the global set of common coastal points – that is, ocean grid points that are adjacent to grid points flagged as land for the 8th of a degree land mask and all of the model and observational MDTs – the initial unfiltered DYCOT CMDT (DYCMDT0) has a mean (unbiased) RMSD relative to the 7 ocean models of 31.7 cm, with the RMSD's ranging from 29.6 cm relative to the Nemo12b model to 32.9 cm relative to the LivC model (see Table 1). After filtering (with the default parameters), with the MDT extrapolated over land using just the altimetry CMDT, the mean RMSD reduces to 18.9 cm and the minimum difference, again provided by the Nemo12b model, falls to 16.1 cm. In this case it is the Ecco2 model that gives the maximum difference of 20.6 cm. Although extrapolating over land using just the TG MDT still reduces the discrepancy with the ocean model CMDTs, the results are not as good as they are using the altimetry CMDT. In this case the mean RMSD is 25.8 cm, with the closest agreement (20.5 cm) given by Nemo12a and the poorest agreement (29.1 cm) again provided by Ecco2. (A global analysis using both the altimetry and TG CMDTs to extrapolate over land is not provided as the coastMDT software crashed when this calculation was attempted for the global domain.)

Somewhat different results emerge when the analysis is restricted to just those common coastal points for which we also have TG-based MDT values (see Table 2). In this case, it is the quarter degree version of Nemo (NemoQ) that gives the best agreement with all of the DYCOT CMDTs and LivS that gives the poorest agreement. Unfiltered the RMSD difference with NemoQ is 15.7 cm, while filtering with either the altimetry- or TG- based land fill gives a reduced RMSD of 8.7 cm in both cases. For the worst case, the unfiltered RMSD difference with LivS is 18.8 cm, while filtering with the altimetry- and TG-based land fill gives RMSD's of 12.6 cm and 13.5 cm, respectively.

If the two observational MDTs are included in the analysis (see Tables 3 and 4), then for unfiltered and altimetry-based land fill CMDTs it is the observational MDT DTU10-TUM13 that provides the closest agreement, with RMSD values of 28.3 cm and 15.0 cm respectively (compared with 29.6 cm and 18.9 cm relative to Nemo12b) when all common coastal points are considered. However, with the TG-based land fill it is the Nemo12a ocean model that still provides the closest agreement. The same pattern is found when the analysis is restricted to the common coastal points with TG MDT values. The DTU10-TUM13 MDT is in closest agreement with the unfiltered and altimetry-based land fill CMDTs, with RMSD values of 14.3 cm and 7.0 cm respectively

(compared with 15.7 cm and 8.7 cm relative to NemoQ), but it is NemoQ that is still in closest agreement with DYCMDTtg. Also including the TG MDT values in the analysis (see Table 5) while changing the mean RMSD's does not change the MDTs that give the closest agreement with the DYCMDTs. The TG MDT does however displace the LivS MDT as giving the poorest agreement (14.2 cm, up from 13.5 cm) with DYCMDTal.

A conclusion from this set of comparisons is that filtering improves the CMDT and that using the altimetry-based MDT to extrapolate the MDT over land gives better results than using only the TG-based MDT. This is not surprising given that the latter uses far fewer observations to fill the land values and that these values are likely noisier. Among the ocean models, it is the Nemo family of models that provides the closest agreement with the DYCOT CMDTs. The geodetic MDT (DTU10-TUM13) agrees somewhat more closely with the DYCMDT0 and DYCMDTal, which is not surprising given that is of the same type as the DYCOT CMDTs. That said, that difference is not great and for some reasons it does not apply when the TG MDT has been used to fill the land/undefined areas.

Finally for the global analysis we consider a direct comparison between the DYCOT CMDTs and the TG MDT values. Unlike for the coastMDT software, this analysis is restricted to just TG locations that are adjacent to land/undefined grid cells on the project land mask. Of the 302 TG MDT values, 118 satisfy this criterion. Prior to filtering the DYCOT CMDT and the TG MDT have an RMSD over these 118 points of 71.7 cm, most of which is due to a bias of 69.1 cm. Upon removing this offset, the RMSD drops to 19.2 cm. Filtering with the altimetry-based land fill reduces this to 13.8 cm (although the bias actually increases a little showing the negative impact of filtering). Unlike the previous comparisons, in this case the TG-based land fill gives the best results, reducing the RMDS to 11.6 cm. However, this is not a fair comparison given that the TG values have been used to obtain the land fill and so the two observations are not independent.

North-east Atlantic
Interestingly, when we consider the regional comparisons with ocean models, although all show a RMSD reduction due to filtering, there is no consistency as to the best approach to extrapolation of the CMDT over land. For the NE Atlantic study region, filtering with the self-fill gives the best result, reducing the mean (min) RMSD from 14.2 (13.5) cm to 8.1 (7.2) cm. The TG-based fill gives the worst result, reducing the mean (min) RMSD to 9.1 (8.2) cm, with the combined fill giving intermediate results. Nemo12a also gives the best agreement with DYCMDT0 and DYCMDTal for the NE Atlantic. However, the lower resolution models Ecco2 and EccoG agree most closely with DYCMDTtg and dyCMDTbt. LivS agrees lest well with all of the DYCOT MDTs in this region.

Figure 1 shows the impact of the various filtering approaches on the CMDT for the Northeast Atlantic coastline. From Figure 1a, which shows the unfiltered DYCMDT0 (black) against the closest matching model MDT (Nemo12a; yellow) it is clear that filtering is essential to obtain a reasonable estimate of the CMDT. Filtering with the self-fill approach (Figure 1b) is quite effective at removing the noise, producing an estimate

of the CMDT that is much more like the best fitting model CMDT, which again is from Nemo12a. With the exception of a residual spike in the geodetic CMDT near grid point 700, particularly good agreement is found between the geodetic and model estimates between coastal points 650 to 1100. This corresponds to the stretch of coastline from the English Channel into the Norwegian Sea. For the more southerly stretch of coastline the geodetic estimate of the CMDT has more structure than the Nemo12a estimate. It is difficult to assess to what extent this is due to residual noise in former or the model estimate being too smooth. Some combination of the two is the most likely explanation. The extent of the noise in the TG-CMDT means that it is not possible to use this estimate to decide one way or the other. The geodetic estimate also shows a large 10 cm jump in the coastal MDT around grid point 1100 not seen in the Nemo12a estimate (or any of the other models).

Figure 1c illustrates the impact that using only TG MDT values to fill the land areas has on the coastal MDT. As one might expect, along stretches of coastline where TG MDT values are present the geodetic estimate is drawn towards these values. This is clear on the stretch of coastline from point 100 to 850, with introduction of a minimum around point 200 and a local maximum at point 250 being particularly obvious. In addition to this pull is a somewhat competing influence of greater smoothing between TG location, as one might expect if one were to filter the MDT with zero (or some other constant) values over land. This is apparent, for instance, in the loss of the peak between grid points 850 and 950, where there was a good match between the geodetic and model CMDTs in figure 1b. Again, it is difficult to be categorical, but the fact that the best agreement between the geodetic and model estimates in this case is less than for the self-fill case shown in Figure 1b suggests that using the TG fill results in a poorer estimate of the CMDT. This is also suggested by visual comparison.

Figure 1d shows that in the case of the combination fill method, the TG estimates have the greatest impact, whereas the self-fill has the greatest influence where there are few TGs. The best agreement is slightly better than for the TG-only fill method, but this is with EccoG model, that looks unrealistic in comparison with Nemo12a for example.

If we also include the two observational estimates in the comparison then we find that the geodetic MDT DTU10-TUM13 replaces Nemo12a as the closest match for the unfiltered and self-fill CMDT estimates, with RMS differences falling slightly from 13.5 to 12.4 cm for the former and 7.2 to 6.7 cm for the latter. However, versions of Ecco remain the closest match for the tg and combined fill methods. This again suggests that the use of the TG MDT to fill land produces a poorer estimate of the CMDT.

Considering only points for which TG MDT estimates are available changes the results a little. In this case, Nemo12a becomes the closest model match for all filtered CMDTs, showing that the agreement with the Ecco models when all coastal points are considered arises for the closer agreement in places where there are no TG-based estimates and both are dampened. DTU10-TUM13 remains the best match in the self-filtered case when the observational MDTs are included in the analysis but Nemo12a again replaces the Ecco

models. Interestingly these estimates remain the closest matches even when the TG MDT estimates are included in the analysis.

Table 6 shows the comparison between the TG CMDT estimates and the DYCOT MDTs. Unsurprisingly the closest match occurs from the TG-based fill method, followed by the combined fill and then the self-fill method.
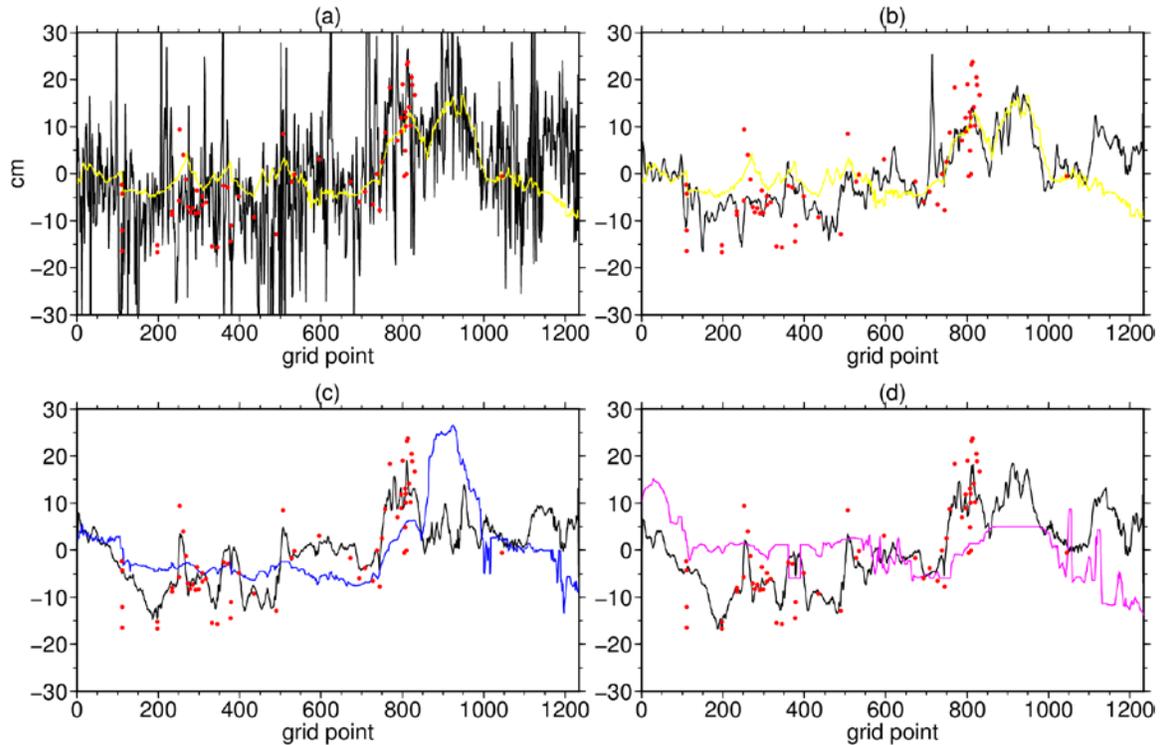
Figure 1. The coastal MDT for the NE Atlantic region (excluding the Med.), showing the DYCOT CMDTs (black), the closest model CMDTs (various colours) and the TG-based CMDT estimates (red dots). (a) DYCMDT0 and Nemo12a; (b) DYCMDTal and Nemo12a; (c) DYCMDTtg and Ecco2; (d) DYCMDTbt and EccoG. The local mean has been removed in all cases.

7
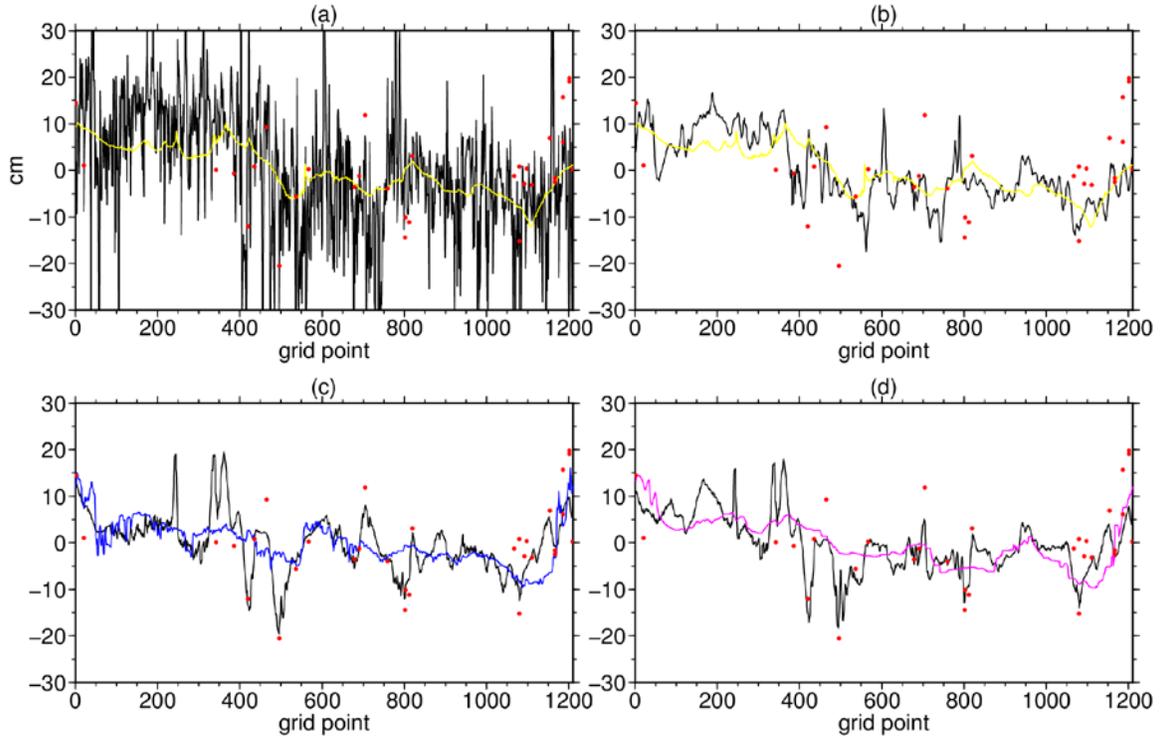
Figure 2. The coastal MDT for the Mediterranean, showing the DYCOT CMDTs (black), the closest model CMDTs (various colours) and the TG-based CMDT estimates (red dots). (a) DYCMDT0 and Nemo12a; (b) DYCMDTal and Nemo12a; (c) DYCMDTtg and Ecco2; (d) DYCMDTbt and EccoG. The local mean has been removed in all cases. The path travels anti-clockwise around the Mediterranean for the southern shore of the Strait of Gibraltar

For completeness Figure 2 shows the CMDTs for the Mediterranean. The results again show the negative influence of using the TG MDT to fill over land.

Agulhas

For the Agulhas region, the mean RMSD between the DYCOT CMDT and the model CMDTs is 21.3 cm prior to filtering (see Figure 3a and Table 1). The best agreement (21.0 cm) is with the CMDT from the Nemo12b model. Somewhat better agreement (17.8 cm) is found with the observational estimate DTU10-TUM13 (Table 3). The unbiased difference with the TG MDT is only 3 mm. However, this is based on just 2 TG observations. Again, it is clear from Figure 3a that the unfiltered DYCOT CMDT is severely affected by noise and filtering is therefore required.

With a mean RMSD relative the ocean models of 8.2 cm it is the self+TG fill method that appears most successful, followed by the self-fill (10.1 cm) and the TG-fill (11.1 cm) approaches. This is somewhat surprising given that only two TG values are available for this region. Examination of Figure 3 shows that this is because it is the self+TG fill that results in the smoothest CMDT. No matter which method is used to fill land values prior to filtering, it is the Ecco2 model that most closely matches the filtered DYCMDTs. On the other hand, NemoQ provides the poorest match for the TG+self fill and Nemo12a for the other two fill methods. This is the only region where these models provide the poorest match. If we also include the two additional observational CMDTs in the comparison

8

then the Aviso CMDT supplants ECCO2 as the closest match to the filtered DYCMDTs. Again the best match (6.5 cm RMSD) is for the TG+self fill method. In this case RMSD difference with the two TG MDT values is 9.6 cm.
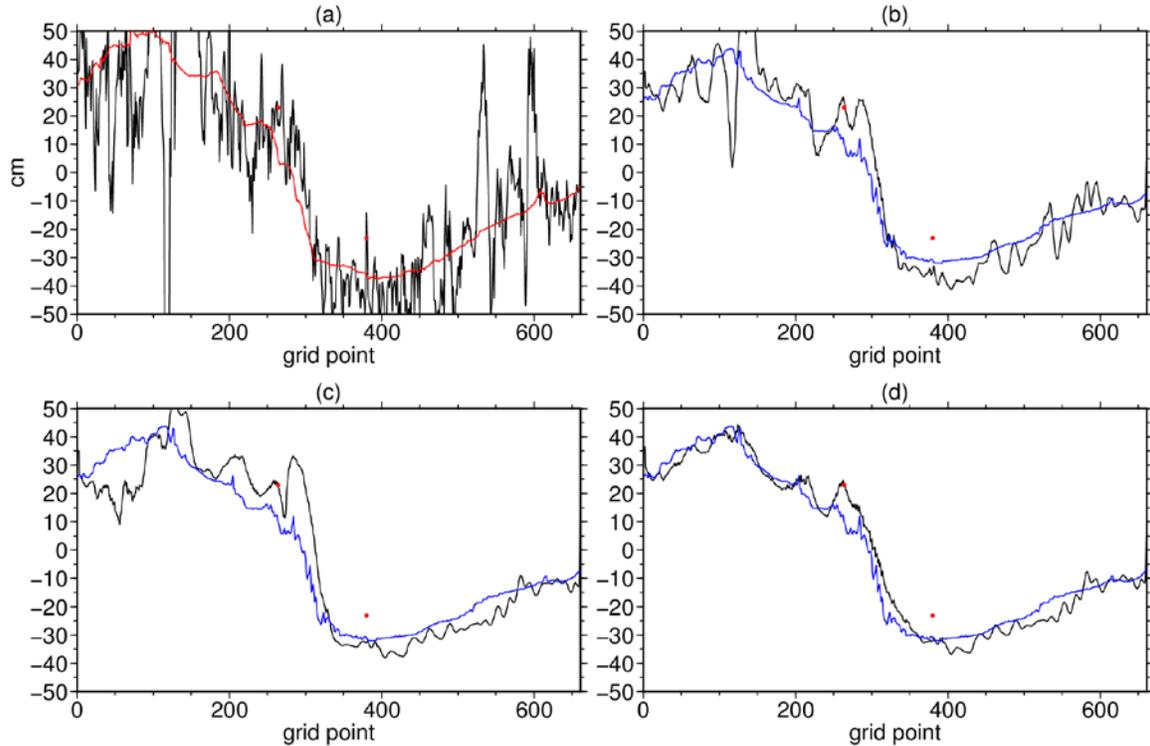
Figure 3. The coastal MDT for the Agulhas region, showing the DYCOT CMDTs (black), the closest model CMDTs (various colours) and the TG-based CMDT estimates (red dots). (a) DYCMDT0 and Nemo12b; (b) DYCMDTal and Ecco2; (c) DYCMDTtg and Ecco2; (d) DYCMDTbt and Ecco2. The local mean has been removed in all cases. The path travels clockwise from the Indian to the Atlantic Ocean with end points at the equator.

South America

For the South America study region, the mean RMSD between the DYCOT CMDT and the model CMDTs is 28.1 cm prior to filtering (see Figure 4a and Table 1). The best agreement (26.6 cm) is with the CMDT from the Nemo12a model. Somewhat better agreement (22.3 cm) is found with the observational estimate DTU10-TUM13 (Table 3). The unbiased difference with the TG MDT is 8.9 cm. However, this is based on just three TG observations. Again, it is clear from Figure 4a that the DYCOT CMDT requires filtering to remove the noise with which it is severely affected.

With a mean RMSD relative the ocean models of 13.6 cm it is again the self+TG fill method that appears most successful when removing noise, followed by the TG-fill (15.5 cm) and the self-fill (17.2 cm) approaches. Again, this is somewhat surprising given that only three TG values are available for this region. In all cases it is the Nemo12a model that remains the closest match to the filtered DYCMDTs. Visual inspection of Figure 4 confirms that with the exception of a few isolated peaks, it is the TG+self fill approach that produces the smoothest CMDT. Given that there are so few TG values to constrain

the land fill it is not obvious why there should be such a dramatic improvement between the self-fill (Figure 4b) and the combined-fill (Figure 4d) CMDTs.

Figure 4. The coastal MDT for the South American region, showing the DYCOT CMDTs (black), the closest model CMDTs (various colours) and the TG-based CMDT estimates (red dots). (a) DYCMDT0 and Nemo12a; (b) DYCMDTal and Nemo12a; (c) DYCMDTtg and Nemo12a; (d) DYCMDTbt and Nemo12a. The local mean has been removed in all cases. The path travels clockwise from the Atlantic to the Pacific Ocean with end points at 13N.

Australia
In terms of the mean RMSD the same ordering is found for Australia, with the altimetry-based land fill, reducing the mean RMSD from 22.6 cm to 9.5 cm, with the combined and TG-based fills reducing it to 10.0 cm and 10.1 cm, respectively. For Australia, it is NemoQ that gives the closest overall agreement, in this case with DYCMDTal, with Nemo12b closest for DYCMDTtg and DYCMDTbt. Again EccoG agrees least well across all variants.
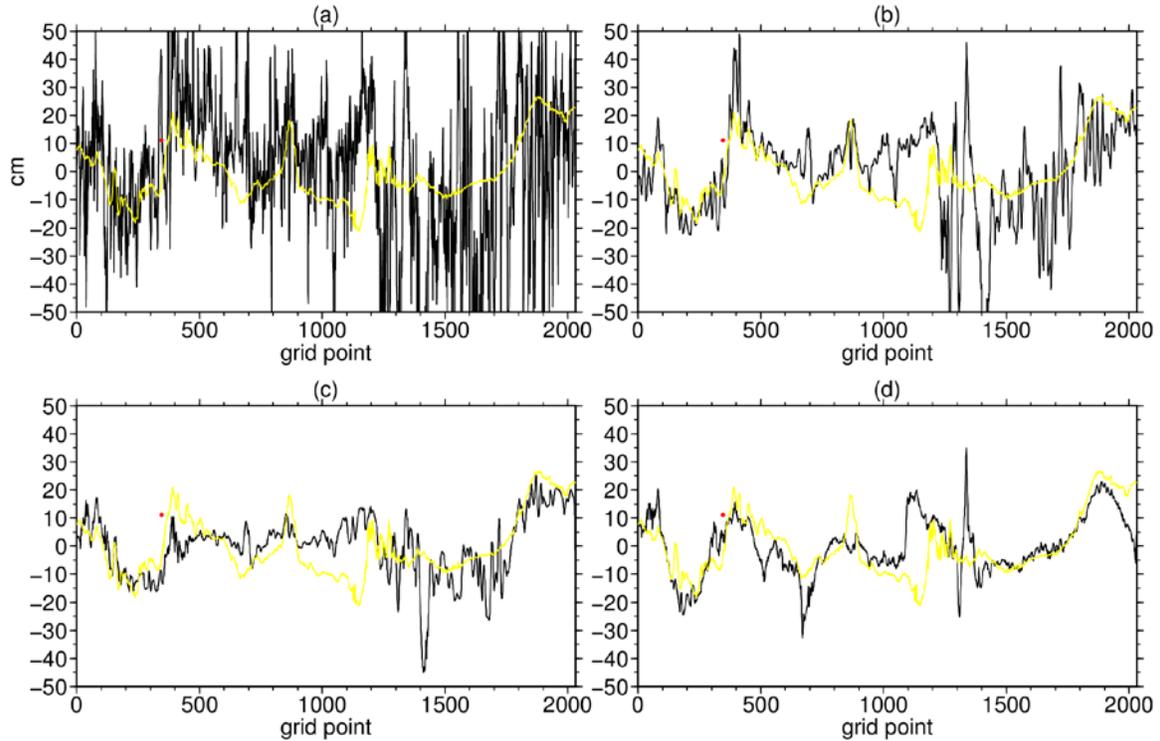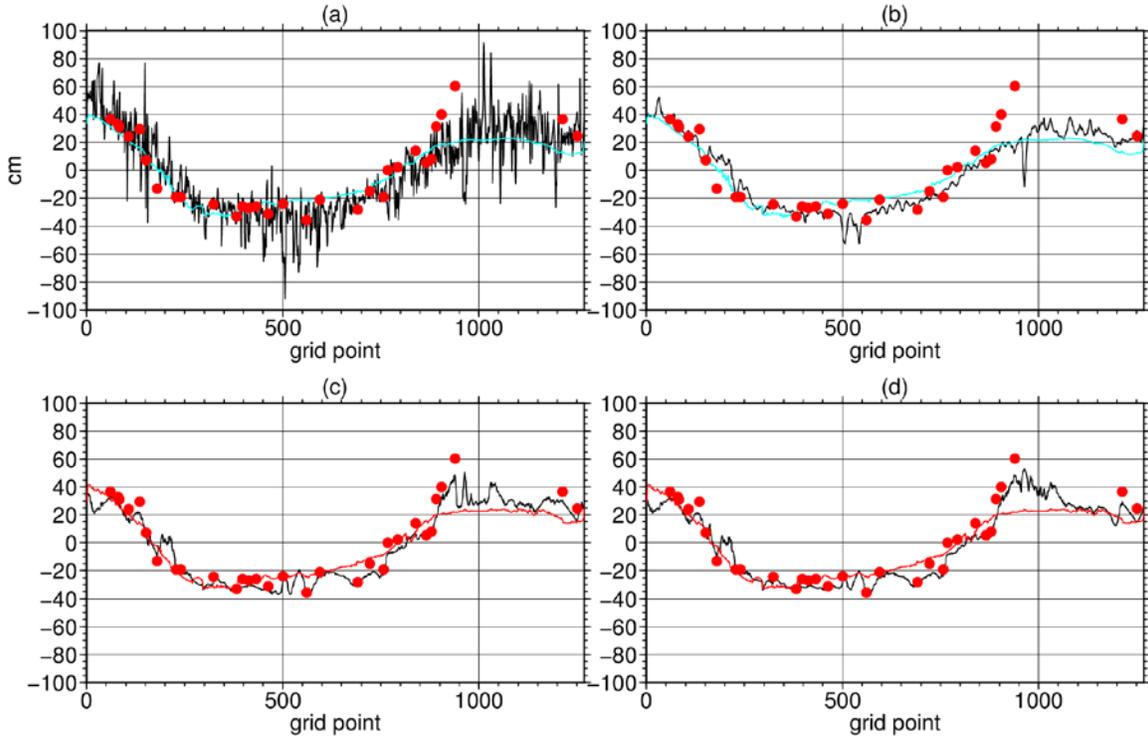
Figure 5. The coastal MDT for the Australia, showing the DYCOT CMDTs (black), the closest model CMDTs (various colours) and the TG-based CMDT estimates (red dots). (a) DYCMDT0 and NemoQ; (b) DYCMDTal and NemoQ; (c) DYCMDTtg and Nemo12b; (d) DYCMDTbt and Nemo12b. The local mean has been removed in all cases. The path travels clockwise from the from the most northerly point.

Pacific Islands

Finally, it is only for the Pacific Islands where the TG-based fill gives the best results, reducing the mean (min) RMSD from 38.6 (37.8) cm to 10.9 (8.5) cm. In this case the alt-based fill gives the worst results with an RMSD of 16.5 cm and the combined fill giving an intermediate value of 16.2 cm. For the Pacific Islands the Nemo12b model gives the closest agreement with the DYCOT CMDTs, except for the best case DYCMDTtg where it is Ecoo2 that most closely matches. Here EccoG agrees least well across all variants.

Table 1. Assessment of the DYCOT CMDTs against ocean models for all common coastal points. RMS differences are given in m. For each entry four values are given. From top to bottom these are: DYCMDT0 (no filtering), DYCMDTal, DYCMDTtg and DYCMDTbt.

Region	RMSD (mean)	RMSD (min)	RMSD (max)	Model (min)	Model (max)
Global	0.317	0.296	0.329	Nemo12b	LivC
	0.189	0.161	0.206	Nemo12b	Ecco2
	0.258	0.205	0.291	Nemo12a	Ecco2
	*	*	*	*	*
Ne Atlantic	0.142	0.135	0.154	Nemo12a	LivS
	0.081	0.072	0.1	Nemo12a	LivS
	0.095	0.087	0.117	Ecco2	LivS
	0.091	0.082	0.113	EccoG	LivS
Agulhas	0.213	0.21	0.217	Nemo12b	LivC
	0.101	0.091	0.109	Ecco2	Nemo12a
	0.111	0.098	0.123	Ecco2	Nemo12a
	0.082	0.069	0.096	Ecco2	NemoQ
Australia	0.226	0.22	0.234	NemoQ	EccoG
	0.095	0.082	0.115	NemoQ	EccoG
	0.101	0.084	0.128	Nemo12b	EccoG
	0.1	0.086	0.118	Nemo12b	EccoG
South America	0.281	0.266	0.301	Nemo12a	LivC
	0.172	0.149	0.197	Nemo12a	EccoG
	0.155	0.133	0.178	Nemo12a	EccoG
	0.136	0.111	0.159	Nemo12a	EccoG
Pacific Islands	0.386	0.378	0.397	Nemo12b	EccoG
	0.165	0.151	0.184	Nemo12b	EccoG
	0.109	0.085	0.129	Ecco2	EccoG
	0.162	0.148	0.179	Nemo12b	EccoG

Table 2. As in Table 1, but with analysis restricted to common coastal points for which we also have TG-based MDT values. (Note, for the Agulhas region there are no such values.)

Region	RMSD (mean)	RMSD (min)	RMSD (max)	Model (min)	Model (max)
Global	0.176	0.157	0.188	NemoQ	LivS
	0.111	0.087	0.126	NemoQ	LivS
	0.111	0.087	0.135	NemoQ	LivS
	*	*	*	*	*
Ne Atlantic	0.157	0.143	0.17	NemoQ	LivC
	0.067	0.049	0.101	Nemo12a	LivC
	0.068	0.051	0.101	Nemo12a	LivC
	0.071	0.055	0.104	Nemo12a	LivC
Australia	0.171	0.142	0.192	EccoG	Nemo12a
	0.077	0.052	0.093	EccoG	Nemo12a
	0.099	0.088	0.119	Nemo12b	LivS
	0.101	0.09	0.122	Nemo12b	LivS
South America	0.321	0.273	0.393	NemoQ	LivC
	0.148	0.124	0.203	NemoQ	LivC
	0.101	0.074	0.161	NemoQ	LivC
	0.154	0.112	0.223	NemoQ	LivC
Pacific Islands	0.149	0.135	0.172	NemoQ	LivS
	0.101	0.074	0.16	Ecco2	LivS
	0.137	0.114	0.192	NemoQ	LivS
	0.131	0.109	0.185	NemoQ	LivS

Table 3. Assessment of the DYCOT CMDTs against ocean models and two observational MDTs (Aviso and DTU10-TUM13) for all common coastal points. RMS differences are given in m. For each entry four values are given. From top to bottom these are: DYCMDT0 (no filtering), DYCMDTal, DYCMDTtg and DYCMDTbt.

Region	RMSD (mean)	RMSD (min)	RMSD (max)	Model (min)	Model (max)
Global	0.313	0.283	0.329	DTU10-TUM13	LivC
	0.184	0.15	0.206	DTU10-TUM13	Ecco2
	0.262	0.205	0.291	Nemo12a	Ecco2
	*	*	*	*	*
Ne Atlantic	0.141	0.124	0.154	DTU10-TUM13	LivS
	0.081	0.067	0.1	DTU10-TUM13	LivS
	0.096	0.087	0.117	EccoG	LivS
	0.092	0.082	0.113	EccoG	LivS
Agulhas	0.208	0.178	0.217	DTU10-TUM13	LivC
	0.095	0.074	0.109	Aviso	Nemo12a
	0.104	0.07	0.123	Aviso	Nemo12a
	0.081	0.065	0.096	Aviso	NemoQ
Australia	0.222	0.203	0.234	DTU10-TUM13	EccoG
	0.091	0.078	0.115	Aviso	EccoG
	0.099	0.084	0.128	Nemo12b	EccoG
	0.098	0.085	0.118	Aviso	EccoG
South America	0.272	0.223	0.301	DTU10-TUM13	LivC
	0.16	0.106	0.197	DTU10-TUM13	EccoG
	0.145	0.107	0.178	Aviso	EccoG
	0.131	0.102	0.159	Aviso	EccoG
Pacific Islands	0.38	0.349	0.397	DTU10-TUM13	EccoG
	0.159	0.125	0.184	DTU10-TUM13	EccoG
	0.111	0.085	0.129	Ecco2	EccoG
	0.156	0.127	0.179	DTU10-TUM13	EccoG

Table 4. As in Table 3, but with analysis restricted to common coastal points for which we also have TG-based MDT values. (Note, for the Agulhas region there are no such values.)

Region	RMSD (mean)	RMSD (min)	RMSD (max)	Model (min)	Model (max)
Global	0.17	0.143	0.188	DTU10-TUM13	LivS
	0.103	0.07	0.126	DTU10-TUM13	LivS
	0.109	0.087	0.135	NemoQ	LivS
	*	*	*	*	*
Ne Atlantic	0.156	0.143	0.17	NemoQ	LivC
	0.064	0.049	0.101	DTU10-TUM13	LivC
	0.066	0.051	0.101	Nemo12a	LivC
	0.069	0.055	0.104	Nemo12a	LivC
Australia	0.163	0.132	0.192	Aviso	Nemo12a
	0.069	0.038	0.093	Aviso	Nemo12a
	0.101	0.088	0.119	Nemo12b	LivS
	0.103	0.09	0.122	Nemo12b	LivS
South America	0.303	0.223	0.393	DTU10-TUM13	LivC
	0.132	0.055	0.203	DTU10-TUM13	LivC
	0.086	0.021	0.161	DTU10-TUM13	LivC
	0.135	0.049	0.223	DTU10-TUM13	LivC
Pacific Islands	0.148	0.135	0.172	NemoQ	LivS
	0.094	0.053	0.16	DTU10-TUM13	LivS
	0.136	0.114	0.192	NemoQ	LivS
	0.128	0.103	0.185	DTU10-TUM13	LivS

Table 5. As in Table 4, but including the TG MDT values in the analysis.

Region	RMSD (mean)	RMSD (min)	RMSD (max)	Model (min)	Model (max)
Global	0.171	0.143	0.188	DTU10-TUM13	LivS
	0.107	0.07	0.142	DTU10-TUM13	TGmdt
	0.106	0.087	0.135	NemoQ	LivS
	*	*	*	*	*
Ne Atlantic	0.155	0.143	0.17	NemoQ	LivC
	0.065	0.049	0.101	DTU10-TUM13	LivC
	0.066	0.051	0.101	Nemo12a	LivC
	0.069	0.055	0.104	Nemo12a	LivC
Australia	0.17	0.132	0.233	Aviso	TGmdt
	0.078	0.038	0.159	Aviso	TGmdt
	0.096	0.049	0.119	TGmdt	LivS
	0.097	0.048	0.122	TGmdt	LivS
South America	0.282	0.089	0.393	TGmdt	LivC
	0.14	0.055	0.214	DTU10-TUM13	TGmdt
	0.098	0.021	0.209	DTU10-TUM13	TGmdt
	0.136	0.049	0.223	DTU10-TUM13	LivC
Pacific Islands	0.159	0.135	0.257	NemoQ	TGmdt
	0.109	0.053	0.242	DTU10-TUM13	TGmdt
	0.136	0.114	0.192	NemoQ	LivS
	0.131	0.103	0.185	DTU10-TUM13	LivS

Table 6. Assessment of the DYCOT CMDTs against the TG MDT.

Region	No of values	bias	RMSD	RMSD (unbiased)	min	max
Global	118	0.691	0.717	0.192	-0.786	0.671
	118	0.705	0.718	0.138	-0.433	0.698
	118	0.7	0.71	0.116	-0.815	0.42
	*	*	*	*	*	*
Ne Atlantic	46	0.726	0.742	0.15	-0.35	0.595
	46	0.728	0.732	0.076	-0.2	0.151
	46	0.742	0.745	0.064	-0.218	0.174
	46	0.743	0.746	0.066	-0.217	0.175
Agulhas	2	0.702	0.702	0.003	-0.003	0.003
	2	0.698	0.705	0.099	-0.099	0.099
	2	0.701	0.708	0.099	-0.099	0.099
	2	0.704	0.71	0.096	-0.096	0.096
Australia	14	0.637	0.676	0.227	-0.377	0.518
	14	0.666	0.684	0.157	-0.395	0.266
	14	0.705	0.707	0.049	-0.086	0.082
	14	0.707	0.709	0.048	-0.086	0.08
South America	3	0.65	0.657	0.089	-0.127	0.064
	3	0.651	0.685	0.214	-0.255	0.267
	3	0.581	0.617	0.209	-0.28	0.222
	3	0.629	0.645	0.145	-0.183	0.173
Pacific Islands	25	0.682	0.745	0.3	-0.778	0.679
	25	0.721	0.757	0.232	-0.446	0.682
	25	0.682	0.696	0.141	-0.227	0.444
	25	0.693	0.711	0.162	-0.229	0.593

WP4200: Scientific Roadmap

1. Synthesis of results.

Introduction

The GOCE++ Dycot project has been reported in a number of Technical Notes, which are here referred to by the deliverable number D1-D7 (this Scientific Roadmap forms part of D8). After preliminary work in Work Package 1, to assess the state of the art and to select data, models and regions of particular interest (D1, D2 and D3), the main work of the project was undertaken in Work Packages 2 (D4 and D5), and 3 (D6 and D7)

WP 2 involved the development and testing of software to calculate an ocean mean dynamic topography (MDT) from the combination of satellite altimetry and geoid or from tide gauge measurements and geoid.

WP 3 involved compilation of tide gauge data and GPS coordinates, and accounting for secular trends (D7), and calculation of coastal MDTs from tide gauges and from satellite altimetry (D6).

This section represents a synthesis of results from these two Work Packages.

Software development and testing

The software was written in the R language and provides the capability to take in both global fields (such as ocean model data, geoid, or mean sea surface), or pointwise data (tide gauge measurements). The global fields were standardised to a regular 0.125 degree latitude/longitude grid, and land masks were calculated to standardise the definition of ocean and land points on this grid (there are three such land masks defined according to whether the grid points contain any ocean, any land, or using a 50% threshold to choose between land and ocean).

A number of issues were recognised as being important for the comparison of these two data types.

1) Satellite altimeter data is conventionally supplied with an inverse barometer (IB) correction applied, so that it represents not the true sea surface position, but where the sea surface would be if the atmospheric pressure took a reference value (the IB-corrected surface is the relevant surface for ocean dynamics and geostrophic currents). Tide gauges represent actual sea level, so an IB correction is needed for the tide gauge data. Corrector surfaces were calculated on the 1/8 degree grid, using the same model as used to correct the altimetry (the Dynamic Atmospheric Correction, which is actually a high frequency

18

ocean model which accounts for more than just the IB correction, but is very close to IB for the long period signals considered here), and also a pure IB correction from the ERA-Interim atmospheric reanalysis dataset.

2) Different permanent tide systems are used for the GPS measurements at tide gauges and the sea surface measurements from satellite altimetry. This can cause latitude-dependent errors of order 20 cm. Corrector surfaces for this effect were also provided. This is briefly described in D4. More detail is given in the Appendix to this Technical Note.

3) The question of how best to smooth the global MDT encounters particular difficulties near to the coast. It is clear that some smoothing is required because small scales in the mean sea surface are often not resolved in the geoid. This is implemented by an iterative block average smoothing. However, it is also clear from model simulations and from theoretical arguments that the along-coast direction is special from the point of view of dynamic topography, and that a smoothing which is optimal for open ocean will typically produce artificially large along-coast gradients in MDT. The preliminary approach which has been taken so far is to set all land values in the local region considered to a constant MDT level at each iteration of the smoother. That constant is calculated as an average of the initial coastal values. While this can have clear advantages locally (see results in D5 and D5), it is not a viable method for comparisons which involve variations of MDT along the coast, as these variations are eliminated by the method. Future work should address the best way to set these land values in a manner which is responsive to the data, but still ensures a sensible along-coast smoothness of the MDT. For the present comparisons, the coastal smoothing is not used (smoothing only involves ocean points, ignoring any land values).

The software testing (D5), following work in WP3, showed the potential for good agreement between tide gauges and satellite-derived MDTs, using the Eigen-6C4 geoid and DTU15 mean sea surface. Regional mismatches had standard deviations varying from 0.034 m to 0.16 m depending on region and smoothing, with biases covering about half that range.

Our two well-surveyed regions showed a mixture of results. The Northwest European Shelf region of the Northeast Atlantic (NSeas1 in D5) showed a standard deviation of less than 0.06 m, and bias of less than 0.02 m with or without smoothing. In the case of Australia, the bias remains less than 0.03 m, but the standard deviation increases to 0.135 m without smoothing, but reduces below 0.06 m after smoothing.

Australia, though defined here as "well surveyed", is actually an intermediate case, as local levelling is over extremely long distances and rarely performed, and in-situ gravity data are rather sparse. A more detailed investigation into Australia is currently being considered for publication (Filmer et al., 2017). This shows agreement with the best ocean models at the level of 0.08 m standard deviation, but highlights certain sites where tide gauge MDTs are out of line with their neighbours to an extent which is

oceanographically unlikely, suggesting that local geoid error is the dominant issue for these sites.

Three poorly-surveyed regions were considered. South East Africa, with only 5 tide gauges, showed biases of 0.04 to 0.06 m and standard deviations of 0.03 to 0.054 m. Similarly, South America, with only 3 tide gauges showed biases of around 0.05 m and standard deviations of under 0.08 m. While these results appear good, especially for Africa, the numbers of gauges are small and the statistics should be interpreted with caution.

The third poorly-surveyed region is the small-island dominated Pacific region. This showed the largest bias (0.08 to 0.09 m) and standard deviation (0.16 to 0.15) of all regions. This result was confirmed separately in a global analysis (D6). This is particularly interesting as there is little reason to suspect the GPS positioning in these cases is any worse than elsewhere, and many tide gauges in this region show excellent agreement with satellite altimetry in the time-dependent signals (D6). The large mismatches and systematic bias point to a short length-scale geoid error. It is plausible that this should cause a bias as the islands all have very similar geology, rising steeply from the ocean floor, and missing gravity data is likely to have a similar influence in each case.

Tide gauge data

Data have been gathered from 302 tide gauges with GPS ties. The ellipsoidal heights of the tide gauge datums have been calculated and tabulated, allowing calculation of the ellipsoidal height of sea level. In addition, it has been noted where the relevant geoid position is for each tide gauge. In cases where a GPS measurement was taken directly at the tide gauge (either as the primary measurement, or coupled with GPS elsewhere to make a differential measurement) this position is the tide gauge position. When the tide gauge connection to GPS is made by levelling, then it is the geoid at the GPS position which is relevant. This work is described in detail in D7.

The GPS heights are corrected to the 2003-2007 reference period using vertical land movement rates based on the ULR GPS solution where available, and tide gauge minus altimetry elsewhere (Wöppelmann and Marcos, 2016). Errors are typically 1-2 mm/yr, leading to errors in the mean heights from this cause of less than 0.02 m.

Obtaining a mean sea level over the reference period can also be problematic if there are periods of missing tide gauge data. Two approaches have been tried to fill gaps in tide gauge data: fitting the temporal variability on nearby tide gauges where they are sufficiently well correlated, or fitting on nearby satellite altimetry data. A comparison of mean values using the two different methods revealed a root-mean-square difference of 0.03 m, suggesting that this is not the major source of error (though not negligible, and occasional values approaching 0.1 m are seen). As the altimeter method is more widely applicable, this method is adopted.

An analysis of geocentric sea level trends showed that the use of secular trends (as used for vertical land motion) is much less useful, as decadal variability dominates. This highlights the importance of using a common reference period, and makes it clear that correction to a different reference cannot be made simply using a linear function of time.
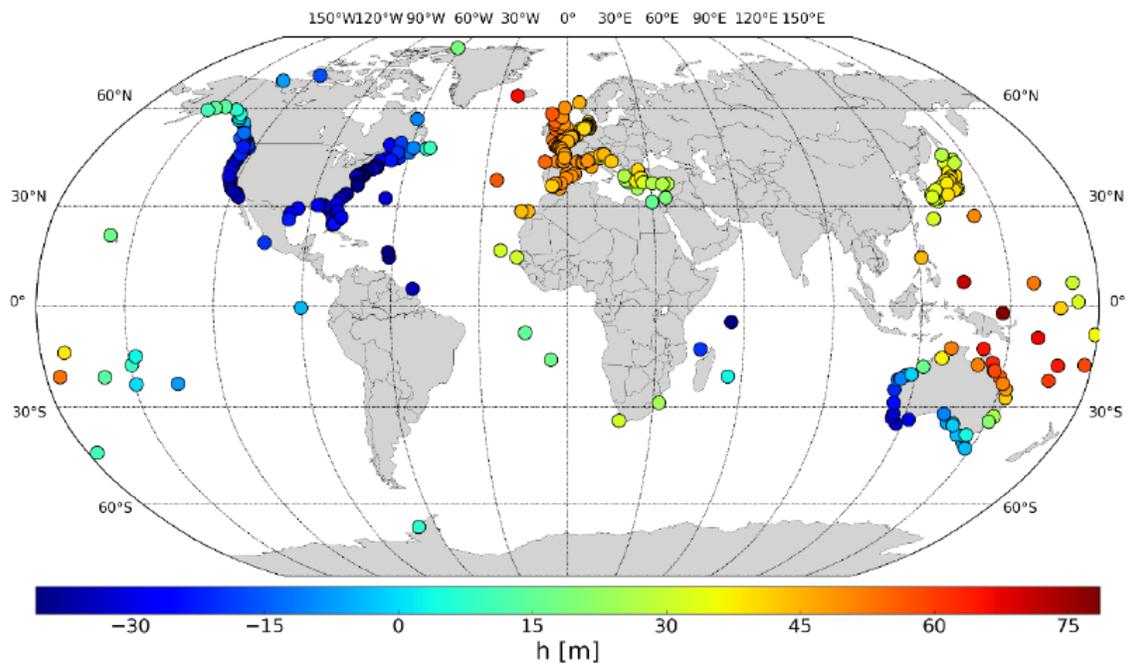
Figure 6: Sites at which tide gauge data with GPS ties are available. Colours show the mean (2003-2007 inclusive) height of sea level at the tide gauges, measured relative to the reference ellipsoid.

Coastal MDT

The tide gauge measurements discussed above have been converted to MDT estimates using a variety of geoids at a variety of truncations, and with different smoothing approaches. The headline results were discussed in the section on software development and testing, but here we give some more detail.

Figure 2 shows the MDT at the 302 tide gauges, compared with a range of global MDTs from ocean models and satellite measurements, extrapolated to the coast. This is updated and improved from the data shown in D6, which prompted the checking of GPS ties for a few outliers.

The ordering of the tide gauges follows the Permanent Service for Mean Sea Level coastal ordering. This starts with Norway, running anticlockwise round Europe, Africa and Asia, then covers Australia and the Pacific, before running anticlockwise around the Americas starting with Alaska and ending with Arctic Canada, before finally moving to Antarctica.
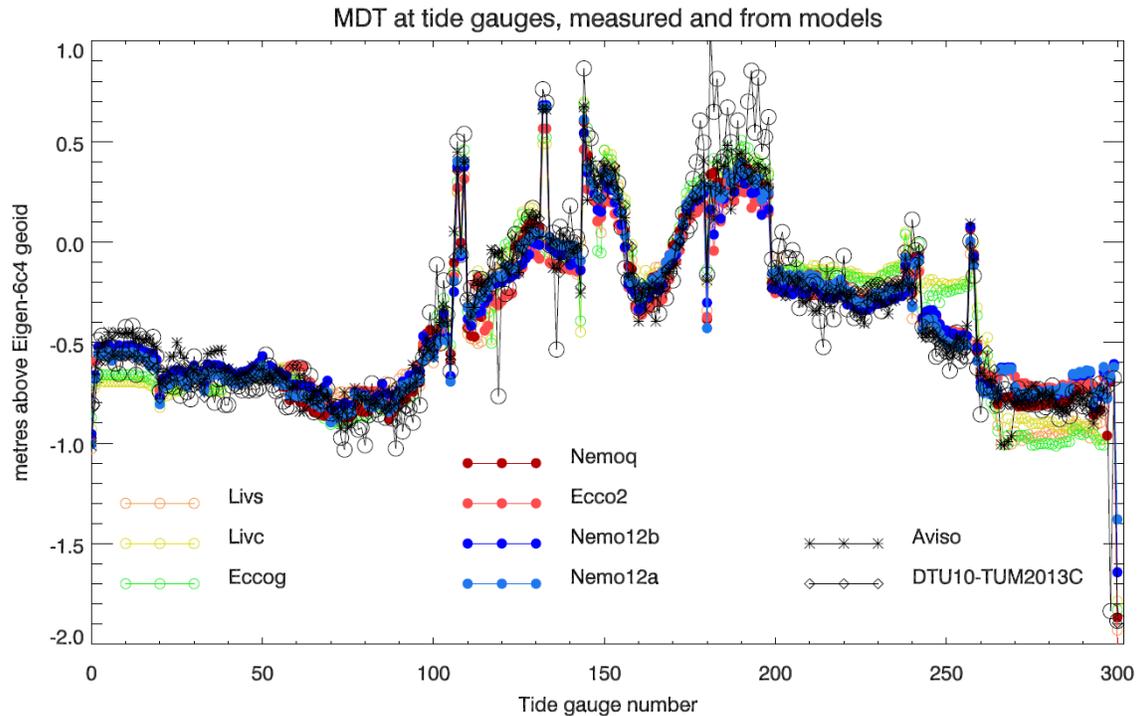
Figure 7: The MDT at 302 tide gauges (black circles) using the Eigen-6C4 geoid to its full resolution, compared with predictions from 7 ocean models (colours), and 2 satellite-derived MDTs (black).

Several things can be seen immediately. The match is generally good, but the tide gauges show a systematic high bias between about numbers 175 and 200, corresponding to the Pacific Islands. The two prominent downward spikes (120 and 137) are Aburatsubo (near Tokyo) and Mikuni (fairly nearby, but on the opposite, north coast of mainland Japan). Tectonic activity is an obvious concern, but the many other Japanese records look good. Other "spikes" are common to tide gauges and models, and represent excursions off the coastline to islands.

The coarse resolution models, Livs, Livc and Eccog, all show significant departures from the observations particularly in the North Atlantic from about 230.

Table 1 shows some summary statistics based on these comparisons. The distribution is clearly non-Gaussian, with long tails (most likely due to local geoid errors) and a central region which is closer to Gaussian. The compactness of the central region gives a measure of model accuracy, and shows clearly that the finer resolution models, and satellite based data, agree better with tide gauges than the coarser models. This is not uniformly the case though. Nemoq, at ¼ degree resolution, does particularly well, whereas Nemo12b, at 1/12 degree, does significantly worse than the very similar

22

Nemo12a (perhaps because this longer model run has had time to drift further from initial conditions).

Table 7: Statistics comparing the coastal MDT from combination of tide gauges with the Eigen-6C4 geoid to full resolution, against 8 different global MDTs extrapolated to the same positions. Values are in metres. The pdfs are non-Gaussian, so they are characterized by half the range which contains the number of values which would be expected to fall within 1 sigma in a Gaussian distribution (1 sigma equiv), or quarter the range for 2 sigma. Also given are the minimum and maximum values (TG-MDT after subtracting the median), and the number of missing values (because some MDTs do not have data in some regions). Where there are no missing values, there are 302 points being compared.

Global MDT	Standard deviation	1 sigma equiv	Half (2 sigma)	min	max	Skewness	Excess Kurtosis	N missing
Nemo12a	0.135	0.103	0.139	-0.600	0.557	0.43	4.57	0
NemoQ	0.130	0.103	0.135	-0.570	0.610	0.63	4.30	0
Aviso	0.132	0.110	0.135	-0.706	0.551	0.07	4.81	3
DTU10-TUM13	0.138	0.114	0.138	-0.711	0.578	0.26	3.59	4
Nemo12b	0.147	0.115	0.160	-0.568	0.626	0.92	3.52	0
Ecco2	0.156	0.129	0.163	-0.453	0.698	1.05	2.60	1
Livs	0.168	0.149	0.181	-0.613	0.767	0.85	2.87	3
EccoG	0.163	0.153	0.164	-0.583	0.531	-0.06	0.50	7
Livc	0.171	0.162	0.173	-0.556	0.537	0.05	0.46	7

Skewness is generally positive, meaning the most extreme mismatches tend to be tide gauges showing higher MDT values than the global fields. Excess kurtosis (kurtosis – 3) is extremely positive (narrow peak and long tails) for the best comparisons, reducing to much smaller values (close to Gaussian) for the coarse resolution ocean models. This is suggestive of two distributions: a roughly Gaussian distribution which depends on the global MDT, and a tail of outliers which is independent of global MDT, and therefore results from local effects at the tide gauges (most likely geoid error). This interpretation is bolstered by the fact that the maximum and minimum errors are poorly related to the accuracy of the bulk of the distribution.

It is clear that the data are able to discriminate between models, especially when ignoring the tails of the distributions. However, by far the most important factor is the quality of the geoid, and in particular its fine scale structure. This is illustrated by Figure 3, which repeats Figure 2 but with a geoid truncated at degree 300. It is further supported by results of a range of methods applied to the calculation of satellite-derived MDT at tide gauge positions (D6).

Finally, for this comparison we show the spatial distribution of these MDT measurements in Figure 4. It is impossible to show much detail in such a map, but it does show the general patterns, and also highlights the fact that the gauge on the east coast of South Africa (Richards Bay) has a value which agrees well with the Aviso global MDT, but that resolution of the thin strip of ocean to the west of the Agulhas current is crucial for this, as there are nearby ocean values which are very different. More detailed examinations reveal similar results for the Gulf Stream, Kuroshio, and East Australian Current.
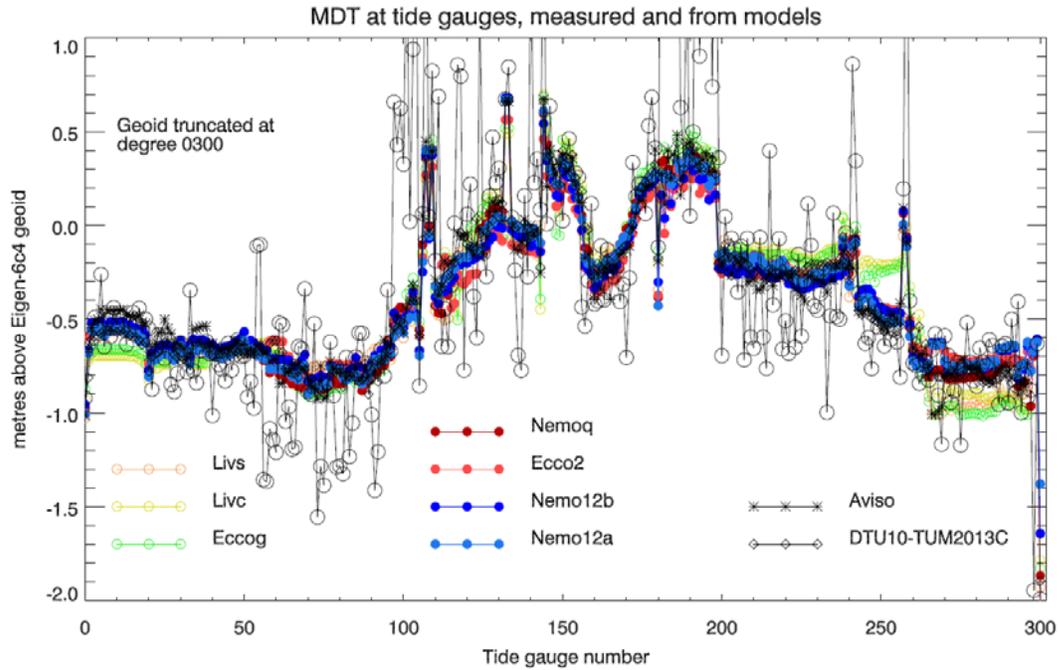
Figure 8: repeat of Figure 2 but with the geoid truncated at degree 300.
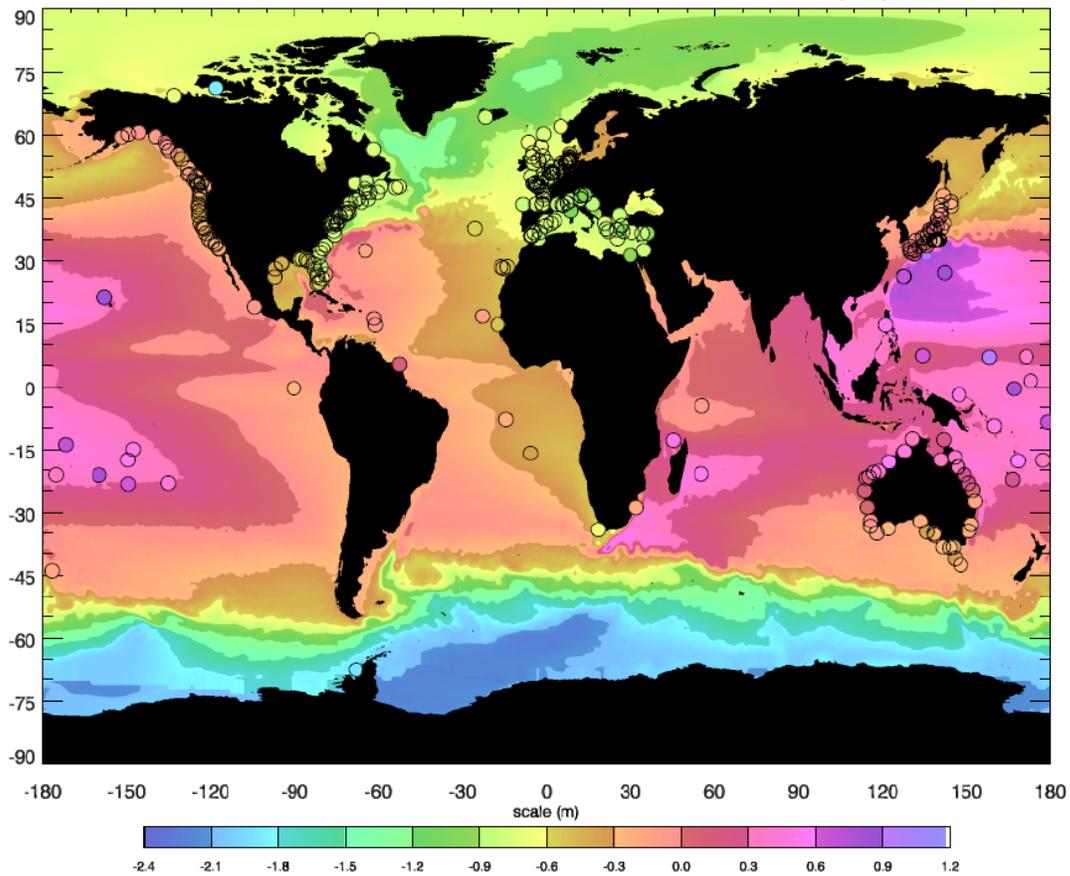
Figure 9: The spatial pattern corresponding to Figure 2, using Aviso+Ecco2 global MDT to compare with the tide gauge MDT.

Further investigations into coherence scales for tide gauge data and model predictions (D6) showed an extremely heterogeneous picture. Neighbourhood correlations between tide gauge time series (running annual means) varied between very small values and very close to 1, with most values above 0.5. In some cases, relatively poor correlations were associated with long distances between tide gauges, but in others they seemed to be indicative of tide gauge "quality", which may mean either accuracy of measurement or representativeness of broader scales. Individual case studies and comparisons with altimetry showed that sometimes dramatic differences between neighbours were due to genuine signal differences from ocean dynamics. Clearly this issue must be accounted for when assigning coastal values by smoothing of global satellite-derived fields.

The model analyses suggested a means to do this, as the higher-resolution models produced quite consistent (but highly geographically variable) estimates of how far along- and off-shore it was necessary to travel in order to encounter a dynamic topography change exceeding a certain threshold. It was suggested that this information could be used to construct an expected signal covariance for use in interpolation and extrapolation of satellite and tide gauge MDTs.

A local analysis into the Norwegian MDT demonstrated the value of coastal altimetry data from CryoSat-2 (D6; Idžanović et al, 2017). In this region, strong levelling ties between tide gauges permit a comparison which is not dependent on direct GPS measurements at each gauge. Similar conclusions were drawn, with good error budgets in the is well-surveyed region: the dynamic topography as modelled has small, and smooth variations across the region, but both geodetic measurements demonstrate small-scale variations of around 0.03 m (levelling) or 0.03-0.05 m (satellite method). The addition of measurements very close to the coast was found to help in avoiding errors due to coastal currents, seen in both the satellite data and ocean model. The remaining error, however, was found to be dominated by small-scale geoid error which can only be addressed by local gravity measurements.

Similar investigations into Australian coastal MDT also highlighted the small-scale geoid error, at larger amplitude in this case, with sporadic mismatches of 0.1-0.2 m (Filmer et al., 2017). In some cases these were found to be in regions of complex coastal geometry (in one case the gauge is some distance from the coast). Again, it was found that addition of CryoSat-2 data had the potential to improve the coastal resolution. In this case, however, another issue was also identified: the availability of tide model data was found to be a limiting factor, which was overcome by switching from the GOT4.8 to the FES2012 tidal model. This highlights the importance of reassessing altimeter correction models as new, more coastal data become available.

An investigation into the accuracy of CryoSat-2 data in the northwest European seas and the Bay of Bengal also confirmed that the CryoSat-2 altimeter is producing accurate measurements in the coastal region.

2 Future directions

The biggest challenge for unified calculation of a coastal and global MDT is clearly the lack of small-scale geoid information for comparison with point measurements from tide gauges, or to combine with satellite measurements of the mean sea surface close to the coast. This is a problem with varying geographical impact, which will ultimately only be overcome by use of local measurements, either of gravity in a region surrounding the point in question, or of geopotential at the point (see later).

A second challenge is the limited number of tide gauges with GPS ties. We have identified 302 such gauges in this project, in comparison to 1007 datum-controlled records which overlap the satellite altimetry era (1993 onwards).

Even without additional data, the present investigations have highlighted a number of ways in which immediate progress can be made based on observations which are currently available or will become available in the next few years.

Here we present recommendations for ways forward on two time horizons: a short-term horizon of a few years, and a longer-term decadal time scale.

Short term recommendations.

Using tide gauge data: Tide gauge measurements are clearly dominated by small scale geoid errors with a highly non-Gaussian and regionally dependent error. The size of these errors is such that a single tide gauge can contribute only weakly to constraining the MDT at the coast. However, in regions with multiple gauges separated by distances short compared to the coherence length scale of the MDT, tide gauge measurements can be used as part of an optimal mapping strategy, if realistic errors can be estimated. We recommend using the small scale variability from gauge to gauge as a proxy for regional errors to feed into such a mapping.

Using satellite data: Equally, and for the same reasons, satellite-derived data are of limited use at individual points, but can be improved with appropriate smoothing. In turn, this smoothing is facilitated if the data can be extended as close to the coast as possible. The immediate recommendation is therefore to make use of the new SAR altimetry, and to prepare for the SWOT mission which is expected to improve the coastal resolution still further, in order to produce and refine new global mean sea surface maps extending the work of DTU16. Care must be taken to ensure appropriate altimeter corrections, such as tide corrections, are used and do not degrade the spatial coverage.

Extending tide gauge data: It has recently been convincingly shown (Larson et al., 2017; Williams and Nievinski, 2017) that the signal to noise ratio of coastal GNSS receivers can, in favourable circumstances, be used to make a geocentric coastal sea level measurement with centimetric accuracy. This sidesteps many of the difficulties with tide gauges, of tracing documentation and levelling ties, as the relevant measurement is made directly, in combination with monitoring of changes in the sensor position. The tide gauge network results should be extended using this new technology. In addition, further

GNSS ties should be encouraged and clearly documented to extend the MDT measurement capability to other tide gauges around the world.

Optimal combination of data: Information on the length scales of variability of the MDT is a necessary precursor of optimal combination. We have found that ocean models with resolutions of about ¼ degree or better provide such information in a manner which is consistent with observational constraints and also consistent between models. We recommend that statistics based on model MDTs be used to constrain this optimal mapping, with the caveats given below.

Given the clearly different natures of coastal and open-ocean MDTs, our recommended strategy is split into two arms. First, a coastal MDT should be computed, combining tide gauge and satellite data, using covariances based on the model-derived along-coast and offshore length scales. Second, the global solution should be computed using appropriate anisotropic smoothing, but constrained to match the predetermined coastal MDT.

Model investigations: The use of model-derived covariances, though necessary for the present, has certain dangers. There is the possibility of over- or under-weighting observations when the model predictions are wrong because of missing processes. The validation to date has shown that, in most circumstances, there are no major errors in the models, but there may be exceptions. In particular, when a tide gauge is in an estuary, it is unclear to what extent processes which are missing from the model may play a role. Examples are interactions with river flow, nonlinear tidal effects on the mean, and wave set-up effects. Attention should be payed to these issues in regional models. The processes are all accounted for in some models, but the focus has thus far been on time-dependent effects rather than the influence on the MDT, which is much harder to validate.

Applicability to different regions: The strategies outlined above will play out very differently in different regions. In well-surveyed regions with many tide gauges, the tide gauge data is likely to play a significant role in constraining the coastal solutions. In poorly-surveyed regions, where tide gauge data are sparse, there will be no along-coast averaging effect, and the sporadic measurements with correspondingly large errors (given the lack of information about short length-scale variability) are unlikely to make a significant contribution. As an example, the Pacific island measurements appear to have both random and systematic errors of order 0.1 m. On the other hand, model data show that the MDT remains within 0.02 m of the coastal MDT out to distances of hundreds of kilometres from most islands (D6), meaning that the satellite data will produce the greater constraint. In order for isolated tide gauges to make a significant contribution, it is crucial that local geoid information be improved, and the improvement be quantified.

<div align="center">

Long-term recommendations

</div>

No presently-foreseeable satellite gravity measurement system is capable of providing geoid measurements on the small scales (order 10 km) required for true point measurements of MDT. Improvements of coastal MDT measurements at a level which

will provide an independent test of ocean and climate models beyond what will be possible in the next few years, will rely on either in-situ (land-based and/or airborne) gravity measurements, or new technology.

An example of the former is the NOAA GRAV-D gravity survey of the US (Johnson, 2009). On decadal timescales, the extension of such measurements to cover a significantly broader region of the world is feasible, though it is unlikely that truly global coverage will be achieved.

The alternative is a new method of determining the geopotential directly at a particular point. This sidesteps the need for global solutions and broad coverage of fine resolution gravity, but it does mean that each measurement is only representative of the particular point at which it is made. The method relies on the development of precise clocks, and the general relativistic result that clocks run at different rates depending on the geopotential surface at which they sit (lower clocks run slower). The fractional change in clock frequency is given by $\frac{\delta f}{f} = \frac{\delta W}{c^2} \approx \frac{g\,\delta h}{c^2}$ where δW is the geopotential change, δh is the height change, and c is the speed of light. The factor $\frac{g}{c^2}$ is approximately 10^{-16} m^{-1}, meaning that centimetric accuracy is attained at $\frac{\delta f}{f} = 10^{-18}$. The present generation of optical clocks is already very close to attaining this accuracy (Margolis, 2014; Petit, 2017). There remains, however, a substantial challenge in comparing such clocks at separate sites (frequency transfer). Nonetheless, frequency transfer at 10^{-16} accuracy has been demonstrated by satellite using the GPS network (Petit et al., 2015). Optical fibre frequency transfer is already at 10^{-18} accuracy (Lisdat et al., 2016), which is important for verification and development, but satellite transfer will become necessary for any system which is to be used widely at satellites.

The development of such highly accurate clocks and satellite frequency transfer capability will have much broader applicability than simply coastal MDT determination, and is an objective that we would strongly encourage. From the present perspective, it is worth noting that this would be as valuable for isolated tide gauges as for those which are closely clustered, and would therefore be of great value in poorly surveyed regions.

In addition to tide gauge measurements, there are still improvements to be made in global mean sea surface determination. We expect the SWOT mission to improve coverage significantly in this regard. A decadal timescale issue will be the development of optimal path length corrections and minimisation of aliasing of high frequency variability, both issues of particular importance in the coastal zone.

References

Filmer, M. S., C.W. Hughes, P.L. Woodworth, W.E. Featherstone, R.J. Bingham (2017), Comparison between geodetic and oceanographic approaches to estimate mean dynamic topography for vertical datum unification. J. Geodesy (submitted).

Idžanović, M., V. Ophaug and O. B. Andersen (2017), The coastal mean dynamic topography in Norway observed by CryoSat-2 and GOCE. Geophys. Res. Lett. 44, 5609–5617, doi:10.1002/2017GL073777

Johnson, B. (2009), NOAA project to measure gravity aims to improve coastal monitoring. Science 325 (5939), 378, doi: 10.1126/science.325_378

Larson, K. M., R. D. Ray, and S. D. P. Williams (2017), A ten-year comparison of water levels measured with a geodetic GPS receiver versus a conventional tide gauge. Journal of Atmospheric and Oceanic Technology, 34, 295-307, doi: 10.1175/JTECH-D-16-0101.1

Lisdat, C. and 34 co-authors, (2016), A clock network for geodesy and fundamental science. Nature Communications 7:12443, doi: 10.1038/ncomms12443

Margolis, H. (2014), Timekeepers of the Future. Nature Physics (10), 82-83, doi: 10.1038/nphys2834

Petit, G. (2015), 1×10^{-16} frequency transfer by GPS PPP with integer ambiguity resolution. Metrologia 52, 301-309, doi: 10.1088/0026-1394/52/2/301

Petit, G. (2017), Frequency standards work in the consultative committee for time and frequency. Presentation at meeting of IAG Joint Working Group 2.1 on Relativistic Geodesy, Hannover, 15-16 May 2017.

Williams, S. D. P., and F. G. Nievinski (2017), Tropospheric delays in ground based GNSS multipath reflectometry— Experimental evidence from coastal sites, J. Geophys. Res. Solid Earth, 122, 2310–2327, doi:10.1002/2016JB013612

Wöppelmann G., and Marcos M. (2016), Vertical land motion as a key to understanding sea level change and variability, Rev. Geophys., 54, 64–92.

Appendix: Dealing with the permanent tide.

Chris W. Hughes, 24 Jan 2017.

Bottom line summary

N = geoid height above the ellipsoid, can be in the zero tide (ZT) or tide free (TF) system.
h = geometrical height above the ellipsoid, in the mean tide (MT) system for altimetry, and in the tide free (TF) system for GNSS.

To within a couple of millimetres, it should be ok to use a slight approximation (the approximation is 0.1 mm at most) of the IERS conventions, which gives:

$N_{MT} = N_{ZT} + A_0$
$N_{MT} = N_{TF} + A_0(1+k_2)$
$h_{MT} = h_{ZT} = h_{TF} + A_0 h_2$

Where $A_0 = D\left(\frac{1}{3} - \sin^2\phi\right)$, ϕ is latitude, and
D = 29.767 cm
k_2 = 0.30190
h_2 = 0.6078

For better than a couple of mm, details matter (precisely which Love numbers k_2 and h_2, and amplitude D, were used in the computation)

More detailed description

The presence of the time-mean Sun and Moon causes:

1) Directly, a gravitational field which lifts equipotentials by an amount

$A_0 = D\left(\frac{1}{3} - \sin^2\phi\right)$, where ϕ is latitude and D = about 29.7 cm,

representing a lift of 9.9 cm at the equator and a drop of 19.8 cm at the poles.

2) Indirectly, a distortion of the Earth which amplifies the geopotential lift by a factor $(1+ k_2)$,
and lifts the surface by an amount $A_0 h_2$. Here, k_2 and h_2 are the degree 2 tidal Love numbers, about 0.3 and 0.61 respectively.

Anything measured in the real world includes this permanent tide, so it is natural for sea level heights above a reference ellipsoid or geoid to be measured with the permanent tide included. This is called the mean tide system.

However, the concept of a reference ellipsoid and matching "Normal" gravity field, as in GRS80 (Moritz, 2000), is developed from the idea of a rotating, self-gravitating body with an ellipsoidal equipotential surface in equilibrium with self-gravitation and rotation rate only, with no external bodies acting, so the reference ellipsoid and matching normal gravity do not include the permanent tide.

Furthermore, spherical harmonic representations of gravity fields list only a single set of coefficients. These represent the difference from the normal potential due to the non-equilibrium mass distribution of the Earth, and the associated radial functions all decay away from the Earth. The coefficients are incapable of representing the direct effect of Sun and Moon, because the associated coefficients would be the second set of spherical harmonics which increase away from the Earth (a correction to C_{20} is possible, but it would only work for one particular geopotential, and would be wrong at all other distances from the Earth). Thus, the geopotential from a set of spherical harmonic coefficients must be missing the direct gravitational contribution of the Sun and Moon. We call this the "zero tide" system.

There is a further complication in that, in calculating time averages, it is usual to remove the time dependent tide from any signal measured. In doing so, it is often the case that the permanent tide (both direct and indirect) is also removed. In fact, it is not the true permanent tide which is removed, but a version which assumes the Earth's elasticity at infinite period (for the permanent tide) is the same as that at the periods of the varying tide, predominantly semidiurnal and diurnal. Thus, the tidal Love number values are those appropriate to the diurnal and semidiurnal tidal frequencies. The true permanent tide has quite different Love numbers appropriate for a nearly fluid Earth, but these are of only academic interest for our purposes.

The result of this is that, for the gravity field we sometimes find measurements in a system in which both the direct and (wrong version of the) indirect mean gravitational effect of the Sun and Moon have been removed. This is called the "conventional tide free" or "conventional non-tidal" system, where "conventional" emphasizes the fact that the diurnal/semidiurnal tidal frequency Love numbers were used. The same thing is true of GNSS measurements of ellipsoidal heights (i.e. heights normal to the reference ellipsoid). In this latter case, the "conventional tide free" system is the convention used in practice, despite an IAG resolution (Resolution 16 of the 18th General Assembly of the IAG, 1983) that mean tide should be used for displacements and zero tide for potentials.

So, to summarise:

Altimetry measures the height of the sea surface relative to the ellipsoid, in the "real world" mean tide system.

Spherical harmonic coefficients for the gravity exclude the potential due to external bodies, and may also exclude the indirect tidal potential induced by those bodies (on the assumption of a frequency independent Love number), so may be in the zero tide or conventional tide free system.

GNSS ellipsoidal heights are given with both direct and indirect effects removed (on the assumption of a frequency independent Love number), and are therefore in the conventional tide free system.

To convert between systems:

Including the mean tide (i.e. in the mean tide system), the geoid departs from the reference ellipsoid by A_0 more than it does in the zero tide system, so if N is geoid height above the ellipsoid:

$N_{MT} = N_{ZT} + A_0$
$N_{MT} = N_{TF} + A_0(1+k_2)$

where MT means in the mean tide system, ZT in the zero tide system, and TF in the tide free or non-tidal system.

For geometrical heights above ellipsoid, there is no direct effect to consider, so the mean tide system is the same as the zero tide system. The surface in the mean tide system is A_0h_2 above the surface in the tide free system, so the conversion is

$h_{MT} = h_{ZT} = h_{TF} + A_0h_2$

where, to recap, $A_0 = D\left(\frac{1}{3} - \sin^2\phi\right)$, where ϕ is latitude.

So far I have only given approximate values of k_2, h_2 and D. Below, I will give various standards for these values

EKMAN REFERENCE VALUES
A standard reference is Ekman (1989) which gives
D = 29.6 cm
$k_2 = 0.3$
$h_2 = 0.62$

(NB Ekman's formula for A_0 is actually $A_0 = 9.9 - 29.6\sin^2\phi$ cm, where the 9.9 should be read as a rounded approximation to 29.6/3)

GOCE HSU REFERENCE VALUES

The GOCE+HSU final summary report gives, on page 47, a set of formulae for converting between tide systems. The formulae for the geoid are as above, with

D = 29.6 cm
k_2 = 0.30129,

which gives corrections at most 0.33 mm different from those using Ekman's values. The k_2 value is the "nominal" value from McCarthy and Petit (2003) (i.e. the IERS conventions). However, the IERS document (section 6.3, page 67) states that the appropriate k_2 value to use here is 0.30190, (it also mentions that the value used for EGM96 was 0.30).

The formula for heights, taken directly from McCarthy and Petit (2003, p83, section 7.1.3) is

$$h_{MT} = h_{ZT} = h_{TF} + \left(-12.06 + 0.01P_2\right)P_2 \text{ cm, where } P_2 = (3\sin^2 \phi - 1)/2$$

which can be rewritten as $h_{TF} + A_0 h_2 \left[1 + 0.00124\left(\frac{1}{3} - \sin^2 \phi\right)\right]$ with h_2 = 0.6078, which implies that D = 29.76 cm.

Ignoring the 0.00124 term, which has an effect of 0.1 mm, this reduces to

$h_{MT} = h_{ZT} = h_{TF} + A_0 h_2$

<u>Final summary from GOCE HSU standards</u>:

$N_{MT} = N_{ZT} + A_0$
$N_{MT} = N_{TF} + A_0(1+k_2)$

$$h_{MT} = h_{ZT} = h_{TF} + A_0 h_2 \left[1 + 0.00124\left(\frac{1}{3} - \sin^2 \phi\right)\right] \approx h_{TF} + A_0 h_2$$

where, $A_0 = D\left(\frac{1}{3} - \sin^2 \phi\right)$, where ϕ is latitude, and
D = 29.6 cm for the geoid (N) formulae
D = 29.76 cm for the height formulae
k_2 = 0.30129
h_2 = 0.6078,

Clearly the HSU standards are mixing together Ekman and IERS values. The different D values cause a maximum change [when multiplied by $\frac{2}{3}(1 + k_2)$] of 1.4 mm. The change in h_2 relative to Ekman (0.6078 vs 0.62), when multiplied by $\frac{2}{3}D$, gives a maximum difference of 3.6 mm (these two changes do partly compensate).

IERS REFERENCE VALUES

From IERS conventions 2003 (McCarthy and Petit, section 7.1.3), the permanent tide in radial displacement is

$$(-12.06 + 0.01P_2)P_2 \text{ cm}$$

where $P_2 = (3\sin^2 \phi - 1)/2$, exactly as in the GOCE HSU document.

However, they also state that this is calculated from H_0 = -31.460 cm where H_0 is the amplitude of V/g (i.e. the lift of geopotentials by the direct gravitational effect) for the permanent tide, in the normalization of Cartwright and Tayler (1971) (this value is also consistent with the Cartwright and Tayler values extrapolated to year 2000). To translate this normalization to a value of D requires multiplying it by the factor $-\frac{3}{2}\sqrt{\frac{5}{4\pi}} = -0.9461747\ldots$, which converts -31.460 to +29.767 cm. The matching Love numbers given are h_2 = 0.6078 and (section 6.3, pp 66-67) k_2 = 0.30190. Therefore the full IERS standard is

$N_{MT} = N_{ZT} + A_0$
$N_{MT} = N_{TF} + A_0(1+k_2)$
$h_{MT} = h_{ZT} = h_{TF} + A_0 h_2 \left[1 + 0.00124\left(\frac{1}{3} - \sin^2 \phi\right)\right] \approx h_{TF} + A_0 h_2,$

where $A_0 = D\left(\frac{1}{3} - \sin^2 \phi\right)$, ϕ is latitude, and
D = 29.767 cm
k_2 = 0.30190
h_2 = 0.6078.

The number 0.00124 is calculated from the 0.01 factor in the original equation. To a fraction of 1 mm (in fact, 0.1 mm) this factor can be neglected, giving approximate height equations:

$h_{MT} = h_{ZT} = h_{TF} + A_0 h_2$

The IERS 2010 conventions (Petit and Luzum, 2010) for permanent tide are the same as the 2003 conventions (McCarthy and Petit, 2003).

34

Size of errors

If we take the IERS case as reference, and add a superscript zero to the constants for this case, then the error in the transform on using a different set of constants is largest at the poles, where it is given by

$$h_{Err} = -\frac{2}{3}[Dh - D^0 h^0]$$

$$N_{Err1} = -\frac{2}{3}[D - D^0]$$

$$N_{Err2} = -\frac{2}{3}[D(1 + k_2) - D^0(1 + k_2^0)]$$

where h_{Err} is the error in the TF to ZT or MT height transform, N_{Err1} is the error in the ZT to MT geoid transform, and N_{Err2} is the error in the TF to MT geoid transform. Using numbers given above, we find the following errors with respect to IERS (ignoring the 0.1 mm term in IERS and HSU height transforms):

Table 8: Errors in mm at poles resulting from non-IERS transformations

	Ekman	HSU
h_{Err}	-1.731 mm	0 mm
N_{Err1}	+1.113 mm	+1.113 mm
N_{Err2}	+1.824 mm	+1.570 mm

We can expect errors of a similar size if the IERS constants are used to perform a transform on heights or geoid heights given in the tide free system, if the Love numbers used when removing tides to generate those heights differed from the IERS values.

References

Cartwright, D. E. and R. J. Tayler, 1971: New computations of the tide-generating potential. Geophys. J. R. astr. Soc (23), 45-74. doi: 10.1111/j.1365-246X.1971.tb01803.x. http://dx.doi.org/10.1111/j.1365-246X.1971.tb01803.x

Ekman, M., 1989: Impacts of geodynamics on systems for height and gravity, Bulletin Geodesique (63), 281-296. doi: 10.1007/BF02520477. http://dx.doi.org/10.1007/BF02520477

GOCE+HSU final summary report available from http://www.goceplushsu.eu/gpweb/gc-cont.php?p=65

McCarthy, D.D. and G. Petit (Eds), (2003) IERS Conventions (2003), available from https://www.iers.org/IERS/EN/Publications/TechnicalNotes/tn32.html

Petit, G., and B. Luzum (Eds), (2010) IERS Conventions (2010), available from https://www.iers.org/IERS/EN/Publications/TechnicalNotes/tn36.html

Moritz, H. (2000): Geodetic Reference System 1980. Journal of Geodesy (2000) 74: 128. doi: 10.1007/s001900050278.
http://dx.doi.org/10.1007/s001900050278